

Copyright
by
Anamika Dubey
2015

The Dissertation Committee for Anamika Dubey
certifies that this is the approved version of the following dissertation:

**Distributed Resource Integration Analysis and Network
Design of Electric Power Distribution Systems**

Committee:

Surya Santoso , Supervisor

Ari Arapostathis

Alexis Kwasinski

Gary Hallock

Abdelhamid Ouroua

**Distributed Resource Integration Analysis and Network
Design of Electric Power Distribution Systems**

by

Anamika Dubey, B.Tech., M.S.E.

DISSERTATION

Presented to the Faculty of the Graduate School of

The University of Texas at Austin

in Partial Fulfillment

of the Requirements

for the Degree of

DOCTOR OF PHILOSOPHY

THE UNIVERSITY OF TEXAS AT AUSTIN

December 2015

Dedicated to my mother

Acknowledgments

I owe the successful completion of my dissertation to the guidance and support of my adviser, committee members, friends, and family, without whose help this work would not have been possible.

First, I would like to express my deepest gratitude to my adviser, Dr. Surya Santoso, for giving me an excellent opportunity and a conducive research environment. I am forever grateful for his constant motivation, immense knowledge, and endless patience that inspired me to do my best. At times, his trust in my potential helped me regain my self-confidence and kept me going. I am indebted to his critical reviews on the quality of my work and writing as it helped me in conducting a well-rounded research. His example helped me translate the challenges of graduate life into the satisfaction of achievement.

My sincere thanks goes to the rest of my committee members: Dr. Ari Arapostathis, Dr. Gary Hallock, Dr. Alexis Kwasinski, and Dr. Abdelhamid Ouroua for their insightful remarks, valuable comments, and constant encouragement. Their critiques and challenging questions helped me in making my research objectives more comprehensive with a broader scope for their applications. I am indebted to their years of experience and knowledge in shaping my research and dissertation.

I would also like to acknowledge the funding agencies for my research: The United Illuminating Company, Electric Power Research Institute, Office of Naval Research, and Electric Ship Research and Development Consortium. My sincere thanks to Mr. Marek Waclawiack, and Mr. Matthew P. Cloud

from The United Illuminating Company and Dr. J. Taylor, Dr. Arindam Maitra, and Dr. Matthew Rylander from EPRI for discussions and insights into the electric vehicle and photovoltaic generation problem.

Let me also thank Dr. Hongbo Sun from Mitsubishi Electric Research laboratories, Boston under whose supervision I completed two summer internships. Working under him was an excellent opportunity as it broadened my perspective regarding the challenges of the current and future power distribution systems.

I thank my fellow labmates and friends: Pisitpol Chirapongsananurak, Swagata Das, David Jonsson, Min Lwin, Kyungwoo Min, Tuan Ngo, and Ben Stevens for stimulating discussions and useful feedbacks, and for their friendly support. I am also grateful to my friends: Swagata Bhattacharjee, Debarati Kundu, Avik Ray, Aparajita Sant, Virag Shah, and Gurtej Singh as they were my family away from home. Thanks for being a respite from the demanding graduate student life and in helping me create wonderful memories.

I would also like to acknowledge my fiancé, Abhishek Sharma, for stirring my interest in research and higher studies. He has always been the most honest critic of my work, thus, helping me keep an objective outlook towards my progress. I am thankful for his encouragement in every aspect of my professional life. Thanks for being an awesome friend, guide, and mentor. This task would have been much more difficult without your support.

I thank my family: my parents, siblings, and grandparents for their support in my life. I am forever grateful to my mother, Dr. Usha Dubey, for her support and encouragement. Had it not been for her sacrifices, I would not be able to pursue my dreams. She taught me to take any challenge in life head-on and never be defeated by circumstances. Also, I am thankful to

my Nana, Mr. Heeralal Mishra, for his unwavering faith in me and his help in every aspect of my life. I am fortunate to have such a loving family and the most awesome siblings. I would also like to acknowledge my father whose loving memories have always been my strength. Lastly, I am grateful for the good grace of the almighty on me and my family.

Distributed Resource Integration Analysis and Network Design of Electric Power Distribution Systems

Anamika Dubey, Ph.D.

The University of Texas at Austin, 2015

Supervisor: Surya Santoso

The integration of high percentages of distributed energy resources and controllable loads into the distribution system coupled with the strict power quality and service reliability requirements at the power distribution level are necessitating a significant change in the planning, operation and control of the traditional power distribution system. The future power distribution circuits should be able to accommodate the new technologies while simultaneously providing a desired level of power quality and service reliability to the customers. This thesis aims to address the current and future grid requirements of both existing as well as new distribution systems with regard to power quality and service reliability issues. Several methods are proposed to evaluate and mitigate power quality and service reliability concerns due to the integration of smart grid technologies into both existing and new distribution circuits. Notably, for the existing distribution circuits, integration studies are simulated to analyze and mitigate the impacts of electric vehicle loads and photovoltaic generation on the distribution voltages. Furthermore, the problem of siting,

sizing and deployment of distributed energy storage systems in meeting distribution planning requirements with regard to integrating distributed generation and providing contingency requirements is also addressed. A new distribution system both grid-connected and operating in islanded mode, however, could be designed to the new requirements. The new distribution circuit could be designed to meet the power quality and service reliability standards directly, thus more efficiently mitigating the concerns. In the thesis, the new distribution circuit design is approached from the perspective of maximizing the service reliability. For the new distribution circuit, approaches to reliability based distribution circuit design are proposed.

Table of Contents

Acknowledgments	v
Abstract	viii
List of Tables	xix
List of Figures	xxi
Chapter 1. Introduction	1
1.1 Existing Distribution Circuits	3
1.1.1 Electric Vehicle Loads	3
1.1.2 Photovoltaic Generation (PV)	5
1.1.3 Distributed Energy Storage Systems	6
1.2 New Distribution Circuits	7
1.2.1 Primary Distribution System	8
1.2.2 Zonal Distribution System	9
1.3 Contributions	10
Chapter 2. Integrating Distributed Resources to Existing Dis- tribution Systems	12
2.1 Distribution Planning	13
2.1.1 Existing Planning Framework	14
2.1.2 Including Distributed Resources to the Planning Framework	16
2.2 Proposed Analysis Framework	18
2.2.1 Distribution Circuit Model	19
2.2.2 Methodology to Evaluate Impacts	20
2.2.3 Approaches to Mitigate Impacts	20
2.3 Analysis Tools	21
2.3.1 Distribution Circuit Simulator	21

2.3.1.1	CYMDIST	22
2.3.1.2	OpenDSS	22
2.3.2	Required Characteristics of the Analysis Tools	23
2.3.2.1	Power Flow	24
2.3.2.2	Fault Study	25
2.3.2.3	Control Study	26
2.3.2.4	Electric Vehicle (EV) Model	27
2.3.2.5	Photovoltaic (PV) System Model	28
2.3.2.6	Energy Storage (ES) System Model	29
2.4	Feeder Circuit Data	30
2.4.1	Circuit Data	31
2.4.1.1	Source Object	31
2.4.1.2	Substation Transformers	32
2.4.1.3	Distribution Lines	32
2.4.1.4	Distribution Service Transformers	33
2.4.1.5	Capacitor Banks	33
2.4.2	Load Data	33
2.4.2.1	Hourly Metered Loading Data at the Substation	34
2.4.2.2	Customer Loads	35
2.4.3	Distributed Energy Resource (DER) Data	35
2.4.3.1	Electric Vehicles (EV)	36
2.4.3.2	Photovoltaic System (PV) Data	36
2.4.3.3	Energy Storage (ES) Data	37

Chapter 3. Electric Vehicles - Modeling, Impacts, and Mitigation 38

3.1	Analysis Approach	40
3.2	Electric Vehicle Charging Technology	42
3.2.1	Background of Electric Vehicle Technologies	43
3.2.2	Electric Vehicle Charging Standards	43
3.2.3	EV Charging - North American (NA) Distribution Circuit	44
3.2.3.1	EV Charging Modes	45
3.2.3.2	Grid Requirements and Restrictions in NA	45

3.3	Modeling EV Charger	46
3.3.1	Literature Review	47
3.3.2	EV Charger Circuit	48
3.3.2.1	Power Processing Unit	49
3.3.2.2	Battery Management Unit	49
3.3.3	Generic Time-Domain EV Load Model	50
3.3.4	Average Value Model for the Electric Vehicle (EV) Loads	52
3.3.4.1	Rectifier Block - AVM Model Derivation	53
3.3.4.2	During Commutation	56
3.3.4.3	After Commutation	56
3.3.4.4	Boost-Converter - Analytical Model	58
3.3.5	Constant-power EV Load Model	59
3.3.6	Application and Validation of the EV load AVM model	62
3.3.6.1	Case 1 - Validation and Comparison of the proposed AVM Model	63
3.3.6.2	Case 2 - Validation against the Actual Measurements	64
3.3.6.3	Case 3 - Application to the Distribution Feeder	66
3.3.6.4	Case 4 - Evaluation of Voltage Drop in the Secondary Circuit due to EV Load Charging	68
3.4	Evaluating and Mitigating the Distribution System Impacts of EV Charging - A Literature Review	69
3.4.1	Impacts of EV Charging on Distribution System	70
3.4.1.1	EV Load Impacts on Electricity Generation Adequacy	71
3.4.1.2	EV Load Impacts on Transformer Aging	72
3.4.1.3	EV Load Impacts on Distribution Power Quality	73
3.4.2	Time-of-Use (TOU) Pricing to Mitigate EV Load Impacts	75
3.4.3	Smart Charging Algorithms to Mitigate EV Load Impacts	76
3.4.3.1	Controlled EV Charging - Maximize Utility Benefits	77
3.4.3.2	Controlled EV Charging - Maximize Customer Benefits	79
3.5	Evaluation of the Impacts of EV Charging on Utility Distribution System	80

3.5.1	Preparing the Distribution Circuit	81
3.5.2	EV Load Impacts at Local Circuit Level	83
3.5.3	EV Charging Impacts at Global Circuit Level	85
3.6	Infrastructural Upgrades to Mitigate EV Load Impacts	87
3.6.1	Increasing Size of the Service Transformer	88
3.6.2	Reconfiguring the Secondary Circuit by adding an Additional Service Transformer	88
3.7	Time-of-Use (TOU) Pricing to Mitigate EV Load Impacts	91
3.7.1	Simulated Charging Scenarios	92
3.7.2	Results and Discussions	95
3.7.3	Optimal Time to begin Off-peak rates in a TOU Scheme	97
3.8	Smart Charging Algorithm	100
3.8.1	Problem Formulation	101
3.8.2	Proposed Methodology	103
3.8.3	Evaluation of the Proposed Charging Scheme	106
3.8.3.1	Impact on Voltage Variability during EV Charging	107
3.8.3.2	Increasing Accommodation Limit with the Proposed Charging Scheme	109
3.9	Conclusion	115

Chapter 4. Integrating Photovoltaic Generation - Impacts and Mitigation 119

4.1	Potential Impacts of PV Integration	121
4.1.1	Voltage Related Issues	121
4.1.1.1	Overvoltage	122
4.1.1.2	Voltage Deviation	123
4.1.1.3	Voltage unbalance	123
4.1.2	Current Related Problems	124
4.1.3	Overcurrent Protection Related Problems	125
4.1.3.1	Sympathetic tripping of relays	126
4.1.3.2	Breaker reduction of reach/Breaker insensitivity	126
4.2	PV Hosting Capacity Problem	127
4.2.1	Definitions	127

4.2.1.1	Customer Penetration Level (C_{pen}^i)	128
4.2.1.2	PV Penetration Level (PV_{pen}^i)	128
4.2.1.3	PV Deployment Scenarios (x_j^i)	128
4.2.2	PV Hosting Capacity - Problem Formulation	128
4.2.3	Monte Carlo Based Method for PV Hosting Problem	130
4.2.3.1	First-hosting Capacity ($H_{1,k}$)	130
4.2.3.2	All-hosting capacity ($H_{100,k}$)	130
4.2.4	Additional Factors Affecting PV Integration Limits	131
4.2.4.1	Effect of the Minimum Load Condition	131
4.2.4.2	Hourly Variations in Circuit Load and PV Generation	132
4.3	Hourly Stochastic Analysis Framework	134
4.3.1	Identify Hourly Effective Minimum Load	134
4.3.1.1	Hourly Minimum Load (Min_{load}^{hr})	136
4.3.1.2	Hourly Existing PV Generation ($PV_{existing}^{hr}$)	136
4.3.1.3	Hourly Effective Minimum Load (Eff_{load}^{hr})	137
4.3.2	PV Deployment Scenarios	137
4.3.3	Hourly PV Impact Analysis	138
4.3.4	Determine PV Hosting Capacity	140
4.4	Accuracy Assessment Framework	140
4.4.1	Impact of Multiple k -run MCS on Hosting Capacity	141
4.4.2	Hosting Capacity Probabilistic Intervals	142
4.4.3	Percentage Accuracy of the Monte Carlo Simulation	143
4.4.3.1	First-hosting Capacity Percentage Accuracy, $Acc_k^\epsilon(H_1)$	144
4.4.3.2	All-hosting Capacity Percentage Accuracy, $Acc_k^\epsilon(H_{100})$	144
4.5	Results and Discussions	145
4.5.1	Characterizing Distribution Circuit	145
4.5.2	PV Hosting Capacity using the Proposed Framework	148
4.5.3	Accuracy of Hosting Capacity Results	151
4.5.4	Impacts of the Number of Monte Carlo Runs	151
4.6	Discussion on Impacts of PV on Bus Overvoltages	153

4.6.1	PV Hosting Capacities for Overvoltage Condition	154
4.6.2	Bus Locations observing Overvoltages	155
4.6.3	Effects of Minimum Load on PV Hosting Capacity . . .	156
4.6.4	Effects of PV Locations on Hosting Capacity	158
4.7	Mitigating Overvoltage Concerns using Smart Inverters	159
4.7.1	Fixed Power Factor Control	160
4.7.2	Volt-Var Control	161
4.7.3	Volt-Watt Control	162
4.7.4	Results	162
4.8	Conclusion	164

Chapter 5. Grid Impacts and Benefits of Deploying Distributed Energy Storage Systems 167

5.1	Operational Uses of Deploying Distributed Energy Storage Systems	169
5.1.1	System-Level Benefits	169
5.1.2	Customer-Level Benefits	171
5.1.3	Energy Storage Deployment	171
	5.1.3.1 Substation-level Deployment	172
	5.1.3.2 Feeder-level Deployment	173
5.2	Distributed Energy Storage Analysis - Proposed Framework	173
5.2.1	Define Application Scenarios	174
5.2.2	Identify Starting Point for ES Analysis	174
5.2.3	Determine ES Size	175
5.2.4	Identify ES Locations	175
5.2.5	Conduct Grid Impact Analysis	176
5.3	Application 1 - Energy storage to meet N-1 Contingency . . .	176
5.3.1	Selected Distribution Circuit	177
5.3.2	Identify Starting Point for ES Analysis	179
5.3.3	Determine Energy Storage Size	180
	5.3.3.1 Percentile Analysis	181
	5.3.3.2 Energy Storage Power System Rating	181

5.3.3.3	Energy Storage Energy System Rating	183
5.3.4	Determine Energy Storage Location	184
5.3.5	Conduct Grid Impact Analysis	184
5.4	Application 2 - Energy Storage to Increase PV Hosting Capacity	186
5.4.1	Selected Distribution Circuit	187
5.4.1.1	Feeder's PV Hosting Capacity	187
5.4.1.2	Assumptions for ES Deployment	189
5.4.2	Energy Storage Size	190
5.4.2.1	Energy Storage Power Subsystem Rating	190
5.4.2.2	Energy Storage Energy Subsystem Rating	191
5.4.3	Energy Storage Location	191
5.4.4	Grid Impact Analysis	191
5.5	Application 3 - Energy Storage to Mitigate PV Variability	192
5.5.1	PV Variability	193
5.5.1.1	Mathematical Analysis of Voltage regulation Concern	194
5.5.1.2	Energy Storage to mitigate Voltage Regulation Concern	196
5.5.2	Selected Distribution Feeder and Assumptions	197
5.5.3	Energy Storage Size	199
5.5.4	Energy Storage Location	200
5.5.5	Energy Storage Control	200
5.5.6	Grid Impact Analysis	201
5.6	Conclusion	205
 Chapter 6. Designing New Distribution Circuits		207
6.1	Shipboard Power Distribution System	208
6.1.1	Primary Distribution System	209
6.1.2	Zonal/Secondary Distribution System	210
6.2	Shipboard Power System Reliability Analysis - A Literature Review	211
6.2.1	Quantify Distribution System Reliability	212
6.2.2	Comparing Distribution System Topologies	214

6.2.3	Optimal Equipment Placement	215
6.3	Proposed Approach to designing Distribution Systems for Improved Reliability	217
6.3.1	Three-dimensional Shipboard Power System Design . . .	218
6.3.1.1	Designing Three-dimensional Topologies	219
6.3.1.2	Reliability Concepts	220
6.3.1.3	Reliability Calculation Method	221
6.3.2	Resilient Distribution Circuit Design	222
6.3.2.1	Network Availability	224
6.3.2.2	Optimal Topology Design Problem	224
6.3.2.3	Proposed Algorithm - Successive Minpath Generation	225

**Chapter 7. Three-dimensional Shipboard Power System Design
227**

7.1	Reliability Calculation	229
7.1.1	Component Reliability Indices	230
7.1.2	System Reliability Indices	231
7.1.2.1	First-Order Interruption Scenarios	232
7.1.2.2	Second-Order Interruption Scenarios	234
7.1.2.3	Second-Order Interruption Scenarios Involving Stuck Break	236
7.1.2.4	System Reliability Indices using Markov Model	236
7.2	Planar Shipboard Power System Topologies	238
7.2.1	Ring Bus	239
7.2.2	Breaker-and-a-Half	239
7.3	Three-Dimensional Shipboard Power System Topologies	241
7.3.1	Three-Dimensional Ring Bus Topologies	244
7.3.2	Three-Dimensional Breaker-and-a-Half Topologies	245
7.4	Results and Discussions	245
7.4.1	Reliability Indices	250
7.4.2	Component Count Comparison	252
7.5	Conclusion	252

Chapter 8. Resilient Distribution Circuit Topology Design	254
8.1 Scope of the Work	257
8.2 Network Availability - Definitions	259
8.2.1 Probabilistic Graph and Network Topology	259
8.2.2 Network Availability	260
8.3 Resilient Network Topology Design	261
8.3.1 Problem Formulation	262
8.3.2 Complexity of the Topology Design Problem	263
8.3.3 Theoretical Discussion	263
8.4 Proposed Algorithm : Successive Minpath Generation	266
8.4.1 Initial Topology Design	267
8.4.2 Availability Calculation	268
8.4.3 Edge Selection and Addition	270
8.5 Results and Discussion	271
8.5.1 Comparison of Existing Circuit Topologies	272
8.5.2 Designed Resilient Circuit Topology	273
8.5.3 Designed Resilient Circuit Topology with Multiple Sources	277
8.6 Conclusion	278
 Chapter 9. Conclusion	 280
 Bibliography	 285
 Vita	 309

List of Tables

3.1	EV Charging Levels and Charger Specifications (NA Standards)	45
3.2	Level-1 (120V/12A) EV Charger Circuit Parameters	50
3.3	Summary of effects of EV charging on the primary wire (the selected secondary circuit has EV loads equivalent to 50-100% of residential loads)	83
3.4	Summary of effects of various factors evaluated on the secondary circuit supplied by a single-phase service transformer (One EV load)	84
3.5	Effects of increasing EV penetration on the primary wire voltages	86
3.6	Effects of EV load clustering on the primary wire voltages . .	86
3.7	Effects of reconfiguring the secondary service using an additional service transformer	91
3.8	Various charging scenarios simulated for both 24-kWh and 16-kWh EV battery loads charged using a 240V/16A EV charger	94
3.9	Characteristic of secondary circuit for unscheduled starting time	96
3.10	Characteristic of secondary circuit for unscheduled starting time	97
3.11	Minimum Feeder Voltages Recorded due to EV Load Charging (pu)	109
3.12	Comparison of three charging methods for each EV penetration level	118
4.1	PV Hosting Results	149
4.2	PV Hosting Results	163
5.1	Percentile values for the required ES capacity based on load demand for years 2013-2017 and using a 3% load growth . . .	184
5.2	Energy served above transformer rating for Years 2013-2017 .	186
5.3	PV Hosting Results	192
6.1	Equipment Configuration Reliability Index Comparison	217
7.1	Component Failure Reliability Indices	231

7.2	System Reliability Indices - Ring Bus Topology	251
7.3	Overall Interruption Rates	251
7.4	System Topology Component Count Comparison	253
8.1	Comparison of different distribution circuit topologies	273
8.2	Comparison of different distribution circuit topologies	275

List of Figures

2.1	Simplified block diagram of battery charging system.	27
2.2	Simplified block Diagram of the PV system model and its control interface. [1]	28
2.3	PV system model in OpenDSS. [1]	29
2.4	ES system model in OpenDSS. [1]	30
3.1	The structure of the North American power distribution system.	44
3.2	The structure of the North American power distribution system.	45
3.3	Simplified block diagram of battery charging system.	48
3.4	Time-domain model for a Level-1 (120V/12A) EV battery charger	50
3.5	Block diagram of PWM control of PFC boost converter	51
3.6	Block diagram of PWM control of DC-DC converter	51
3.7	Reduced-order time-domain model for a Level-1 (120V/12A) EV battery charger	52
3.8	Equivalent time-domain model for the generic EV battery charger	53
3.9	a) Two-switch conduction configuration, b) Four-switch conduction configuration	55
3.10	Piece-wise representation of the RMS AC current (i'_{ac})	55
3.11	Boost converter - power factor correction stage	59
3.12	One-line diagram of the charging facility	60
3.13	Power demand measured at the secondary service	61
3.14	Daily load shape profiles for an 8 kWh EV load (charger efficiency is 90%)	61
3.15	An example EV load shape profile of a 16 kWh EV load being charged by a Level-2 charger (240V/16A-3.84kW)	62
3.16	Current and voltage waveforms for the EV charger models: (a) output DC voltage (V_{load}); (b) DC current (i_{dc}) waveform; (c) supply side AC current (i'_{ac}) waveform	65
3.17	One-line diagram of the secondary circuit under evaluation	66
3.18	Supply side AC current (i_{ac}) waveform	66

3.19	(a) Distribution feeder model under evaluation; (b) Switching model for a Level-2 (240V/16A) EV charger	67
3.20	Current and voltage waveforms for the EV charger with PWM control: (a) output DC load voltage (V_{load}) for an EV charger; (b) rectified DC current (i_{dc}) waveform for an EV charger; (c) AC current (i_{ac}) waveform measured at the transformer secondary	69
3.21	One-line diagram of the distribution feeder model (Application of the EV load AVM model)	70
3.22	Voltage waveforms (v_{load}) at the load node with and without EV load using the: (a) switching model; (b) AVM model . . .	71
3.23	One line diagram of the residential distribution circuit (Courtesy of the electric utilities).	82
3.24	Largest additional voltage drop recorded in secondary circuits populated with four EVs with respect to the size of the service transformer	89
3.25	Secondary circuit selected for the analysis (Courtesy of the electric utilities).	90
3.26	Secondary circuit selected for the analysis (Courtesy of the electric utilities).	91
3.27	Probability Density Function for EV charger starting time (unscheduled starting time)	94
3.28	Probability Density Function for EV charger starting time (randomized starting time)	95
3.29	Load shape profiles with off-peak rates beginning at 11 pm and 12 am (24-kWh EVs)	99
3.30	Voltage profiles with off-peak rates beginning at 11 pm and 12 am (24-kWh EVs)	99
3.31	One line diagram for the 120V/240V secondary distribution circuit (Courtesy of the electric utilities).	107
3.32	Voltage profile at the EV load location for each charging method.	108
3.33	Daily load demand profile at the service transformer for each charging method.	109
3.34	EV accommodation capacity for uncontrolled charging case. .	111
3.35	EV accommodation capacity, when EV loads are charging under optimal TOU schedule (off-peak rates beginning at 12 am). .	112
3.36	Percentage of secondary customers reporting under-voltage violation for uncontrolled charging and charging under TOU schedule.	113

3.37	Load demand profile at the substation transformer at 100% EV penetration for each charging method.	114
4.1	Overvoltage scenario.	122
4.2	Voltage deviation scenario.	123
4.3	Voltage deviation scenario.	124
4.4	Reverse power flow scenario.	125
4.5	Sympathetic tripping in case of three-phase fault.	126
4.6	Effects of minimum load on voltage rise due to PV.	132
4.7	Duration of daily daytime minimum load recorded over a year.	133
4.8	Typical per-unit PV generation profile on a clear sunny day.	133
4.9	Proposed hourly stochastic analysis framework for determining circuit's PV hosting capacity.	135
4.10	5 th percentile minimum load corresponding to hour = 12.	136
4.11	The stochastic analysis framework - Generate PV Deployment Scenarios	138
4.12	The stochastic analysis framework - Identify PV Size	139
4.13	First-hosting capacity using multiple <i>k-run</i> MCS, where $k = 100$	142
4.14	Probabilistic interval for first-hosting capacity.	143
4.15	Largest voltages recorded for 50% hosting capacity interval ($h_{1,k}^{50}$).	144
4.16	One-line diagram of the selected distribution feeder (Courtesy of the electric utilities).	146
4.17	Hourly effective load calculated for the selected feeder.	147
4.18	Obtaining a statistically representative minimum load condition.	148
4.19	Hourly PV hosting capacities obtained using proposed framework.	149
4.20	Maximum voltages recorded for each PV deployment scenario corresponding to hour 12.	150
4.21	Probability of observing an overvoltage corresponding to 10% to 99% probabilistic interval for first-hosting capacity.	152
4.22	Probability of observing an overvoltage corresponding to 10% to 99% probabilistic interval for all-hosting capacity.	152
4.23	Hosting capacity percentage accuracy vs. tolerance parameter.	153
4.24	Hosting capacity percentage accuracy vs. the number of Monte Carlo runs.	154

4.25	PV locations and sizes corresponding to PV deployment scenario for the first overvoltage violation (Courtesy of the electric utilities).	155
4.26	Heat plot for primary bus voltages corresponding to the first overvoltage violation scenario.	156
4.27	Number of primary buses observing overvoltage during the minimum load condition for each PV deployment scenario.	157
4.28	Hosting capacity vs. Minimum load.	157
4.29	PV hosting results for each selected PV deployment locations .	158
4.30	Impact of PV deployment location on PV hosting capacity. . .	159
4.31	Volt-Var Curve followed by smart inverters to control the VAR output of the PVs.	161
4.32	Volt Watt Curve followed by smart inverters to control the active power output of the PVs.	163
4.33	PV hosting capacity with smart inverter control.	164
5.1	Operational uses of energy storage systems [115].	170
5.2	One-line Diagram of the Distribution Circuit Selected for Analysis (Courtesy of the electric utilities).	177
5.3	Simulated N-1 Contingency Case (Courtesy of the electric utilities).	178
5.4	Yearly load shape profile measured at the Node A (Year 2013). .	179
5.5	Percentile plot of ES size based on overload recorded for Years 2013-2017.	182
5.6	Percentile plot of the energy served above transformer rating for Year 2013-2017.	183
5.7	Potential Locations for Energy Storage Deployment to meet N-1 contingency requirement (Courtesy of the electric utilities). . .	185
5.8	Application of energy storage is the substation mitigating transformer overloading during an N-1 contingency scenario.	186
5.9	One-line diagram of the selected distribution feeder (Courtesy of the electric utilities).	188
5.10	PV hosting capacity for overvoltage concern (Additional + Existing PV generation).	190
5.11	A typical PV generation profile with cloud transients.	193
5.12	A simplified one-line diagram of the distribution feeder connected to PV.	194

5.13	Change in voltage.	195
5.14	Mitigating PV voltage variation concern using ES.	196
5.15	One-line diagram of the selected distribution feeder with existing PV locations and generation capacities (Courtesy of the electric utilities).	198
5.16	Energy Storage Locations (Courtesy of the electric utilities).	201
5.17	Voltage profiles (with and without energy storage), with energy storage located at FeederEnd1 (Courtesy of the electric utilities).	202
5.18	Largest voltage variation measured at PV bus 2 for different ES locations (Courtesy of the electric utilities).	203
5.19	a) PV irradiance profile with high variability, b) Existing PV generation at the selected feeders from 12:00 pm to 1:00 pm using the high variability PV profile.	204
5.20	Voltage profiles (with and without energy storage) at; a) substation, b) FeederEnd1, c) PVBUS1, d) PVBUS2.	205
6.1	A shipboard distribution system in BAAH topology.	209
6.2	Comparison of (a) ring bus; (b) breaker-and-a-half; and (c) double breaker, double bus topologies.	210
6.3	A zonal electric distribution (ZED) system in grid topology.	211
6.4	Equipment interruption rates for ring bus, BAAH, and DBDB topologies. For Radar and Zonal loads, the number of interruptions per year for BAAH topology are very small (not visible on the graph).	214
6.5	Optimal equipment placement within the breaker-and-a-half topology (BAAH).	216
6.6	Flowchart for the proposed optimal topology design algorithm	225
7.1	Markov model of a first-order interruption scenario.	233
7.2	Markov model of a second-order interruption scenario.	235
7.3	Markov model of a second-order interruption scenario.	237
7.4	A shipboard distribution system with ring bus topology.	240
7.5	A shipboard distribution system with breaker-and-a-half topology (version one) - BAAHv1.	241
7.6	A shipboard distribution system with breaker-and-a-half topology (version two) - BAAHv2.	242
7.7	Designed three-dimensional SPS topology - 3D topology 1.	243

7.8	Designed three-dimensional SPS topology 2 - 3D topology 2. .	244
7.9	Three-dimensional ring bus topology by connecting upper and lower decks of the ship.	246
7.10	Three-dimensional ring bus topology by connecting upper and lower decks of the ship.	247
7.11	Three-dimensional BAAHv2 topology by connecting upper and lower decks of the ship.	248
7.12	Three-dimensional BAAHv2 topology by connecting upper and lower decks of the ship.	249
7.13	Comparing overall interruption rates.	252
8.1	Defining operational and failed networks for a distribution circuit. A network is identified as operational if and only if there is a path from the supply node to each load node. The network fails if any one of the load nodes are disconnected from the supply node.	261
8.2	Initial topology design- spanning tree.	268
8.3	Distribution circuit topologies, a) Radial b) Loop and c) Grid.	272
8.4	Resilient distribution circuit topology with, a) $A(G) > 0.98$ b) $A(G) > 0.99$ c) $A(G) > 0.995$	275
8.5	Resilient distribution circuit topologies designed for the 30-node system.	276
8.6	A distribution circuit supplied by multiple power sources and the pseudo source node added to solve the resilient circuit design problem.	277
8.7	Resilient distribution circuit topologies for the distribution circuits supplied by two power sources.	279

Chapter 1

Introduction

The utility distribution systems are designed to deliver reliable electric power economically to the electrical consumers at their place of consumption. Distribution system planning is essential to provide a cost-effective, reliable, and quality power supply. A distribution planning problem can be modeled to satisfy multiple design requirements including the ability to efficiently serve the load demand, minimize feeder losses, adaptability to change in the supply and demand, service continuity during outage, etc. An optimization problem satisfying all design constraints could be complicated. To simplify the problem, the distribution circuit requirements are prioritized, and the planning is done by solving multiple smaller optimization problems. Traditionally the distribution system is planned for the lowest cost that can provide the power supply reliably to the connected loads. The reliability of the circuit operation and quality of the service are ensured by installing the equipment systems on top of the earlier designed distribution circuit. Thus, to date the traditional distribution planning algorithms do not include power quality and grid reliability directly into the distribution circuit design problem.

However, over the last decade, the electric power grid has been transforming in an unprecedented way, necessitating a significant change in the way we design, operate, and control the traditional power systems. Starting with the high penetration of distributed generation, the integration of electric vehicle

technology, bi-directional power flow, and smart metering the energy sector is going through vast and rapid technical and policy related transformations. The inherent variability of renewable generation and the vulnerability of traditional power systems to the demand and generation stochasticity can potentially result in grid-related problems, thus necessitating it to include the impacts of new technologies into the distribution planning framework. Additionally, in recent years, with the increased dependence on electric power systems and the increased complexity of the distribution circuits, ensuring a higher level of reliability is becoming increasingly important. Particularly, in the case of microgrids operating independent of the grid, for example, an all-electric ship, where service continuity is crucial, the distribution planning problem should be approached from the perspective of improving the service reliability.

This dissertation aims to address the current and future grid requirements of both existing as well as new distribution systems with regard to power quality and service reliability issues. Several methods are proposed to evaluate and mitigate the power quality and service reliability concerns due to the integration of smart grid technologies into both existing and new distribution circuits. Since redesigning an existing distribution circuit is both uneconomical and impractical, methods are proposed to evaluate the impacts and to mitigate the concerns of integrating smart grid technologies into the existing distribution systems. A new distribution system both grid-connected and operating in islanded mode, however, could be designed to meet the power quality and service reliability standards directly, thus, more efficiently mitigating the concerns. In the thesis, the new distribution circuit design is approached from the perspective of maximizing the service reliability. Therefore, for the cases where a new distribution system can be economically implemented, approaches

to reliability based distribution circuit design problem are proposed.

In sum, the objectives of this work are to 1) evaluate existing utility distribution circuit for voltage and power quality issues and suggest control schemes to mitigate power quality concerns, and 2) design a reliable distribution circuit topology for a new distribution system such as an electric ship power system.

1.1 Existing Distribution Circuits

The general objectives regarding the existing distribution system are: 1) to develop methods for evaluating the effects of smart grid technologies on distribution circuit power quality, and 2) to propose mitigation schemes for enabling the integration while maintaining the desired levels of power quality. First, the effects of smart grid technologies such as electric vehicles (EVs), photovoltaic systems (PVs), and distributed energy storage (ES) systems on the circuit's power quality are evaluated. Once the power quality concerns are understood, suitable control schemes to mitigate the effects and to improve the distribution circuit power quality are proposed. The detailed objective and approach for the analysis is discussed here.

1.1.1 Electric Vehicle Loads

This work evaluates the impacts of integrating EV loads on utility distribution circuits and presents their solutions. The aim is to understand, identify, and mitigate EV charging effects on a residential distribution circuit. The analysis begins with evaluating the effects of EV charging on both primary and secondary services voltages. A three-phase model is simulated for the distribution circuit under evaluation. The representative models for EV charger and EV battery collectively termed EV load are developed using dif-

ferent modeling techniques. Three different EV load models are developed: a time-domain model, an average-value model [2, 3], and a constant-power model. Note that each model is suited for a specific type of impact analysis. Several circuit parameters affecting the distribution circuit voltage quality are identified, and their effects on the distribution circuit are evaluated. To evaluate the impacts, several EV deployment scenarios are simulated, and the load flow analysis is executed for a day in a 15 min interval, termed daily load flow solution. The results of daily load flow solutions with and without EV loads are compared. The proposed impact analysis approach identifies several factors such as EV load location, size, distribution, and percentage penetration affecting primary and secondary distribution voltage quality while EV loads are charging [4–7]. The study concludes that EV load charging may increase the peak load demand potentially overloading service transformers and may result in unnecessary voltage drops in the secondary service voltages.

Given the impacts of EV charging on transformer loading and service voltage quality, the study presents the following infrastructural upgrades to mitigate EV load concerns: increasing the size of service transformer, and reconfiguring the distribution circuit using an additional service transformer. Since, infrastructural upgrades require significant efforts and cost, to mitigate EV load concerns we present both indirect and direct control algorithms for EV charging. The impact of indirectly controlling EV charging using TOU pricing is discussed first, followed by the proposed approach to identify an optimal time to begin off-peak rates in a TOU pricing scenario while avoiding EV customer inconvenience [8]. It is observed that the simultaneous charging of EV loads during off-peak hours under a TOU schedule may result in a second peak in the load demand. To address this concern a smart charging algorithm

directly controlling EV charging rate and time while aiming to minimize the voltage variations at each EV load node is proposed. By reducing voltage variations, the proposed algorithm optimally shifts the EV load demand to off-peak load hours, thus mitigating loading concerns as well [9].

1.1.2 Photovoltaic Generation (PV)

A high penetration of residential photovoltaic (PV) panels can potentially cause a number of operational issues on the distribution circuit. This study further evaluates the impacts of integrating large percentages of distributed photovoltaic systems (PVs) on the existing distribution circuits. First, the representative models for the distribution circuit and the PV system are developed. Depending on the existing percentages of PV penetration, PV panel efficiency, solar irradiance data, and the yearly load demand profiles of the conventional loads, the distribution circuit is evaluated for any existing voltage regulation concerns.

The increasing PV penetration and the undesirable impacts of PVs on distribution circuit necessitate the task of determining the largest PV capacity a given distribution circuit can accommodate without violating circuit's operational limits. The obtained PV capacity is referred to as the circuit's PV hosting capacity. The PV hosting capacity can be defined with respect to several impact criteria, for example, system overvoltage, thermal stress, harmonics, etc. This study presents a Monte Carlo based hourly stochastic analysis framework to determine circuit's PV hosting capacity. In the proposed approach, Monte Carlo method is used to simulate the scenarios of probable PV locations and sizes while the hourly analysis framework is used to include the daily variations in load and PV generation. A mathematical formulation

of the hosting capacity problem for bus overvoltage concerns is presented first, followed by the proposed stochastic analysis approach [10]. A thorough interpretation of PV hosting results is presented, and various factors that may affect feeder's voltage quality are identified [11]. Additionally, a method to evaluate the percentage accuracy of the hosting capacity results is proposed as well. Once voltage regulation effects are assessed, mitigation schemes to increase the PV hosting capacity of the distribution circuit are proposed. The application of smart inverters in mitigating PV impacts is investigated. Multiple control methods including active and reactive power regulation using smart inverter are implemented, and circuit's PV hosting capacity is calculated.

1.1.3 Distributed Energy Storage Systems

In recent years, the advancement of smart-grid technologies and the integration of distributed photovoltaic (PV) generation have led to an increase in distributed energy storage (ES) deployments. This calls for a standard methodology, analytics, and tools to quantitatively evaluate the effectiveness of energy storage solutions. In this thesis, a framework for the integration of ES systems including impacts analysis of integrating ES and identifying ES sizes and locations is presented. The proposed framework begins with identifying application scenarios for ES deployment. Based on the selected application scenarios, the starting point for the analysis including ES deployment type, planning duration, feeder load conditions, and existing and future PV generation are identified. The ES size both power and energy system ratings are calculated, and potential ES locations are determined. Finally, the grid impact analysis is conducted to quantify the benefits of deploying ES and in meeting the desired grid service objective.

In this study, the ES is implemented for following application scenarios: 1) meet substation N-1 contingency requirement, 2) increase feeder's PV hosting capacity, and 3) mitigate voltage variability concerns due to PV generation variability. The study details the method to size, place, and control ES for each application scenario.

1.2 New Distribution Circuits

On the contrary to existing distribution circuits, for a new distribution circuit, the study aims to design an economical and reliable distribution circuit topology. To date, the distribution circuit design problem is approached from the perspective of minimizing the circuit losses. The future distribution circuit requires a shift in the circuit design paradigm, from minimizing circuit losses to optimizing service reliability and power quality. For example, the critical loads such as weapons, communication systems, and propulsion systems of an electric ship, require a reliable and space efficient distribution circuit topology. As service reliability is becoming an increasingly important issue, the study aims to explore the design of a reliable distribution circuit topology.

The objective of this work is to investigate and develop network topologies for an all-electric shipboard power system (SPS), that will ensure quality and continuity of service as well as survivability in the event of outage or failure. For this reason, the work is based on a two-level distribution topology: the primary distribution system, and the secondary zonal electric distribution (ZED) system. These two systems interact in much the same way that primary networks and secondary circuits operate in terrestrial power distribution systems designed in a mesh topology, such as those found in urban centers. In fact, it is important to note that while the specifics of this work applies to shipboard

distribution systems, the concepts addressed can be applied to many types of small-scale distribution systems, such as substations or microgrids. In sum, the proposed framework aims to - 1) develop analytics to compare the reliability of the distribution system topologies, and 2) investigate approaches to improve the reliability and service availability of an SPS.

1.2.1 Primary Distribution System

As for the shipboard's primary distribution system, the prior work to ensure a higher level of service continuity focused on evaluating several existing topologies such as a ring bus and a breaker-and-a-half topology, and selecting the best circuit topology. It is observed that the overall systems reliability also depends upon the relative placement of loads and generation units within the system. To obtain an optimal equipment arrangement in a given SPS topology, an equipment placement algorithm based on particle swarm optimization (PSO) is developed as well in the prior work [12].

In this study, we propose to investigate the gains in reliability that can be achieved through designing three-dimensional (3D) shipboard primary distribution system topologies. Ship's planar topologies are extended into three-dimensional (3D) structures by distributing equipment loads to different planar SPS designs and connecting those using vertical tie-buses. Note that a 3D topology can be unfolded into multiple planar nets by simply disconnecting vertical tie-buses. A 3D topology adds structural robustness to the ship's primary distribution system. Since equipment loads are distributed in multiple decks of the ship, in an event of damage to one of the ship's decks, equipment loads in non-damaged decks may remain operational. Additionally, 3D topologies also result in a slight improvement in the service reliability when

compared with the respective planar configurations [13].

1.2.2 Zonal Distribution System

Generally, to ensure maximum level of service availability for zonal loads, a grid topology is deployed for the zonal electric distribution (ZED) system. However, due to the physical space constraints, designing a ZED topology with a required level of availability while using a minimum number of conductors would be more suitable. In this work, an algorithm is developed to find an resilient distribution topology that minimizes the number of conductors (or design economy) while satisfying a required service reliability measure of electric service. Here, the reliability for ZED systems is quantified in terms of network availability, which is defined as the steady-state probability of a network being in an operational state.

First, ship's ZED systems designed in several existing distribution circuit topologies including radial, loop, and grid are compared for their reliability and design economy. A novel mathematical formulation and an efficient graph theory-based algorithm to solve the topology design problem is developed [14] next. Using the algorithm, an optimal distribution circuit topology is designed while satisfying a given network availability requirement. The proposed algorithm, termed as successive minpath generation, is evaluated using 15 and 30 node ZED systems, supplied by single as well as multiple power sources. The findings confirm that the algorithm is significantly efficient in designing reliable circuit topologies. Compared to grid topology, the proposed approach results in ZED systems with network availability more than 0.99 by using 3 fewer and 12 fewer conductors for a 15-node and a 30-node ZED, respectively.

1.3 Contributions

With the advent of distributed energy resources and increased service quality and reliability standards, new methods for distribution planning and design are required for the future distribution systems. This thesis explores the control and design of distribution networks in order to address the grid requirements of both existing as well as new distribution systems. For existing distribution circuits, the impacts of integrating distributed generation and controllable loads are evaluated and their solutions are proposed. As for the new distribution systems, methods to design new distribution circuits with consideration to improved service reliability and continuity are developed.

For existing distribution circuits, first, the impacts of the EV load charging on the utility distribution circuit are evaluated. Simulation models for the distribution circuits, conventional loads, and the EV loads are developed. For an EV load, three different models were developed namely; a time-domain mode, an AVM model [2,3], and a constant-power model. Next, several factors affecting secondary circuit voltage profile due to charging of the electric vehicles (EVs) are identified and evaluated [4–7]. Several methods to mitigate EV charging impacts are investigated including infrastructural upgrades, indirect controlled charging using TOU pricing [8], and directly controlled charging using the proposed smart charging algorithm [9]. Next, the voltage regulation issues of integrating high percentages of the PV systems into the distribution circuit are evaluated. An hourly stochastic analysis framework is proposed to determine the largest PV generation capacity a feeder can accommodate [10,11]. The obtained PV capacity is termed as feeder’s PV hosting capacity. The application of smart inverter in mitigating feeder voltage regulation issues of integrating large percentages of PV systems into the grid are investigated

as well. The thesis further presents a method for integrating energy storage systems into the existing distribution circuit. The application of ES systems for the distribution circuit are evaluated using multiple application scenarios. The study evaluated the benefits of integrating ES both at substation-level and at feeder-level. For the substation-level application, the ES is deployed to meet N-1 contingency requirement for the substation transformer. As for the feeder-level applications, the use of ES in increasing feeder's PV accommodation limit and in mitigating voltage variation concerns due to PV generation variability is investigated.

The objectives for new distribution circuit are explored using an all-electric shipboard power system (SPS). Methods to design a reliable distribution circuit topology for an SPS, both at primary and zonal distribution levels are proposed. For ship's primary distribution system, the reliability gains obtained from designing a three-dimensional (3D) shipboard power system are explored. Several planar SPS topologies are extended to 3D structures by distributing loads to different levels of the ship, where each level is designed in a planar SPS configuration and different planes are connected using vertical tie-buses [12, 13]. At the zonal distribution level, a reliable network topology is developed using graph theory foundation. A successive minpath generation approach is developed and implemented to design a reliable circuit topology supplied by both single and multiple power sources [14]. Although the methods for new distribution circuit design are explored using shipboard power system, the proposed approaches are applicable for designing any new distribution circuit connected to the grid or working in an islanded mode.

Chapter 2

Integrating Distributed Resources to Existing Distribution Systems

An electric distribution system is required to supply a cost-effective, reliable, and quality power supply to the electrical consumers at their place of consumption. A distribution system planning is essential to achieve the objectives of the utility distribution system. Traditionally, the distribution systems are planned for the lowest cost that can provide the power supply reliably to the connected loads. In the past few years, with the rapid adoption of electric vehicles and distributed generation technologies, the distribution system paradigm is changing. Additionally, energy storage is receiving increasing attention by utility engineers and regulators alike for its potential to solve a wide number of technical challenges in the management of electric power. The distribution planning framework should include the impacts and solutions of integrating new technologies into the distribution system.

In this chapter, first, a short discussion on the traditional distribution planning methods followed by the requirement for integrating new technologies to the planning framework is presented. Next, the proposed approach to evaluating and mitigating the impacts of integrating variable loads and distributed generation is detailed. The method to incorporating the benefits of deploying energy storage systems into the distribution grid is also presented. Furthermore, the analysis tools required for simulating the proposed methodology and

the specifics regarding the feeder data requirement are detailed as well. For the distribution system analysis, a distribution simulator supporting detailed feeder and equipment modeling with advanced distribution system analysis capabilities is required. This study uses Open Distribution System Simulator (OpenDSS) [1], an open source distribution system simulator for the planning analysis. OpenDSS is a comprehensive simulation tool for electric utility distribution systems. The program supports all frequency domain (sinusoidal steady-state) analyses commonly performed for utility distribution systems. Additionally, it supports sequential power flows that can be simulated over successive time intervals for a specified period of time. This capability allows us to perform daily and yearly load flow studies with consideration to the variations in EV charging profiles, PV generation profiles, ES charging and discharging profiles, and daily and yearly conventional load variations.

2.1 Distribution Planning

Distribution system planning is essential to achieve the objectives of the utility distribution systems of providing economical and reliable power supply. The planning ensures that the forecasted loading figures can be met by the planned stage-by-stage deployments. Traditionally, the distribution system is planned for the lowest cost that can provide the power supply reliably to the connected loads. The primary concern has been to provide a cost-effective power supply to the customer load demand while maintaining the required reliability and voltage quality. In the past few years with the rapid adoption of electric vehicles and distributed generation technologies, the distribution system paradigm is changing. Additionally, energy storage is receiving increasing attention by utility engineers and regulators alike for its potential to solve

a wide number of technical challenges in the management of electric power. The distribution planning, therefore, need to include the impacts and benefits of incorporating distributed generation and energy storage systems into the distribution system.

2.1.1 Existing Planning Framework

Traditionally, distribution systems are designed for the lowest cost that meets the desired service reliability and demand security [15]. The planning objective is set to minimize the installation cost of the substations and feeders plus implied costs associated with maintenance and operation while satisfying several constraints related to allowable voltage regulation, reliability, and service availability, etc.

A power distribution system should be able to provide a reliable power supply economically to consumers. A few essential features of the power distribution system are as follows [15]:

1. Coverage - The supply system should be able to reach each consumer willing to purchase power covering the entire utility territory.
2. Capacity - The system should have sufficient capacity to meet the peak load demand of the consumers.
3. Reliability - The power should be delivered reliably with satisfactory continuity of the supply.
4. Voltage quality - A stable voltage should be maintained regardless of the load level and feeder conditions.

Based on the above requirements, traditionally the distribution planning is categorized in three stages: long-term planning, network planning, and construction planning. First, load forecasting models are used to determine the

location of the primary substation. The long-term planning is used to determine the most optimal network arrangements and associated investments with respect to the future developments. The substation is prepared for a long-term plan for example 10 years. Next, the planning is escalated to the network level, and the locations of service transformers and conductor configurations are determined. The network arrangement is determined based on the reliability criteria. The network level planning also includes appropriate sizing, siting and feeder layout selection. Additionally, the distribution system needs to be planned for feeder voltage control and feeder protection. Finally, the component planning stage begins which includes actual engineering and design of distribution components. The major components of the traditional distribution planning algorithms are as follows:

1. Load forecasting - The distribution planning and expansion depend upon the prospective load growth in the utility service territory. Distribution utilities directly meter their customers and have access to the extensive load database. The metered load demand and the information regarding the development projects in the locality are used to predict the potential load growth and to make planning or expansion decisions.
2. Planning for reliability - Distribution system reliability is measured in terms of customer reliability indices (SAIDI, SAIFI, CAIDI, etc.). The evaluation of reliability for a distribution system is not unique but incremental. This is because the expansion and reinforcements are done considering their impact on reliability. In fact, multiple expansion options are weighted for their reliability benefits and the one providing the best cost-benefit ratio is implemented.
3. Frequency and voltage support - To maintain voltage quality and stabil-

ity, voltage regulation equipment including capacitors and var compensators are implemented in the distribution circuit. The planning includes sizing and siting of the voltage regulation equipment depending upon the feeder and load characteristics.

4. Power system protection - Finally, the protection system including selecting the numbers and locations of reclosers and sectionalizers is designed and installed. Fuse-recloser coordination and overcurrent protection schemes are implemented as well.

2.1.2 Including Distributed Resources to the Planning Framework

In recent years, with the advancement of smart-grid technologies and the integration of distributed resources including electric vehicles technology, distributed PV generation, and energy storage units, the electric distribution system is transforming in an unprecedented way. Additionally, because of the strict requirements enforced for the quality and reliability of electric supply, the challenges for the electric distribution service providers are increasing. Distribution planning now faces complex analytical scenarios with power flow in different directions driven by generation and storage technologies connected in medium and low voltage networks. Additionally, the intermittent generation from distributed energy resources and variable and controllable loads may pose voltage, loading, and protection related concerns.

For an instance, several research articles have speculated that if charging infrastructure is not planned properly, the widespread adoption of EVs over the distribution circuit can significantly increase the substation load demand and might necessitate generation capacity expansion of the existing distribution grid. Furthermore, the increased peak load demand due to EV load charging

may overload the service transformer and result in transformer overheating. This could potentially deteriorate the transformer's life and increase the economic burden on distribution utilities. Additionally, increased EV penetration may result in sustained secondary service under-voltages, violation of the recommended under-voltage limits, and unbalance in three-phase power supply. Evidently, the growing presence of EVs on the grid necessitates including EVs to the distribution planning framework.

Similarly, it has been projected that deploying large percentages of distributed generation specifically PV systems may result in voltage, loading, and protection related concerns. Voltage issues arise due to excess PV generation resulting in bus overvoltage conditions, undesirable voltage deviations/ variations, and voltage unbalance conditions. Loading issues arise when service transformers and conductors are overloaded and thermal limits are violated. Note that loading concerns may decrease the life-span of the feeder equipment due to overheating and necessitate grid upgrades. Protection-related issues occur when protection equipment such as relays, reclosers, breakers, network protectors and fuses operate improperly. Such misoperations occur when PV interferes with the existing protection equipment. Given the impacts of PV generation on the distribution grid and the rapid adoption of the PV generation at the distribution level, a planning framework incorporating the impacts and solutions of potential PV deployments is required.

Furthermore, it is recognized by the utilities and the researchers alike that many of the challenges due to the integration of the distributed generations and variable loads can be solved using energy storage (ES) systems. This has propelled the deployment of the distributed energy storage systems in the past few years. Additionally, energy storage technology is an important potential

option for utilities, system operators, and end users to increase reliability and reduce the cost of electricity. The energy storage systems may be especially important as a flexibility asset to address the integration of variable generation resources such as wind and solar. However, the widespread use of energy storage is unlikely without the additional development of the technology and examples of its successful applications. Therefore, a planning framework while incorporating potential benefits of energy storage deployments is required.

2.2 Proposed Analysis Framework

As discussed before, with the increased penetration of distributed resources, there is the pressing need to include new technologies into the distribution planning framework. In this section, our methodology to including various distributed technologies into the distribution system analysis framework is presented. The approach is to evaluate the potential impacts of new technologies into the grid and to propose potential solutions to mitigate the impacts. The analysis requires a complete electrical model of the distribution circuit starting from the substation down to the individual customer loads including equipment models for three-phase transformers, three-phase primary, laterals, secondary networks, and service transformers. Therefore, a suitable distribution system simulator enabling detailed feeder modeling and analysis is required. This study is done using OpenDSS [1] an open-source distribution system simulator. The details regarding the requirements of the analysis tools and properties of OpenDSS are discussed in the later sections of this chapter. In addition to the detailed feeder model, a realistic impact study requires a representative load model for the secondary customer loads. In this study, the customer loads are modeled as a constant power load with an associate load

shape profile. The daily and yearly load shape profile measured at the substation meter is used to generate the customer load profiles. Next, models for the additional equipment systems added to the distribution feeder for example, EV, PV, and ES systems are developed either using the selected distribution system simulator or analytical methods. OpenDSS has in-built models for PV and ES systems. As for the EV loads, we have developed three representative models namely a time-domain model, an average value model, and a constant power model each suitable for a different impact study. Once the impacts are evaluated, methods to mitigate the concerns are accessed. The steps are detailed as follows.

2.2.1 Distribution Circuit Model

As discussed before, a detailed feeder model starting from the substation down to individual customer locations is required for implementing the proposed impact analysis framework. A detailed feeder model for actual distribution circuits under evaluation is simulated in OpenDSS. Additionally, representative models for customer loads and equipment loads are also developed using the load demand data available at the substation and customer load characteristics. In order to evaluate the impacts, representative models for the new technology to be integrated in the feeder are developed as well. OpenDSS supports equipment models for PV and ES systems. In this study representative models for EV loads are developed using MATLAB [16] and OpenDSS [1] (see Chapter 3). The feeder, load, and equipment data required for the distribution circuit modeling in OpenDSS are detailed in the later sections of this chapter.

2.2.2 Methodology to Evaluate Impacts

A framework is required to systematically evaluate the impacts of the integration of distributed resources. The proposed formulation aims to develop several representative scenarios for integrating the distributed resources into the feeder and for accessing their impacts on the feeder voltages. For example, for EV integration analysis, several factors affecting distribution voltage quality due EV load charging are identified. The analysis is done by simulating several EV deployment scenarios at the primary and secondary circuit level. Additionally, large-scale EV deployment scenarios are simulated to analyze the impacts of EV integration on overall distribution system voltage quality. As for the PV integration, the objective is to identify the maximum PV penetration that can be accommodated into a given distribution circuit without resulting in the violation of the acceptable voltage limits. Although, the proposed PV analysis method is implemented to primarily determine PV limits for overvoltage conditions, the approach is generic and can be implemented for other voltage, current, or protection related impacts as well.

2.2.3 Approaches to Mitigate Impacts

Once the impacts are understood, methods to mitigate the feeder voltage quality concerns are developed. For EV loads, first several practical methods to mitigate voltage related concerns such as increasing transformer size and reconfiguring the feeder are implemented. Next, the impact of EV charging with Time-of-use (ToU) pricing and a method to device optimal ToU schedule is presented. Finally, a controlled charging method aiming to minimize voltage variation concern in the feeder due to EV charging is implemented. As for PV integration, the use of smart inverters in increasing PV integration limit is

explored. The thesis further explores the utility of deploying ES systems in facilitating PV integration and mitigating voltage related concerns arising due to PV generation variability.

2.3 Analysis Tools

This section presents a discussion on the analysis tools required for implementing the proposed framework of distribution planning analysis. A distribution simulator is required to evaluate the impacts and benefits of including distributed resources in the traditional planning framework. The selected distribution simulator must support detailed feeder and equipment modeling with advanced distribution system analysis capabilities. First, a short discussion on a few distribution system simulators is presented. Then the required characteristics of the simulation platform including the available circuit, equipment models, and solution algorithms are discussed. For the purpose of the discussion, OpenDSS is used as an example, and the available solution interface and circuit models are elaborated.

2.3.1 Distribution Circuit Simulator

The benefits of incorporating distributed energy resources into the distribution circuit can be evaluated only by simulating potential planning scenarios on an actual detailed feeder model. The planning framework to incorporate the impacts and benefits of distributed energy resources requires a detailed feeder model. A distribution system simulator is required to simulate the detailed feeder model for the planning analysis. This study uses OpenDSS, an open source distribution system simulator. Another distribution system simulator CYMDIST [17], widely used by utilities is briefly discussed as well. The

analysis also requires an interface to conveniently simulate multiple planning objectives and potential future load and generation scenarios. In this study, we have used MATLAB [18] as the interface to OpenDSS for simulating multiple planning scenarios on the selected feeders. This section also details the characteristics and requirements of the interface required to connect the distribution system simulator to the programming environment.

2.3.1.1 CYMDIST

The CYMDIST [17] distribution analysis software is a suite of applications composed of a network editor, analysis modules, and user-customizable model libraries. The program is designed for planning studies and simulating the behavior of electrical distribution networks under different operating conditions and scenarios. It includes several built-in functions that are required for distribution network planning, operation, and analysis. The analysis functions such as load flow, short-circuit, and network optimizations can be applied to balanced or unbalanced distribution networks that are built with any combination of phases and configurations. Although CYMDIST is versatile in its application modules, a more flexible simulation platform is desired for including new technologies into the distribution planning framework. The analysis requires a simulation platform more flexible in modeling new components and in simulating multiple planning scenarios of different time-scales.

2.3.1.2 OpenDSS

The OpenDSS [1] is a comprehensive electrical system simulation tool for electric utility distribution systems. The program supports all frequency domain (sinusoidal steady-state) analyses commonly performed for utility dis-

tribution systems planning and analysis. Additionally, it supports sequential power flows that can be simulated over successive time intervals (e.g., hourly or yearly) for a specified period of time. This capability allows us to perform the daily and yearly load flow study for the distribution system with consideration to the daily variations in EV charging schedule, PV generation profile, ES charging and discharging profiles, and daily and yearly conventional load variations. One of the major benefits of OpenDSS is its extraordinary capability to support planning and analysis of distributed generation (DG) technologies. OpenDSS is able to capture both the time- and location-dependent value of DG, thus providing a valuable analysis platform for DG integration.

OpenDSS can be implemented as both a stand-alone executable program and an in-process Component Object Model (COM) server DLL designed to be driven by a variety of existing software platforms. The executable version has a basic text-based user interface on the solution engine to assist users in developing scripts and viewing solutions. The COM interface is implemented on the in-process server DLL version of the program to allow users to use the features of the program to perform new types of studies. Through the COM interface, the user is able to design and execute custom solution modes. In this study OpenDSS is executed using MATLAB program. The external execution of OpenDSS provides powerful analytical capabilities as well as excellent graphics for displaying results.

2.3.2 Required Characteristics of the Analysis Tools

Once the distribution circuit model is available, the next task is to perform power system analysis on the selected distribution feeder. The distribution system analysis tools must fully capture the static, quasi-static (time-series),

and dynamic impacts of distributed resources under a wide range of time-scales. The basic features of the required distribution system analysis tool are as follows:

1. The simulator must support power flow analysis for radial/looped networks including time-series analysis in several solution modes supporting a wide range of time-scales. The power flow algorithm must support balanced, and unbalanced load flow analysis.
2. The tool should provide the capability for transient/dynamic analysis required for evaluating the impacts of dynamic phenomenon such as flicker, the interaction of different control elements, and fault studies during islanding.
3. The simulator must provide analysis platform to include the control equipment such as shunt capacitors, voltage regulators, on-load tap changers, etc. and support typical and user-defined control algorithms.
4. Additionally, the simulator must incorporate pre-defined models or provide the flexibility to design models of the new equipment systems and their control blocks. Also, the simulator should be sufficiently flexible in incorporating control algorithm while allowing both time-dependent and location-dependent deployments of distributed energy resources.

2.3.2.1 Power Flow

The power flow study results in a detailed information about the distribution feeder for a given timestamp or a given time period (24-hour, 1-year, etc.). The analysis details the feeder losses, voltage levels, line currents, active and reactive power flows, capacitor and tap positions, etc. Depending upon the planning criteria, the power flow may need to be executed for a single time

step (snapshot), for 1 day (daily), or for 1 year (yearly). OpenDSS supports power flow simulation in several solution modes including the standard single snapshot mode, daily mode (24 hour), dutycycle mode (≥ 1 sec), Monte Carlo mode while considering the variation in the customer load with respect to the time. Additionally, the program supports detailed harmonic load flow analysis required for underspending the impacts of the new technologies on voltage and current harmonics.

2.3.2.2 Fault Study

Fault study or short-circuit analysis is yet another power system analysis algorithm required to be solved for the distribution planning. The short-circuit analysis determines the current and voltage levels for a given distribution feeder in the event of a fault. The fault study is very crucial when designing the protection system for the distribution feeder. Additionally, deploying distributed energy resources may change the fault current levels thus necessitating modifications in the existing protection architecture. Therefore, fault study is crucial to distribution planning analysis especially when PV and ES are to be integrated within the distribution planning framework.

OpenDSS supports several fault study modes including conventional fault flow, snapshot fault study, and Monte Carlo fault study. The conventional fault study mode simulates faults for all buses and reports currents and voltages on all phases for all types of faults: All-phase fault, SLG faults in each phase, LL and LLG faults. The snapshot fault mode allows the user to place one or more faults on the system at selected buses while defining the type of fault and the value of the fault resistance. In the Monte Carlo mode, the fault is applied at random locations as specified in the simulation. Monte Carlo fault

study is useful in understanding the impacts of DG integration on the existing distribution system protection scheme. For example, a Monte Carlo fault study can be used to estimate the typical voltage levels observed at a DG site for various faults on the utility system and to compute voltage sag indices.

2.3.2.3 Control Study

In a utility distribution circuit, shunt capacitors and voltage regulators are placed along the feeder for voltage support. The status of the voltage support equipment changes depending upon the load condition. For a representative simulation, the distribution simulator must support control system modeling. Particularly when distributed energy systems are deployed, the controls may vary more frequently depending upon the PV variability or ES control interface.

OpenDSS supports the modeling of standard utility distribution system control for capacitor and regulator elements. The capacitor control monitors the voltage and current at a terminal of a power delivery equipment and sends switching messages to the capacitor object. Depending upon the status of the power delivery element, the capacitor state is changed. The regulator control object emulates a standard utility voltage regulator or LTC control. In OpenDSS, control elements are modeled separately from the power-carrying elements, thus, providing significant flexibility in creating user-defined control models. The control blocks for PV systems and ES systems are also available in OpenDSS.

2.3.2.4 Electric Vehicle (EV) Model

A simple low-cost EV charger circuit is composed of single-phase rectifier with boost converter (or any other filter) as power factor correction stage followed by a DC-DC converter for insulation of battery from AC grid (see Figure 2.1). The manner in which power is delivered to batteries is also very crucial to th battery life. Hence, EV charger also includes a control circuit for battery power management. The charging circuit consists of two parts:

1. Power processing unit - This unit ensures that the AC power supplied by the grid to the battery is processed to DC supply of appropriate voltage and current levels.
2. Battery management unit - Battery management unit consists of sensors and control circuitry to monitor the charging current, voltage, and state-of charging (SOC) and accordingly control the charging status.

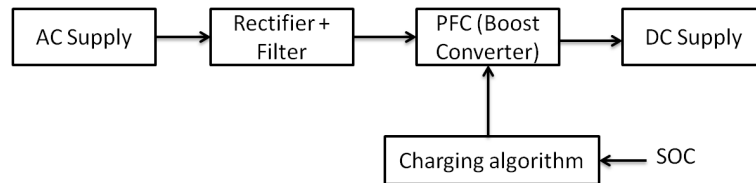


Figure 2.1: Simplified block diagram of battery charging system.

The integration analysis of EV load charging on distribution circuit requires a representative model of the EV charger and battery. In this work, three different models for EV loads are developed: time-domain model, average-value model, and constant-power model. The detailed time-domain model is developed in PSCAD and used to simulate the switching dynamics of the EV load. An average-value model capturing the average dynamics of the EV charger is developed using MATLAB. Additionally, a constant-power model

is also simulated and implemented in OpenDSS and used for the distribution feeder analysis.

2.3.2.5 Photovoltaic (PV) System Model

A simplified block diagram for the entire PV system, from solar cells to the grid is illustrated in Figure 2.2. The inverter control, which provides volt-var, volt-watt, and dynamic reactive current control modes is shown as well in the figure. A PV system consists of one or more solar cell modules or panels that take insolation from the sun (direct and indirect) and convert that into a DC signal. The DC signal is passed on to an input filter capacitor. Following the input filter capacitor, a DC to AC inverter transforms the current from the DC stage into a grid synchronized AC signal.

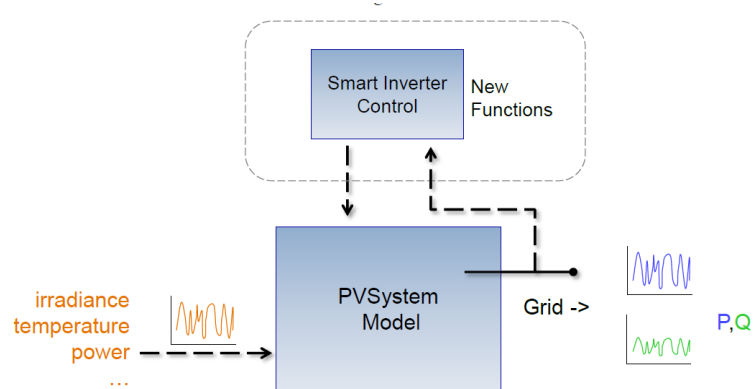


Figure 2.2: Simplified block Diagram of the PV system model and its control interface. [1]

OpenDSS provides an in-built distribution system model for PV systems capable of simulation studies in time steps greater than or equal to 1s. The model assumes the inverter is able to find the max power point (mpp) of the panel quickly. This simplifies the modeling of the individual components (PV panels and inverter). The PV system is modeled as a power delivery

object producing power, according to some generation function. In this case, the active power, P , is a function of the irradiance, temperature, and rated power at the mpp (P_{mpp}) at a selected temperature and at an irradiance of 1.0 kW/m^2 (see Figure 2.3). For PV system, reactive power is specified separately from the active power and may be specified as either fixed kvar values or a fixed power factor value.

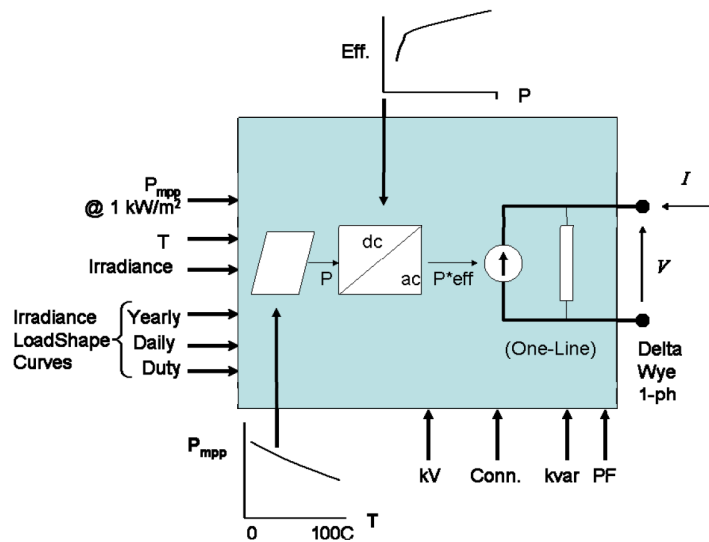


Figure 2.3: PV system model in OpenDSS. [1]

2.3.2.6 Energy Storage (ES) System Model

The storage element is essentially a generator that can be dispatched to either produce power (discharge) or consume power (charge) within its power rating and its stored energy capacity. In OpenDSS, energy storage is modeled as a generator. The storage element can also produce or absorb reactive power (vars) within the kVA rating of the inverter (see Figure 2.4). The ES model available in OpenDSS supports time-varying simulation modes includ-

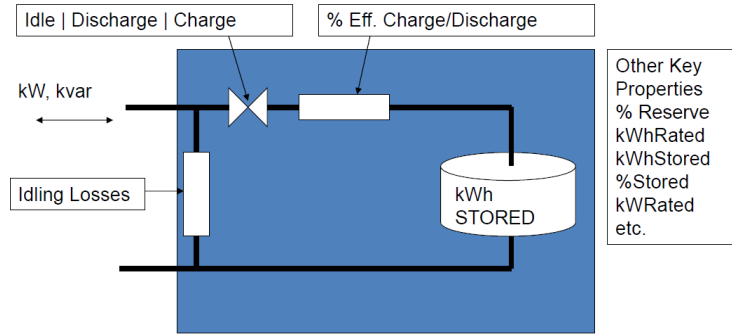


Figure 2.4: ES system model in OpenDSS. [1]

ing snapshot, daily, yearly, and duty cycle simulation study. For ES integration study, daily or yearly modes are typically required to understand the use of ES in providing for peak load management and looking at general energy issues over a period of time. As for short term power variations such as generation variability due to cloud transients affecting solar PV generation, a duty cycle mode would be required to study the effectiveness of storage. In addition to equipment model and solution interfaces, OpenDSS also provides several control models for ES systems. The control modes help in simulating the cases to demonstrate the utility of ES in providing grid benefits.

2.4 Feeder Circuit Data

A discussion on the feeder data required for the distribution system planning study with distributed energy resources is presented in this section. The feeder data requirements are categorized into three sections: circuit data, load data, and distributed energy resource (DER) data. The circuit data details the substation characteristics, circuit topology, feeder characteristics such as impedance, length, and rated nominal and emergency loadings, and locations

and types of distribution equipment including distribution transformers, regulators, capacitors, and loads. The load data information includes load characteristics including rated load demand, power factor, allocation factor, load profiles, etc. The DER data includes location, capacity, and control data corresponding to EV, PV, and ES systems.

2.4.1 Circuit Data

The planning framework proposed in this dissertation requires a detailed circuit model. A simplified electronic one-line diagram showing substation, feeders, capacitor banks, feeder regulators, and lumped load points should first be made available. Information regarding substation characteristics, distribution lines, capacitors, service transformers, and customer loads is required to simulate the actual feeder model of the given distribution feeder. In the following section, the details required for each equipment type for the proposed planning analysis are discussed.

2.4.1.1 Source Object

The source object specifies the equivalent circuit for the upstream transmission and generation system supplying for the selected distribution substation. The source object is represented as two-terminal voltage sources behind an impedance. The impedance is equal to the Thevenin equivalent of the transmission and generation system upstream from the substation transformer. The required data are as follows:

- Line-to-line voltage (kV) at the source bus,
- Short-circuit currents or MVA at the high-voltage side bus for each substation (three-phase and line-ground), or the equivalent impedance at

the high-side (transmission-side) of the substation.

2.4.1.2 Substation Transformers

The substation transformer is connected to the sub-transmission level and steps down the voltage to the distribution levels. The following details are required for modeling the substation transformer:

- Number of transformer banks at the substation,
- Transformer connections for all transformers in the substation,
- High- and low-side voltages for each transformer in the substation,
- Transformer size, X/R ratio, leakage impedance (% on substation MVA),
- Substation bus configuration and number of feeders served from each bus (i.e., which banks feed which feeders in parallel, etc.),
- Substation load tap changer (LTC) control settings or regulator settings if not LTC.,
- Characterization of the territory (rural/urban/suburban),
- Any AMR and AMI penetration along the circuit.

2.4.1.3 Distribution Lines

The distribution line details should include conductor size, type, length, construction, emergency ampacity, and the sequence impedance for each segment of circuit. Additionally, the latitude and longitude coordinates of each feeder bus should be specified to determine the topology of the feeder. Note that the conductor data could be provided in a different format as well. For example, instead of linecode data, the conductor detail could be provided in terms of line geometry and wire data. Please refer to OpenDSS manual for detail [1].

2.4.1.4 Distribution Service Transformers

Distribution transformers or service transformers connect the primary distribution lines to the secondary networks. The distribution transformer steps down the primary distribution voltages (13.2 kV) to secondary levels (120V, 240 V, 480 V). The necessary details for the simulation are the same as for the substation transformer. The required data are as follows:

- Primary and secondary buses connected to the transformer,
- Transformer MVA rating,
- High- and low-side voltages for each xfmr in the substation,
- Transformer size, X/R, leakage impedance (% on sub MVA).

2.4.1.5 Capacitor Banks

The planning analysis also requires information about the capacitor banks installed in the feeder. The required data for capacitors are as follows: bus connection, cap bank sizes, control mechanism (fixed, voltage, current, kvar, time, etc.), control settings (on/off settings, delay), and three-phase connection configurations (grounded-wye/ungrounded-wye).

2.4.2 Load Data

A detailed description of load models, loading characteristics, and metered loading data is required for the planning analysis. Note that the analysis needs to be simulated for yearly, daily, and in minutes resolution. Therefore, yearly load demand data measured at the substation meter, preferably in hourly or 15-minute resolutions, needs to be acquired. In addition to the metered load demand, information regarding the rated load demand, power factor, and load allocation factor is required for each customer load supplied by the circuit.

Additional information about the load type and load shape for each customer load, or class of load, is optional, but useful, in simulating close to real feeder operating conditions.

2.4.2.1 Hourly Metered Loading Data at the Substation

The yearly active and reactive power generation at the substation meter should be made available. The load demand data is useful in identifying feeder's typical maximum and minimum load conditions. Additionally, the peak reactive power demand is used to determine the status of the capacitor banks for the base case simulation. The capacitor banks are adjusted so that during the base case simulation the reactive power matches the peak reactive power demand.

An ideal (complete) data-set of the metered loading data would consist of the following:

- Apparent energy (MVAh),
- Real energy into and out of the load (MWh) and Absolute real energy (MWh),
- Reactive energy into and out of the load (Mvarh), Absolute Reactive Energy (Mvarh),
- Apparent Power Total (MVA),
- Real Power Total (MW),
- Reactive Power Total (Mvar),
- Per phase real and reactive power,
- Frequency,
- Line Voltages, Line Currents,
- Line Voltages THD, Line Currents THD,

- Power Factor Total, PF A, PF B, PF C,
- Displacement Power Factor Total,
- Displacement PF A, Displacement PF B, Displacement PF.

2.4.2.2 Customer Loads

As discussed before, the load data corresponding to each customer load present in the distribution feeder is required for the analysis. The following details for each customer load are required.

- Rated load demand at individual customer locations (kW, power factor, allocation factor),
- Type of customer loads (residential/commercial). Information regarding the customer class categories.
- Base load profiles for different customer load classes and subclasses. Information on base load profile characteristics for different customer classes and subclasses.
- Total loads on other circuits. If possible, the MW/Mvar without other circuits' capacitors in service (un-corrected reactive power)
- Load duration curves (15 min interval data, or minute interval) aggregate for the circuit, as well as individual customers', classes or subclasses.

2.4.3 Distributed Energy Resource (DER) Data

The objective of this work is to evaluate and mitigate the impacts of integrating modern technologies such as electric vehicles (EVs), photovoltaic systems (PVs), and distributed energy storage (ES) systems in the distribution circuit. The task includes designing circuit and equipment models, identifying simulation criteria, evaluating grid impacts of the new technologies, and

developing control strategies to mitigate the impacts and facilitate the integration. Therefore, for the analysis, the following additional data corresponding to electric vehicles, photovoltaics (PV) systems, and energy storage (ES) units are required.

2.4.3.1 Electric Vehicles (EV)

For a realistic analysis of EV load impacts, details regarding existing or expected EV penetration level for the given feeder are required. Additionally, the data regarding EV charging levels, average miles driven by EV consumers, and EV charger locations should be provided. Note that if the information regarding EV consumers is not available, potential EV charging scenarios may be simulate to evaluate the possible impacts on the given distribution circuit. The desired information regarding the EV chargers is listed below.

1. Existing or future electric vehicle penetration level,
2. Electric vehicle charging levels (Level 1, Level 2, or Level 3),
3. Existing or planned EV charger location and power levels.

2.4.3.2 Photovoltaic System (PV) Data

For the given distribution feeder the details regarding the existing PV generation system is required. This includes the location, size, and efficiency of the deployed PV panels and typical 24-hour PV generation profiles characterizing the typical PV variability for the given feeder. The following information is required for including existing PV into the distribution feeder model. Note that the details regarding the location and size of the existing PV is required while rest of the data regarding irradiance, temperature curve and PV efficiency curve are optional.

1. Existing PV locations and size along the feeder,
2. Solar Irradiance data,
3. 24-hr temp shape curve,
4. P-T curve (rated P_{mpp} vs temperature),
5. PV efficiency curve.

For realistic analysis a high resolution PV generation data is required. The PV generation profile is particularly required for the evaluation of the impacts of PV variability of distribution voltages. The data is required to understand and evaluate benefits of deploying ES for voltage management in an event of cloud transients. Typically, a PV generation data should be provided in 1 sec resolution for the entire year or longer.

2.4.3.3 Energy Storage (ES) Data

The data corresponding to the energy storage system must be prepared if the feeder is equipped with the energy storage systems. The following data list is required for modeling the energy storage unit.

1. Existing ES locations and size along the feeder,
2. Operating/control algorithms for the existing ES systems,
3. Future ES deployment penetrations and possible locations along the feeder,
4. Possible ES application/operating mode (if known),
5. Operational range, ramp rates, etc. (if known).

Chapter 3

Electric Vehicles - Modeling, Impacts, and Mitigation

The promise of clean and efficient transportation coupled with the advances in battery technologies and generous federal incentives are promoting transportation electrification and in the near future, electric vehicles (EVs) are expected to dominate the vehicle market [16, 19–21]. The success of EV technology depends on the availability and easy access of EV charging stations. Utilities are rapidly installing EV charging stations, both at residential and commercial locations. In North America, a residential EV charging station provides a 120V (Level-1) or a 240V (Level-2) voltage supply to the connected EV, either using a normal wall outlet or a dedicated charging circuit. Commercial chargers are generally high-power fast AC/DC chargers installed in heavy traffic corridors and at public charging stations. Since commercial chargers are still in the primary stages of deployment, the most common charging method used by EV owners is overnight charging using residential charging stations, primarily Level-2 chargers. The increasing number of residential EV chargers may result in several challenges for the distribution system, necessitating the system level analysis of the impacts of EV integration into the residential distribution circuits and its solutions.

The EV integration study presented in literature has primarily focused on the following issues, namely the impacts of EV loads on: electricity generation

adequacy [21–27], transformer aging [27–31], and distribution system power quality [4–7, 27–41]. A short literature review of the impacts of EV loads addressing the above issues is presented in this chapter. In short, it is speculated that if charging infrastructure is not planned properly, the widespread adoption of EVs over the distribution circuit can significantly increase the substation load demand and might necessitate generation capacity expansion of the existing distribution grid. Furthermore, the increased peak load demand due to EV load charging may overload service transformers, resulting in transformer overheating, thus deteriorating the transformer’s life and increasing the economic burden on distribution utility companies. Additionally, increased EV penetration may result in sustained secondary service undervoltage conditions, violation of undervoltage limits, and unbalance in three-phase power supply thus deteriorating the service voltage quality.

In literature, several methods to mitigate the EV impacts are proposed. The mitigation strategies are primarily grouped into two categories. In the first approach, utilities indirectly control EV charging using Time-of-Use (TOU) pricing [42–48]. The decreased off-peak electricity rates in a TOU pricing scenario motivates EV owners to charge their vehicles during off-peak hours, thereby significantly decreasing the peak load demand and mitigating transformer overloading and heating concerns. In the second approach, utilities directly control EV charging rate and time of EV customers using smart charging algorithms [49–68]. To date, algorithms proposed to control EV load charging aim to achieve two objectives. One is to maximize utility benefits by shifting EV charging to off-peak load hours, and the other is to maximize customer benefits by optimally charging EVs aiming to decrease the customer’s total electricity cost in a real-time electricity market. Both smart charging

methods have certain limitations. By shifting the EV charging profile to off-peak hours, the first method ignores customer inconvenience. As for the other method, many utilities still do not deploy real-time electricity pricing for the residential customers, rendering the method inapplicable. Furthermore, none of the smart charging methods directly aims to decrease EV load impacts on feeder voltages.

This study presents the impacts of integrating EV loads on utility distribution circuits and their solutions. The objective is to understand, identify, and mitigate EV charging impacts on a residential distribution circuit. A detailed literature review including EV charging impacts and solutions is presented first. The chapter further details the proposed approach to evaluating EV load impacts on the distribution system and presents several mitigation schemes to address the EV charging concerns. The proposed mitigation schemes include infrastructural upgrades, indirect EV charging control using TOU pricing, and direct EV charging control using smart charging algorithms.

3.1 Analysis Approach

This study is conducted to help utilities in evaluating impacts of EV loads on their distribution circuits. In particular, the study evaluates how EV loads affect the voltages on the primary and the secondary wires and identifies operating and system conditions that give rise to poor voltage quality in terms of additional voltage drops due to the EV load charging. Once the EV charging effects are understood, several mitigation plans are developed to solve the EV load grid integration issues. To evaluate the EV load effects, three different EV load models are simulated namely; time-domain model, average-value model, and constant power model. A time-domain model simulates the complete EV

charger model with its switching dynamics and is mainly used to evaluate the effects of EV loads during short-circuit or fault conditions. An average value model (AVM) simulates an analytical model for EV load by averaging the switching actions involved in one power cycle. AVM models are used to evaluate steady-state effects of EV charging such as voltage drop concerns due to the EV load charging. In a constant power model, the EV load is represented as a constant power load with an associated load shape, thereby further simplifying the EV load model. A constant power model is used to simulate daily load flow solutions evaluating the effects of EV load charging i.e. increased load demand and voltage drop concerns, over a day.

Next, a complete electrical model of distribution circuits from the substation down to individual customer loads including three-phase transformers, three-phase primary, laterals, secondary networks, and service transformers is specified in the three-phase steady-state load flow model. The evaluation of the impacts of EV loads on the distribution circuit voltage quality requires simulation and comparison of load flow solutions, with and without EV loads. This is done by analyzing the load flow at a suitable interval over one day, referred to as ‘daily load flow solutions’. In this study, the load flow solutions are simulated every 15 minute. Clearly, this analysis requires daily load shape profiles for all conventional loads present in a given distribution feeder. The required load shapes for each conventional load are generated and assigned using the kW consumption data (measured at the substation) over a year, and the stratified pricing information, provided by utilities. The effects of a Level-2 (low) and a Level-2 (high) EV charger with respective power ratings of 3.84 kW (240V/16A) and 7.2 kW (240V/30A) charging a 16kWh/24kWh EV load are evaluated. A charging efficiency of 90% is assumed for all EV chargers con-

sidered in this study. The proposed impact analysis approach identifies several factors such as EV load location, size, distribution, and percentage penetration affecting primary and secondary distribution voltage quality while EV loads are charging. The study concludes that EV load charging may increase in the peak load demand potentially overloading service transformers and may result in unnecessary voltage drops in the secondary service voltages.

Given the impacts of EV charging on transformer loading and service voltage quality, the following infrastructural upgrades to mitigate EV load concerns are presented: increasing the size of service transformer, and reconfiguring the distribution circuit using an additional service transformer. Since, infrastructural upgrades require significant efforts and cost, to mitigate EV load concerns the study presents both indirect and direct control algorithms for EV charging. The impact of indirectly controlling EV charging using TOU pricing is discussed first, followed by the proposed approach to identify an optimal time to begin off-peak rates in a TOU pricing scenario while avoiding inconveniencing EV customers. It is observed that the simultaneous charging of EV loads during off-peak hours under a TOU schedule may result in a second peak in the load demand. To address this concern a smart charging algorithm directly controlling EV charging rate and time while aiming to minimize the voltage variations at each EV load node is proposed. By minimizing voltage variations, the proposed algorithm optimally shifts the EV load demand to off-peak load hours, thus mitigating loading concerns as well.

3.2 Electric Vehicle Charging Technology

This section presents a review of the current electric vehicle (EV) charging technologies. A brief discussion of different EV technologies including the types

of EV batteries is presented, followed by a discussion on EV charging standards and EV charging levels for North American (NA) distribution circuits.

3.2.1 Background of Electric Vehicle Technologies

There are three types of EV technologies currently available on the market; hybrid electric vehicles (HEVs), plug-in hybrid electric vehicles (PHEVs) and battery electric vehicles (BEVs) [6]. HEVs contain an internal combustion engine that runs on conventional liquid fuel but is also supplemented by an electric motor and onboard battery. PHEVs contain both an internal combustion engine and an electric motor and battery. The battery can be charged in three different ways; by plugging in, by the combustion engine, or by regenerative braking. BEVs also referred as all-electric vehicles, do not contain internal combustion engine. Instead, they use batteries to store electricity and run on the stored electricity [6].

Since, HEVs do not require a separate charging infrastructure, this study concerns with PHEVs and BEVs only, collectively referred as EVs. EV batteries are quite different from the batteries used in consumer electronic devices such as laptops and cell phones; they should be light in weight and small in size while able to handle up to a hundred kW of power and high energy capacity (up to tens of kWh). Currently, two major battery technologies are used in EVs [6], nickel metal hydride (NiMH) and lithium ion (Li-ion).

3.2.2 Electric Vehicle Charging Standards

The EV charging is either provided using a normal wall outlet or a dedicated charging circuit (e.g. wall box or charge pole). Usually EV charging is provided by a 120V (Level-1) or a 240V (Level-2) voltage supply (see Figure

) in North America. The EV's charge couplers are described in SAE J1772 and for residential and public EV charging the Type 1 coupler (SAE J1772) is preferred for the U.S. market. Although, the couplers are specified for up to 690 V AC and up to 250 A at 50 to 60 Hz, Level-1 (up to 16 A) and Level 2 (up to 32A) are most commonly implemented [41]. Fast charging circuits, for example, CHAdeMO and the Combined Charging System usually deployed close to highways or on parking sites are also becoming popular. The impacts of fast chargers are however not discussed herein.

3.2.3 EV Charging - North American (NA) Distribution Circuit

The NA power system maintains its tri-phase characteristic down to the mid-voltage (MV) level. At the MV level, electric power is distributed to the low-voltage (LV) level through a pole-mounted transformer. On the LV side of the transformer, a single-phase three-wire supply provides power at 120V and 240V to each consumer, as shown in Figure 3.1.

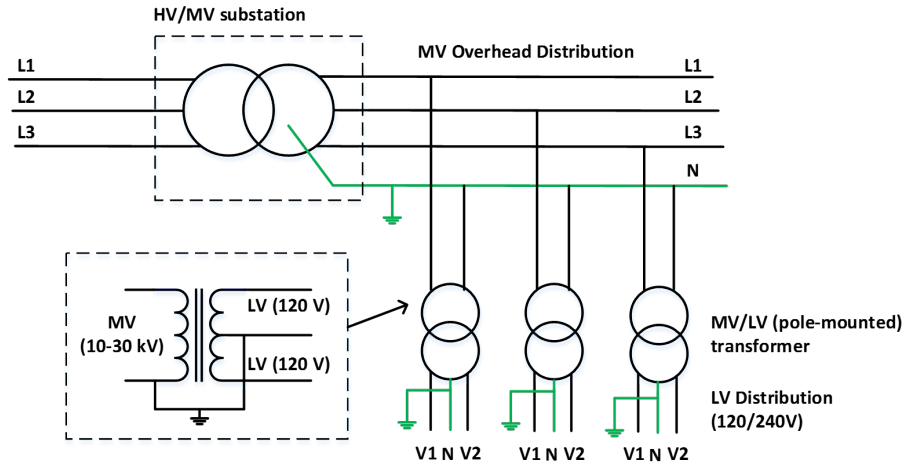


Figure 3.1: The structure of the North American power distribution system.

3.2.3.1 EV Charging Modes

The Society of Automotive Engineers (SAE) is responsible for the standardization of EV charging stations. SAE Surface Vehicle Recommended Practice J1772 (SAE J1772) is the NA standard for EV electrical connectors. SAE identifies three charging levels (see Table 3.1) depending upon the energy transfer rate. Note that, Level-1 and Level-2 chargers are deployed at the residential facilities while Level-3 chargers are used at commercial charging stations. Figure 3.2 shows the connection of EVs to the power distribution circuit for Level-1 and Level-2 charging.

Table 3.1: EV Charging Levels and Charger Specifications (NA Standards)

Charging Level Type	Voltage Level	Power Level
Level-1	120 VAC	Up to 1.8 kW
Level-2	208-240 VAC	Up to 19.2 kW
Level-3 or DC Charging	480VDC	50 kW-150 kW

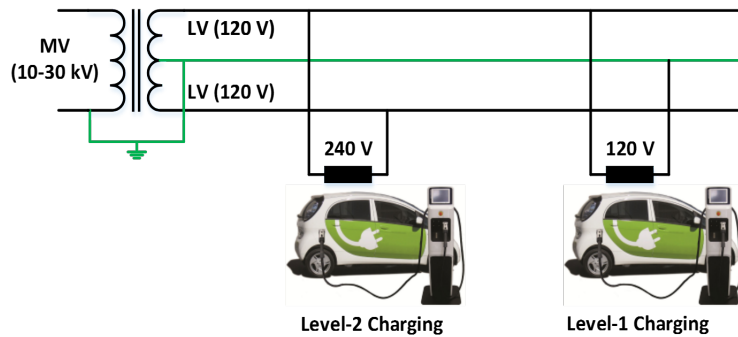


Figure 3.2: The structure of the North American power distribution system.

3.2.3.2 Grid Requirements and Restrictions in NA

For a reliable power distribution, grid requirements and restrictions are imposed when connecting loads, such as EVs, to the distribution circuit. For

the NA distribution system, ANSI C84.1-2011 [62] provides the national standard for voltage regulation. As per the standard, typically, the service voltage should range within $\pm 5\%$ of the nominal voltage rating and the three-phase voltage unbalance should not exceed 3%.

3.3 Modeling EV Charger

The power quality impacts of the EV load charging on distribution circuits requires a representative model of the EV charger. In this study, three different models for EV load are developed: time-domain model, average-value model and constant-power model.

A time-domain model simulates the actual device behavior with its switching actions and is useful in evaluating the EV load during fault conditions. EV load time-domain model is deployed for the evaluation of the overcurrent protection coordination while EV loads are charging. Due to the converter's high switching frequency, a time-domain model can take a significant amount of time to run and therefore is not suitable for the voltage quality study. An average model (or small-signal model) eliminates the switching actions of the device by using appropriate averaging techniques. To facilitate voltage quality study, an average-value model (AVM) of the EV load is developed by averaging the effects of switching actions which happen within one power cycle. Furthermore, an even more simplified EV load model using the actual field measurements and EV load characteristics, referred to as constant-power model, is developed. The constant-power model is more flexible in simulating daily load flow solutions and in performing voltage quality and harmonics evaluations. All three EV load models are explained in the following section. Note that, the voltage quality analysis conducted in this chapter uses the constant-power

EV load model.

3.3.1 Literature Review

The electric vehicle (EV) battery chargers connected to a secondary distribution circuit often raise voltage regulation concerns both in the primary distribution lines and secondary wires. To evaluate the concerns and to provide a better understanding of the impacts of EV loads on the distribution voltages, a representative simulation model of EV chargers must be developed. Switching models or detailed device-level models of EV chargers are accurate in mimicking a wide range of charging conditions. However, these simulation models usually take a significant amount of time to run due to the converter's high switching frequency. Furthermore, the evaluation of voltage regulation issues in the primary and secondary circuits requires running hundreds of multi-hour load demand scenarios making the detailed model impractical. In addition, voltage regulation is not an electromagnetic transient phenomenon, therefore the use of detailed model is not necessary. For these reasons, a small-signal model of EV chargers is called for. The small signal model averages the effects of fast switchings in the device that occur within one power cycle, thus making the simulation fast and less computationally intensive.

An EV charger circuit is composed of a single-phase rectifier with a boost converter as the power factor correction stage, followed by a DC-DC converter for insulation of the battery from the AC supply [69]. An equivalent switching model of the EV charger based on empirical data obtained for a range of actual EVs is presented in [70]. However, the model is manufacturer specific as it is empirically derived. A model for a population of EV loads is developed in [71]. As such, this model does not represent device-level characteristics

and is mainly intended to evaluate the effects of a large number of EV loads on system harmonics. A detailed EMTP-RV model or switching model for a Level-1 (120V/12A) battery charger is presented in [72]. Since the developed model is a switching model, it takes a significant amount of time to run and is therefore not suitable for evaluation of voltage regulation concerns. Average-value modeling is the most general method used for developing the small-signal models for power electronic equipment. Average-value models for DC-DC converters and various three-phase rectifier circuits have been developed in [73–80]. A mathematical model for electric vehicle charging demand specifically for rapid charging stations is developed in [81]. The developed EV charging model considers both spatial and temporal uncertainty of electric vehicle charging demand.

3.3.2 EV Charger Circuit

A battery charger takes power from an electric energy supply (mostly AC voltages) and delivers power to battery packs. Since battery packs take DC power, the supply power needs to be processed by battery chargers. The manner in which the power is delivered to the batteries is also very crucial to battery life, hence a charger also includes a control circuit for battery power management [80, 82]. Evidently charging circuit consists of two parts as described below.

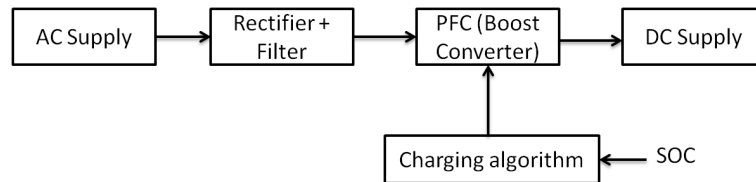


Figure 3.3: Simplified block diagram of battery charging system.

3.3.2.1 Power Processing Unit

Power processing unit of a general EV charger consists of an AC-DC converter. The general architecture is shown in Figure 3.3. Due to safety requirements and standards, battery chargers are generally isolated from the AC power grid. Traditionally, battery chargers consist of AC-DC full bridge rectifier followed by a capacitor (to reduce voltage ripples). The supply side current injected by such a converter is not sinusoidal and is rich in harmonics, hence undesirable. A power factor correction stage (PFC) (generally using a boost converter) with an appropriate control circuit is used to improve the supply current waveforms. In commercial chargers, the boost converter uses pulse width modulation (PWM) control to provide power factor correction at the input terminals. As a result, the charger operates at near unity power factor with minimum low frequency harmonic current content during normal operation. From modeling perspective, power processing unit till the power factor correction stage is sufficient enough to study the impact of a battery charger on AC grid.

3.3.2.2 Battery Management Unit

Battery management unit determines the efficiency and performance of the battery charger. It consists of a micro-controller and sensors to monitor the status of charging current, voltage, and battery's state-of charging (SOC). Micro-controller contains charging algorithms, which enables it to determine when to start and stop the charging process. Conventional charging methods include passive charging, constant current (CC) charging, constant voltage (CV) charging and CC-CV charging. Recently a pulsed current charging method is gaining popularity as a fast charging algorithm.

3.3.3 Generic Time-Domain EV Load Model

A generic time domain model for an EV load being charged by a Level-1 (120V/12A) battery charger is simulated and shown in Figure 3.4 [72]. The model consists of an AC-DC full bridge rectifier followed by a power factor correction (PFC) stage, a DC-DC insulation stage, and a battery load. Table 3.2 presents the circuit parameters for the EV load model shown in Figure 3.4. For the EV load being charged by a Level-2 EV charger, all circuit parameters shown in Table 3.2 are assumed identical, with the exception that V_{ac} is changed to 240 V.

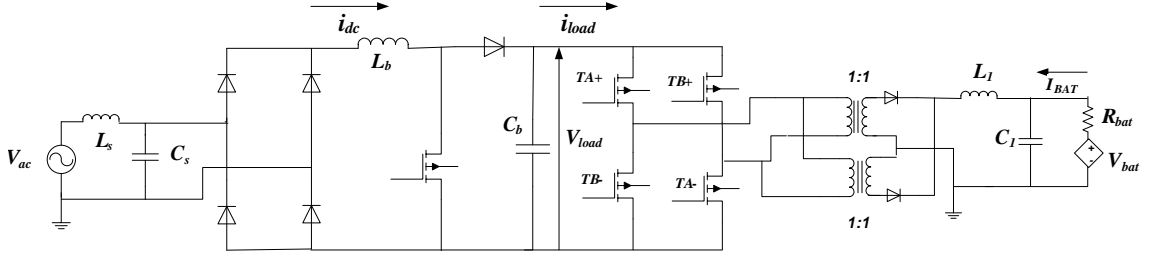


Figure 3.4: Time-domain model for a Level-1 (120V/12A) EV battery charger

Table 3.2: Level-1 (120V/12A) EV Charger Circuit Parameters

Supply side circuit parameters	Boost converter circuit parameters	DC-DC converter circuit parameters	Battery model
$V_{ac} = 120\text{V}$	$L_b = 1.8 \text{ mH}$	$L_1 = 5 \text{ mH}$	$R_{bat} = 0.1 \Omega$
$L_s = 0.5 \text{ mH}$	$C_b = 500 \mu\text{F}$	$C_1 = 50 \mu\text{F}$	$V_{bat} = 384 \text{ V}$
$C_s = 10 \mu\text{F}$			

The PFC stage ensures a sinusoidal supply-side current control methodology for which is shown in Figure 3.5. The difference between the output of the boost converter (V_{load}) and the reference voltage (in this case 370 V) is used to generate an error signal which is then fed to the voltage controller, $G_v(s)$. The

output of the voltage controller is then multiplied by the haversine to generate a reference signal for the boost inductor current. Using this current as the reference and the measured current from the boost inductor (i_{dc}), a new error signal is formed which is fed into the current controller, $G_i(s)$. The output of the current controller is then compared with a ramp signal to provide PWM control of the switch resulting in a sinusoidal supply current.

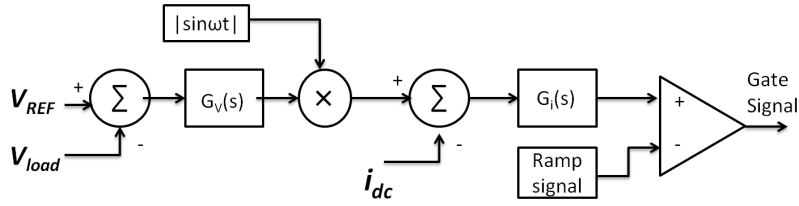


Figure 3.5: Block diagram of PWM control of PFC boost converter

The full-bridge DC-DC converter associated with the insulation stage is controlled using the PWM technique, the block diagram for which is shown in Figure 3.6. The PWM scheme controls all four switches using bi-polar voltage switching. The difference between the reference ($I_{REF} = 3.65$ A) and the measured battery current (I_{BAT}) is fed to a PI controller and the output is compared against a 50 kHz ramp signal. The output determines the transistor pairs needed to be switched on, (TA+,TA-) or (TB+,TB-).

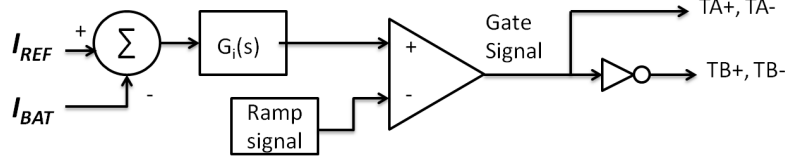


Figure 3.6: Block diagram of PWM control of DC-DC converter

A 330V-10kWh Li-ion battery is used as the battery load. The battery model used in this case is a 384 V DC voltage source (fully charged voltage of battery) behind a 0.1Ω series resistance.

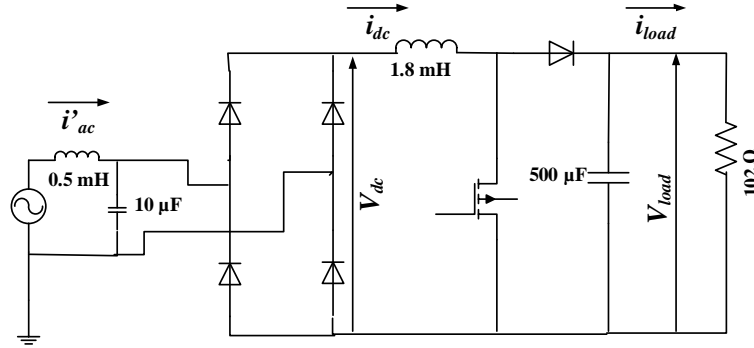


Figure 3.7: Reduced-order time-domain model for a Level-1 (120V/12A) EV battery charger

Furthermore, a reduced-order model for an EV load charged by a Level-1 (120V/12A) EV charger is also developed as shown in Figure 3.7. In the reduced-order model the DC-DC converter and the battery are replaced by an 102Ω resistor. Similarly, equivalent resistance for the reduced-order model of an EV load being charged by a Level-2 EV charger (240V/16A) is simulated by replacing the DC-DC converter and the battery load by a 58Ω resistor.

3.3.4 Average Value Model for the Electric Vehicle (EV) Loads

In this section an AVM for the reduced-order EV load model is developed [2], [3]. Specifications for the EV charger assembly are the same as in the time-domain model, shown in Figure 3.7. The AVM model for the EV load is developed in two stages for which the time-domain model is divided into two blocks :

- Rectifier block - converting AC supply voltage to low ripple DC voltage and
- Boost converter block - for power factor correction

In order to break the model into two stages it is required to introduce an isolation between the two blocks. This is achieved by dividing the boost converter inductance into two equal halves (L_b and L_{dc}) and introducing a very low capacitance (C_{dc}) between the two stages, as shown in Figure 3.8. Since the capacitance introduced is very low, overall circuit behavior of the EV charger shown in Figure 3.8 remains unaffected. The equivalent switching model is shown in Figure 3.8.

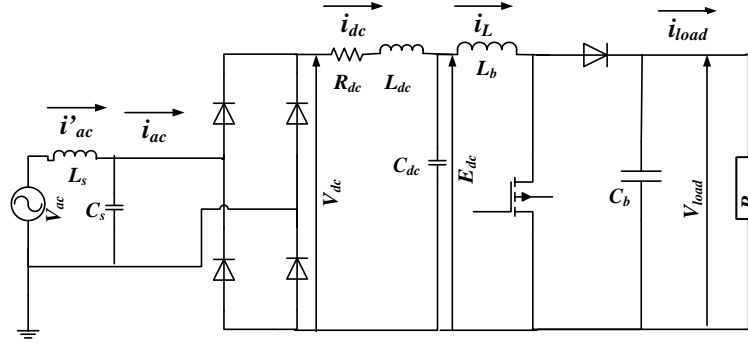


Figure 3.8: Equivalent time-domain model for the generic EV battery charger

3.3.4.1 Rectifier Block - AVM Model Derivation

The AVM model for a three-phase rectifier is developed by assuming that the DC current flowing through the filter inductor is smooth enough to be represented approximately by a first order Taylor series [83]. In (3.1), current i_{dc0} is the instantaneous DC current flowing through the inductor (L_{dc}) halfway through commutation, u is the overlap angle and k is the rate of rise of DC current with respect to $\theta = \omega t$.

$$i_{dc} = i_{dc0} + k\left(\theta - \frac{u}{2}\right) \quad (3.1)$$

Although an EV load is a constant current device, i.e. it draws a constant RMS supply side current and a constant RMS DC current, the current

waveforms are not constant. The PWM control for the EV charger modifies DC current waveform as haversine wave making the instantaneous value of DC current variable. Hence, an AVM cannot be developed for instantaneous values of current waveforms. Since, for an EV charger, the RMS values of AC and DC current waveforms remain constant, the AVM can be derived for the RMS values of current waveforms. In this work, the AVM is developed for the RMS value of the DC current waveform and for the derivations herein, (3.1) represents the RMS value of the DC current waveform. Since the PWM control results in a sinusoidal supply (AC) current, the harmonic distortion in current waveforms could be assumed to be minimal and the actual current and voltage waveforms could be reproduced from their RMS values, obtained using the developed AVM model. The analytical derivation for the AVM of the rectifier block is presented below.

Generally, a single-phase bridge rectifier exhibits a two-switch conduction configuration (see Figure 3.9(a)). However because of the presence of source impedance, during commutation the current cannot be transferred instantaneously from the outgoing device to the incoming device and thus the rectifier exhibits a four-switch conduction configuration (see Figure 3.9(b)).

In order to represent current delay during commutation, the RMS current on the supply side (i'_{ac}) is expressed as the difference of two current waveforms i_1 and i_2 . Currents i_1 and i_2 flow in opposite directions through the source impedance as shown in Figure 3.10. It is clear that during positive half cycle commutation mode, i_1 increases from 0 to I_0 and i_2 decreases from I_0 to 0. Then i_1 and i_2 currents stay at I_0 and 0 respectively until the next commutation. Similarly during negative half cycle commutation mode, i_2 increases from 0 to I_0 and i_1 decreases from I_0 to 0. Then i_2 and i_1 currents stay at

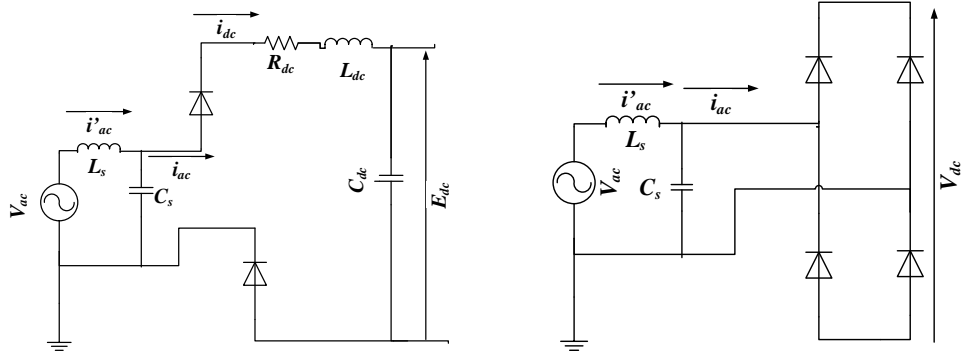


Figure 3.9: a) Two-switch conduction configuration, b) Four-switch conduction configuration

I_0 and 0 respectively until the next commutation. Note that, I_0 is the RMS value of supply side AC current (i'_{ac}) waveform after commutation. Using the above discussion and Figure 3.10, for entire power cycle:

$$\begin{aligned}
 i'_{ac} &= i_1 - i_2 \\
 i'_{ac} &= i_{ac} + C_s \int V_{dc} dt \\
 i_{dc} &= i_1 + i_2 - C_s \int V_{dc} dt
 \end{aligned} \tag{3.2}$$

where i_{dc} is the RMS DC current.

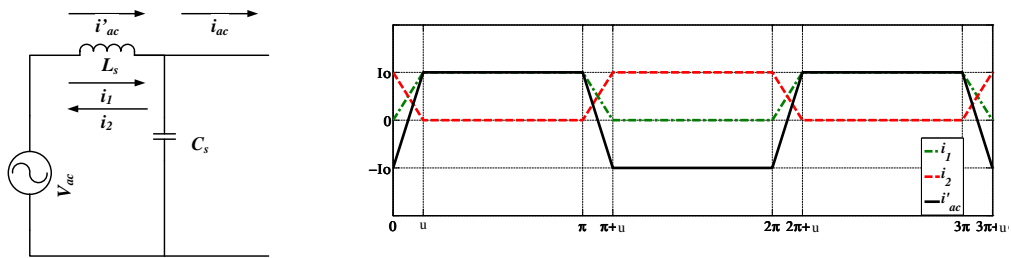


Figure 3.10: Piece-wise representation of the RMS AC current (i'_{ac})

3.3.4.2 During Commutation

Applying Kirchhoff's voltage law (KVL) to the commutation circuit in Figure 3.9(b), the following equation is obtained. Note that, during commutation, $V_{dc} = 0$.

$$V_{ac} = L_s \frac{di'_{ac}}{dt} \quad (3.3)$$

Substituting (3.2) in (3.3), eliminating i_2 and substituting i_{dc} and V_{dc} , then integrating from 0 to θ yields:

$$i_1(\theta) = \frac{\sqrt{2}V_a}{2\omega L_s}(1 - \cos(\theta)) + \frac{1}{2}(k\theta) \quad (3.4)$$

At the end of the commutation, current i_1 will be equal to DC current i_{dc} . By substituting $i_1(u) = i_{dc}(u)$ in (3.1), where u is angle of commutation:

$$i_1(u) = i_{dc}(u) = i_{dc0} + \frac{1}{2}(ku) \quad (3.5)$$

At the end, commutation (overlap) angle is given as:

$$u = \cos^{-1} \left(1 - \frac{2\omega L_s i_{dc0}}{\sqrt{2}V_a} \right) \quad (3.6)$$

3.3.4.3 After Commutation

Applying Kirchhoff's voltage law (KVL) to the circuit in Figure 3.9(a), we get:

$$V_{dc}(\omega t) = \sqrt{2}V_a \sin \omega t - \omega L_s \frac{di_1}{d\omega t} + \omega L_s \frac{di_2}{d\omega t} \quad (3.7)$$

Clearly (3.7) is applicable for all time. By averaging (3.7) over $0 \leq \theta \leq \pi$, the average value for dc voltage $\bar{V}_{dc}(t)$ can be obtained.

$$\bar{V}_{dc} = \frac{1}{\pi} \int_0^\pi \left[\sqrt{2}V_a \sin \omega t - \omega L_s \frac{di_1}{d\omega t} + \omega L_s \frac{di_2}{d\omega t} \right] d\omega t \quad (3.8)$$

The bar over the variables in the equations indicate that these are averaged values.

During commutation $V_{dc} = 0$. Hence, for $0 < \theta \leq u$, i_1 is derived by (3.5) and $i_2 = i_{dc} - i_1$. For the period $u < \theta \leq \pi$, i_2 is zero and using (3.1), $i_1 = i_{dc} + C_s \int V_{dc} dt$. Using above arguments, substituting (3.5) and (3.1) in (3.8), and solving for \bar{V}_{dc} we get:

$$\begin{aligned}\bar{V}_{dc}(t) &= \frac{2\sqrt{2}}{\pi}V_a - \frac{2\omega L_s}{\pi}i_{dc0} + L_s \left(1 - \frac{u}{\pi}\right) \frac{d\bar{i}_{dc}}{dt} + \frac{C_s L_s}{\pi} \bar{V}_{dc}(t) \\ &= g \left(\frac{2\sqrt{2}}{\pi}V_a - \frac{2\omega L_s}{\pi}i_{dc0} + L_s \left(1 - \frac{u}{\pi}\right) \frac{d\bar{i}_{dc}}{dt} \right)\end{aligned}$$

where

$$g = \frac{1}{1 - \frac{C_s L_s}{\pi}} \quad (3.9)$$

Also applying KVL on the ‘DC’ side, we get:

$$\bar{V}_{dc} = E_{dc} + L_{dc} \frac{d\bar{i}_{dc}}{dt} + R_{dc} i_{dc0} \quad (3.10)$$

Substituting (3.10) in (3.9) we get:

$$\frac{d\bar{i}_{dc}}{dt} = \frac{\frac{2g\sqrt{2}V_a}{\pi} - \left(\frac{2g\omega L_s}{\pi} + R_{dc}\right) i_{dc0} - E_{dc}}{L_{dc} + gL_s \left(1 - \frac{u}{\pi}\right)} \quad (3.11)$$

Eq. (3.11) represents the DC current dynamics of the single phase bridge rectifier circuit.

Using (3.2), and the RMS current waveform in Figure 3.10, the supply side AC current waveform for one power cycle is given by (3.12). Note that the supply side AC current waveform is represented as i_{ac}^{wave} .

$$i_{ac}^{wave}(\theta) = \sqrt{2}a \cdot \sin(\theta) ; 0 < \theta \leq u$$

$$\begin{aligned}
&= \sqrt{2} \left(i_{dc} + C_s \int V_{dc} dt \right) \sin(\theta) ; u < \theta \leq \pi \\
&= -\sqrt{2} b \cdot \sin(\theta - \pi) ; \pi < \theta \leq \pi + u \\
&= -\sqrt{2} \left(i_{dc} + C_s \int V_{dc} dt \right) \sin(\theta - \pi) ; \text{else}
\end{aligned}$$

where

$$\begin{aligned}
a &= 2 \left(\frac{\sqrt{2} V_a}{2\omega L_s} (1 - \cos(\theta)) + \frac{k}{2}(\theta) \right) - i_{dc} \\
b &= 2 \left(\frac{\sqrt{2} V_a}{2\omega L_s} (1 - \cos(\theta - \pi)) + \frac{k}{2}(\theta - \pi) \right) - i_{dc} \quad (3.12)
\end{aligned}$$

The DC current waveform is generated using (3.13). Note that the DC current waveform is represented as i_{dc}^{wave} .

$$\begin{aligned}
i_{dc}^{wave}(\theta) &= \sqrt{2} a \cdot \sin(\theta) \quad ; 0 < \theta \leq u \\
&= \sqrt{2} (i_{dc}) \sin(\theta) \quad ; u < \theta \leq \pi \\
&= \sqrt{2} b \cdot \sin(\theta - \pi) \quad ; \pi < \theta \leq \pi + u \\
&= \sqrt{2} (i_{dc}) \sin(\theta - \pi) ; \text{else} \quad (3.13)
\end{aligned}$$

3.3.4.4 Boost-Converter - Analytical Model

The circuit diagram for the boost-converter part of the EV load time-domain model is shown in Figure 3.11. The average value model for a boost converter is given as:

$$\begin{aligned}
L_b \frac{d\bar{i}_L(t)}{dt} &= E_{dc} - (1 - d)\bar{V}_{load}(t) \\
C_b \frac{d\bar{V}_{load}(t)}{dt} &= (1 - d)\bar{i}_L(t) - i_{load} \\
i_{load} &= \frac{V_{load}}{R_{load}} \quad (3.14)
\end{aligned}$$

where d is the duty cycle of the converter, given by.

$$\bar{q}(t) = d = \frac{T_{on}}{T_{on} + T_{off}} \quad (3.15)$$

where, $q(t)$ represents status of the switch or switching signal. (ON: $q(t) = 1$, OFF: $q(t) = 0$)

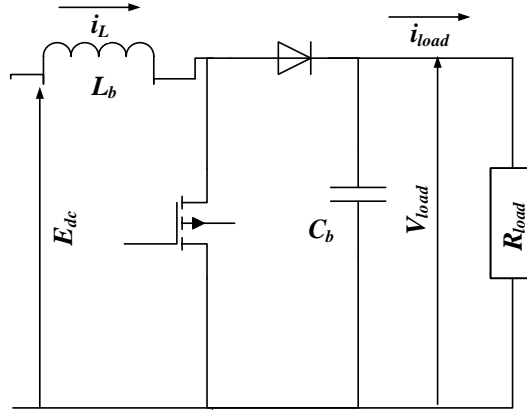


Figure 3.11: Boost converter - power factor correction stage

3.3.5 Constant-power EV Load Model

The voltage variations recorded over a day in the distribution feeder is a steady-state event; hence a steady-state model for the EV load would be sufficient in conducting the voltage quality analysis. This section describes the constant power EV load model simulated for voltage quality study. The simulation of steady-state model requires an understanding of the steady state behavior of EV loads. To understand the steady state characteristics, field measurements were taken at an EV charging facility. Figure 3.12 shows the one-line diagram of the charging facility under consideration. The charging station shown in Figure 3.12 is equipped with four Level-2 (240V-15A) chargers.

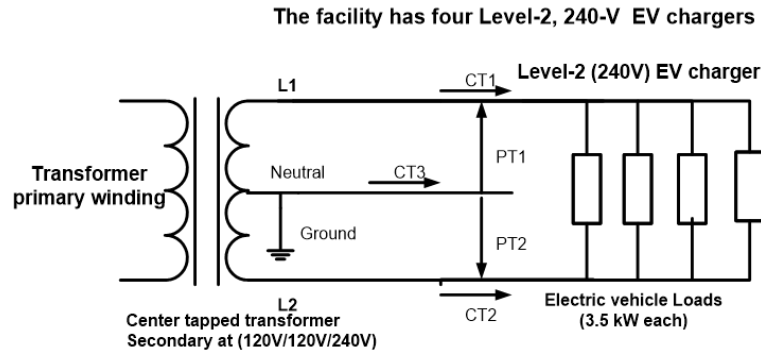


Figure 3.12: One-line diagram of the charging facility

The measurement conditions are specified as follows. Four EVs were being charged between measurement time, 0 and 420 s for a total power demand of 13.9 kW or 3.5 kW per EV with line current of 15 A. Later between 420 s and 470 s, two EVs were being charged while the other two went offline. A representative snapshot for the measurement of EVs' power demand is shown in Figure 3.13. It can be seen that the power demand remains constant while EV loads are charging. Clearly, the field measurements suggest that the EV loads draw constant power when plugged in for charging. This observation is justified by the fact that the commercial charging circuits are equipped with advanced control strategies, designed to draw a constant current while maintaining a constant charging voltage, thus supplying a constant power to the EV. The constant power demand justifies a constant power model for the EV loads.

For the voltage quality evaluations, the daily load shape profile for the EV load is also required. Therefore, based on the type of EV battery, vehicle traffic, and the type of charging facility (residential or commercial facility) to which the EV load is connected to, the load shape profile for the EV load is generated.

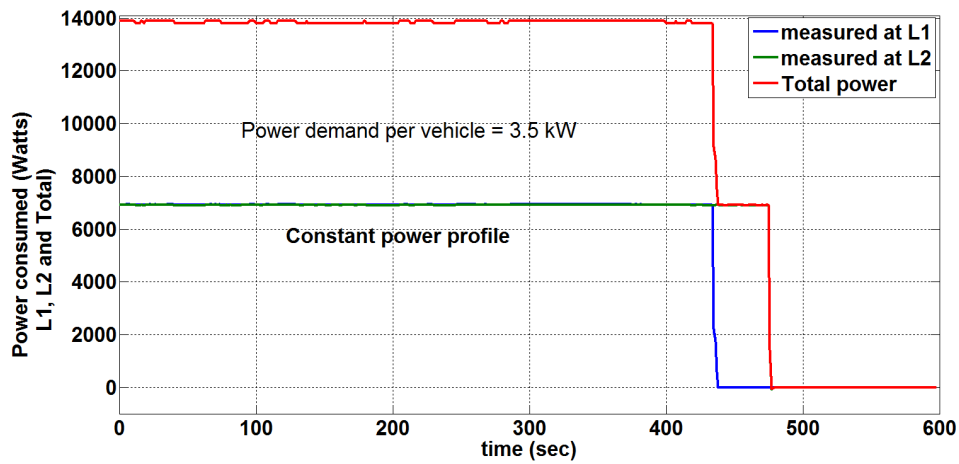


Figure 3.13: Power demand measured at the secondary service

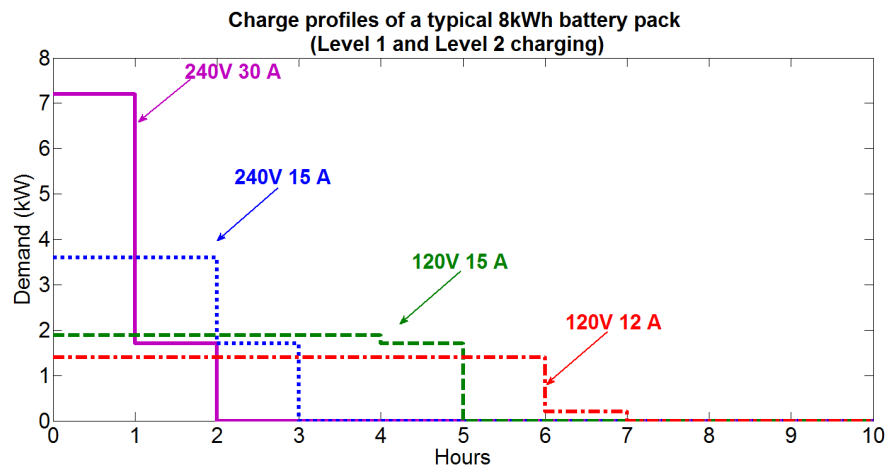


Figure 3.14: Daily load shape profiles for an 8 kWh EV load (charger efficiency is 90%)

An example load shape profile of an EV load with an 8-kWh battery pack is shown Figure 3.14 [79]. The electrical demand over time for an EV load is clearly not constant for all time. In a battery charger, the kW demand remains constant until the state of charge (SOC) of the battery reaches 90%. After which, the rate of charge is decreased until the battery is fully charged. Based

on the observations drawn from the measurements and Figure 3.14, a daily load shape profile for a 16 kWh EV load with 20% SOC [69], being charged by a 240V-16A Level 2 EV charger connected to a residential facility, is developed and shown in Figure 3.15. The load shape profile of EV load is developed using the constant power load characteristic and a fixed EV charging starting time. To simulate the worst case scenario, the EV load demand is assumed to overlap with the peak demand hours of the service transformer i.e. 6 -10 pm.

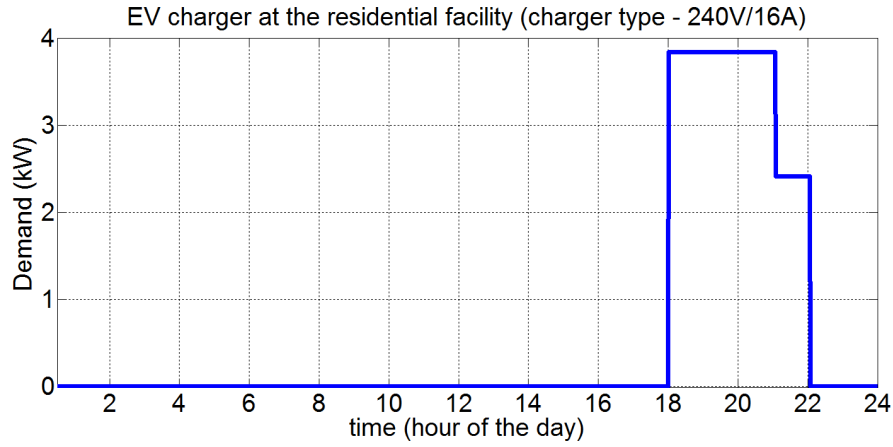


Figure 3.15: An example EV load shape profile of a 16 kWh EV load being charged by a Level-2 charger (240V/16A-3.84kW)

3.3.6 Application and Validation of the EV load AVM model

This section illustrates the application of the AVM model for an EV load being charged by a Level-2 (240V/16A) EV charger in evaluating the secondary circuit voltage drops due to the EV load charging. The section also validates the AVM against the time-domain model. The selected parameters for the battery charging system shown in Figure 3.8 are given as follows: $L_s = 0.5$ mH, $C_s = 10 \mu\text{F}$, $L_{dc} = 0.9$ mH, $L_b = 0.9$ mH, $C_{dc} = 1$ pF, $C_b = 500 \mu\text{F}$. The

value of the supply voltage (V_{ac}) is 240 V and the equivalent load resistance ($R_{load} = 58 \Omega$) is used.

The system is subjected to four case studies. In Case 1, a Level-1 EV charger of rating 120V/12A is simulated and validated against the switching model. Case 2 validates both the AVM model and switching model of the EV charger against the actual measurements taken at an EV charging facility. In Case 3, a simple distribution feeder model is simulated. Three Level-2 (240V/16A) EV chargers are connected to phase A of the secondary distribution transformer. Case 4 validates the accuracy of the AVM model in evaluating the effects of EV load on the secondary network voltage profile. These case studies are discussed in details below.

3.3.6.1 Case 1 - Validation and Comparison of the proposed AVM Model

An AVM model for a Level-1 (120V/12A) EV battery charger is developed in Matlab/Simulink [18]. The AVM is validated against an equivalent switching model developed using PSCAD/EMTDC [84]. The RMS supply voltage for the charging system is $V_{ac} = 120$ V. To simulate the reduced-order model, the DC-DC converter and the battery load are replaced by an equivalent load resistance (R_{load}) equal to 102Ω . It should be noted that for the developed AVM model, the PWM control is maintaining the battery charging voltage at 370 V.

Figure 3.16 shows the load voltage (V_{load}), rectified DC current (i_{dc}) and supply current (i'_{ac}) waveforms for the proposed AVM model and the switching model. The load voltage is constant at approximately 370 V. The rectified DC current (i_{dc}) waveform has a peak value of 17.5 A. Also, the AC current

waveform is sinusoidal for the proposed AVM model with the peak value of 17.5 A, the same as in the switching model. Hence, the RMS value of supply side AC current is approximately 12.3 A as required by a Level-1 (120V/12A) EV charger. Graphs generated by the proposed AVM model clearly overlap with the graphs generated by the switching model, thus validating the AVM model.

3.3.6.2 Case 2 - Validation against the Actual Measurements

Real time measurements are taken at a charging facility using a power quality analyzer. The secondary network voltage and current profiles during EV charging are recorded. The charging facility is populated with two 3.5 kW EV loads. The one-line diagram of the secondary network chosen for the measurements is shown in Figure 3.17.

An equivalent switching model and an AVM model is developed for this case. Both AVM and switching models are validated against the actual measurements taken at the charging facility. The supply-side current waveforms are shown in Figure 3.18. From Figure 3.18, the peak value of supply side current is 41 A, which gives peak current contribution per charger equal to $\frac{41}{2}$ A. Hence RMS current supplied to each EV charger is $\frac{41}{2\sqrt{2}} = 14.5$ A. Also, current required by each 3.5 kW EV load at a voltage level of 240 V is equal to $\frac{3.5}{0.24} = 14.58$ A, which is same as RMS current supplied to each EV load in Figure 3.17. Hence, the above argument validates the supply side current profile for the measurements taken.

Clearly the supply side AC current measured for both switching model and AVM model overlap with the actual measurements taken, thus validating both models.

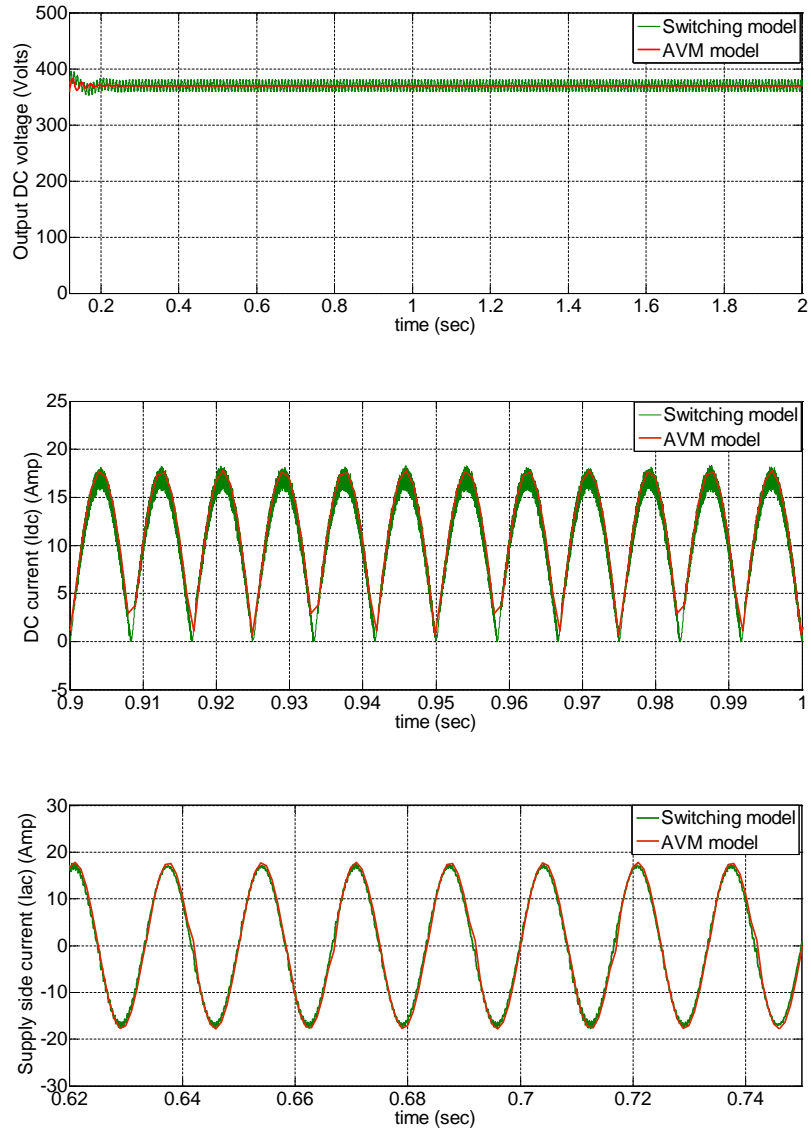


Figure 3.16: Current and voltage waveforms for the EV charger models: (a) output DC voltage (V_{load}); (b) DC current (i_{dc}) waveform; (c) supply side AC current (i'_{ac}) waveform

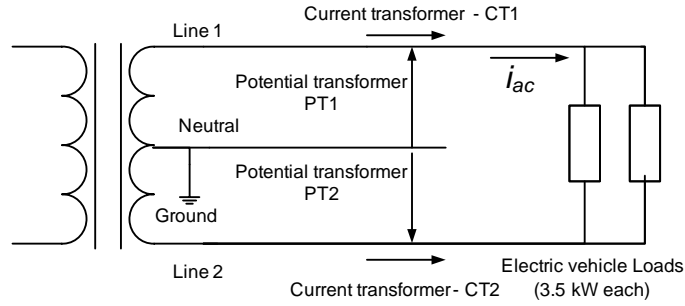


Figure 3.17: One-line diagram of the secondary circuit under evaluation

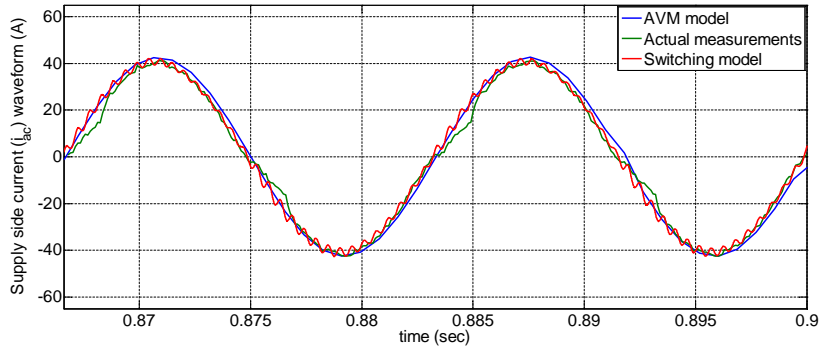


Figure 3.18: Supply side AC current (i_{ac}) waveform

3.3.6.3 Case 3 - Application to the Distribution Feeder

A simple distribution feeder model is simulated in this section and the EV charging characteristics are validated for the equivalent AVM model. A three-phase 13.8 kV source is connected to a 10 km long distribution line. The distribution line is supplying a single-phase center-tap distribution transformer of voltage rating 7.97kV/240V, and two single-phase loads as shown in Figure 3.19(a). Three Level-2 (240V/16A) EV chargers are connected to the secondary side of the center tap transformer. To simulate the reduced-order model for the Level-2 EV charger (Figure 3.19(b)), the DC-DC converter and the battery load are replaced by an equivalent load resistance of 58 Ω . For the

AVM model, PWM control is maintaining battery charging voltage at 370 V.

AVM model is validated against the switching model for the center-tap transformer secondary (AC) current, DC current inside one of the EV chargers, and battery charging voltage. Figure 3.20 shows the load voltage (V_{load}), rectified DC current (i_{dc}) waveform for a particular battery charger, and the transformer secondary current (i_{ac}) waveform for both models.

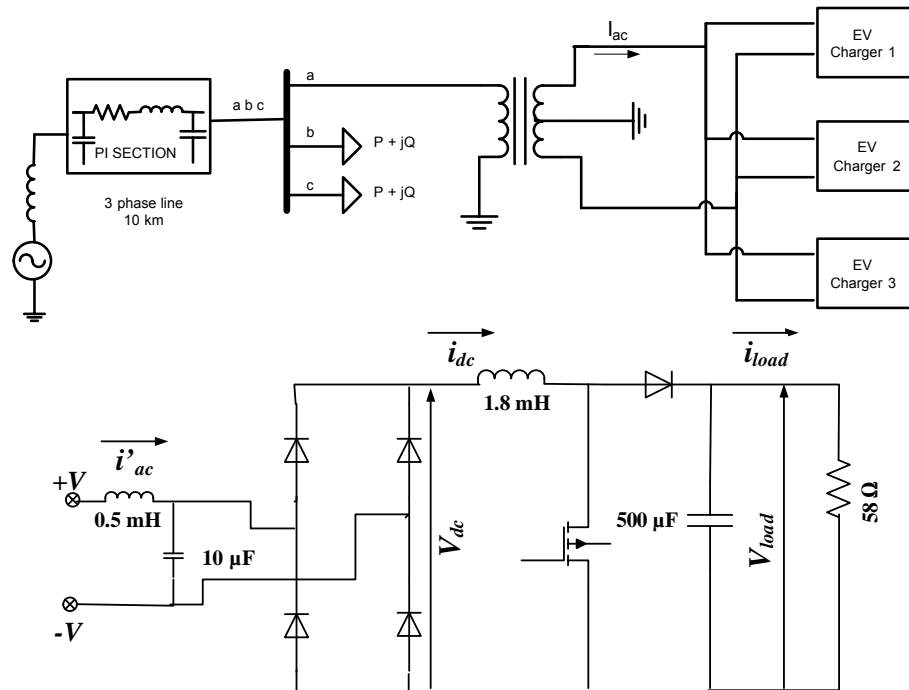


Figure 3.19: (a) Distribution feeder model under evaluation; (b) Switching model for a Level-2 (240V/16A) EV charger

As expected due to PWM control, the load voltage is constant at 370 V. The AVM model is averaging the DC current waveform generated by the switching model, thus validating the AVM model. Also, the rectified DC current (i_{dc}) has a peak value of 23 A. The DC current waveform is a fully rectified sine wave (haversine). The current waveforms on the secondary side

of the center-tap transformer are sinusoidal for both models. The peak value of the current waveform is 70 A giving the peak current contribution per EV charger equal to $\frac{70}{3}$ A. Hence, the RMS current required per EV charger comes out to be $\frac{70}{3\sqrt{2}} = 16.3$ A, as required by the Level-2 (240V/16A) EV charger. Graphs generated by the AVM model clearly overlap with the graphs generated by the switching model, thus validating the AVM model.

3.3.6.4 Case 4 - Evaluation of Voltage Drop in the Secondary Circuit due to EV Load Charging

The one-line diagram of a 13.8 kV distribution feeder model under evaluation is shown in Figure 3.21. A single-phase center-tap distribution transformer of voltage rating 7.97kV/240V is connected to phase A of one of the three phase lines. The service transformer is connected to a 500 m long secondary feeder. The secondary circuit supplies two 2.5 kW conventional loads and a 240V/16A (3.84 kW) EV charger.

The RMS voltage profile is recorded at the load node for both the AVM model and switching model, with and without the EV load. The RMS voltage profiles for both models are shown in Fig. 3.22. Without EV load, both models record 116.9 V RMS voltage at the load node. The RMS voltage drops to 112.7 V when one 240V/16A EV load is connected to the network. Both, the AVM and switching models record an additional voltage drop of 4.2 V (3.5 %) due to EV load charging. This case concludes that the AVM model satisfactorily evaluates steady state effects of EV load charging on the secondary network voltage profile.

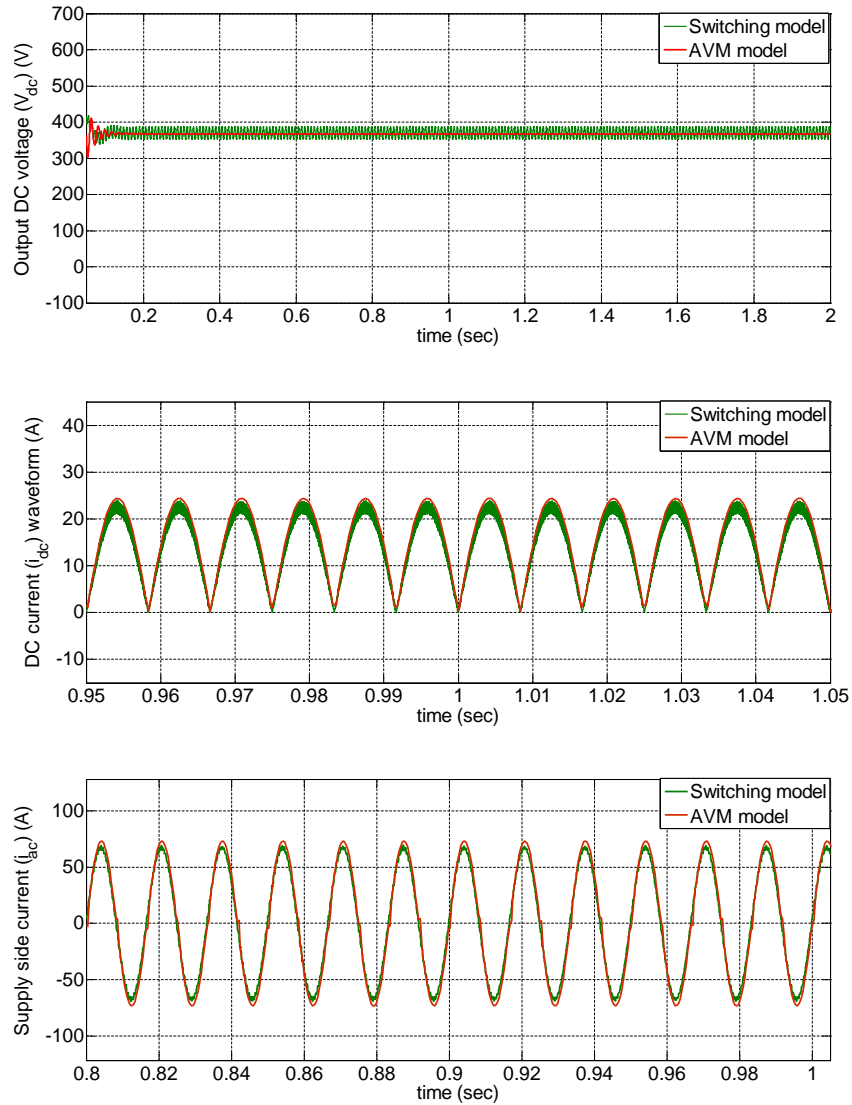


Figure 3.20: Current and voltage waveforms for the EV charger with PWM control: (a) output DC load voltage (V_{load}) for an EV charger; (b) rectified DC current (i_{dc}) waveform for an EV charger; (c) AC current (i_{ac}) waveform measured at the transformer secondary

3.4 Evaluating and Mitigating the Distribution System Impacts of EV Charging - A Literature Review

This section presents a detailed literature review on the impacts and mitigation of EV charging on the distribution system. The impact analysis details

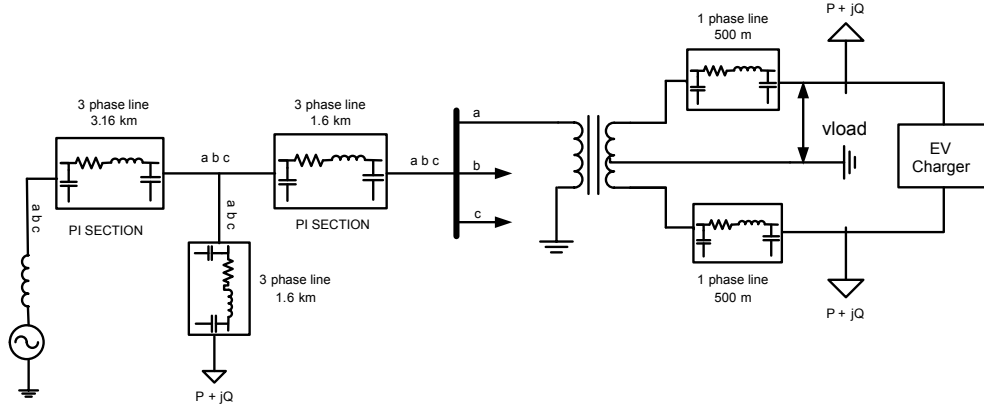


Figure 3.21: One-line diagram of the distribution feeder model (Application of the EV load AVM model)

the evaluation of the EV load impacts on generation adequacy of the existing distribution circuits, on transformer aging due to overloading, and on distribution system power quality. Several mitigation schemes proposed in literature including indirect control using TOU rates and direct control using smart charging algorithms are detailed next.

3.4.1 Impacts of EV Charging on Distribution System

The growing EV charging infrastructure comes with several challenges for the existing distribution system. These challenges have been thoroughly evaluated in the past few years. In the existing literature, EV impact analysis is primarily conducted to evaluate the effects of EVs on electricity generation adequacy, transformer aging, and distribution system power quality. It is speculated that EV charging during peak load hours may increase the peak load demand and necessitate generation capacity expansion. Additionally, increased EV load demand may overload substation and service transformers thus deteriorating transformers' life. Additionally, EV charging may result

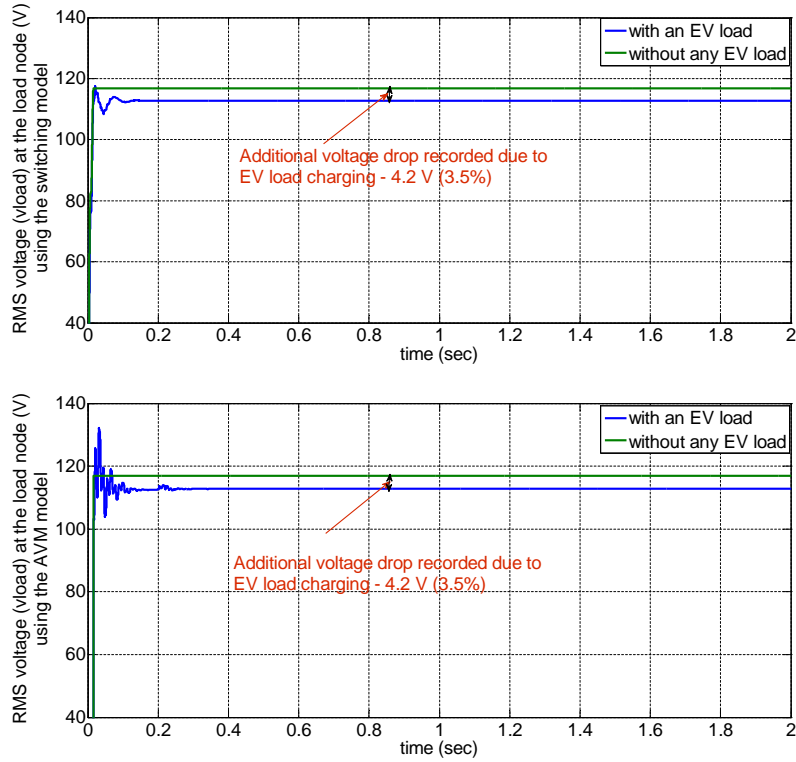


Figure 3.22: Voltage waveforms (vload) at the load node with and without EV load using the: (a) switching model; (b) AVM model

in power quality issues including voltage drops, power unbalances, and voltage/current harmonics.

3.4.1.1 EV Load Impacts on Electricity Generation Adequacy

Several EV integration studies [21–27] have analyzed the existing and planned generation capacity to meet current and future EV demands. These studies conclude that the requirement for new power plants due to EV charging is unlikely if EVs do not increase the system peak load demand. In other words, if vehicles are charged during off-peak hours, EV charging will not

have a significant impact on the power generation adequacy. It is observed that without controlled charging, a large-scale EV deployment could decrease supply adequacy, and, therefore, will necessitate the construction of additional power plants. Specifically, [28] concludes that depending on the time and place of the vehicle additions, EV charging could require additional power generation or increase the utilization of existing capacity and possibly reduce the reserve margins thus resulting in serious reliability concerns.

3.4.1.2 EV Load Impacts on Transformer Aging

The large-scale EV deployment is likely to cause problems in the distribution system such as increased load demand, an increase in system losses, and additional voltage drops in distribution voltages [4–7, 27–41]. The increased load demand due to EV loads can overload service transformers and increase system losses. Furthermore, EV charging can create new load peaks exceeding the service transformer’s rated capacity, thereby, accelerating equipment aging [29–31]. Specifically, [29] characterizes the impacts of EV charger characteristics particularly system harmonics on distribution transformer life. The analysis results in a quadratic relationship between the transformer life and the total harmonic distortion (THD) of the battery charger current. In order to have a reasonable transformer life expectancy, it is suggested that the current THD should not exceed 25-30%. Similarly, [30] evaluates the impacts of EV charging on transformer capacity overloading and concludes that a time-controlled EV charging can successfully mitigate the transformer overloading concerns. An EV charging analysis using actual load consumption data from Austin, Texas, during a typical summer day is conducted in [85]. The study anticipates that in such areas a high density of EVs may reduce distribution

transformer life unless EV charging is managed adequately. A separate study concludes that depending upon charging condition, EV charging may have both positive and negative effects on transformer aging [20]. An increased peak load demand may decrease transformer life expectancy; however, if EVs are primarily charged during off-peak hours, a flatter load profile could reduce the daily expansion and contraction of the transformer, resulting in a positive effect on transformer's life. In another study [86], authors evaluate the impacts of EV loads on distribution transformers and conclude that the existing distribution assets are able to support a number of electric vehicles without resulting in any adverse impacts.

3.4.1.3 EV Load Impacts on Distribution Power Quality

EV charging is also likely to cause power quality problems in the distribution circuit including, but not limited to undervoltage conditions, power unbalances, voltage and current harmonics. As the number of EVs increases so is the electricity demand required to charge their batteries. An EV load being charged by a Level-2 charger can almost double the peak load demand of the homeowner [6]. The increased load demand due to EVs leads to additional voltage drops in the secondary service voltages, thus affecting the service voltage quality.

Several studies have been conducted to evaluate the impacts of EV charging on distribution voltages. The existing methods simulate multiple representative EV charging scenarios and project the potential impacts of EV charging using distribution circuit analysis tools. For example, [32] evaluates the impacts of the additional demand due to EV charging on system power losses and voltage deviations. The study further recommends using a controlled charging

method to mitigate the EV charging impacts. In [33], the impacts of quick EV charging on the power distribution system particularly on power system harmonics are evaluated and the maximum EV penetration level while avoiding serious harmonic impacts is determined. Furthermore in [35], the impacts of EV integration on the power system loading and voltage profile are evaluated and the benefits of several charging scenarios i.e. dumb charging, timed charging, and controlled charging on service voltage quality are quantified. Similarly, [36] investigates the effects of EV charging on distribution voltages, line drops, and system losses and [37] evaluates EV impacts particularly on voltage limits, power quality, and power imbalance. In [4–7], several circuit parameters, both at local and global level affecting distribution voltages during EV charging are evaluated. Based on the analysis, it is concluded that that a large-scale EV deployment could violate recommended limits for secondary wire voltages and might result in voltage unbalance. Another study uses actual measurements and survey data to determine EV charging characteristics including feeder load demand, EV charging starting time, battery state-of-charge (SOC), and proposes a stochastic approach to analyze the impacts of EV charging [39]. A Monte Carlo approach to evaluate the impacts of EV charging on feeder voltage quality including under/over voltages and voltage imbalances is proposed in [40]. Ref. [41] presents a comparative analysis on EV charging impacts of typical NA and EU distribution circuits.

Since maintaining an appropriate voltage level for residential customers is a matter of prime importance for utility companies, a detailed analysis of the impacts of EV charging on distribution voltages is required. In Section 3.5, we present our approach to evaluating the voltage quality impacts of EV loads on residential customers.

3.4.2 Time-of-Use (TOU) Pricing to Mitigate EV Load Impacts

The EV impacts analysis concludes that EV load charging during peak load hours can lead to undesirable grid impacts, such as an increase in the peak load demand and undervoltage conditions, thus necessitating the grid expansions. Thus, an uncontrolled charging of EV loads can limit the percentage penetration of EV loads into the distribution grid [4–7, 27–41]. To avoid EV charging during peak load hours, utility companies deploy a TOU pricing structure. In a TOU scheme, the electricity usage are rated differently during peak and off-peak hours (lower rate), which motivates the customers to utilize the electricity generated during off-peak hours [43–45]. The schedule to begin peak and off-peak rates in a TOU scheme is referred to as a TOU schedule. In [45], the customer’s response to time-varying rates for EV charging is investigated. The study aimed to understand the behavior and choices of EV customers to different EV tariff structures. The study concluded that EV customers were responsive to TOU prices, and most of the EV owners programmed their vehicle to charge during the off-peak tariff periods. Therefore, TOU pricing can successfully stimulate EV charging during off-peak hours and flatten the demand profile [43–45].

Implementing TOU pricing is a useful demand-side management scheme. However, if while designing the TOU schedule the total demand and load profile of EV load is not taken into consideration, the effects of EV charging under a TOU schedule might get worse [46–48]. The reduced electricity rates during off-peak hours may result in simultaneous charging of multiple EV loads causing an even higher increase in peak load demand and thus larger additional voltage drops. To date, the implemented TOU schemes do not consider EV loads while setting up the TOU schedule. This calls for the development of an

optimal TOU schedule that considers the EV load demand and thus minimizes the effects of EV load charging.

An optimized TOU schedule taking EV load demand into consideration is developed in [48]. The paper proposed an approach to minimize peak value and peak-valley difference of the load demand. However, the proposed TOU structure in [48] does not take the convenience of EV owners into consideration. An optimal TOU schedule that benefits both utility companies and customers while taking EV charging into consideration is developed and presented here [8]. The objective is to develop a practical approach for setting up a TOU schedule based on customer load demand, EV charging demand, and service transformer loading constraint. The selected time to begin off-peak rates in a TOU scheme should minimize the effects of EV charging on the secondary service voltages while ensuring that EVs are fully charged by 7 am (worst case), thus maximizing grid and customer benefit simultaneously. The analysis suggests that the optimal time to begin off-peak rates is between 11 pm and 12 am, but no later than 12 am [8].

3.4.3 Smart Charging Algorithms to Mitigate EV Load Impacts

The TOU pricing structure that essentially aims to minimize the EV loading during peak load hours by shifting the EV demand to off-peak hours is not an optimal solution for significantly higher levels of EV penetration. Under TOU pricing, the simultaneous charging of several EV loads can create a second peak in load demand, during off-peak hours [46]. The second peak will essentially limit the number of EVs that can be included in the distribution circuit. It should be noted that even after implementing TOU rates, a significant amount of power system capacity remains underutilized. This is because

in the TOU pricing scenario all EV loads begin to charge simultaneously at the beginning of off-peak rates. The power system could be utilized more efficiently if the EV charging rate and time are controlled to optimize a desired grid objective [49,50]. The grid objective could be, including, but not limited to, flattening the overall load shape profile, minimizing the charging cost, or minimizing power losses. This calls for the development of smart charging algorithms aiming to accommodate a higher percentages of EVs into the grid without causing any negative impact on the distribution feeders.

Given the potential benefits of the smart charging scheme, several articles [51–68] have addressed the problem and have proposed algorithms to determine the EV schedule while optimizing for a given grid objective. The objectives are primarily divided into two categories, maximizing utility benefits and maximizing the benefits of EV owners.

3.4.3.1 Controlled EV Charging - Maximize Utility Benefits

Several articles sought to address the first objective, i.e. maximizing utility benefits are summarized as follows. To maximize utility benefits, an aggregator is generally deployed by the utility and the decision for EV charging rate and time is made based on the current load demand or electricity pricing level. For example, Clement et al. [51] proposed a coordinated charging scheme to minimize system power losses. The authors proposed a dynamic programming algorithm to determine the EV charging profiles for each EV load, under both deterministic and stochastic setting. An EV charging strategy is proposed in [52] while aiming to minimize the peak load demand. Both local and global control strategies based on quadratic programming are proposed to control EV load charging based on the local load information and overall global load

information, respectively. Sortomme et al. [53] established the relationship between feeder losses, load factor, and load variance and formulated several optimal charging algorithms to minimize the impact of EVs on the distribution system. A real time EV charging control strategy aiming to minimize the total electricity generation cost and associated grid energy losses is proposed in [54]. Furthermore, [55] proposes a demand response strategy to decrease the potential impacts of new load peaks created by EV integration while minimizing the infrastructure investments. Also, in [56] the authors propose a different demand response (DR) strategy to accommodate EV charging while keeping the peak demand unchanged, thus maximizing the grid usage. In [57], authors aim to flatten the total load demand and formulated the optimal EV charging scheduling problem as a discrete optimization problem. In [58] and [59], the optimal charging control for EVs is achieved by optimizing the energy usage of the distributed EVs for V2G frequency regulation services. In [60] a near real-time algorithm while taking the dynamic nature of EV charging demand into account is proposed. The EV charging problem is formulated as a receding horizon optimization problem while taking the transformer and line capacity limits, phase unbalance, and voltage stability constraints into account. Ref. [61] proposes another receding-horizon optimization approach to obtain EV charging schedule while including the future EV penetration into the algorithm. Authors claim that the proposed approach, after including future EV deployments, results in a flatter demand profile and better demand-side management.

3.4.3.2 Controlled EV Charging - Maximize Customer Benefits

In a TOU/real-time electricity market, EV charging rate and time can be controlled to follow the TOU/real-time rate structure, thereby minimizing the cost of EV charging for the EV owners. Several researchers have utilized this property and have proposed controlled charging techniques by actively adjusting the EV charging rate and time based on a real-time electricity market, thus maximizing benefits for the EV customers. For instance, a control model for EV charging based on real-time electricity price information is introduced in [62]. In [63], a quadratic programming technique is used to optimize the charging-discharging process such that the charging cost is minimized while maximizing the discharging profit. A heuristic method is proposed in [64] to control the EV charging rate and time in response to the TOU pricing schedule. A real time V2G control algorithm with price uncertainty is proposed in [65], aiming to maximize the profit to each EV owner. The profit includes the payment received by the EV owners from the utility company for selling power minus the cost of purchasing power from the grid. In [66], both global and local optimal EV control strategies are proposed while aiming to minimize the total cost of electricity paid by EV owners for EV charging. Similarly, [67] solves the EV charging scheduling problem by jointly maximizing the aggregator's profits and EV owner's costs. A linear programming based optimal control strategy is proposed for the static charging scenario while a heuristic is developed for the dynamic scenario. In [68], the customer benefits are maximized by optimizing for the local grid level constraints. The authors propose an EV charging strategy targeting to deliver the maximum amount of energy to the EV loads while maintaining the circuit parameters (substation demand and feeder voltages) within the specified limits.

The proposed smart charging algorithms in literature have a few limitations. By optimally scheduling EV charging rate and time to maximize utility benefits, the proposed algorithms ignore customer inconvenience. Additionally, many utilities do not implement real-time price for the residential customers thus rendering the optimal EV charging methods to maximize EV customers' charging benefits inapplicable. In Section 3.8, we propose a controlled charging algorithm aiming to minimize voltage variations during EV charging thus resulting in a flat voltage profile at each EV customer location. The proposed algorithm takes EV charging start and end time as a user input thus avoiding customer inconvenience and obtains an optimal EV charging schedule while minimizing the voltage impacts of EV charging.

3.5 Evaluation of the Impacts of EV Charging on Utility Distribution System

In the following section, we present our approach to evaluate EV load impacts on the distribution circuit, primarily focusing on the voltage quality issues of integrating EVs into the system. The analysis first aims to identify several factors affecting distribution voltage quality while EV loads are charging. This is done by simulating several EV deployment scenarios at local secondary circuit and global distribution circuit level [4–6]. The local circuit analysis aims to understand the effects of EV load charging at the local distribution circuit level. The objective is to evaluate several distribution circuit parameters that can potentially affect the distribution circuit voltage quality. Using this analysis, utilities can determine potential conditions leading to poor voltage quality and can take specific mitigating actions for the customers most susceptible to EV charging impacts. The local level effects will

be evaluated at both secondary and primary voltage levels. Next, large-scale EV deployment scenarios are simulated to analyze EV integration impacts on overall distribution voltage quality [7]. The analysis is termed global circuit analysis and is conducted to understand the EV charging effects on a larger scale. This analysis will help to understand the EV capacity of distribution circuit, helping in planning, expanding or forming strategic policies concerning the distribution circuit. For example, based on identified most affected areas, utilities can find out an optimal location to deploy distributed energy storage units or distributed generation plants to mitigate the impacts. The details regarding the simulation method and impact analysis can be found [5].

3.5.1 Preparing the Distribution Circuit

This study is performed using two typical real-world 13.8-kV radial distribution circuits, one serving predominantly 120/240V single-phase three-wire residential loads, and the other service both single-phase residential and three-phase commercial loads. The selected real-world 13.8-kV radial distribution circuit serving predominantly 120/240V single-phase three-wire residential loads is shown in see Figure 3.23. The distribution circuit has approximately 7,000 buses and supplies over 13,000 devices, where a majority of the customer loads are single-phase. For the analysis, a complete electrical model of the distribution circuit from the substation down to individual customer loads including three-phase transformers, three-phase primary, laterals, secondary networks, and service transformers is specified in the three-phase steady-state load flow model. A daily load shape profile for all secondary network loads is generated and assigned using load demand data measured at the substation and the stratified billing rates. The EV loads are modeled as a constant power

load with an associated load shape. Load shapes of EV loads are then generated based on the temporal diversity in EV load charging patterns and the characteristics of the EV charging station. The study presented herein is carried out for Level-2 EV chargers with power ratings of 3.84-kW (240V/16A) and charging efficiency of 90% charging a 16-kWh EV battery. To evaluate the impacts of EV loads on the distribution voltages, three-phase load flow analysis with consideration to the load shape profile of EV loads and conventional loads is performed for a day at every 15-minute time interval. Finally, the EV load effects both at the local and global secondary circuit level are evaluated.



Figure 3.23: One line diagram of the residential distribution circuit (Courtesy of the electric utilities).

3.5.2 EV Load Impacts at Local Circuit Level

Several factors affecting the primary and secondary service voltage quality due to EV charging are identified and evaluated. A detailed summary of various potential factors that could affect voltage quality is presented in Tables 3.3 and 3.4.

Table 3.3: Summary of effects of EV charging on the primary wire (the selected secondary circuit has EV loads equivalent to 50-100% of residential loads)

Circuit parameters under evaluation	Different conditions evaluated for	Short-circuit capacity (MVA)		Largest additional voltage drop in the	
		Primary Wire	Secondary Wire	Primary Wire	Secondary Wire
Location of the service transformer w.r.t the substation	Remote from the substation	42.5	0.174	0.13%	4.41%
	Nearby the substation	240	0.178	0.023%	4.32%
Comparison of short-circuit capacity	Primary Wire	Higher short-circuit capacity at the primary wire of the nearby service transformer			
	Secondary Wire	Comparable short-circuit capacities at the load node of both secondary services (remote/nearby)			
Comparison of additional voltage drop	Primary Wire	Essentially experience very minor voltage drops during EV charging (0.13% vs. 0.023%)			
	Secondary wire	Comparable secondary service voltage drops are recorded at both locations of the service transformer (remote/nearby)			

Fortunately, the most severe voltage drop occurs at the EV load node itself. Other non-EV load nodes are not impacted unless they lie along the path of the EV charging current. It has been observed that EV loading does not cause a significant additional voltage drop in the primary wires. However, the secondary service voltages are affected more significantly due to EV loading.

Table 3.4: Summary of effects of various factors evaluated on the secondary circuit supplied by a single-phase service transformer (One EV load)

Circuit parameters under evaluation	Different conditions evaluated for	Largest voltage drop		Condition for the largest voltage drop
		Residential circuit	Mixed circuit	
Location of the service transformer w.r.t the substation	Remote from the substation	1.7%	1.65%	Comparable voltage drop (comparable short-circuit capacity)
	Nearby the substation	1.69%	1.64%	
Location of the EV load w.r.t. the service transformer	Remote from the service transformer	1.7%	1.65%	EV load is remote from the service transformer
	Nearby the service transformer	0.8%	0.14%	
Size of the EV load	240V/16A	1.7%	1.65%	EV load of size 240V/30A
	240V/30A	3.24%	3.14%	
An EV load added adjacent to an existing EV load	One EV load	1.7%	1.65%	Additional EV load increases the voltage drop
	One + One EV loads	3.2%	2%	

The key observations drawn from the analysis are as follows:

1. EV loads result in more severe voltage drops in the secondary circuit as compared to the primary feeder. The short-circuit capacities at both remote (174 kVA) and nearby (178 kVA) secondary circuits are relatively low, thus resulting in significant additional voltage drops at both locations while EV loads are charging. On the other hand, the short-circuit capacities at the primary distribution circuits, both remote (240 MVA) and nearby (42.5 MVA), are too high for EV loads to significantly affect the voltage profiles.
2. It has been observed that two similar secondary circuits possess approximately the same short-circuit capacity at their load nodes (120V/240V) irrespective of their relative locations from the substation, i.e., nearby

(178 kVA) or remote (174 kVA) from the substation. This results in approximately equal additional voltage drops due to EV load charging for both locations of the secondary service.

3. An EV load within the secondary circuit at the farthest load node from the service transformer causes a greater voltage drop than the case when the EV load is located at the load node closer to the service transformer. The difference in the largest additional voltage drop depends upon the short-circuit capacity measured at the respective load nodes. The lower the short-circuit capacity, the higher the additional voltage drop.
4. The voltage drop due to a 240V/30A EV load is approximately double that of a 240V/16A EV load. Also, an EV load added adjacent to an existing EV load worsens the voltage quality of the secondary circuit under evaluation.

3.5.3 EV Charging Impacts at Global Circuit Level

The effects of increasing EV penetration on the distribution circuit voltages are summarized in Table 3.5. The largest additional voltage drops for the primary wires are recorded for different percentages of EV penetration. The number of EV loads per secondary service is increased from 1 to 4. Mean and standard deviation of the distribution of additional voltage drops recorded at various primary wires are also reported. The largest additional voltage drop increases with the increase in the number of EV loads. It should be noted that the EV charging time coincides with the duration of peak load hours for the secondary loads. Also, to evaluate the worst case condition, all EVs are assumed to be charging simultaneously.

The effects of the EV load clustering on the primary wire voltages are

Table 3.5: Effects of increasing EV penetration on the primary wire voltages

Total number of EV loads	Percentage voltage drop recorded for 13.8 kV primary wires			
	Additional loading due to EV (%)	Largest additional voltage drop	Mean value	Standard deviation
669	35.27%	1.35%	0.95%	0.24%
1338	71.13%	2.77%	1.95%	0.51%
2007	107.77%	4.25%	3.04%	0.80%
2676	144.92%	5.7%	4.19%	1.09%

summarized in Table 3.6. The analysis suggests that the clustering of EV loads leads to an imbalance in the three-phase power demand. As a result, one of the phases (Phase C, in this case) of the primary wire records an increase in the supply voltage (also shown in Table 3.6). Again, all EVs are charging simultaneously and the charging time coincides with the secondary service peak load hours. Based on the analysis the following observations are made:

Table 3.6: Effects of EV load clustering on the primary wire voltages

Total number of EV loads	Effects on the primary wire voltages		
	Additional loading due to EV load (%)	Largest additional voltage drop	Largest increase in service voltage (Phase C)
22	1.16%	0.45%	0.22%
44	2.33%	0.88%	0.45%
66	3.52%	1.35%	0.68%
88	4.75%	1.81%	0.91%

1. The primary of service transformers farther away from the substation tends to experience more severe additional voltage drops. Load nodes in secondary services supplied by these transformers experience much

higher additional voltage drops than those experienced at the primary of the transformers. Hence, the secondary services farther away from the substation are of prime concern for the utilities in terms of voltage quality problems due to EV loads.

2. Higher EV penetration results in a higher additional voltage drop at the primary wire.
3. As for EV load clustering, the largest additional voltage drop increases significantly for the primary phase supplying for the EV load clusters. Further, clustering of EV loads causes an imbalance in the load demand which may result in voltage increase in one or both of the other phases.

3.6 Infrastructural Upgrades to Mitigate EV Load Impacts

It has been shown in the previous section that EV charging has considerable effects on the secondary service voltages and the service transformer load demands. This calls for the evaluation of effective mitigation actions addressing the effects of EV charging. This section evaluates the mitigation of EV charging impacts by upgrading the distribution system infrastructure. The mitigation schemes evaluated are increasing the kVA rating of the service transformer, and reconfiguring the secondary circuit using an additional service transformer. The analysis is conducted using the 13.8-kV residential distribution circuit, shown in Figure 3.23. The impacts of EV charging on feeder voltages before and after implementing the mitigation schemes are compared.

It has been observed that increasing the kVA rating of the service trans-

former although mitigates the transformer load demand concerns; it results in a negligible decrease in the feeder voltage drops. The largest additional voltage drop due to EV load charging decreases significantly on reconfiguring the secondary circuit by adding an additional service transformer. Adding a service transformer and reconfiguring the secondary circuit, however, require additional infrastructural expenses.

3.6.1 Increasing Size of the Service Transformer

This section summarizes the effects of increasing the size of a service transformer on the secondary service voltage drops during EV load charging. The secondary service served by a 50 kVA service transformer remote from the substation is selected for the analysis. The secondary service is populated with four 240V/16A EV loads. The kVA rating of the service transformer is increased to three times of its nominal value in the steps of 10 kVA. A comparison of the largest additional voltage drops recorded in the secondary circuit with respect to the size of service transformer is shown in Figure 3.24. The largest additional voltage drops due to EV charging decreases only by approximately 0.2% when service transformer rating is increased to thrice its nominal rating. Based on the analysis, increasing the size of a service transformer does not significantly improve the secondary service voltage quality.

3.6.2 Reconfiguring the Secondary Circuit by adding an Additional Service Transformer

The effects of reconfiguring the secondary circuit by adding an additional service transformer in mitigating the secondary circuit voltage drop concerns are evaluated in this section. A 50-kVA service transformer supplying five

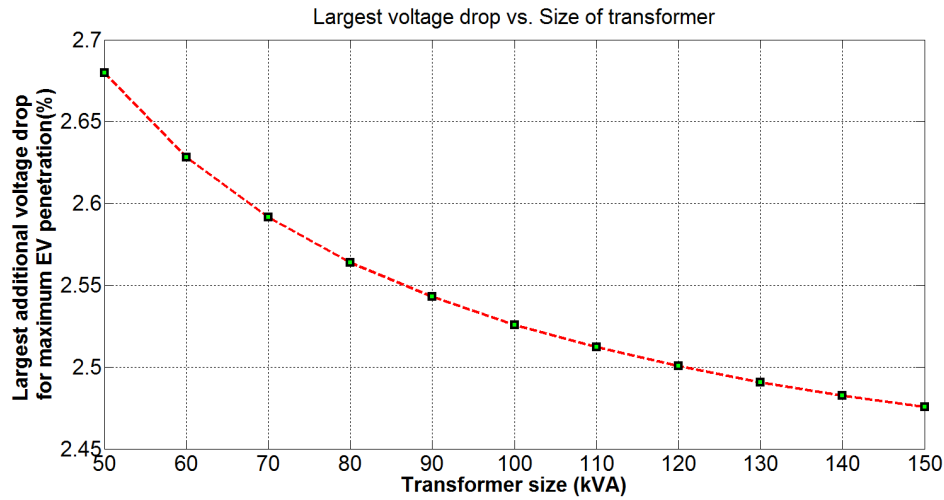


Figure 3.24: Largest additional voltage drop recorded in secondary circuits populated with four EVs with respect to the size of the service transformer

secondary loads is selected for the study (Figure 3.25). The circuit is loaded with four EV loads and the largest additional voltage drop due to EV load charging is recorded. This is referred to as the base case in the following discussion.

An additional 50-kVA service transformer is added to split the secondary circuit into two circuits, as shown in Figure 3.26. The original transformer is now supplying two loads, and the new transformer is supplying the remaining three loads while each service transformer is supplying two EV loads. The voltage profile with and without the EV loads (at the load node) is recorded and compared to the base case. In order to validate further that the size of the transformer does not play a significant role in mitigating secondary circuit voltage, an additional case is simulated. The kVA rating of both transformers is decreased to 25-kVA, making their sum 50 kVA. The additional voltage drop in the secondary circuit is recorded with and without EV loads, with the same

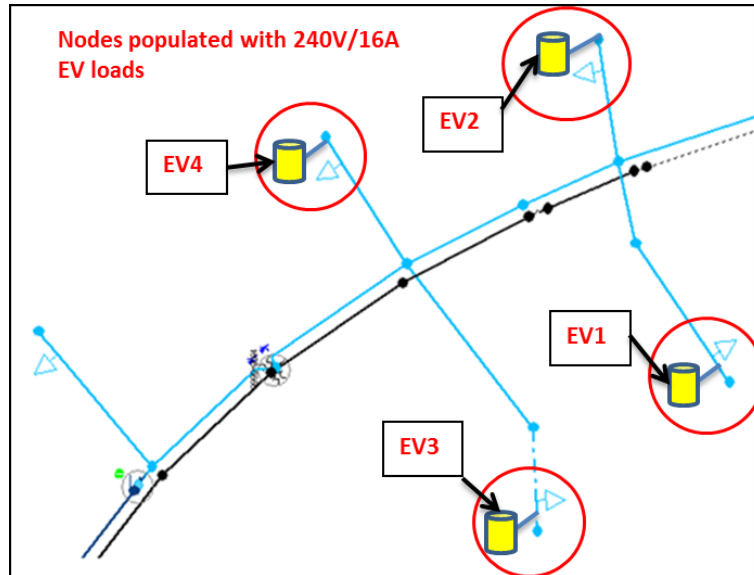


Figure 3.25: Secondary circuit selected for the analysis (Courtesy of the electric utilities).

arrangement of EV loads as in the base case. The results are summarized in Table 3.7.

It is observed that splitting and reconfiguring the secondary circuit using an additional service transformer significantly decreases the additional voltage drops due to EV load charging. Furthermore, the mitigation of secondary circuit voltage drops due to an additional service transformer depends upon its location; placing the additional transformer closer to the new secondary circuit results in a larger mitigation in the voltage drop concerns. The primary disadvantage of this method is the additional infrastructural cost incurred due to the additional service transformer, rendering the method expensive in terms of efforts and cost

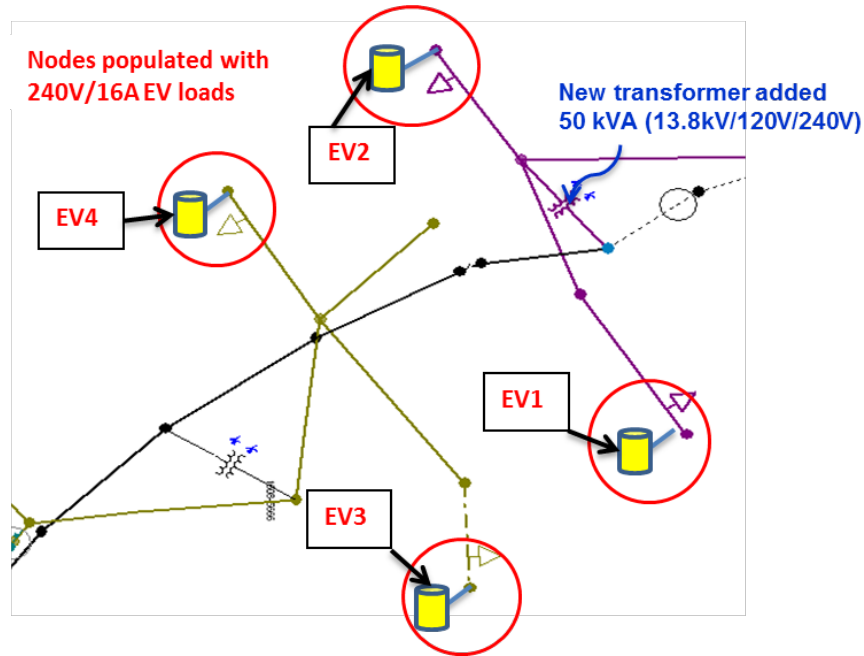


Figure 3.26: Secondary circuit selected for the analysis (Courtesy of the electric utilities).

Table 3.7: Effects of reconfiguring the secondary service using an additional service transformer

Number of EV load node	Largest additional voltage drop in the secondary circuit		
	Base case circuit	Case 1 - Splitting the circuit into two (using 50 kVA + 50 kVA transformers)	Case 2 - Splitting the circuit into two (using 25 kVA + 25 kVA transformers)
EV 1	3.2 V (2.61 %)	0.46 V (0.37 %)	0.62 V (0.49%)
EV 2	3.29 V (2.68 %)	0.54 V (0.43 %)	0.69 V (0.55 %)
EV 3	2.77 V (2.55 %)	1.77 V (1.57 %)	1.93 V (1.27%)
EV 4	2.32 V (1.88 %)	1.34 V (1.08 %)	1.51 V (1.21%)

3.7 Time-of-Use (TOU) Pricing to Mitigate EV Load Impacts

The infrastructural upgrades implemented to mitigate EV load concerns such as resizing/adding a service transformer and reconfiguring the secondary

circuit require significant efforts and cost. To avoid any unnecessary cost, utilities implement TOU pricing structure. TOU pricing encourages EV owners to charge their EVs during off-peak hours, thus flattening the load demand profile and reducing the additional voltage drops resulting from EV charging [43, 44].

A few studies have projected that if the off-peak rates in a TOU schedule are not set to an optimal time, the effects of EV charging can get worse [46–48]. This is because the reduced electricity prices during off-peak hours will result in the simultaneous charging of multiple EV loads and may result in an even higher increase in peak load demand and thus larger additional voltage drops. To date, utility companies do not consider EV loads while setting up the TOU schedule. This calls for the development of an optimal TOU schedule that considers the EV load demand and thus minimizes the effects of EV load charging.

In this section, we develop a practical method to set up an optimal TOU schedule that benefits both the utility and customers while taking EV charging into consideration. The aim is to develop a practical approach for setting up the time to begin off-peak rates in a TOU schedule so that the largest additional voltage drops and substation peak load demand are decreased while ensuring EVs are fully charged by 7 am, thus avoiding customer inconvenience. A summary of our evaluation approach and results are discussed in this section. Please refer to [8] for the detailed approach and results.

3.7.1 Simulated Charging Scenarios

The effects of time-controlled charging of the EV loads in mitigating voltage quality concerns are evaluated in this section. Various time-controlled

charging scenarios with EV charging beginning at different hours of the day are simulated. A 50-kVA service transformer remote from the substation is selected for the analysis. The secondary circuit supplied by the transformer is loaded with four EV loads. The analysis is performed for a 240V/16A Level-2 EV charger, with 20% SOC on the incoming vehicle. The EV load profile is specified by the charging scenario under evaluation. Various charging scenarios considered in this section and their evaluation parameters are summarized in Table 3.8. It should be noted that the charging scenarios specified in Table 3.8 are simulated for both a 24-kWh (Nissan Leaf [87]) and a 16-kWh (Chevy Volt [88]) EVs.

The unscheduled charging scenario represents the case when the TOU rates are not implemented and the starting time of EV charging is not scheduled by the utilities. Under this scenario, residential customers do not program their EVs to begin charging at a particular time. The PDF given in Figure 3.27 represents the uncertainty in the EV charger starting time for this case. Multiple Monte-Carlo runs are simulated by randomizing the EV chargers' starting times (using Figure 3.27). The largest increase in load demand and the largest additional voltage drops are recorded for each case. As mentioned in Table 3.8, 100 runs are simulated and the load flow results recorded for each case are averaged to obtain the voltage profile and the load shape profile for the unscheduled EV charging scenario.

Next, the time-controlled charging scenarios with simultaneous starting of EV loads are simulated for different hours. The start time of EV charging is varied in the range of 8 pm to 3 am and all EVs are assumed to begin charging simultaneously at that hour. The largest increase in load demand and the largest additional voltage drop for each case is recorded individually

Table 3.8: Various charging scenarios simulated for both 24-kWh and 16-kWh EV battery loads charged using a 240V/16A EV charger

Charging scenario	Probability Density Function (PDF) for EV charging starting time	Number of Monte Carlo runs
Unscheduled charging	Gaussian distribution with mean at 8 pm (Figure 3.27)	100 runs
Simultaneous charging at 8 pm, 10 pm, 11 pm, 12 am, 1 am, 2 am, and 3 am	No PDF, all EVs start charging at the same time	Not required (there is no randomness in starting time)
Randomized charging at 8 pm, 10 pm, 11 pm, 12 am, 1 am, 2 am, and 3 am	Positive half of Gaussian distribution with mean at the time of the controlled charging (Figure 3.28)	100 runs

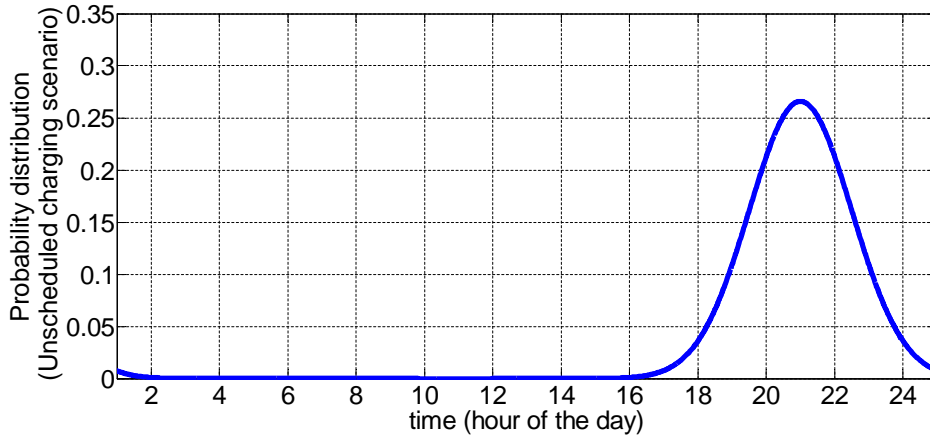


Figure 3.27: Probability Density Function for EV charger starting time (unscheduled starting time)

and reported for the comparison.

To make the analysis of time-controlled charging of the EV loads more general, randomness is added to the EV charger start time. Multiple cases are simulated by shifting the EV charger start time to different hours of the day, ranging from 8 pm to 3 am. For each hour, multiple Monte-Carlo runs

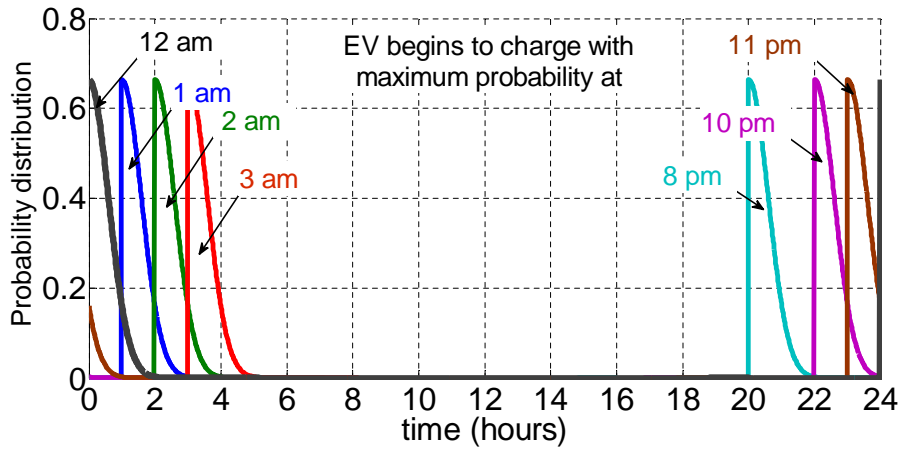


Figure 3.28: Probability Density Function for EV charger starting time (randomized starting time)

are simulated by randomizing the EV chargers' start times using the PDF for that hour (Figure 3.28). The largest increase in load demand and the largest additional voltage drops are recorded for each case. The load flow results corresponding to multiple Monte-Carlo runs are averaged to obtain the voltage profile and load shape profile for the randomized charging scenario beginning at a particular hour. The process is repeated for different hours ranging from 8 pm to 3 am.

3.7.2 Results and Discussions

Table 3.9 represents the additional voltage drop and the increase in peak load demand recorded on charging EV loads under the unscheduled charging scenario. Clearly, a significant voltage drop is recorded when the starting time for EV load charging is not scheduled. Note that the analysis is done for both 24 kWh (Nissan Leaf [87]) and 16 kWh (Chevy Volt [88]) EVs. A 24 kWh EV load requires around 6 hours 30 minutes, while a 16 kWh EV

load requires around 4 hours to fully charge from 20% state of charge (SOC) using a 240V/16A charger. This is the minimum SOC generally allowed by EV manufacturers [69].

Table 3.9: Characteristic of secondary circuit for unscheduled starting time

EV battery size	EVs fully charged by	Increase in peak load demand (kW) due to EV charging	Largest additional voltage drop
24 kWh	6 am	12.6 kW	4.7 V (3.9%)
16 kWh	3:30 am	11.4 kW	4.2 V (3.5%)

Next, the results for various ‘time-controlled charging scenarios’ simulated for both 24-kWh and 16-kWh EV loads are discussed. For both 24 kWh and 16 kWh EV loads, the increase in peak-load demand decreases as the starting time of EV charging is shifted to the off-peak load hours, i.e. to any time after 8 pm. A second peak in load demand is seen when the starting time of EV loads is shifted to any time after midnight. However, the second peak recorded for any of the time-controlled charging scenarios is not as significant as that due to EV charging under the unscheduled charging scenario. As the start time of EV charging is shifted from 8 pm to 3 am, the largest additional voltage drop decreases. Also, when the starting time of EV charging is 1 am or 2 am, no additional voltage drop is recorded in the secondary circuit. Note that, all EV loads might not be fully charged in the morning upon shifting the EV charging starting time to any time after midnight. The merits and drawbacks of few time-controlled charging scenarios are presented in Table 3.10.

Note that the optimal time to begin off-peak rates should minimize the effects of EV charging on secondary service voltage drops while ensuring EVs are fully charged by 7 am. Clearly, the time-control scenario should at least

Table 3.10: Characteristic of secondary circuit for unscheduled starting time

Charging begins at	Merits	Drawbacks
8 pm	Both 24-kWh and 16-kWh EVs are fully charged before 7 am	The largest additional voltage drop increases and is 0.6% more than the unscheduled charging case.
11 pm	Both 24-kWh and 16-kWh EVs are fully charged before 7 am and the increase in the peak load demand and the additional voltage drop is less than the unscheduled charging case (24-kWh/16-kWh).	The increase in the peak load demand and an additional voltage drop in the secondary service is still significantly high.
12 pm	All 16-kWh EVs are fully charged before 7 am. Also the additional voltage drop decreases significantly	24-kWh EVs might be charged to only 90% before 7 am if randomness is assumed in the EV charger starting times.
1 am	No additional voltage drop is recorded.	24-kWh EVs are not fully charged before 7 am

be an improvement upon the ‘base case’ (unscheduled starting time) in terms of the largest additional voltage drop and increase in the peak load demand.

Based on the observations the optimal time to begin off-peak rates in a ToU pricing scenario is established. The analysis suggests that the optimal time to begin off-peak rates in a ToU pricing scenario is as early as 11 pm, but no later than 12 am (midnight). If EV charging were to begin at these hours the effects of EV charging on the secondary service voltage drop would be minimal while ensuring that EVs are fully charged by 7 am.

3.7.3 Optimal Time to begin Off-peak rates in a TOU Scheme

The analysis suggests that the optimal time to begin off-peak rates in a TOU pricing scenario is between 11 pm and 12 am (midnight) [8]. Note that a 24-kWh EV load requires around 6 hours 30 minutes, while a 16-kWh EV

load requires around 4 hours to fully charge from 20% SOC using a 240V/16A charger. The off-peak rates should begin at a time such that the effects of EV charging on the secondary service voltages and load demands are minimized while ensuring EVs are fully charged by 7 am. Since, a 24-kWh battery takes a longer time to recharge, the best time to begin off-peak rates will mainly depend upon the 24-kWh EV loads.

The impacts of TOU schedule beginning at 11 pm and 12 am on the 24-kWh EV loads are detailed here. Figure 3.29 and Figure 3.30 show the load shape profiles and voltage profiles when four 24-kWh EV loads are charging under TOU schedules beginning at 11 pm and 12 am. Upon starting off-peak rates at 11 pm, and assuming there are four 24-kWh EVs (each is equipped with a 240V/16A charger) in a given secondary service, and that most EV owners would program their vehicles to start charging at or soon after 11 pm, a largest additional voltage drop of 1.8 V (1.5%) is recorded with an increase in peak load demand of approximately 4 kW. Furthermore, on beginning off-peak rates at 11 pm, all 24-kWh EVs with an initial SOC of 20% are fully charged by 7 am. If off-peak rates begin at 12 am and most EV owners program their vehicles to start charging at or soon after 12 am, no increase in peak demand and no additional voltage drop are recorded in the secondary circuit; however, in this case, 24-kWh EV loads that begin to charge after 12:30 am with an initial SOC of 20% are only charged up to 90% by 7 am.

TOU pricing scheme is a popular method of implementing time-controlled charging of EV loads. The optimal time selected to begin off-peak rates should minimize the effects of EV charging while ensuring EVs are fully charged by 7 am, thus optimizing both grid and customer benefits. Based on our analysis, we conclude that the optimal time to begin off-peak rates is between 11 pm

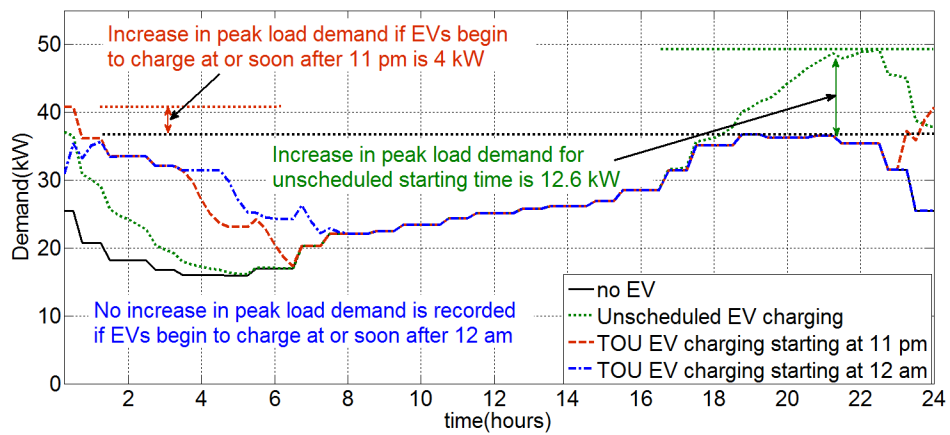


Figure 3.29: Load shape profiles with off-peak rates beginning at 11 pm and 12 am (24-kWh EVs)

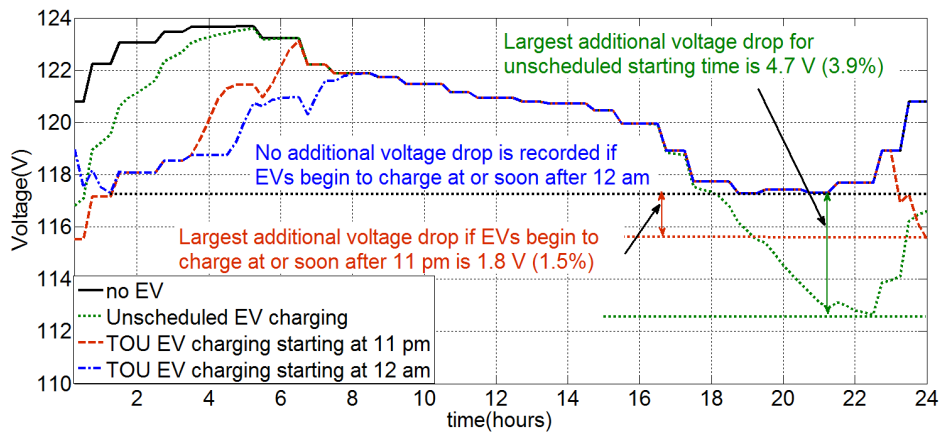


Figure 3.30: Voltage profiles with off-peak rates beginning at 11 pm and 12 am (24-kWh EVs)

and 12 am (midnight). Furthermore, we also demonstrate that scheduling off-peak rates at 11 pm or 12 am is a trade-off between secondary service voltage quality and customer satisfaction.

3.8 Smart Charging Algorithm

A TOU pricing structure can successfully shift EV charging to off-peak load hours, thus mitigating the EV charging impacts on peak load demand and secondary voltage drops. The simultaneous charging of a large number of EV loads under a TOU schedule, however, may result in a second peak in the load demand during off-peak hours [46]. The second peak can essentially limit the number of EVs that can be accommodated into the distribution circuit. It is observed that even after implementing TOU rates, a significant amount of power system capacity remains underutilized. Several studies conclude that the direct control of EV charging rate and time using a smart charging algorithm may help in utilizing the power system more efficiently. An optimal EV charging schedule can be obtained by optimizing for a desired grid or customer objective. Several articles [51–68] have proposed smart charging algorithms to directly control EV charging schedule while aiming to either maximize utility benefits or EV customers' benefits. The utility benefits are maximized by optimally shifting EV load demand to off-peak hours. As for customer benefits, methods are proposed to control EV charging while decreasing EV charging cost in a real-time electricity market. The smart charging methods proposed in the literature have certain limitations. By shifting EV charging to off-peak hours, the first approach ignores the convenience of EV owners. The second approach is limited in its application as many utilities still do not deploy real-time electricity pricing for the residential customers [89]. Furthermore, none of the methods directly aims to decrease EV charging impacts on the service voltages.

In this section, a smart EV charging algorithm while aiming to minimize the voltage quality impacts of residential EV chargers is proposed [9]. The al-

gorithm aims to find an optimal charging schedule for each EV in the system by locally minimizing the voltage variation at each EV load node, thus flattening the service voltage profile. To avoid customer inconvenience, the algorithm takes customers' inputs regarding EV charging start and end times. Since the secondary wire voltage drop is observed due to an increase in the load demand during EV charging, minimizing voltage variations optimally shifts the EV load demand to off-peak load hours, thus mitigates both voltage quality and service loading impacts of EV charging. Simulation results conclude that the proposed controlled charging method is efficient in mitigating both voltage drop and transformer loading concerns, even when 100% of residential loads are deployed with EV loads. Additionally, it is demonstrated that the proposed method helps in efficiently utilizing the distribution grid when compared with EV charging scenario under TOU schedule.

3.8.1 Problem Formulation

The problem is formulated as an optimal control problem aiming to minimize daily voltage variation by controlling the daily EV charging profiles. The voltage deviation is measured as the difference between the base voltage (1 p.u.) and voltage at each EV load node, over a day, as shown in (3.16). The mathematical formulation for the problem statement is given as follows.

Let there be M electric vehicles connected to a distribution circuit, with battery capacity E_i where $i \in \{1, \dots, M\}$. The battery content of each vehicle is represented by $Q_i(t)$. The battery content at any time depends upon the EV charger power level. Let EV charger power levels be represented by variable $P_i(t)$. The target is to minimize the overall voltage variability in the secondary

wires supplying for the EVs. The voltage variability is given by

$$V_{var}(t, \mathbf{Q}(t), \mathbf{P}(t)) = \sum_{i=1}^M (1 - V_i(t, \mathbf{Q}(t), \mathbf{P}(t))) \quad (3.16)$$

where,

$$\mathbf{Q}(t) = \begin{bmatrix} Q_1(t) \\ \vdots \\ Q_M(t) \end{bmatrix} \text{ battery content of each EV at time } t,$$

$$\mathbf{P}(t) = \begin{bmatrix} P_1(t) \\ \vdots \\ P_M(t) \end{bmatrix} \text{ EV charger power level at time } t, \text{ and}$$

$V_i(t, \mathbf{Q}(t), \mathbf{P}(t))$, is per unit voltage at time t and at the node supplying for i^{th} EV, when battery states are given by $Q(t)$ and charging power given by $P(t)$.

The proposed controlled charging algorithm is formulated as an optimal control problem, where, $V_{var}(t)$ defines the cost function, and $Q(t)$ corresponds to the state variable which evolves as per the control variable $P(t)$. The objective is to minimize $V_{var}(t)$ over time $t \in (0, T)$, by optimizing the EV charger power levels and ensuring the batteries are completely charged at the end of the charging period ($t = T$), where charging begins at $t = 0$. The cost function is defined as the following:

$$J = \int_0^T V_{var}(t, \mathbf{Q}(t), \mathbf{P}(t)) dt \quad (3.17)$$

Next, the optimal control problem for the proposed controlled charging of EV is formulated as follows:

$$\min(J) = \min \left(\int_0^T V_{var}(t, \mathbf{Q}(t), \mathbf{P}(t)) dt \right) \quad (3.18)$$

Subject to

$$\dot{Q}_i(t) = P_i(t) \quad \forall i \in \{1, \dots, M\} \quad (3.19)$$

For optimal control problem, the control variable $P_i(t)$ should be bounded and integrable. Therefore, the control variable is defined as:

$$0 \leq P_i(t) \leq P_i \quad \forall i \in \{1, \dots, M\} \quad (3.20)$$

where, P_i is peak charging power of the charger supplying for i^{th} EV.

Next, we will define the initial and terminal conditions for the state variable $Q_i(t)$. The initial time is taken as zero and initial and final conditions for the battery content for M vehicles are given as following.

$$\begin{aligned} Q_i(0) &= Q_{i,0} & \forall i \in \{1, \dots, M\} \\ Q_i(T) &= E_i & \forall i \in \{1, \dots, M\} \end{aligned} \quad (3.21)$$

where

$Q_{i,0}$, is the initial battery content of the i^{th} EV when plugged in for charging, i.e. at $t = 0$.

E_i , is the battery capacity of the fully charged i^{th} EV, at time T (specified by EV owners).

$(0, T)$ is the charging period.

3.8.2 Proposed Methodology

This section describes the methodology to solve the EV charging problem formulated in the previous section. Since the battery charger power level could only be varied in some discrete steps, the optimal control problem is discretized. Further, the load flow solution to calculate the voltage variability is also executed in discrete time steps, so a discrete optimization model is more practical.

Here, the discrete version of proposed EV charging problem is solved using dynamic programming. The EV charging period $(0, T)$ is discretized in 15 min intervals, resulting in T time stages equal to the number of hours EVs are charging multiplied by 4. Since the EV charging study is conducted for residential chargers, EV charging hours are from 6 pm to 6 am, resulting in $T = 48$ time stages. The battery contents of M EVs are discretized for T stages and the battery content of i^{th} EV at time t is given by $Q_{t,i}$. Also, the charging power level at a time step t for i^{th} EV is represented by $P_{t,i}$.

The optimal control problem for EV charging (3.18)-(3.21) formulated in previous section is discretized in this section (3.23)-(3.25). The discrete version of the controlled EV charging problem is expressed in a backward recursive formulation to be solved using dynamic programming approach. Let, $f_{t+1}(\mathbf{Q}_{t+1})$, represents the total optimal voltage variability measured from time period $t + 1$ to T .

$V_{var}(t, \mathbf{Q}_t, \mathbf{P}_t)$, is the voltage variability at time t with \mathbf{Q}_t battery content and \mathbf{P}_t EV charger power level.

$\mathbf{Q}_t = \begin{bmatrix} Q_{t,1} \\ \vdots \\ Q_{t,M} \end{bmatrix}$ is an M dimensional vector with each element $Q_{t,i}$ representing battery content for the i^{th} EV at time t .

$\mathbf{P}(t) = \begin{bmatrix} P_{t,1} \\ \vdots \\ P_{t,M} \end{bmatrix}$ is an M dimensional vector with each element $P_{t,i}$ representing EV charger power for the i^{th} EV at time t .

The possible values for charging power $P_{t,i}$ are also discretized and it is assumed that $P_{t,i}$ can take three values: P_i (charger working at peak charging power), $P_i/2$ (charger working at half its peak charging power), and 0 (charger is off). The discrete charging power results in R_i discrete values for EV battery

content ($Q_{t,i}$) at time t . R_i is given by (3.22), where P_i , is the peak charging power available at the charger supplying for the i^{th} EV.

$$R_i = \frac{E_i - Q_i^0}{P_i/8} \quad (3.22)$$

The problem formulation is given as follows:

$$f_t(\mathbf{Q}_t) = \min (V_{var}(t, \mathbf{Q}_t, \mathbf{P}_t) + f_{t+1}(Q_{t+1})) \quad t = 1, 2, \dots T \quad (3.23)$$

Subject to

$$\mathbf{Q}_t = \mathbf{Q}_{t+1} - \mathbf{P}_t \Delta t \quad (3.24)$$

$$\begin{aligned} Q_i^0 &\leq Q_{i,t} \leq E_i && \forall i \in \{1, \dots M\} \\ P_{t,i} &= \begin{cases} 0 \\ P_i/2, \\ P_i \end{cases} && \forall i \in \{1, \dots M\} \\ Q_{i,T} &= E_i && \forall i \in \{1, \dots M\} \end{aligned} \quad (3.25)$$

where

$Q_{i,0}$, is the initial battery content of the i^{th} EV when plugged in for charging. P_i is the peak charging power available at the charger supplying for the i^{th} EV.

Since state variable Q_t is an M dimensional vector, the ‘‘curse of dimensionality’’ arises in the dynamic programming formulation. This is avoided by sequentially solving for each electric vehicle charging profiles using dynamic programming technique successive approximation (DPSA) [49]. DPSA decomposes the multidimensional problem to a sequence of one-dimensional problems, each solving for optimal charge profile for an EV.

In the following section, the proposed controlled charging scheme is evaluated for its effectiveness in mitigating voltage quality issues. The results for

the controlled charging algorithm are compared against two cases: the uncontrolled charging scenario and the charging scenario with an optimal TOU schedule (off-peak rate beginning at 12 am).

3.8.3 Evaluation of the Proposed Charging Scheme

In the following section, the proposed controlled charging scheme is evaluated for its effectiveness in mitigating voltage quality issues. The analysis is first done for 16-kWh EV loads charged by Level-2 (240V/16A) chargers with a peak charging power (P_i) equal to 3.84 kW and 90% of charging efficiency. The initial (Q_i^0) and the final battery capacity (E_i) for each EV are 3.2 kWh (20% SOC) and 16 kWh (100% SOC), respectively. It is also assumed that each EV can start charging as early as 6 pm and must be fully charged by 6 am. Note that for all cases, the initial SOC of the vehicle is 20%. A more practical SOC for vehicles using travel statistics could be used, but since the objective of this section is to evaluate the proposed charging strategy, the starting SOC of the vehicle is irrelevant. Besides, using the minimum allowed SOC permits us to evaluate the charging strategies under the worst possible conditions.

The proposed algorithm is evaluated for its effectiveness in mitigating secondary circuit undervoltage concerns. The results for the controlled charging algorithm are compared against two cases: the uncontrolled charging scenario and the charging scenario with an optimal TOU schedule (off-peak rate beginning at 12 am). The three charging methods are compared for the number of EVs the selected distribution circuit can accommodate without violating the feeder undervoltage limit (< 0.95 pu). The number of EVs that can be accommodated by a given distribution circuit without violating the feeder undervoltage limit is referred to as the EV accommodation capacity of the circuit

3.8.3.1 Impact on Voltage Variability during EV Charging

In this section, the results for uncontrolled charging and charging under optimal TOU schedule are compared against the proposed controlled charging algorithm. An example secondary circuit, which is supplied by a 13.8kV/120V distribution transformer and supplies for 8 customer loads, is selected (see Figure 3.31). Four EVs are connected at the customer load locations and each EV charging method i.e. uncontrolled charging, charging with optimal TOU schedule, and proposed controlled charging, is evaluated. The load demand at the service transformer and voltage profiles at each EV load node are recorded for each charging method.

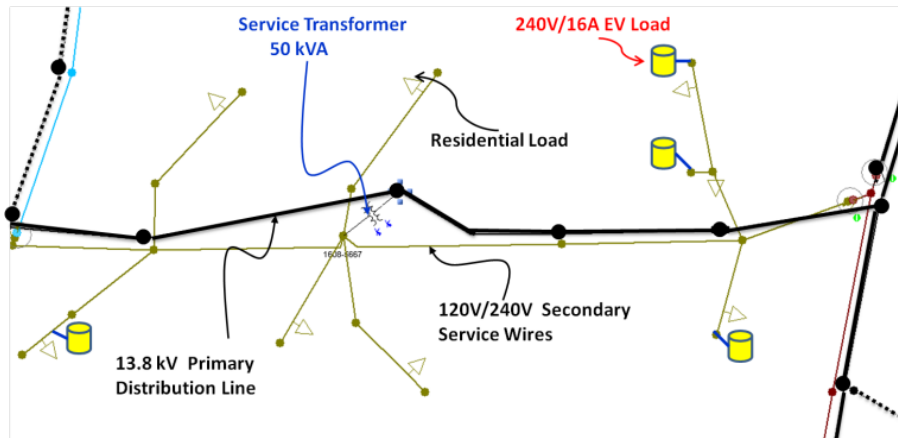


Figure 3.31: One line diagram for the 120V/240V secondary distribution circuit (Courtesy of the electric utilities).

The voltage profile at an EV load node for each charging method is shown in Figure 3.32. It can be seen from the figure that the proposed charging algorithm successfully minimizes the voltage variability at the EV load node and maintains the node voltage near 1 pu. Using the proposed charging method, the total EV load demand is optimally scheduled so that the voltage devia-

tions at each EV load node with respect to 1 pu are minimized. The minimum voltages recorded at each EV load node for the three charging methods are shown in Table 3.11. From the customer’s perspective, the proposed algorithm efficiently mitigates under-voltage concerns and decreases the voltage variability

A rather important observation is made when the impacts of proposed charging scheme are evaluated on the service transformer load demand. The daily load demand profiles for the service transformer are shown in Figure 3.33. The proposed charging algorithm results in a smoother load demand at the service transformer location. Additionally, the proposed charging algorithm fills the off-peak load demand valley and balances the service transformer load demand. Although mitigating the transformer load demand is not modeled as the control objective, the proposed charging method efficiently shifts the EV load demand to off-peak load hours. The proposed algorithm therefore mitigates the service transformer load demand issues as well, and thus is able to meet utility concerns efficiently.

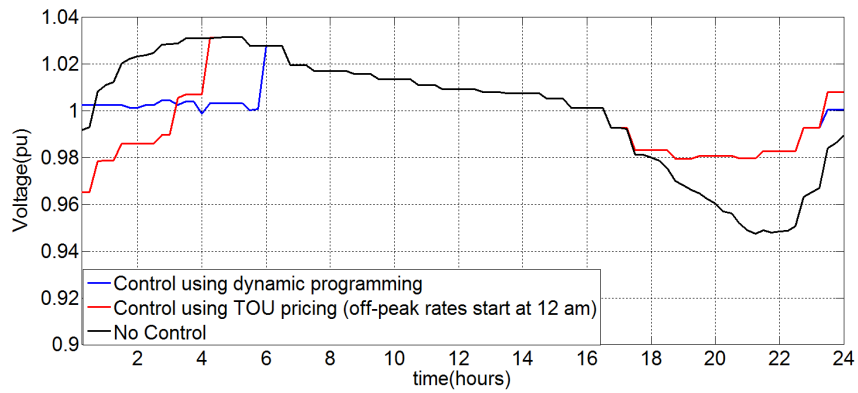


Figure 3.32: Voltage profile at the EV load location for each charging method.

As for the EV charging using optimal TOU schedule, the EV load demand

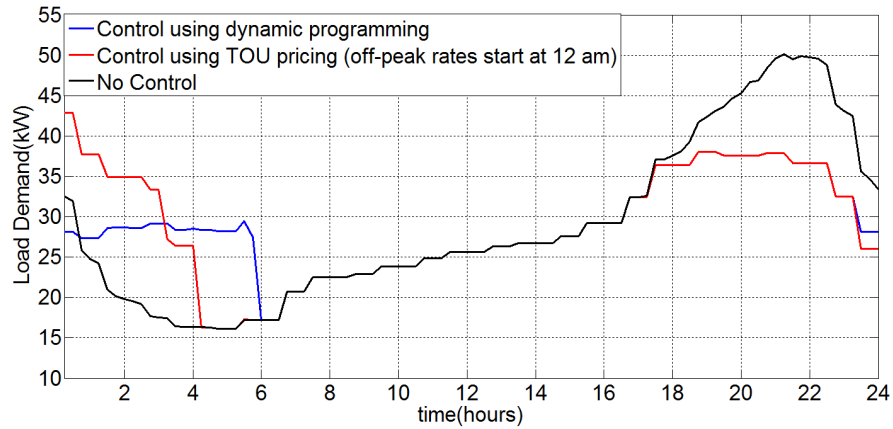


Figure 3.33: Daily load demand profile at the service transformer for each charging method.

shifts to off-peak load hours but results in a second peak in the load demand. The load demand for second peak (42.5 MW), however, is lower than the peak demand recorded for uncontrolled EV charging (50 kW). As for the proposed controlled charging method, no additional peak load demand is recorded while EV loads are charging.

Table 3.11: Minimum Feeder Voltages Recorded due to EV Load Charging (pu)

EV Load	Uncontrolled Charging	Charging with TOU pricing	Controlled Charging
EV 1	0.9611	0.9790	1.002
EV 2	0.9475	0.9654	1.00
EV 3	0.9557	0.9718	1.003
EV 4	0.9579	0.9741	1.004

3.8.3.2 Increasing Accommodation Limit with the Proposed Charging Scheme

The EV accommodation capacity of a distribution circuit is defined as the number of EVs the circuit could accommodate without violating ANSI

under-voltage limit (0.95 pu). The EV accommodation capacity is defined for both primary and secondary wire voltages. Since the future EV deployment and EV charger locations are unpredictable, stochastic analyses are required to better understand the impacts of future EV loads on distribution circuits. The stochastic analysis evaluates multiple EV deployment scenarios by randomly varying EV locations and percentage penetration. This analysis therefore helps in understanding the impacts of EV location and penetration on the distribution feeder voltages.

To make the stochastic analysis systematic, EV deployment scenarios are simulated in the following order [67]. First, for a 5% customer penetration level, EV loads with Level-2 240V/16A chargers and 16-kWh batteries are deployed at randomly selected customer locations. Note that customer penetration is defined as the percentage of total customer loads deployed with EV loads. The customer locations are selected by uniformly sampling the pool of secondary customers (total = 1473) supplied by the distribution feeder. Each EV charging method (uncontrolled, TOU, and smart charging) is implemented for each EV load at a given customer penetration level. A load flow analysis is carried out for each charging method and the minimum primary and secondary voltages are recorded. The customer penetration is increased in an increment of 5% and additional EV loads are deployed at the remaining customer load locations. The process is repeated until the customer penetration level reaches 100%. This gives 20 EV deployment scenarios, one at each customer penetration level {5%, 10%, ..., 100%}. Next, the above process is repeated 100 times, resulting in 2000 EV deployment scenarios, 100 at each customer penetration level. A daily load flow analysis is performed on the 2000 EV deployment scenarios and the minimum voltages over a day are recorded. The above process

is called a stochastic EV analysis.

Figure 3.34 shows the result of the stochastic EV analysis corresponding to the uncontrolled charging case. In Figure 3.34, each point represents the result corresponding to one EV deployment scenario. The graph consists of 4000 points, 2000 points corresponding to the minimum voltages recorded for the primary and secondary wires corresponding to 2000 EV deployment scenarios. From Figure 3.34, the primary wire voltages do not violate the undervoltage limit, even with 100% customer penetration. For the secondary wire voltages, the under voltage limit is violated at the 5% customer penetration level (73 EV loads). The minimum secondary voltage decreases to 0.92 pu with 5% customer penetration and 0.87 pu with 100% customer penetration.

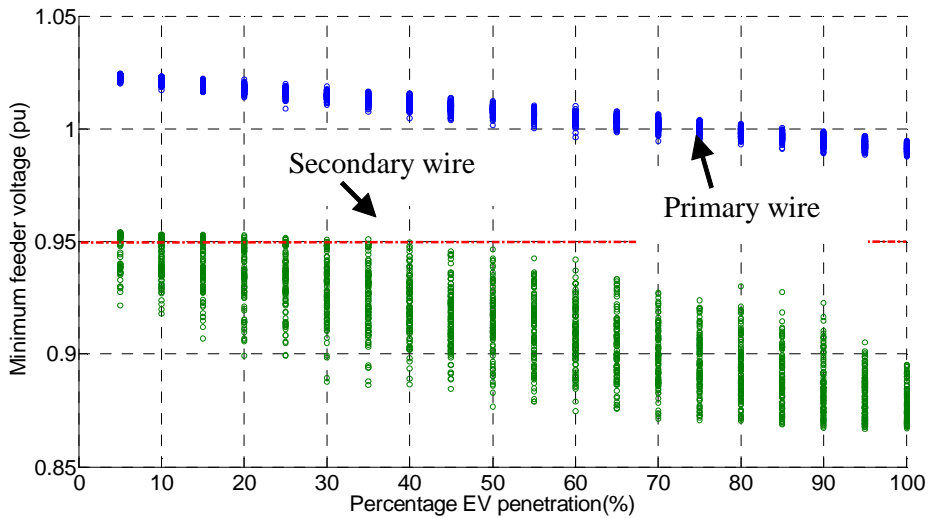


Figure 3.34: EV accommodation capacity for uncontrolled charging case.

Next, the EV accommodation capacity is calculated for the case when EV loads are charging under TOU pricing schedule with off-peak rates starting at 12 am (see Figure 3.35). From the figure, the first voltage violation is

recorded at 10% EV penetration (147 EV loads). Thus, TOU pricing increases the circuit accommodation capacity to 10%. Furthermore, the lowest voltages recorded for each EV deployment scenario increases on implementing TOU pricing structure. Also, the customer penetration increases to 70% to record an under-voltage under each EV deployment scenario, which was 40% for uncontrolled charging case.

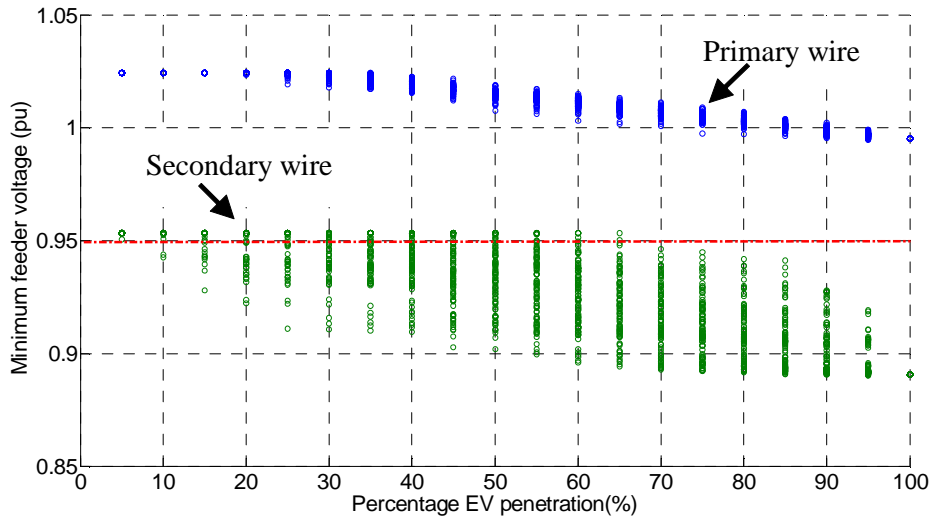


Figure 3.35: EV accommodation capacity, when EV loads are charging under optimal TOU schedule (off-peak rates beginning at 12 am).

Next, to understand the quantitative improvement provided by TOU pricing at the secondary voltage level, the percentage of secondary customers recording under-voltage for each EV deployment scenario are plotted for both uncontrolled charging scenario and charging under TOU pricing schedule. Note that at each customer penetration level the percentage of secondary customer experiencing a voltage violation (voltage < 0.95 pu) decreases significantly on implementing the TOU pricing schedule (see Figure 3.36). With 100% EV penetration (1473 EV loads), the percentage of secondary customers recording

under-voltage decrease to 0.8% in a TOU schedule, as compared to 2.8% for uncontrolled charging.

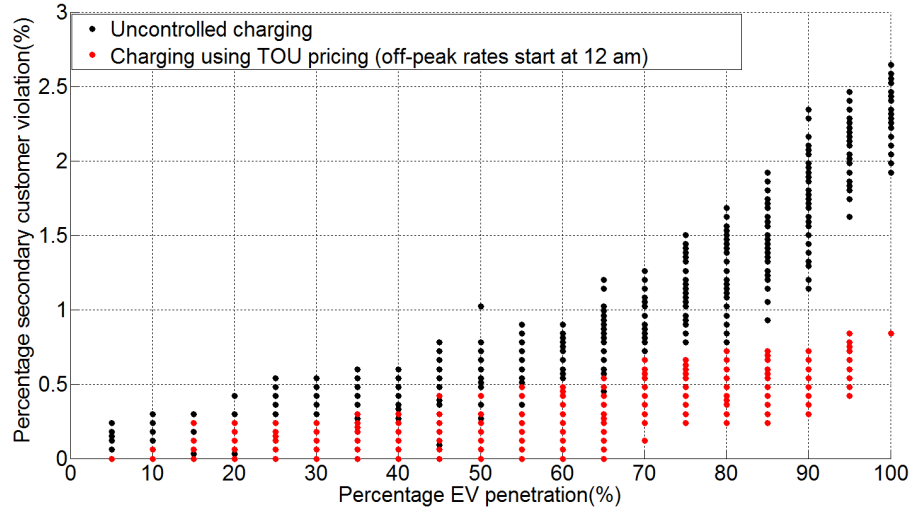


Figure 3.36: Percentage of secondary customers reporting under-voltage violation for uncontrolled charging and charging under TOU schedule.

Next, the proposed controlled charging method using dynamic programming is implemented at each customer penetration level. First, at each customer penetration level, the charging scenario resulting in the lowest voltages in secondary wire are identified. Then the proposed smart charging algorithm is implemented, aiming to minimize the voltage variations at each EV load node. The analysis is based on the assumption that the best improvement provided by the control charging algorithm can be observed by improving the worst-performing EV deployment case. Therefore, the algorithm is implemented for the EV deployment scenario, resulting in the lowest minimum voltages in secondary wires at each customer penetration level.

Using the proposed algorithm, an optimal charging schedule is determined for each EV load present in the circuit. The circuit peak load demand, min-

imum primary and secondary wire voltages, and number and percentage of customers reporting under-voltage violations are recorded and compared in Table 3.12 for the three charging strategies

A comparison of three charging methods at each customer penetration level for the worst-performing EV deployment scenario is shown in Table 3.12. From the table, using the proposed charging method, we are able to improve the EV accommodation capacity of the grid by 70%. Even with more than 75% and until 100% EV penetration, only one case of secondary voltage violation is recorded at the secondary customer location. Also, the minimum voltage with 100% EV penetration is only 0.946 pu, against 0.891 for the charging scenario using TOU pricing and 0.867 for the uncontrolled charging scenario. Furthermore, until 70% EV penetration, no additional peak load demand is recorded at the substation transformer when EV loads are charged using the proposed algorithm.

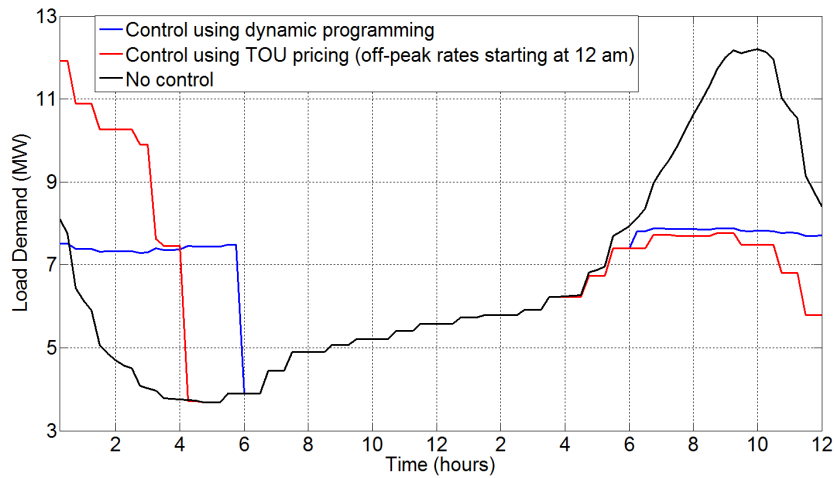


Figure 3.37: Load demand profile at the substation transformer at 100% EV penetration for each charging method.

The peak load demand recorded at the substation transformer without any EV load is 7.7 MW. It should be noted that when EV charging is done under optimal TOU schedule, no additional peak load demand is recorded until 30% EV penetration (441 EV load). Therefore, the optimal TOU schedule is able to mitigate the load demand concerns till 30% EV penetration. If EV load penetration is increased beyond 30%, a second peak at the substation transformer appears during off-peak load hours. From the table, the proposed charging method is able to accommodate up to 70% of EV without increasing the substation transformer peak load demand.

To further understand the impacts of three charging schemes on substation load demand, the load demand profiles at 100% customer penetration level is recorded (see Figure 3.37). For uncontrolled charging case, the peak load demand with EV charging increases to 12.5 MW from 7.7 MW (without any EV). As for the case with EV charging under TOU pricing, at 100% customer penetration, a significantly large second peak (at midnight) in load demand is recorded (11.9 MW). The proposed control charging algorithm performs the best, and even at 100% customer penetration, the load demand increases to only 7.88 MW.

3.9 Conclusion

The objective of this study to understand, identify, and mitigate the impacts of EV charging on distribution circuit voltages. To investigate the EV charging impacts, analytical models for EV charger units and EV battery loads are developed. This study presents three different models for EV loads: a time-domain model, an average-value model, and a constant power load model. Next, a thorough literature review on the evaluation and mitigation of

the impacts residential EV charging on distribution circuit is presented. Our analysis on the impacts of EV load charging concludes that residential EV charging is likely to affect secondary circuit voltages more than the primary wires. Furthermore, if a controlled charging method is not deployed, higher penetration of EV load may result in increased peak load demand and undesirable secondary service voltage drops. In conclusion, the local and global circuit analysis conducted for the selected distribution circuit suggests the following:

1. The location of secondary service with respect to the substation transformer does not affect the additional voltage drop due to EV load charging.
2. An EV load located close to the service transformer results in lower additional voltage drops as compared to one located farther from the service transformer.
3. Doubling the size of EV charger or adding an EV load to the secondary circuit almost doubles the additional voltage drop.
4. Increasing EV load penetration may lead to significantly higher voltage drops in secondary wires as compared to the primary wire voltages.
5. EV load clustering results in an unbalance in the load demand, thus increasing the voltages at few secondary service locations.

Next, several practical methods deployed by utilities to mitigate EV charging concerns are evaluated. The analysis concludes the following:

1. Increasing the size of service transformer, though it mitigates load demand concerns, is unable to mitigate the voltage drop issues.
2. The additional voltage drops due to EV load charging are efficiently mitigated by upgrading the distribution circuit using an additional transformer; however, the method requires infrastructural changes and hence

is expensive.

3. Implementing a TOU schedule efficiently shifts the EV load charging to off-peak load hours.

We also determine an optimal time to begin off-peak rates in TOU schedule. The proposed optimal TOU schedule performed well up to 30% customer penetration with EV, but resulted in second peak in load demand on further increasing the customer penetration.

A smart controlled charging algorithm to mitigate voltage quality issues due to EV charging is proposed next. The algorithm aims to minimize the voltage variation at each load node while taking customer inconvenience into account. An optimal EV charging profile is determined for each EV load by minimizing the overall voltage variation by optimally controlling the EV charger power level. The proposed algorithm is validated for its effectiveness. We conclude that the proposed charging method significantly decreases the substation load demand by optimally shifting the EV load demand to off-peak load hours. Although designed to mitigate voltage variability issues at secondary customer level, the proposed algorithm is also able to deliver utility benefits by minimizing the substation peak load demand.

Table 3.12: Comparison of three charging methods for each EV penetration level

% EV penetration	Num. of EV loads	Peak load demand			Minimum secondary voltage			Num. of secondary customer violations		
		Charging Method			Charging Method			Charging Method		
		1	2	3	1	2	3	1	2	3
5	73	8.02	7.77	7.77	0.922	0.951	0.953	4	0	0
10	147	8.26	7.77	7.77	0.918	0.943	0.953	5	1	0
15	220	8.51	7.77	7.77	0.907	0.928	0.953	5	4	0
20	294	8.75	7.77	7.77	0.899	0.923	0.953	7	4	0
25	368	8.98	7.77	7.77	0.899	0.911	0.953	9	4	0
30	441	9.20	7.77	7.77	0.888	0.911	0.953	9	4	0
35	515	9.47	7.91	7.77	0.886	0.910	0.953	10	5	0
40	589	9.69	8.21	7.77	0.887	0.910	0.953	10	5	0
45	662	9.93	8.52	7.77	0.885	0.903	0.953	13	7	0
50	736	10.16	8.82	7.77	0.877	0.902	0.953	17	7	0
55	810	10.40	9.13	7.77	0.879	0.900	0.953	15	8	0
60	883	10.60	9.44	7.77	0.875	0.896	0.953	15	8	0
65	957	10.84	9.75	7.77	0.876	0.894	0.953	20	9	0
70	1031	11.11	10.06	7.77	0.871	0.893	0.953	21	11	0
75	1104	11.36	10.36	7.78	0.871	0.893	0.946	25	11	1
80	1178	11.58	10.68	7.82	0.871	0.892	0.946	28	12	1
85	1252	11.79	10.99	7.85	0.869	0.891	0.946	32	12	1
90	1325	12.03	11.30	7.85	0.867	0.891	0.946	39	12	1
95	1399	12.28	11.61	7.88	0.867	0.891	0.945	v41	14	1
100	1473	12.52	11.92	7.88	0.867	0.891	0.945	44	14	1

*Charging method 1 - uncontrolled charging

*Charging method 2 - charging under TOU pricing schedule (off-peak rates beginning at 12 am)

*Charging method 3 - proposed controlled charging using dynamic programming

Chapter 4

Integrating Photovoltaic Generation - Impacts and Mitigation

The integration of distributed energy resources (DER), especially residential photovoltaic (PV) systems into the distribution circuit has rapidly increased in the past decade [90]. Since utility distribution systems are designed for centralized power generation and are optimized for the unidirectional power flow, the integration of DER may disrupt system's normal operating conditions. In literature, several studies have been conducted to determine the impacts of PV systems on distribution circuit operations. A high PV penetration may result in several operational issues, including, but not limited to voltage quality problems [91–100], increased thermal stress, additional feeder losses [101], and a higher number of capacitor switching and regulator tap operations [102, 103]. Also, a study [104] conducted using recorded field data from a residential community in Austin, Texas concludes that PV sources may adversely affect distribution system power factor.

The increasing PV penetration and the undesirable impacts of PVs on distribution circuit necessitates the task for determining the largest PV capacity a given distribution circuit can accommodate without violating circuit's operational limits. The obtained PV capacity is referred to as the circuit's PV hosting capacity. The PV hosting capacity can be defined with respect to several impact criteria, for example, system overvoltage, thermal stress, harmon-

ics, etc. However, given the strict regulations enforced for the bus overvoltage [105] condition, in this work the PV hosting capacity is defined and calculated for bus overvoltage concerns.

Several methods to determine the feeder's maximum PV penetration limit have been proposed [106–113], however, the existing methods have a few limitations. A simplified feeder model was used in [107–109] thus, not representing the actual circuit conditions. In [106–109] the PV systems were simulated only at a few specific locations, thus not considering the stochasticity of potential residential PV panel sizes and locations. In [107, 108], small test feeders were used, thus questioning the method's application for an actual distribution circuit. In [111–113], a stochastic analysis framework is used to obtain the PV hosting capacity of actual distribution feeders. The method simulates large numbers of potential PV deployment scenarios by varying residential PV panel locations and sizes. The method however, poorly considers representative load condition for hosting capacity calculation. Additionally, the accuracy of the PV hosting results is not quantified, which is required given that the framework is stochastic. Moreover, the PV hosting capacity will depend upon the hourly variations in load demand and PV generation, which none of the proposed methods take into consideration.

In this chapter, an hourly stochastic analysis framework addressing the limitations of the existing PV hosting methods is developed. In order to understand the PV hosting problem better, first a mathematical formulation for the feeders' PV hosting capacity problem is developed. The impacts of the circuit loading and hourly variations in PV generation on feeder voltages and hosting capacity are discussed next. To solve the PV hosting problem, an hourly stochastic analysis framework based on percentile load calculation is

presented. The proposed framework includes the effects of hourly variations in load demand and PV generation profile while calculating the PV hosting capacity. The accuracy of the obtained PV hosting capacity is quantified using the proposed accuracy assessment approach. Although, in this study, the PV hosting capacity is calculated for the circuit overvoltage concerns, the approach is applicable to calculate PV hosting capacity with respect to any other operating criteria.

4.1 Potential Impacts of PV Integration

There are three categories of concerns related to the impact high PV penetration has on the distribution grid: voltage, loading, and protection-related. Voltage issues include bus overvoltages, voltage deviations, and unbalanced conditions in a three-phase system. Loading issues arise when service transformers and conductors are overloaded, and thermal limits are violated. Protection-related issues occur when protection elements, such as relays, reclosers, breakers, network protectors, and fuses misoperate. Such misoperations occur when PV interferes with the existing protection elements in the distribution grid. Each of the three issues are explained in detail in the following sections.

4.1.1 Voltage Related Issues

Importantly, high PV penetration can degrade the voltage quality at the point of common coupling (PCC), where the load is connected. Voltage quality is expected to be in accordance with the specifications of American National Standard Institute (ANSI) [105]. It is possible for high PV penetration to cause the voltage at the PCC to increase when power is over-generated (over-

voltage), unbalanced, or having a significantly ramp-up or down deviation. The following sections elaborate on each of these conditions.

4.1.1.1 Overvoltage

Overvoltage is common on a sunny day when the load is low, and the PV panels are generating at their maximum capacity, typically during the afternoon (10 to 2 pm). An overvoltage condition due to local generation is more likely to be observed when PV is located at the feeders remote from the substation. An example overvoltage scenario with PV located at the remote feeder end is shown in Figure 4.1. Without PV, the typical voltage profile for the feeder is a drooping curve with lower voltages recorded towards the feeder end. On adding PV generation, the voltages recorded at feeder end increases thus potentially resulting in an overvoltage condition.

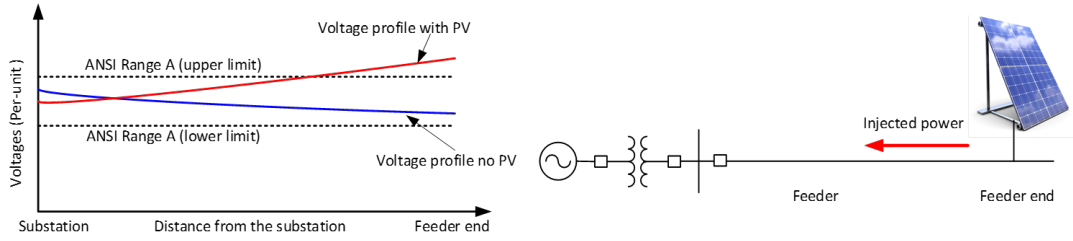


Figure 4.1: Overvoltage scenario.

The maximum allowable range of voltage at any bus is 5% of the rated voltage, i.e., 1.05 per-unit (p.u.), as specified by ANSI C84.1. The per-unit values are obtained by scaling the quantity by their rated values.

$$V_i < 1.05 \text{ p.u.} \quad (4.1)$$

where, V_i is the voltage at any bus i in the distribution feeder.

4.1.1.2 Voltage Deviation

Voltage deviation occurs in PV systems when PV power generation suddenly ramps up or ramps down. This occurs typically when there is cloud interference on the PV panel. The voltage deviation problem is more critical during the maximum load conditions. The steady-state voltage deviation of PV integration should be within the limits specified by ANSI C84.1:

$$V_i - V_i^b < \epsilon \text{ p.u.} \quad (4.2)$$

where,

V_i is the voltage at a bus i after PV integration.

V_i^b is the voltage at a bus i prior to PV integration.

Voltage deviation at a primary wire should not vary more than 3% and the secondary by 5%. Therefore, $\epsilon = 0.03$ p.u. for primary wires and $\epsilon = 0.05$ p.u. for secondary wires.

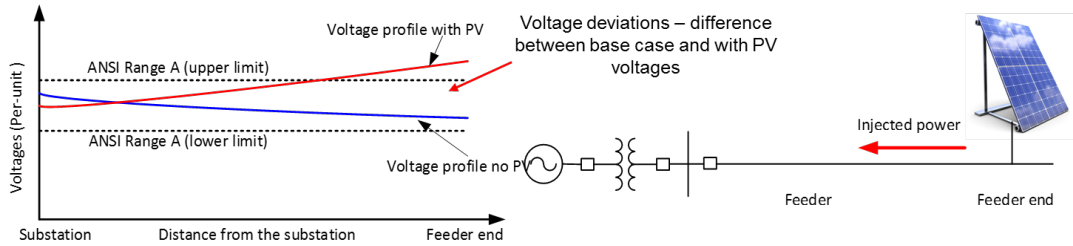


Figure 4.2: Voltage deviation scenario.

4.1.1.3 Voltage unbalance

The unplanned integration of PV on residential rooftops (mostly single-phase connections) can cause voltage unbalance in the three-phase system. This phenomenon occurs when more power is injected (into the distribution

grid) in a single phase than in the other two phases. The ANSI C84.1 limits voltage unbalance to less than 3%.

Power losses and line overloading can occur when power injection is unbalanced in the three-phase system of the distribution network. This voltage unbalance problem, however, can be rectified by modifying the circuit topology in two ways. First, the single-phase load can be transferred from the highest loaded phase to one of the other two more lightly loaded phases. Second, the PV can be connected to the highest loaded phase.

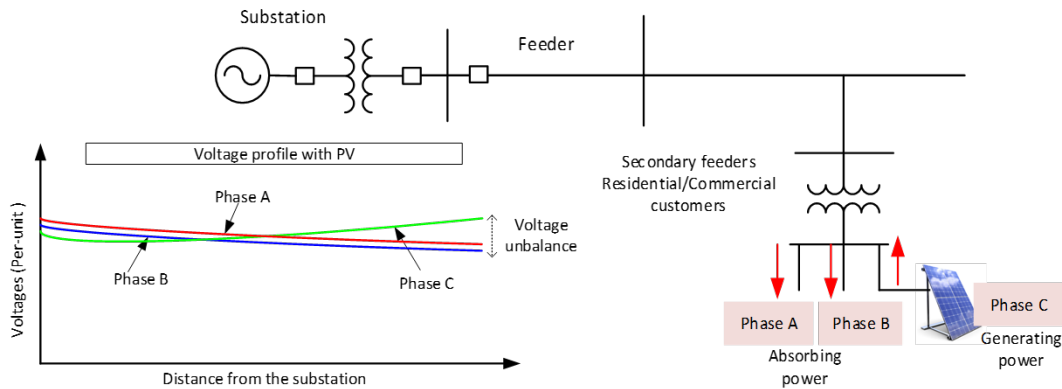


Figure 4.3: Voltage deviation scenario.

4.1.2 Current Related Problems

The net transformer load demand profile exhibits a characteristic "duck" curve: power is over-generated during the day, but peak electric demand occurs in the evening, as PV output decreases [114]. This case illustrates a reverse power flow condition when the transformer load becomes negative during the day; i.e. the power is fed back to the grid (see Figure 4.4).

Reverse power flow is a major concern in secondary grids and spot networks, which are common in big cities. Unlike radial distribution circuits,

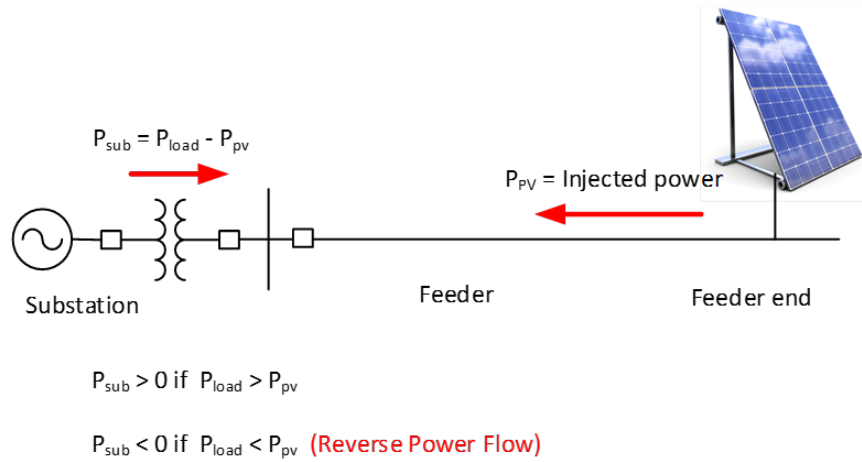


Figure 4.4: Reverse power flow scenario.

these networks contain protectors that are designed to open in case of even a small fraction of reverse power flow. It is specified in IEEE Std. 1547-2003 that the PV integration should not cause the opening of the network protectors. Therefore, if the distribution circuit is laid out in spot or grid topology, then the PV installed capacity is not allowed to cause any reverse power flow. For a radial network, the presence of On-Load Tap Changer (OLTC) transformers pose a limit on the reverse power flow. This is because tap changing transformer have reduced capability to handle reverse power. For instance, the Y-y single resistor tap changer transformers with 23 MVA rating have 42% reverse power capability. The reverse power capability of the transformer depends on vector group, the size of transformers, the resistance of the bridging resistor and power factor [115].

4.1.3 Overcurrent Protection Related Problems

The conventional grid has protection elements such as overcurrent relays, circuit breakers and fuses to interrupt fault current in the grid. With the

integration of a high PV penetration, a number of instances of misoperation of these protection devices have been reported. Two of the main concerns due to the fault contribution by PV are sympathetic tripping and reduction of breaker reach.

4.1.3.1 Sympathetic tripping of relays

Sympathetic tripping is an unnecessary isolation of the healthy feeder due to a fault in an upstream parallel feeder. A scenario with a fault at a parallel feeder of a circuit is illustrated in Figure 4.5. In Figure 4.5, both the substation and the PV panel connected to Feeder 1 contribute to the fault. The relay trips when the current magnitude contributed by the PV in Feeder 1 exceeds the setting of the relay at the head of the feeder. The relay isolates the healthy feeder, interrupting service in the feeder.

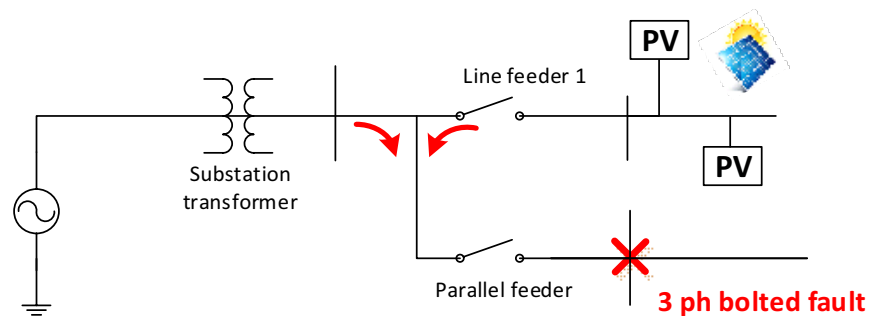


Figure 4.5: Sympathetic tripping in case of three-phase fault.

4.1.3.2 Breaker reduction of reach/Breaker insensitivity

A breaker is expected to identify and isolate any fault in a distribution system. However, high PV penetrations can cause the breaker to go blind to

the faults in the grid. Such a case can arise when the substation fault current is recorded below the breaker's reach. This problem occurs when there is a high impedance fault and also high reverse power flow from the distributed generation towards the substation. Therefore, it is required to evaluate the PV capacity that can be accommodated in the distribution grid without reducing the reach of the breaker.

4.2 PV Hosting Capacity Problem

A feeder's PV hosting capacity is defined as the largest PV generation that can be accommodated without violating the circuit's operational limits. This study is concerned with the overvoltages recorded in the primary wires due to PV integration. An overvoltage violation is recorded if any primary bus in the feeder records a voltage greater than 1.05 pu. The hosting capacity problem aims to determine the largest PV generation that can be integrated into a given feeder without resulting in an overvoltage violation. Since, the locations and sizes of the future residential PV panels are not known, the hosting capacity problem requires simulating and analyzing a large number of potential PV deployment scenarios. Although, the methodology is developed for feeder overvoltage concerns, the proposed framework can be applied to determine the hosting capacity for other impact criterion as well.

4.2.1 Definitions

This section defines the terms used in the mathematical formulation of the PV hosting capacity problem in the following sections.

4.2.1.1 Customer Penetration Level (C_{pen}^i)

Customer penetration level defines the number of customers (in percentage) equipped with PV panels in a given distribution circuit. Thus, an i^{th} customer penetration level is obtained by populating $i\%$ customers with PV panels, where $0 \leq i \leq 100$. Note that, for a given customer penetration level, by varying individual PV panel location and size multiple PV deployment scenarios are possible.

4.2.1.2 PV Penetration Level (PV_{pen}^i)

PV_{pen}^i is defined as the total PV generation in kW added to the distribution circuit corresponding to the i^{th} customer penetration level (C_{pen}^i). Thus, corresponding to each customer penetration level (C_{pen}^i), a PV penetration level (PV_{pen}^i) is obtained.

4.2.1.3 PV Deployment Scenarios (x_j^i)

A PV deployment scenario characterizes the locations and sizes of individual PV panels at each customer load location for a given customer penetration level. Corresponding to each customer penetration level, multiple potential PV locations and sizes each characterizing a PV deployment scenario, are possible. Here, a PV deployment scenario, x_j^i , represents j^{th} PV deployment scenario corresponding to i^{th} customer penetration level.

4.2.2 PV Hosting Capacity - Problem Formulation

The results of a large number of potential PV deployment scenarios are quantified using two representative PV hosting capacities, minimum-hosting (H_{min}) and maximum-hosting capacity (H_{max}). The minimum-hosting capac-

ity (H_{min}) is defined as the lowest PV generation resulting in the first case of overvoltage condition. The maximum-hosting (H_{max}) capacity is defined as the lowest PV generation corresponding to which all PV deployment scenarios in all report an overvoltage condition.

Mathematically, PV hosting capacity problem for a given distribution circuit is defined as follows. Let,

- S be the set of discrete customer penetration levels indexed by i , $S \in \{1, 2, \dots, i, \dots, 100\}$.
- PV_{pen} be the set of all PV penetration levels indexed by customer penetration level, i , $\{PV_{pen}^1, PV_{pen}^2, PV_{pen}^3, \dots, PV_{pen}^i, \dots, PV_{pen}^{100}\}$.
- X^i be the set of all PV deployment scenarios corresponding to C_{pen}^i , indexed by j , $\{x_1^i, x_2^i, \dots, x_j^i, \dots, x_{L_i}^i\}$.
- V_{max}^i be the set of largest primary voltages recorded for all deployment scenarios corresponding to C_{pen}^i . $V_{max}(x_j^i)$ is the largest primary voltage recorded for PV deployment scenario x_j^i , $\{V_{max}(x_1^i), V_{max}(x_2^i), \dots, V_{max}(x_j^i), \dots, V_{max}(x_{L_i}^i)\}$
- L_i be the total number of PV deployment scenarios corresponding to C_{pen}^i .

The hosting capacity problem is defined as follows. Determine H_{min} and H_{max} , where:

$$H_{min} = \min_{i \in S} \{PV_{pen}^i \mid \max(V_{max}^i) > 1.05\} \quad (4.3)$$

$$H_{max} = \min_{i \in S} \{PV_{pen}^i \mid \min(V_{max}^i) > 1.05\} \quad (4.4)$$

4.2.3 Monte Carlo Based Method for PV Hosting Problem

The minimum- and maximum-hosting capacity as defined in (4.3) and (4.4) can be obtained only after simulating all possible PV deployment scenarios, which is impractical. The PV hosting analysis is therefore, done by simulating a finite number of PV deployment scenarios using the Monte Carlo approach. The PV hosting problem based on Monte Carlo approach is defined in this section.

For a given distribution circuit, let k number of PV deployment scenarios are simulated at each customer penetration level, each representing one Monte Carlo run. Since in this study, k Monte Carlo runs/scenarios are simulated at each customer penetration level, the method is termed k -run Monte Carlo study (k -run MCS). The feeder's hosting capacity is characterized using the first- and all-hosting capacity defined as follows:

4.2.3.1 First-hosting Capacity ($H_{1,k}$)

The first-hosting capacity is equal to the lowest PV penetration for which at least one scenario in a k -run MCS observes an overvoltage condition.

4.2.3.2 All-hosting capacity ($H_{100,k}$)

The all-hosting capacity is defined as the lowest PV penetration such that all k scenarios (i.e. 100%) in a k -run MCS observe an overvoltage condition.

The first-hosting capacity ($H_{1,k}$) and all-hosting capacity ($H_{100,k}$) are obtained by solving (4.5) and (4.6).

$$H_{1,k} = \min_{i \in S} \left\{ PV_{pen}^i \mid P(V_{max,k}^i > 1.05) \geq \frac{1}{k} \right\} \quad (4.5)$$

$$H_{100,k} = \min_{i \in S} \left\{ PV_{pen}^i \mid P(V_{max,k}^i > 1.05) = 1 \right\} \quad (4.6)$$

where,

- X_k^i : Set of k PV deployment scenarios simulated using Monte Carlo method at C_{pen}^i , $\{x_1^i, x_2^i, x_3^i, \dots, x_k^i\}$.
- $V_{max,k}^i$: Set of maximum primary voltages recorded for k PV deployment scenarios simulated at C_{pen}^i , $\{V_{max}(x_1^i), V_{max}(x_2^i), \dots, V_{max}(x_k^i)\}$.

4.2.4 Additional Factors Affecting PV Integration Limits

The PV hosting problem formulated in the previous section models the uncertainty in the locations and sizes of the future PV panel deployments. However, there are additional factors that may impact PV hosting capacity. The bus voltages are closely related to the circuit load demand and overvoltage concerns are most likely to arise when the circuit is lightly loaded. The hourly variations in the circuit load and PV generation profile may also affect the feeder's PV hosting capacity. This section presents a discussion on the impacts of the above two factors on circuit voltages.

4.2.4.1 Effect of the Minimum Load Condition

To understand the impact of circuit loading on circuit voltages, the circuit's minimum load is increased and the largest circuit voltages at multiple additional PV penetration levels are recorded (see Figure 4.6). From the figure, at a given PV penetration level, as the feeder's minimum load increases, the largest circuit voltage decreases. For example, for PV penetration equal to 6 MW, on varying minimum load from 0.2 pu to 0.7 pu of the peak load demand, the largest primary voltage decreases from 1.075 pu (overvoltage limit violated) to 1.045 pu (within overvoltage limit). Thus, the PV integration

limit depends significantly upon the minimum load condition, consequently selecting a non-representative load may result in an inaccurate hosting capacity.

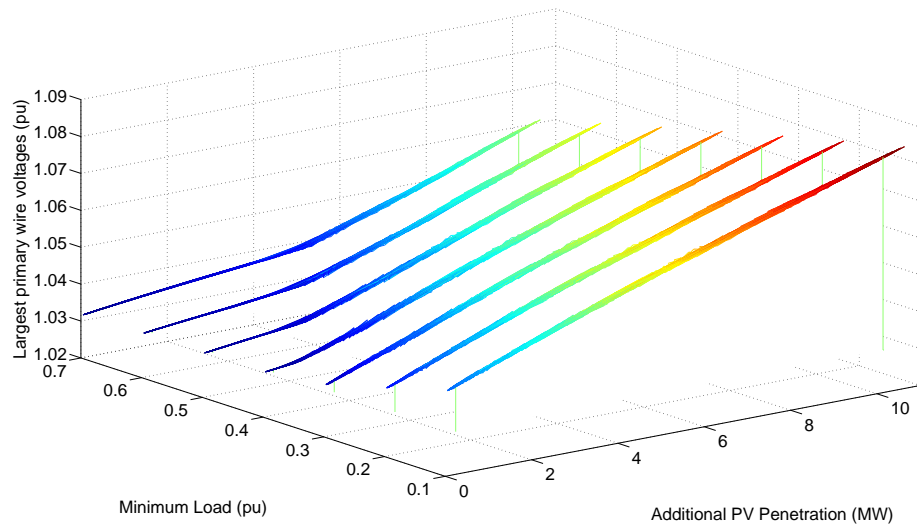


Figure 4.6: Effects of minimum load on voltage rise due to PV.

4.2.4.2 Hourly Variations in Circuit Load and PV Generation

In the stochastic analysis framework presented in [112], the mean or median value of the daily daytime minimum load demand recorded over a year is selected as the circuit's representative minimum load, and the PV analysis is done for the obtained load. However, for the majority of days, the minimum load is recorded either in the early morning or later in the evening (see Figure 4.7), when PV generation is low (see Figure 4.8). Thus, the PV analysis based on the statistical minimum load gives a conservative estimate of the feeder's hosting capacity.

Additionally, the PV hosting capacity obtained using the mean or median

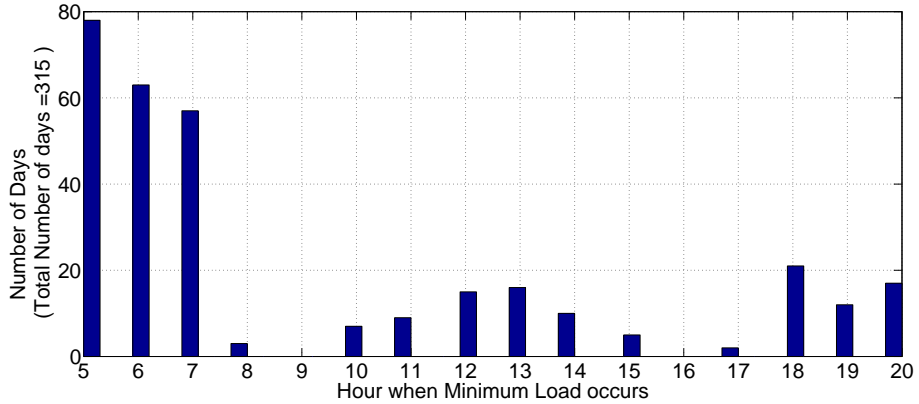


Figure 4.7: Duration of daily daytime minimum load recorded over a year.

value of the daily daytime minimum load demand is unable to statistically quantify the possibility of observing feeder overvoltage condition. In other words, the study cannot determine the potential number and hour of overvoltage violations when PV capacity equal to the feeder’s PV hosting limit is deployed. We recommend that the PV hosting analysis should be conducted in an hourly interval using a statistically representative minimum load condition.

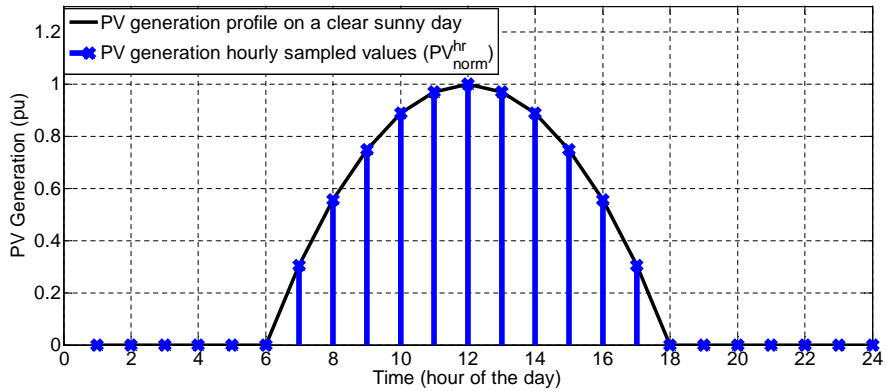


Figure 4.8: Typical per-unit PV generation profile on a clear sunny day.

4.3 Hourly Stochastic Analysis Framework

This section presents the proposed hourly stochastic analysis framework for solving the PV hosting capacity problem. The additional factors related to circuit loading and hourly variations in load and PV generation are included in the proposed framework. The PV hosting capacity is calculated for the statistically representative minimum daytime load demand, termed effective minimum load (Eff_{load}^{hr}). A percentile analysis is done on the measured yearly load demand to obtain Eff_{load}^{hr} . Future PV scenarios are characterized by simulating multiple PV deployment scenarios (x_j^i) using the Monte Carlo approach. For each hour, using Eff_{load}^{hr} , load flow analysis is conducted and the largest primary wire voltages are obtained. Based on the hourly load flow analysis, PV hosting capacities ($H_{1,k}$ and $H_{100,k}$) are calculated (see Figure 4.9).

4.3.1 Identify Hourly Effective Minimum Load

The hourly effective minimum load (Eff_{load}^{hr}) for a given distribution circuit is calculated using the yearly load demand measured at the substation. The measured load demand at the substation includes the generation from the existing PV panels. To obtain the net feeder load demand, the demand satisfied by the existing PV panels should be added to the measured load demand. For each day of the year, the measured load demand and the existing PV generation are sampled in an hourly interval (see Figure 4.8) and a percentile analysis is done to obtain Eff_{load}^{hr} , as detailed in the following section.

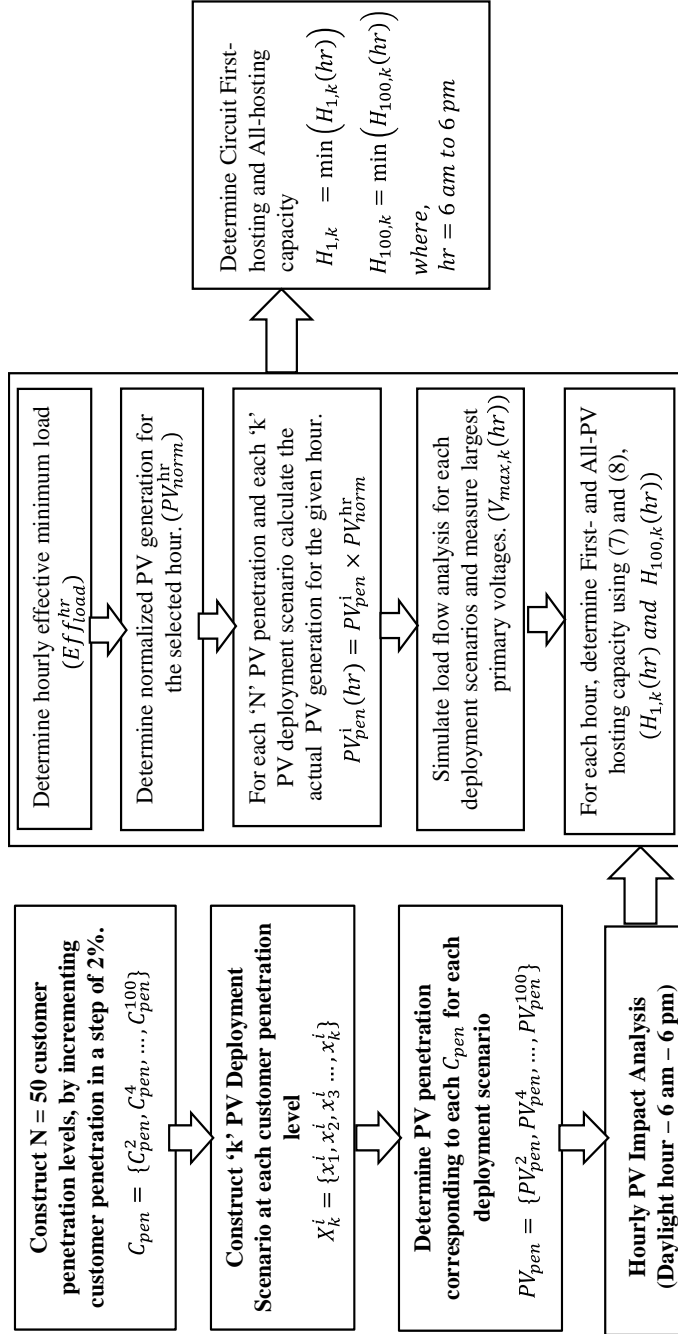


Figure 4.9: Proposed hourly stochastic analysis framework for determining circuit's PV hosting capacity.

4.3.1.1 Hourly Minimum Load (Min_{load}^{hr})

The measured yearly load demand is sampled in an hourly interval and for each hour the 5th-percentile value, termed Min_{load}^{hr} is obtained. Here, for a given hour, the yearly load demand will be higher than the Min_{load}^{hr} for 95% of the time (see Figure 4.10). Thus, Min_{load}^{hr} characterizes circuit's measured minimum load demand. It should be noted that the measured load includes the circuit's existing PV generation. The effective minimum load demand (Eff_{load}^{hr}) is obtained by adding the hourly existing PV generation to Min_{load}^{hr} .

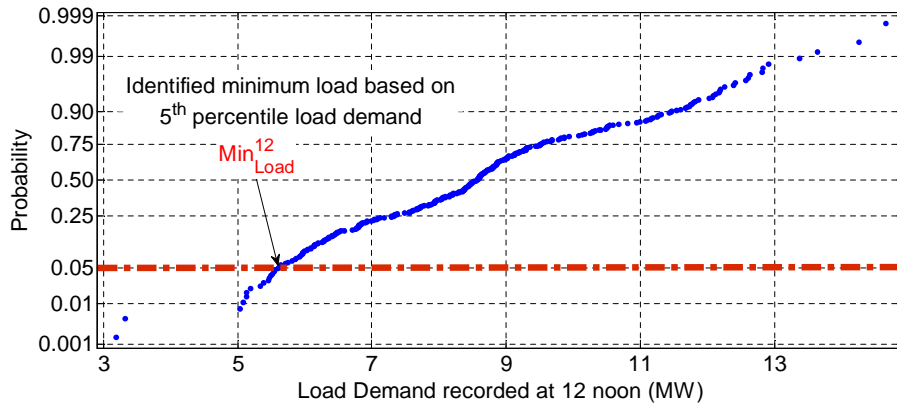


Figure 4.10: 5th percentile minimum load corresponding to hour = 12.

4.3.1.2 Hourly Existing PV Generation ($PV_{existing}^{hr}$)

A representative value for the existing PV generation for each hour of the day is calculated. Here, the PV generation profile for a clear sunny day (see Figure 4.8) is used to obtain $PV_{existing}^{hr}$. The normalized PV generation profile shown in Figure 4.8 is multiplied to the peak existing PV generation capacity of the feeder and sampled in an hourly interval to obtain $PV_{existing}^{hr}$.

4.3.1.3 Hourly Effective Minimum Load (Eff_{load}^{hr})

Hourly effective minimum load is defined as the actual 5th-percentile value of the yearly feeder load demand. Since, hourly minimum load demand (Min_{load}^{hr}) includes the existing PV generation ($PV_{existing}^{hr}$) present in the circuit, Eff_{load}^{hr} is obtained by adding $PV_{existing}^{hr}$ to Min_{load}^{hr} (4.7).

$$Eff_{load}^{hr} = Min_{load}^{hr} + PV_{existing}^{hr} \quad (4.7)$$

It should be noted that an hourly load demand lower than the Eff_{load}^{hr} is likely to be observed 5% of the days over a year. Then, ignoring the accuracy of the Monte Carlo simulations, for 95% of days during the year, the actual PV hosting capacity will be at least equal to or greater than the PV hosting capacity calculated using the feeder's effective minimum load demand. Thus, if a PV capacity equal to the calculated hosting capacity is deployed, the circuit is not likely to observe an overvoltage condition for at least 95% of the days over the year.

4.3.2 PV Deployment Scenarios

The method to simulate PV deployment scenarios by varying PV panel locations and sizes is detailed in this section. Using the Monte Carlo approach, k PV deployment scenarios (X_k^i) are simulated at each customer penetration level ($Cust_{pen}^i$) by associating a uniform random variation in PV panel locations [112]. Additionally, the PV panel size at each customer location is determined based on the customer type (commercial or residential) and the corresponding distributions for the PV panel size [38]. By associating variations in PV deployment locations and sizes, the proposed framework results in multiple unique deployment scenarios.

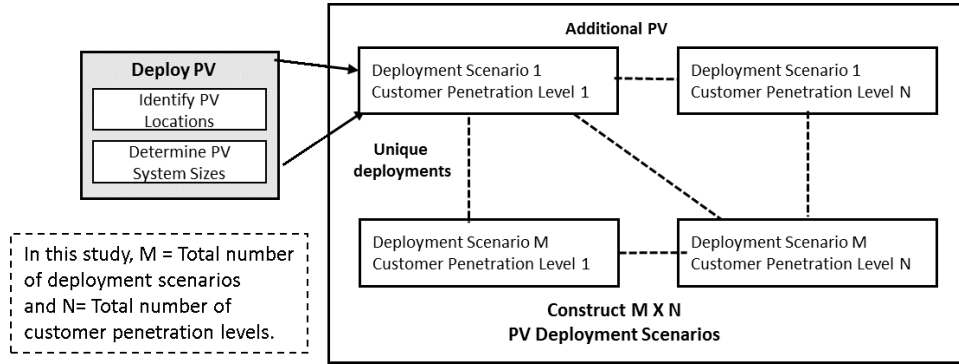


Figure 4.11: The stochastic analysis framework - Generate PV Deployment Scenarios

The method to systematically simulate j^{th} PV deployment scenario, where $j \in \{1, 2, \dots, k\}$ is as follows. First, a 2% of customers ($Cust_{pen}^2$) are selected randomly using a uniform distribution from the pool of customers served by the distribution feeder. At each of the selected customer locations, a PV panel is deployed. The installed PV capacity at each selected customer location is determined based on the customer load type and the corresponding peak load demand using the method described in Figure 4.12. The customer penetration is increased in an increment of 2% and additional PV systems are deployed by selecting locations from the remaining customer loads not connected to PV panels. The customer penetration level is increased and the deployment process is repeated until it reaches 100% ($Cust_{pen}^{100}$). This constitutes one set of PV deployment scenario corresponding to each customer penetration level. The above process is repeated k times, to obtain a total of k PV deployment scenarios (X_k^i) at each i customer penetration level.

4.3.3 Hourly PV Impact Analysis

The PV impacts are analyzed in an hourly interval while including the impacts of hourly variations in PV generation and circuit loading. The hourly

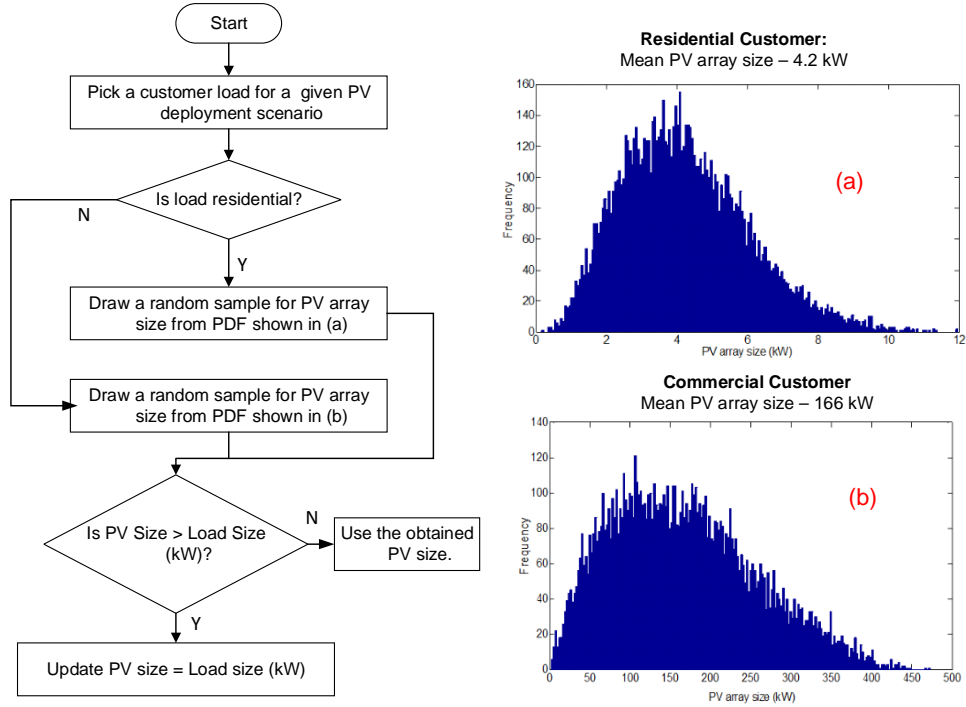


Figure 4.12: The stochastic analysis framework - Identify PV Size

impact analysis is done for the daylight hours starting from 6 am to 6 pm. To evaluate the impacts of PV generation on circuit voltages, a steady-state load flow analysis is simulated for each PV deployment scenario corresponding to each customer penetration level. Note that for a given hour, hr , the steady-state load flow analysis is simulated at the circuit loading equal to $Ef f_{load}^{hr}$ (4.7). For each hour, the net active power generation of each PV panel is prorated based on the parabolic hourly PV generation profile (see Figure 4.8)(4.8). Using the load flow analysis, the largest primary voltages ($V_{max,k}(hr)$) are recorded corresponding to each PV deployment scenario.

$$PV_{pen}^i(hr) = PV_{pen}^i \times PV_{norm}^{hr} \quad (4.8)$$

where,

- $PV_{pen}^i(hr)$: PV generation at hour = hr corresponding to i^{th} PV penetration.
 PV_{norm}^{hr} : Normalized PV generation at hour = hr .

4.3.4 Determine PV Hosting Capacity

Based on the hourly load flow analysis, the first-hosting ($H_{1,k}(hr)$) and all-hosting capacity ($H_{100,k}(hr)$) are determined for each hour using (4.9) and (4.10), respectively. Here, $V_{max,k}^i(hr)$ is the set of maximum primary voltages recorded for k PV deployment scenarios simulated for i^{th} customer penetration level at hour = hr . Finally, feeder's first-hosting ($H_{1,k}$) and all-hosting capacity ($H_{100,k}$) are obtained by taking a minimum of the respective hourly values (see Figure 4.9).

$$H_{1,k}(hr) = \min_{i \in S} \left\{ PV_{pen}^i(hr) \mid P(V_{max,k}^i(hr) > 1.05) \geq \frac{1}{k} \right\} \quad (4.9)$$

$$H_{100,k}(hr) = \min_{i \in S} \left\{ PV_{pen}^i(hr) \mid P(V_{max,k}^i(hr) > 1.05) = 1 \right\} \quad (4.10)$$

4.4 Accuracy Assessment Framework

A distribution circuit may be supplying for thousands of customer loads. For example, the circuit analyzed in this study is supplying for 1218 customers (see Section 4.5). Thus, for a 2% customer penetration ($\simeq 25$ customers), the total possible number of PV deployment scenarios will be equal to $\binom{1218}{25} = 1.4581 \times 10^{50}$. The Monte Carlo approach, however simulates only a finite number of scenarios. Given the large number of possible PV deployment scenarios, it is important to quantify the accuracy of the hosting capacity results obtained using the proposed Monte Carlo approach.

The method to define and quantify the percentage accuracy of the PV hosting capacity results is presented in this section. The percentage accuracy

is defined for the hosting capacity results obtained using a k -run MCS. The framework is based on the hosting capacity probabilistic intervals identified using the distribution of the hosting capacity results. The probabilistic interval defines the percentage of times the hosting capacity result obtained from an independent k -run MCS is expected to lie within a given percentage interval. For instance, the p^{th} probabilistic interval for the hosting capacity, both first-hosting and all-hosting, is defined as the interval that contains $p\%$ of the corresponding hosting capacity results obtained using multiple k -run MCS. The corresponding hosting capacity obtained using a k -run MCS is accurate for $p\%$ of the time if its p^{th} probabilistic interval is accurate.

4.4.1 Impact of Multiple k -run MCS on Hosting Capacity

Given a large number of possible PV deployment scenarios, for a different k -run MCS a different hosting capacity is likely to be observed. This observation is illustrated using the first-hosting capacity. We simulated 200 sets of independent k -run MCS, where the number of Monte Carlo runs, $k = 100$ (100 -run MCS). The PV hosting capacity is calculated based on the proposed framework, resulting in 200 values for first-hosting capacity ($H_{1,k}$). The distribution for ($H_{1,k}$) is shown in Figure 4.13. From Figure 4.13 it can be observed that using a 100 -run MCS, the first-hosting capacity ($H_{1,k}$) for the feeder can be obtained anywhere from 5.9 MW to 6.1 MW. Since the absolute minimum value cannot be obtained unless we simulate all possible deployments, it is necessary to determine the accuracy of the results obtained using a k -run MCS.

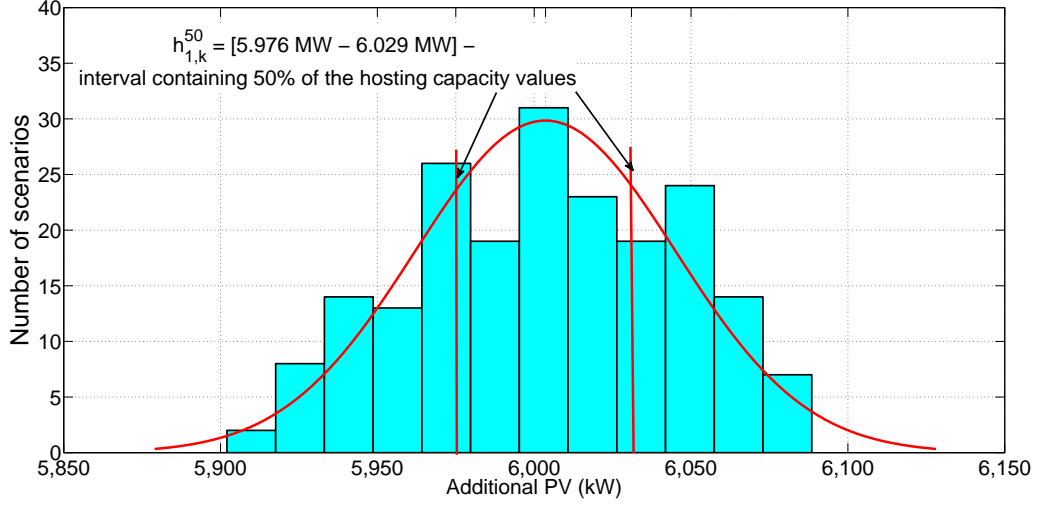


Figure 4.13: First-hosting capacity using multiple k -run MCS, where $k = 100$.

4.4.2 Hosting Capacity Probabilistic Intervals

We begin with obtaining the probability distribution functions (PDF) for both first-hosting ($H_{1,k}$) and all-hosting capacity ($H_{100,k}$). The PDF is then used to obtain the probabilistic intervals for both hosting capacities. The approach to obtain probabilistic intervals is illustrated using $H_{1,k}$.

The PDF (χ_{h1}^k) for $H_{1,k}$ is obtained by approximating the distribution shown in Figure 4.13 using a Gaussian distribution. For the obtained PDF (χ_{h1}^k), $\mu = 6.002$ MW and $\sigma = 41.52$ kW.

$$H_{1,k} \sim \chi_{h1}^k = N(\mu, \sigma^2) \quad (4.11)$$

Using χ_{h1}^k , the p^{th} probabilistic interval for the first-hosting capacity ($h_{1,k}^p$) is calculated using (10).

$$h_{1,k}^p = \left\{ F^{-1} \left(\frac{1-p}{2} \middle| \mu, \sigma \right), F^{-1} \left(\frac{1+p}{2} \middle| \mu, \sigma \right) \right\} \quad (4.12)$$

Here, $x = F^{-1}(y|\mu, \sigma)$ is defined as $\{x : (F(x|\mu, \sigma) = y)\}$. where,

$$y = F(x|\mu, \sigma) = \frac{1}{\sigma\sqrt{2\pi}} \int_{-\infty}^x e^{-\frac{(t-\mu)^2}{2\sigma^2}} dt$$

The probabilistic intervals for the first-hosting capacity ($h_{1,k}^p$) calculated for $p = 10\%$ to 99% are shown in Figure 4.14.

The distribution for the largest voltages recorded for multiple PV deployments corresponding to each probabilistic interval ($h_{1,k}^p$) is obtained next. The corresponding distribution for $p = 50\%$ is shown in Figure 4.15. Note that $h_{1,k}^p$ will be accurate if the probability of observing an overvoltage for the corresponding deployment scenarios is positive but sufficiently small. Also, by definition if $h_{1,k}^p$ is accurate, then $H_{1,k}$ will be accurate at least for $p\%$ of time.

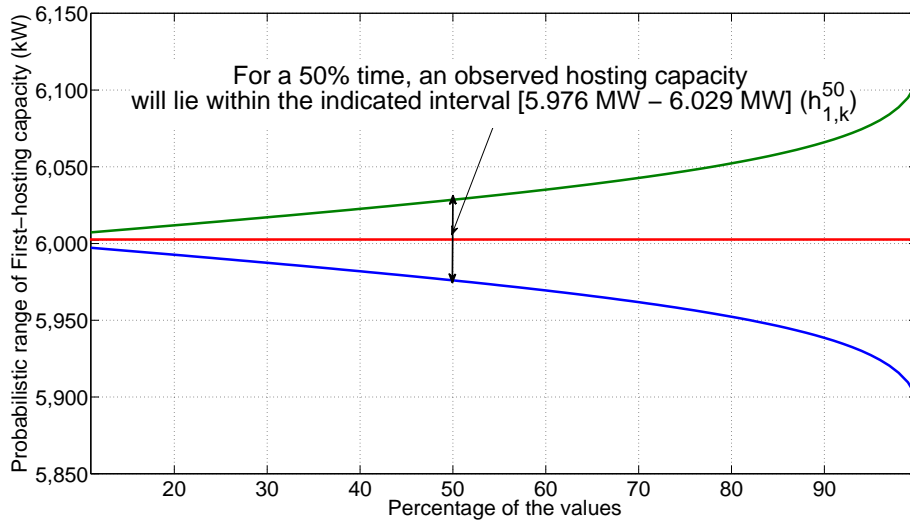


Figure 4.14: Probabilistic interval for first-hosting capacity.

4.4.3 Percentage Accuracy of the Monte Carlo Simulation

For a k -run MCS, the percentage accuracy of feeder's first-hosting and all-hosting capacity is characterized using $Acc_k^\varepsilon(H_1)$ and $Acc_k^\varepsilon(H_{100})$, respectively.

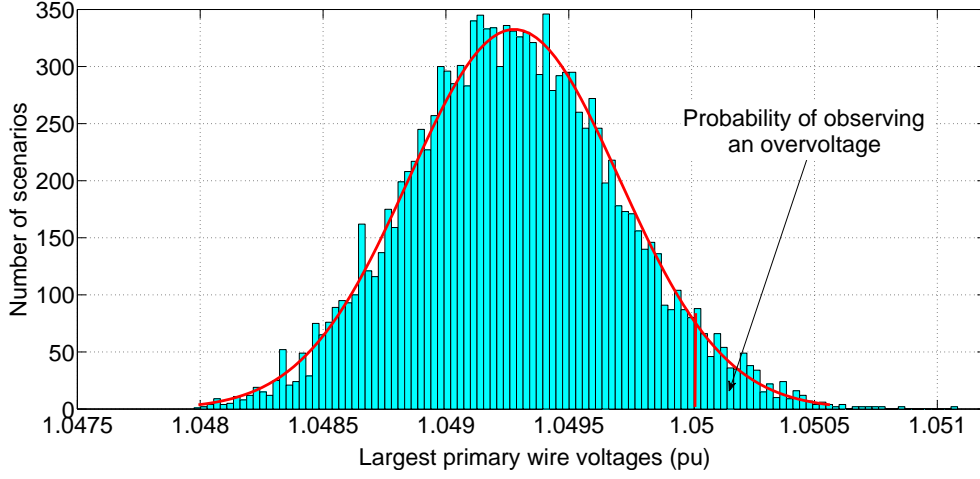


Figure 4.15: Largest voltages recorded for 50% hosting capacity interval ($h_{1,k}^{50}$).

4.4.3.1 First-hosting Capacity Percentage Accuracy, $Acc_k^\varepsilon(H_1)$

First-hosting capacity ($H_{1,k}$) obtained using a k -run MCS is expected to be accurate for $p\%$ time if the probability of observing an overvoltage for PV deployment scenarios in p^{th} probabilistic interval is greater than zero but sufficiently small, as characterized by the tolerance parameter (ε). $Acc_k^\varepsilon(H_1)$ is equal to the maximum p^{th} probabilistic interval satisfying the above definition.

4.4.3.2 All-hosting Capacity Percentage Accuracy, $Acc_k^\varepsilon(H_{100})$

All-hosting capacity ($H_{100,k}$) obtained using a k -run MCS is expected to be accurate for $p\%$ time if the probability of observing an overvoltage for PV deployment scenarios in p^{th} probabilistic interval is less than or equal to one but sufficiently high, as characterized by the tolerance parameter (ε). $Acc_k^\varepsilon(H_{100})$ is equal to the maximum p^{th} probabilistic interval satisfying the above definition.

Based on the above definitions, the hosting capacity accuracy, $Acc_k^\varepsilon(H_1)$

and $Acc_k^\varepsilon(H_{100})$, are obtained using (4.13) and (4.14), respectively.

$$Acc_k^\varepsilon(H_1) = \max_{0 \leq p \leq 100} \{p \mid 0 < P(V_{max,k} | h_{1,k}^p > 1.05) \leq \varepsilon\} \quad (4.13)$$

$$Acc_k^\varepsilon(H_{100}) = \max_{0 \leq p \leq 100} \{p \mid (1 - \varepsilon) < P(V_{max,k} | h_{100,k}^p > 1.05) \leq 1\} \quad (4.14)$$

where,

- $V_{max,k}$: Set of largest voltages recorded for each Monte Carlo scenario corresponding to each k -run MCS.
- $h_{1,k}^p$: p^{th} probabilistic interval for first-hosting capacity.
- $h_{100,k}^p$: p^{th} probabilistic interval for all-hosting capacity.
- ε : the tolerance parameter.

4.5 Results and Discussions

The proposed PV analysis framework is used to determine the PV hosting capacity for an actual 12.47-kV distribution circuit. The results of the PV integration analysis obtained using the proposed hourly stochastic analysis framework are compared against those obtained using the statistical minimum load condition. The accuracy of the PV hosting results are calculated and the impacts of tolerance parameter and the number of Monte Carlo runs on the PV hosting accuracy are determined.

4.5.1 Characterizing Distribution Circuit

The selected 12.47-kV distribution circuit is supplied by a 24-MVA substation transformer and is connected to a total of 1.196 MW of PV system. The distribution circuit serves 1218 customer loads out of which 71% are residential customers. For voltage support, the distribution circuit is connected

to seven capacitor banks, as shown in Figure 4.16. Among the seven capacitor banks, six are rated at 600 kvar each. Of these six capacitor banks, two are kvar controlled, two are time-controlled, and the other two are fixed. The seventh capacitor bank is kvar controlled and rated at 900 kvar. The three-phase circuit model for the distribution system starting from the substation down to single-phase individual customer load location is simulated.

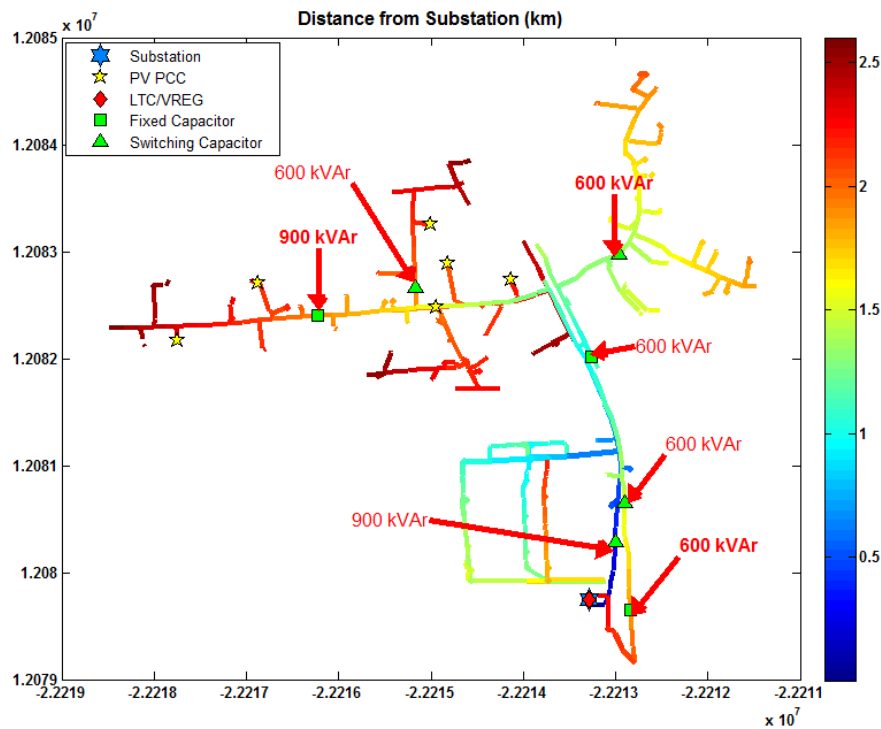


Figure 4.16: One-line diagram of the selected distribution feeder (Courtesy of the electric utilities).

The yearly load demand data measured at the substation for Year 2013 is available. Using the method discussed in Section 4.3, the effective minimum load ($Ef f_{load}^{hr}$) is calculated for each hour of the day (see Figure 4.17). The

effective minimum load accounts for the existing PV in the circuit. From Figure 4.17, the hourly effective minimum load varies from 4.8 MW to 6.8 MW, resulting in a variation of approximately 2 MW.

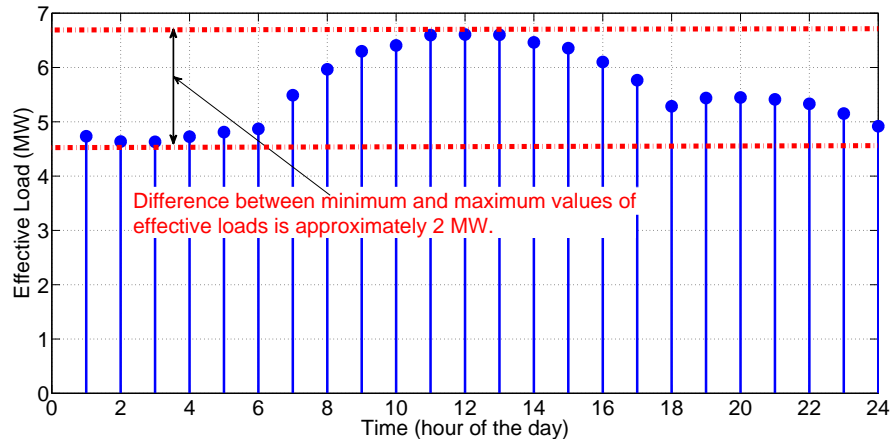


Figure 4.17: Hourly effective load calculated for the selected feeder.

Additionally, using the yearly load demand measured at the substation for the year 2013, the representative minimum loads for the distribution circuit are obtained. The minimum load condition is obtained using a statistical analysis carried on the yearly load demand for the feeder. First, the monthly average sunrise and sunset times are identified and, using this data, the daily minimum daytime load demand is obtained. Next, a histogram plot for the minimum daytime load demand is generated (see Figure 4.18), and the mean and the median of the distribution are calculated. The analysis yields a mean value equal to 6.1792 MW and a median value equal to 6.13 MW. Based on the statistical analysis, a minimum load equal to 6 MW is selected for the analysis.

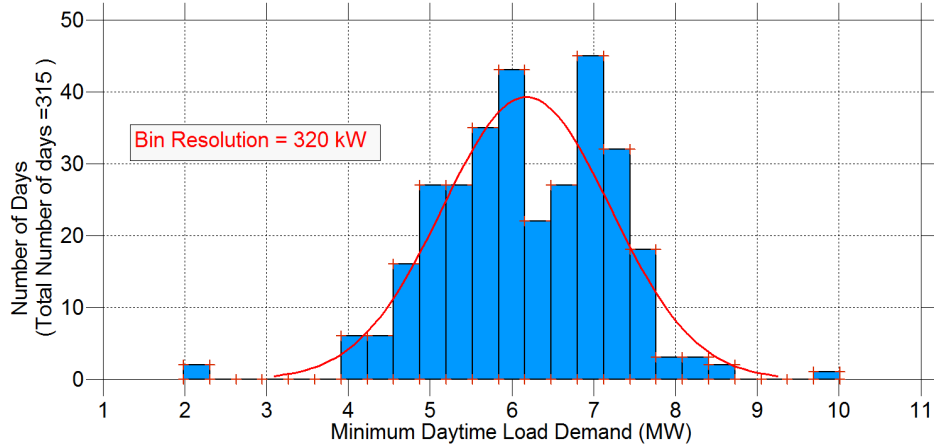


Figure 4.18: Obtaining a statistically representative minimum load condition.

4.5.2 PV Hosting Capacity using the Proposed Framework

Multiple PV deployment scenarios (x_j^i) are simulated using the Monte Carlo simulation approach. Since C_{pen}^i is varied from 2% to 100% in a step of 2%, a total of 50 penetration levels are simulated. In this study we have simulated 100 PV deployment scenario corresponding to each C_{pen}^i . Thus, a total of 5000 cases are simulated for the PV impact analysis.

Using $Ef f_{load}^{hr}$, PV hosting capacities are calculated for each hour of the day. The hourly first-hosting and all-hosting capacities are shown in Figure 4.19. The minimum of the obtained hourly hosting capacities is taken as the circuit's actual PV hosting capacity. From Figure 4.19, the minimum values for both first-hosting capacity and all-hosting capacity are obtained at 12 pm. Therefore, the hosting capacities calculated at 12 pm represent circuit's actual PV hosting capacity (see Table 4.1).

The PV hosting results are compared against those obtained for a fixed minimum loading condition. The minimum load is obtained using a statistical analysis carried on the yearly load demand for the feeder. Based on the

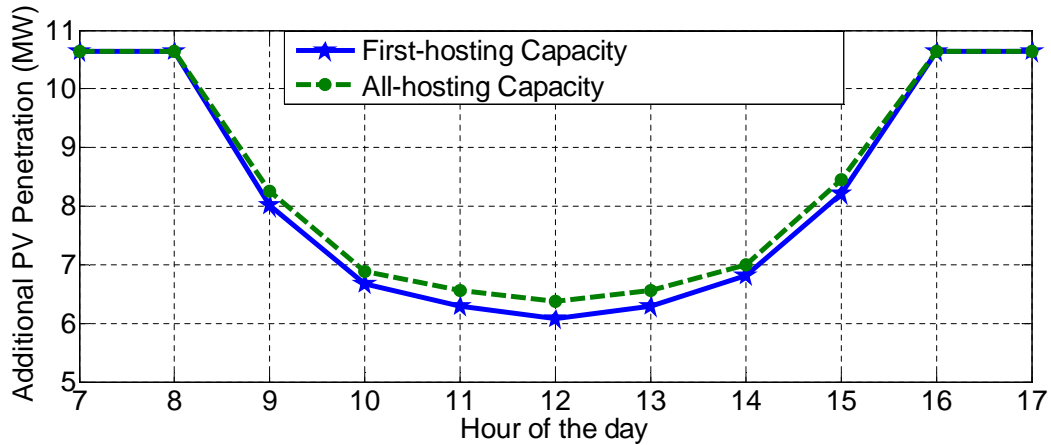


Figure 4.19: Hourly PV hosting capacities obtained using proposed framework.

statistical analysis a minimum load equal to 6 MW, which corresponds to the mean of the daily daytime minimum load demand, is selected for the analysis. The PV hosting capacities are calculated for the corresponding circuit load, and the results are summarized in Table 4.1.

Table 4.1: PV Hosting Results

Cases		Additional PV Size (kW)
Using Hourly Analysis	First-hosting Capacity ($H_{1,k}$)	6,084
	All-hosting Capacity ($H_{100,k}$)	6,374
Using Statistical Minimum Load	First-hosting Capacity ($H_{1,k}$)	5,454
	All-hosting Capacity ($H_{100,k}$)	5,722

The results for primary bus voltages corresponding to all 100 PV deployment scenarios (x_j^i) simulated for all 50 customer penetration levels (C_{pen}^i) at 12 pm are shown in Figure 4.20. Note that each point in the figure corresponds to the maximum primary bus voltage recorded for a particular PV scenario.

The circuit records first violation for primary bus voltages on adding 6.084 MW of additional PV, while an all-hosting capacity comes out to be 6.374 MW. In between the first- and all-hosting capacities, some scenarios record an overvoltage violation while others do not.

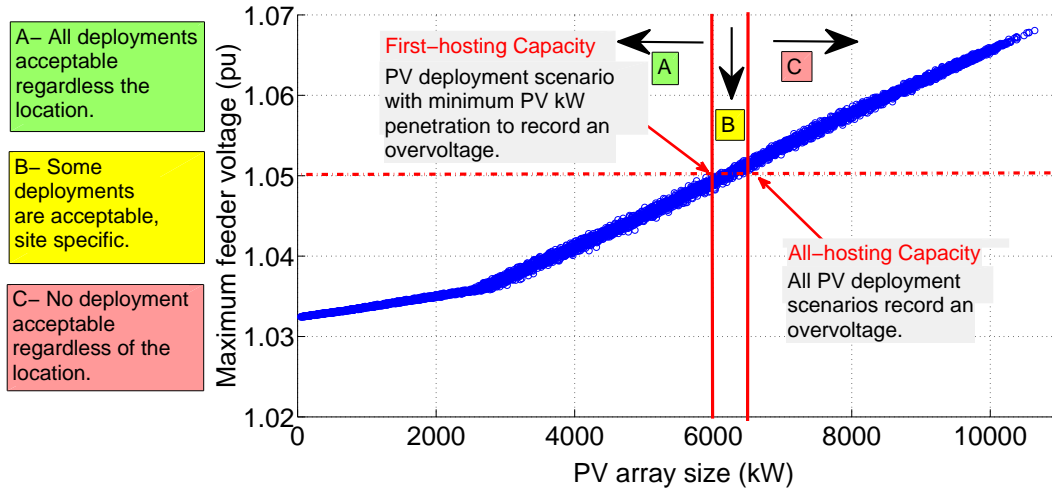


Figure 4.20: Maximum voltages recorded for each PV deployment scenario corresponding to hour 12.

Assuming Monte Carlo simulation can capture the representative PV deployments, the first-hosting capacity ($H_{1,k} = 6.084$ MW) is the minimum PV penetration resulting in an overvoltage violation for at least one PV deployment scenario. Since 5^{th} percentile minimum load is selected, any PV generation less than $H_{1,k}$ will not result in an overvoltage for 95% of the days over the year. For 5% of the days when the daily minimum load demand may be lower than the selected 5^{th} percentile minimum load, an overvoltage may be recorded on adding an additional PV generation less than $H_{1,k}$. It should be noted that this interpretation is not possible for the PV hosting capacity obtained using a fixed minimum load condition. Therefore, the hourly analysis

coupled with percentile load estimation helps in interpreting the PV hosting results.

4.5.3 Accuracy of Hosting Capacity Results

The accuracy of the first- and all-hosting capacities is calculated using the proposed accuracy assessment framework in Section IV. The tolerance parameter, ε , is assumed to be 0.05. The accuracy is calculated for the stochastic analysis using 100 PV deployment scenarios at each customer penetration level, i.e. a *100-run* MCS. Figure 4.21 shows the results for first-hosting capacity. The probability of observing an overvoltage for each probabilistic interval of the hosting capacity is obtained and plotted. Using Fig. 12, for $\varepsilon = 0.05$, $Acc_k^\varepsilon(H_1) = 98\%$, implying that the first-hosting capacity obtained using a *100-run* MCS is expected to be accurate 98% of the time over the year. Similarly, the accuracy of all-hosting capacity is obtained (Figure 4.22). From the figure, the all-hosting capacity calculated using an independent *100-run* MCS, is expected to be accurate 98% of the time for $\varepsilon = 0.05$.

The impact of the tolerance parameter on the accuracy of hosting capacities is analyzed next. Figure 4.23 shows the percentage accuracy of first- and all-hosting capacities with respect to the tolerance parameter (ε). As expected, as the tolerance is increased the accuracy of hosting capacity increases. Also, for $\varepsilon = 0.06$, both $Acc_k^\varepsilon(H_1)$ and $Acc_k^\varepsilon(H_{100})$ are greater than 99%.

4.5.4 Impacts of the Number of Monte Carlo Runs

As discussed before, the hosting capacity accuracy also depends upon the number of Monte Carlo runs/scenarios. Increasing the number of Monte Carlo runs can better approximate the PV deployment scenario and increase the

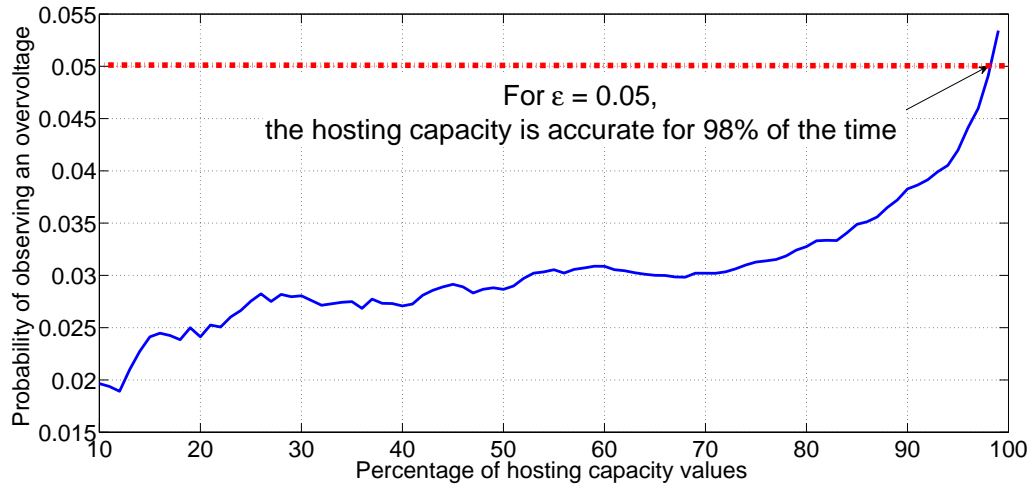


Figure 4.21: Probability of observing an overvoltage corresponding to 10% to 99% probabilistic interval for first-hosting capacity.

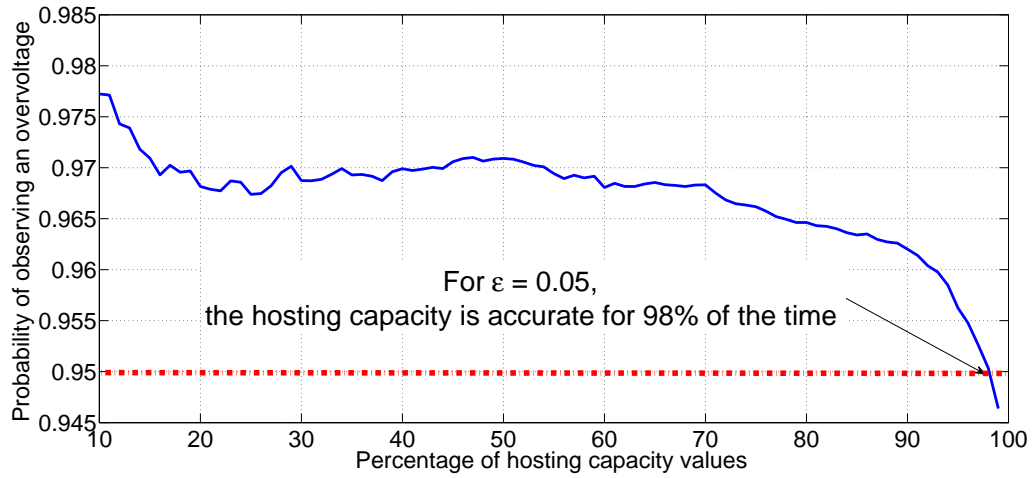


Figure 4.22: Probability of observing an overvoltage corresponding to 10% to 99% probabilistic interval for all-hosting capacity.

confidence in the obtained hosting capacity values. Therefore, it is important to understand the impact of the number of Monte Carlo runs on the percentage accuracy of the hosting capacity.

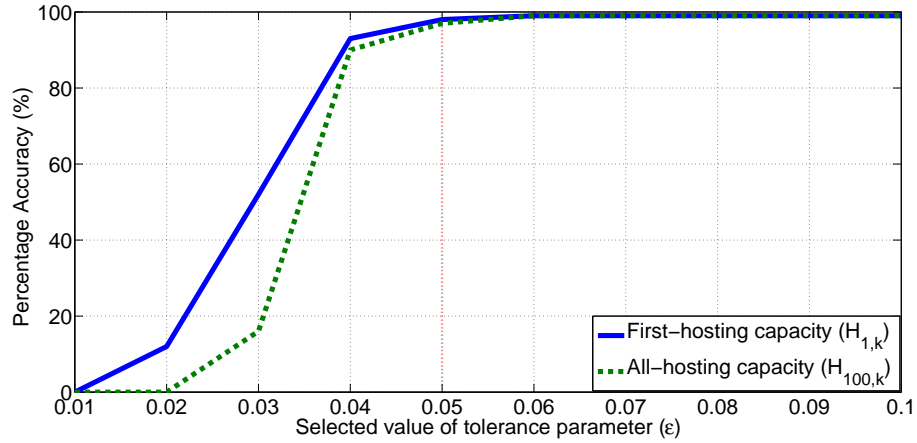


Figure 4.23: Hosting capacity percentage accuracy vs. tolerance parameter.

The PV hosting capacity is calculated for different numbers of Monte Carlo runs. The tolerance parameter is assumed to be 0.05. The number of Monte Carlo runs are varied from 45 to 200 at each customer penetration level, and the percentage accuracy of both first- and all-hosting capacity are obtained. Figure 4.24 shows the relation between hosting capacity accuracy and the number of Monte Carlo runs. From the figure, as the number of runs increases the percentage accuracy increases, in fact, more than 90% accuracy is obtained only by simulating 75 Monte Carlo runs at each customer penetration level.

4.6 Discussion on Impacts of PV on Bus Overvoltages

The PV system impacts on system overvoltages are discussed here in detail. For overvoltage violations, lower PV hosting capacities are observed during the minimum load condition, implying that PVs affect the distribution voltages most when the circuit is lightly loaded. In the following discussion, first, the PV size and location resulting in the largest impacts on feeder voltages are

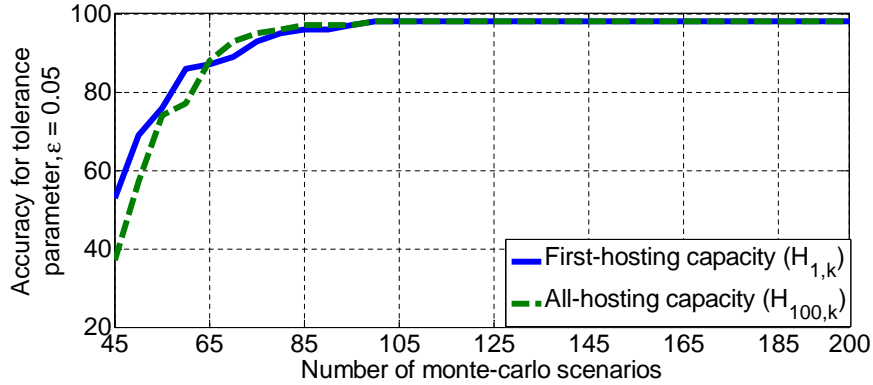


Figure 4.24: Hosting capacity percentage accuracy vs. the number of Monte Carlo runs.

characterized. The numbers and locations of buses observing an overvoltage violation are also identified. Finally, the impacts of feeder loading and PV deployment locations on hosting capacity are evaluated.

4.6.1 PV Hosting Capacities for Overvoltage Condition

Increasing the PV penetration increases the likelihood of overvoltage violation, but there are additional factors as well. Even after the first violation scenario, we observe several scenarios with a higher PV penetration but not reporting an overvoltage. The objective of this section is to observe the PV deployment scenario corresponding to the first violation and to identify the factors potentially resulting in an overvoltage.

Figure 4.25 shows the locations and sizes of PV systems corresponding to the first violation scenario. The first violation is observed for a customer penetration of 52%. From the figure, it can be observed that for this scenario, large PV systems were located farther away from the substation. These nodes generally have low short-circuit capacities and therefore, installing a large PV

system may result in an overvoltage violation. Thus, locating large PVs farther away from the substation is more likely to result in an overvoltage violation

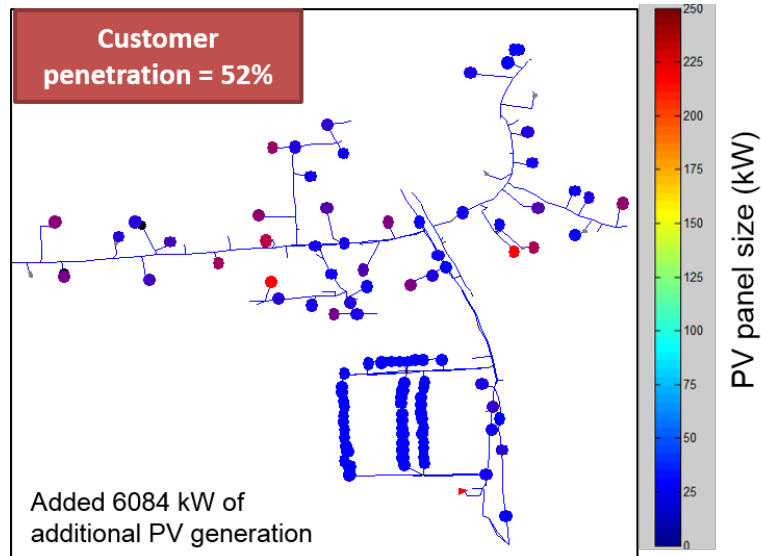


Figure 4.25: PV locations and sizes corresponding to PV deployment scenario for the first overvoltage violation (Courtesy of the electric utilities).

4.6.2 Bus Locations observing Overvoltages

Corresponding to the first violation case, the bus locations reporting overvoltages are identified (see Figure 4.26). This analysis helps in understanding which buses are the first to observe an overvoltage violation due to PV integration. In Figure 4.26, a heat-chart is plotted representing all buses with voltages more than 1.05 pu in red and the rest in orange. From the figure, it is observed that all buses observing overvoltages are farther away from the substation.

Next, for each PV deployment scenario, the number of primary buses recording an overvoltage violation are identified (see Figure 4.27). From the

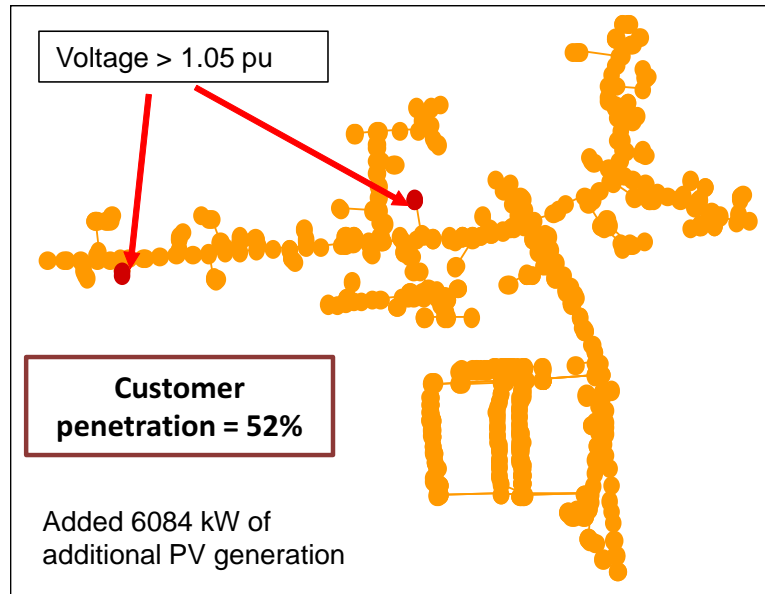


Figure 4.26: Heat plot for primary bus voltages corresponding to the first overvoltage violation scenario.

figure, it is observed that for the PV hosting corresponding to the first violation, only three primary buses report an overvoltage violation. As the PV penetration is increased, the number of primary buses reporting an overvoltage violation increases rapidly. In fact, for all violation case, around 300 primary buses observe an overvoltage condition. Therefore, increasing PV penetration not only increases the maximum bus voltage, but also the number of customers observing a violation.

4.6.3 Effects of Minimum Load on PV Hosting Capacity

The objective of this section is to understand the impact of the minimum load on the circuit's PV hosting capacity. For this study, the minimum load for the circuit is increased from 4 MW to 12 MW in a step of 1 MW, and the stochastic steady-state PV analysis is simulated at each loading condition.

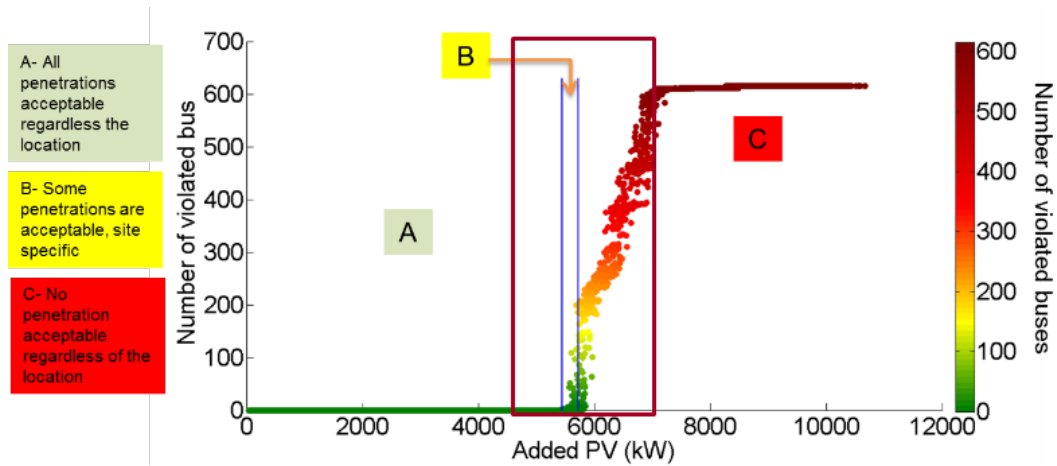


Figure 4.27: Number of primary buses observing overvoltage during the minimum load condition for each PV deployment scenario.

The corresponding first hosting capacity is calculated at each loading condition and is shown in Figure 4.28. It is observed that on increasing the minimum load, the PV hosting capacity of the circuit increases. In fact, for every 1 MW increase in the minimum load, the circuit can accommodate approximately 543 kW of additional PV capacity.

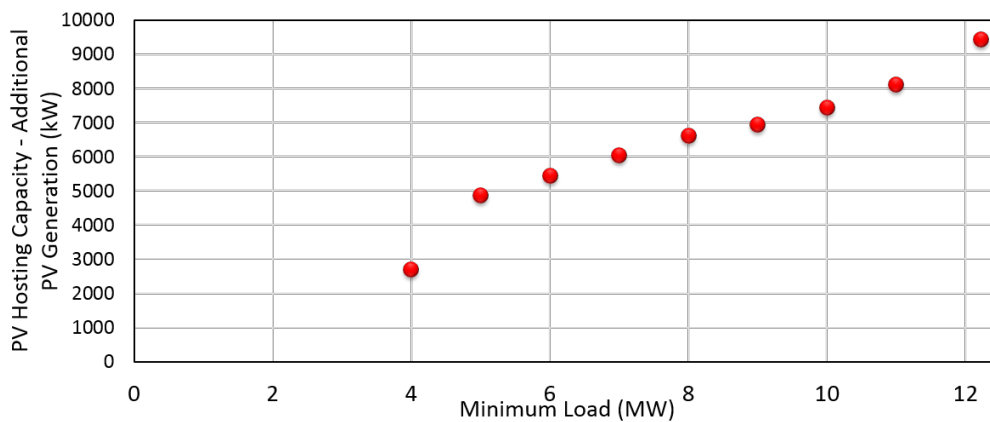


Figure 4.28: Hosting capacity vs. Minimum load.

4.6.4 Effects of PV Locations on Hosting Capacity

In the previous section, we observed that a few PV deployment scenarios may have a higher impact on system voltages, based on the relative PV sizes and locations. It may not be possible to schedule the locations of customer-owned PVs, but utility-owned PVs may be installed at those locations which potentially have the least impact on the circuit voltages. For this purpose, an additional analysis typically for the utility-owned PV system is conducted.

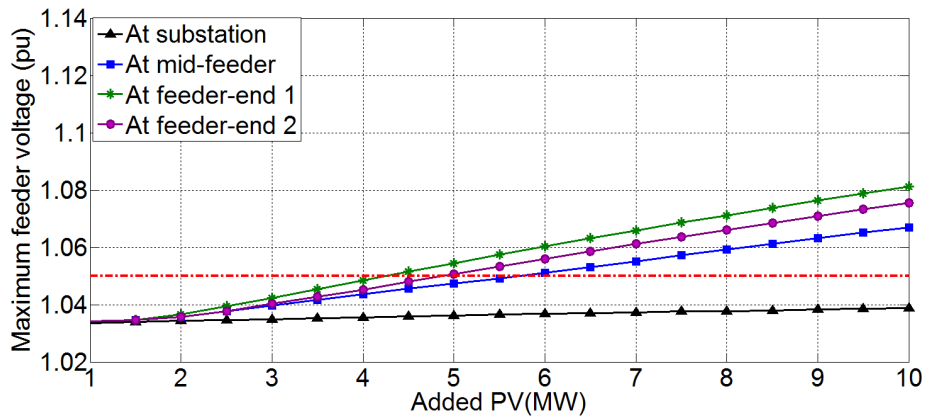


Figure 4.29: PV hosting results for each selected PV deployment locations

For this study, four locations for PV deployment are selected, at substation, mid-feeder, and at two feeder ends (see Figure 4.16). A 500-kW three-phase PV system is selected for the analysis. The number of PV systems is increased from one to twenty, thus adding a total of 10 MW of additional PV at each location. For each location and each number of PV systems, the highest primary wire voltage is recorded (see Figure 4.29). The hosting capacity is calculated for each location by identifying the additional PV capacity leading to an overvoltage violation. From Figure 4.29, no violation is recorded when PV systems were placed at the substation. The hosting capacity is lowest at

the feeder ends. To further understand the locational impacts, the distance of the PV deployment location from the substation is increased in an approximate step of 0.25 miles. As the distance from the substation increases the PV hosting capacity of the circuit decreases, as shown in Figure 4.30.

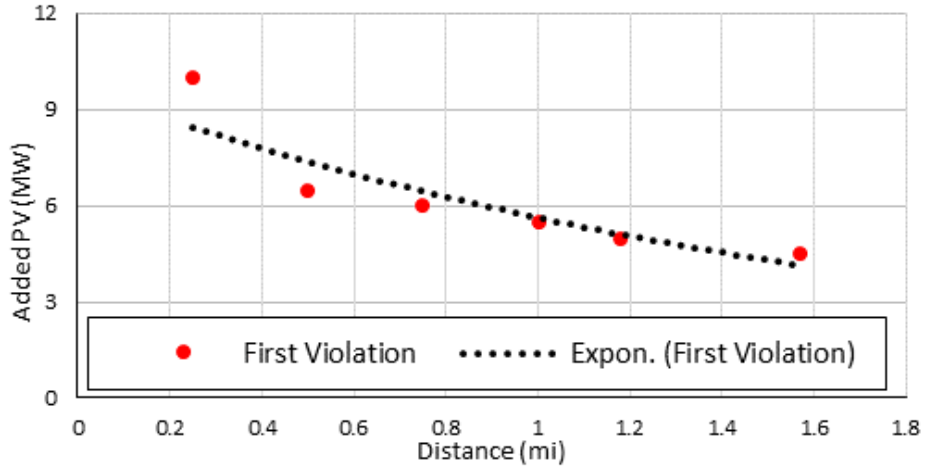


Figure 4.30: Impact of PV deployment location on PV hosting capacity.

4.7 Mitigating Overvoltage Concerns using Smart Inverters

As detailed in the previous sections, integrating large percentages of PVs into the distribution system may result in overvoltage conditions, thus deteriorating the feeder voltage quality. In the previous section, the largest PV generation capacity that a given distribution circuit can accommodate is calculated using the stochastic analysis framework. The obtained generation capacity is termed as feeder's PV hosting capacity. Note that we have considered PV panels with unity power factor for PV hosting capacity calculations. Therefore, the use of PV-based reactive power or other PV-based means of

regulating voltage were not considered. The simplest PV models with no capability for generating or absorbing reactive power were simulated in the previous discussion.

The objective of this section is to investigate the application of implementing smart inverter controls in mitigating feeder overvoltage concerns. In this section, the use of smart inverter in increasing feeder's PV hosting capacity by controlling the PV power output is demonstrated. Three voltage regulation methods are implemented: 1) Fixed power factor control, 2) Volt-Var control, and 3) Volt-Watt control. The details regarding each control method and PV hosting results are presented in the following sections.

4.7.1 Fixed Power Factor Control

Usually, the PV panels operate at unity power factor, meaning they only generate active power. The smart inverter connecting the PV panel to the grid can be used to modify the power factor of the PV panel, thus allowing it to absorb or generate reactive power. Since the objective is to avoid overvoltage concerns due to excess PV generation, the PVs must be programmed to operate at negative power factor implying they are absorbing reactive power. The smart inverter can be programmed to allow PV panels to operate at a lagging power factor. Note that the negative power factor (PF) means that the flow of active and reactive power is opposite. In this section, the results for the feeder's PV hosting capacity when PV panels are operating at $PF = -0.99$ and $PF = -0.98$ are presented.

4.7.2 Volt-Var Control

This function allows a control on the reactive power output of the PVs according to, 1) the voltage at the point of connection (the terminals of the PV system), and 2) the available apparent power capacity of the inverter at that point in time. For the volt-var control implemented in this study, the reactive power generated or absorbed by the smart inverter follows the curve shown in Figure 4.31. In Figure 4.31, the available reactive power ($Q_{available}$) is calculated using (4.15).

$$Q_{available} = \sqrt{(S_{PV})^2 - (P_{PV})^2} \quad (4.15)$$

where,

S_{PV} - is the apparent power rating of the smart inverter connected to PV.

P_{PV} - is the current active power generation of the PV panel.

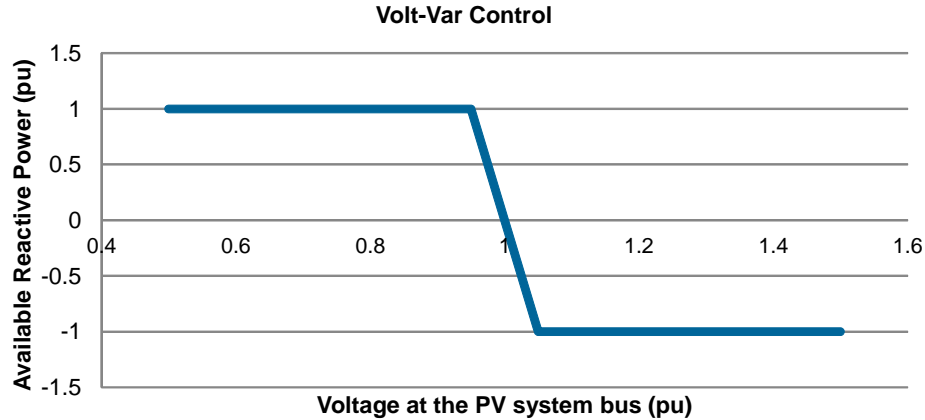


Figure 4.31: Volt-Var Curve followed by smart inverters to control the VAR output of the PVs.

Note that from Figure 4.31, for bus voltages between 0.5 pu and 1 pu, the $Q_{available}$ is positive meaning that the PV panel exhibits a capacitive behavior.

Since, bus voltages are in an undervoltage condition, the smart inverter is programmed to supply reactive power in order to avoid undervoltage. When bus voltages are between 1 pu to 1.5 pu, the $Q_{available}$ are negative implying PV has an inductive behavior. In this case, the PV is programmed to absorb reactive power in order to avoid overvoltage.

4.7.3 Volt-Watt Control

Same as the Volt-Var control, the Volt-Watt control function allows controlling the real power output from the PVs. The smart inverters only control the active power output of the PV panel based on the bus voltages at the point of connection. The plot shown in Figure 4.32 is used to control the PV panel active power. For bus voltages between 0 to 1 pu at terminal of PV system, the active power generation at the PV panel is not modified. However, from bus voltages between 1 and 1.1 pu, the PV generation is controlled to avoid bus overvoltages. Beyond 1.1 pu, the active power output of the PV panels is set to zero.

4.7.4 Results

The above three control methods are implemented and the PV hosting capacities for the selected feeder (see Figure 4.16) are calculated. The PV hosting capacity is obtained using the hourly stochastic analysis method proposed in this chapter. The results are compared against the simplest PV models with no capability of regulating feeder voltages using active or reactive power support. The results are shown in Table 4.2 and Figure 4.33.

From Figure 4.33, on implementing smart inverter based controls, the PV hosting capacity of the feeder increases for each control method. The feeder

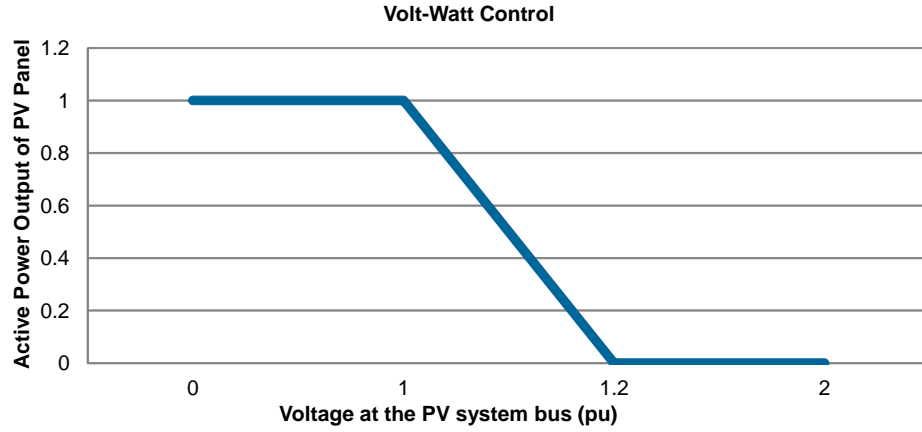


Figure 4.32: Volt Watt Curve followed by smart inverters to control the active power output of the PVs.

Table 4.2: PV Hosting Results

Cases		Additional PV Size (kW)
PF = 1	First-hosting Capacity ($H_{1,k}$)	6,084
	All-hosting Capacity ($H_{100,k}$)	6,374
PF = -0.99	First-hosting Capacity ($H_{1,k}$)	8,775
	All-hosting Capacity ($H_{100,k}$)	8,979
PF = -0.98	First-hosting Capacity ($H_{1,k}$)	>10,000
	All-hosting Capacity ($H_{100,k}$)	>10,000
Volt/Var	First-hosting Capacity ($H_{1,k}$)	8,438
	All-hosting Capacity ($H_{100,k}$)	8,896
Volt/Watt	First-hosting Capacity ($H_{1,k}$)	8,371
	All-hosting Capacity ($H_{100,k}$)	8,741

is able to accommodate 2 MW of additional PV on enabling smart inverter control for active and/or reactive PV generation. It is also observed that the fixed power control with PV panels operating at 0.98 lagging power factor

results in the largest increase in the feeder’s PV hosting capacity.

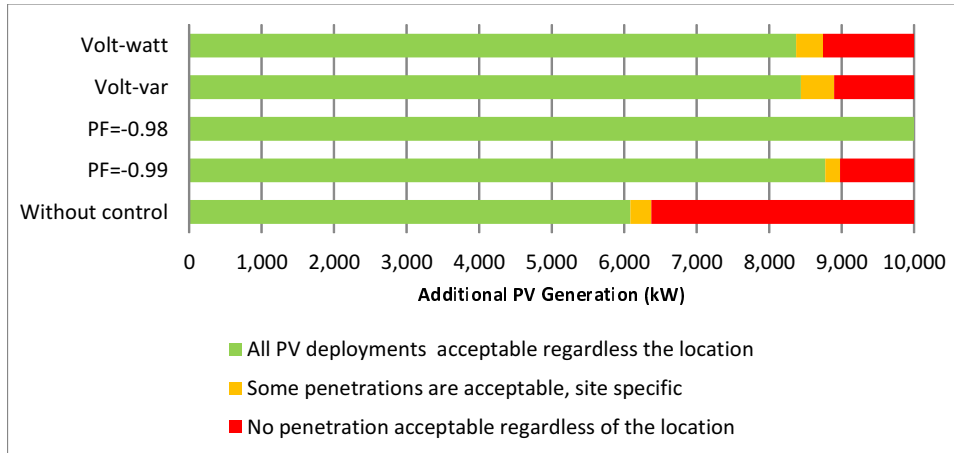


Figure 4.33: PV hosting capacity with smart inverter control.

4.8 Conclusion

This chapter presents a novel framework to understand and solve the impacts of PV integration on feeder voltages. First, a mathematical formulation for the hosting capacity problem is developed. To solve the formulated problem, an hourly stochastic analysis approach is proposed. The method is illustrated by calculating the hosting capacity of an actual 12.47-kV feeder for overvoltage concerns. The results obtained using the proposed method are compared against those obtained using a fixed minimum load condition. It is concluded that the proposed approach results in a better estimate of the feeder’s PV hosting capacity. Next, an approach to evaluating the percentage accuracy of the hosting capacity results is developed. The method aims to identify the percentage of time a hosting capacity obtained using a *k-run* MCS is expected to be accurate. The percentage accuracy is determined with respect to a tolerance parameter (ε). The results conclude that for $\varepsilon = 0.05$,

both first- and all-hosting capacities calculated using a 100-*run* MCS are expected to be accurate for 98% of time.

Additional factors related to bus overvoltage concerns resulting from PV integration are also investigated. To do so, the study analyzes the impacts PV panel size, location, and distribution on the bus overvoltage violations. Furthermore, the buses most affected due to PV integration and the impacts of feeder's minimum load condition on PV hosting capacity are also examined. Based on the analysis, the following conclusions are drawn:

1. The voltage quality impact of PV system varies with the loading condition.
2. For the same customer penetration, the PV system impact varies with the PV deployment scenario, depending on the relative PV locations and sizes.
3. PV deployment scenarios with larger PVs at farthest load nodes result in higher impacts on the voltage quality.
4. Primary buses farther away from the substation are more likely to observe overvoltages.
5. On increasing the system's minimum load, the PV hosting capacity increases.
6. As the distance of PV system location with respect to substation increases, the PV hosting capacity decreases.

Next, methods to mitigate feeder overvoltage concerns due to PV generation using smart inverters are investigated. Three control methods namely fixed power factor, volt-var control, and volt-watt control are implemented. It is observed that on implementing smart inverter control methods, the PV hosting capacity of the feeder increases.

It should be noted that the PV hosting capacity obtained using the proposed framework is still conservative as the PV variability over the year based on seasons and based on PV panel locations is not included. However, given the hourly analysis framework, the seasonal and location dependent PV data can be statistically analyzed to obtain a representative hourly PV generation profile at each PV location. The obtained hourly PV profiles can be used instead of the clear sky PV profile in the proposed analysis framework.

Although, the results are demonstrated using overvoltage condition, the proposed framework can be applied to determine the hosting capacity for other impact criterion, such as voltage deviation, voltage imbalance, etc. In sum, by developing a mathematical formulation, an hourly stochastic analysis framework, and an approach to quantify the percentage accuracy of the results, this work presents a comprehensive understanding of the PV hosting capacity problem.

Chapter 5

Grid Impacts and Benefits of Deploying Distributed Energy Storage Systems

In recent years, due to the advances in smart-grid technologies and the integration of distributed photovoltaic (PV) generation systems, the electric distribution network has been changing rapidly. These infrastructure changes pose multiple challenges for electric distribution service providers with regard to quality and reliability of the power supply. Energy storage (ES) systems have been identified as a potential solution to maintain strict power quality and reliability standards by both utilities and researchers. Including ES technology in distribution plans can enable utilities, system operators, and end users to increase power reliability and reduce the cost of electricity. Additionally, ES systems aid distribution grid flexibility as they can help integrate variable generation resources such as wind and solar. Given various applications of ES systems, a distribution system planning framework is called for, that incorporates the potential impacts and benefits of ES deployments.

The impact and value of integrating ES systems into the distribution circuit have been assessed in several technical studies [116–121]. So far, however, these technical studies have not quantified the benefits of various ES system sizes and deployment locations. Because ES deployment has been increasing, it is necessary to evaluate its value and impact on the distribution system. As such, methods that can evaluate the grid impacts and benefits of ES are

needed. Grid integration tools should be able to identify suitable ES applications, sizes, and deployment locations by using domain-specific knowledge.

This chapter presents a methodology to evaluate impacts and benefits of integrating ES systems into the distribution circuit. The purpose of this task is to develop a consistent methodology to understand the potential grid impacts and benefits of various ES deployment scenarios (utility-connected as well as customer-sited) on the distribution system. The presented analysis framework begins with identifying application scenarios for ES deployment for a given distribution feeder. Depending upon the feeder characteristics, the ES may be required to provide one or more utility or customer level benefits. Next, based on the application scenarios, ES is sized for both power and energy subsystem ratings. To understand the impacts of ES locations, multiple location scenarios by placing ES at different bus locations along the feeder are simulated. Finally, a time-series three-phase load flow analysis is simulated to understand the impacts of ES in meeting the respective application scenarios.

In this chapter, the effectiveness of ES is investigated for the following three application cases:

1. **Satisfy N-1 contingency requirement** : For this application case, ES is deployed to satisfy the N-1 contingency requirement for the substation transformer. The ES application period is assumed to be 3 to 5 years.
2. **Increase PV hosting capacity** : ES is deployed to increase feeder's PV hosting capacity so that the feeder can accommodate a total PV generation capacity equal to 75% of the feeder's peak load demand.
3. **Feeder voltage management** : In this application scenario, the ES is deployed to provide voltage regulation service through volt-var control. This analysis assumes PV systems connected to the feeder cause

unacceptable levels of voltage variations.

5.1 Operational Uses of Deploying Distributed Energy Storage Systems

Figure 5.1 portrays the operational uses where energy storage could be deployed across the electric value chain including generation, transmission, distribution, and end-user locations [116]. Using the figure, the operational uses for ES systems can be broadly categorized as having system-level benefits or customer-level benefits. For system-level benefits, ES systems are deployed to meet grid service objectives, that are directly beneficial to utility companies. As for customer-level benefits, ES systems are deployed at individual customer locations to meet objectives directly beneficial to customers. The following section illustrates both the system-level and customer-level benefits through multiple cases.

5.1.1 System-Level Benefits

This section details ES applications as seen from the system-level, i.e., from the perspective of utilities. ES systems are deployed to specifically meet service objectives directly beneficial to utility companies. A few system-level benefits of ES deployment are as follows.

1. **Distribution system upgrade deferral** - For this application, ES systems are deployed to defer any immediate or future distribution system upgrades, including substation and distribution lines, by decreasing the yearly peak load demand.
2. **Distributed energy resource (DER) integration** - ES can be used to integrate large percentages of distributed generation resources. Since

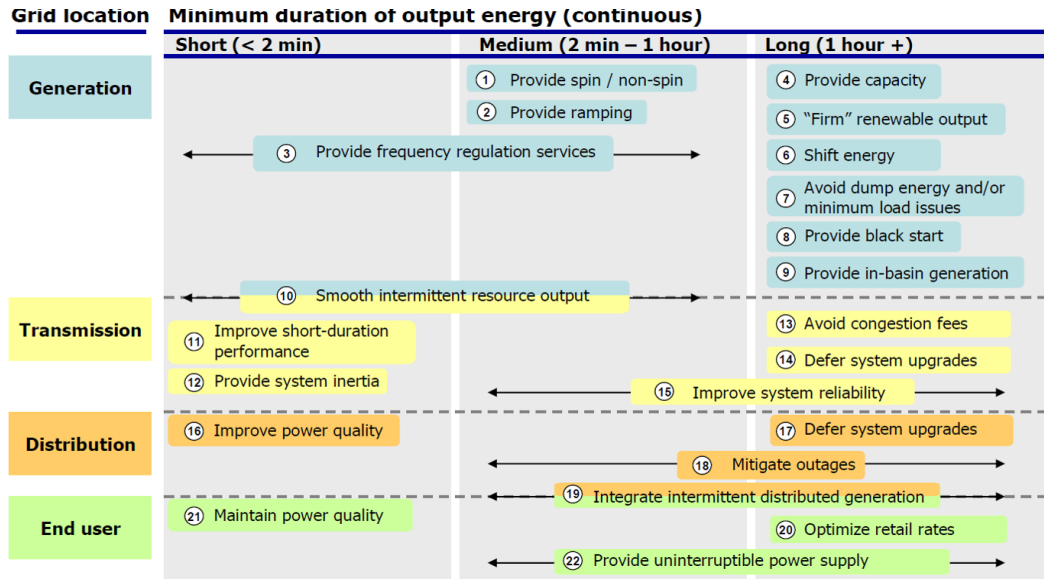


Figure 5.1: Operational uses of energy storage systems [115].

distributed energy resources (DERs) tend to generate during off-peak hours, ES can be programmed to shift the load from peak load to off-peak load hours, thus facilitating DER integration.

3. **Time-of-Use/electricity price shift** - ES can be used to decrease the cost of electricity in a real time or TOU price market. For this purpose, ES is programmed to charge when the electricity rates are higher and discharge when the rates are lower, thus decreasing the yearly cost of the electricity.
4. **Regulation Services** - ES can be programmed to provide ancillary services for frequency regulation based on the circuit's open access transmission tariff.

5.1.2 Customer-Level Benefits

As for the customer-level benefits, ES systems are planned and deployed to meet specific customer requirements. For this application case, ES systems are deployed at the end-user premises to provide service benefits to either commercial or residential customers. A few customer-level benefits of integrating ES systems are listed below.

1. **Reliability benefits** - The energy storage systems can be deployed at a few selected commercial customer locations to provide improved service reliability. In the event of an outage, ES will discharge to support the connected loads, thus decreasing both the Customer Average Interruption Frequency Index (CAIFI) and the Customer Average Interruption Duration Index (CAIDI).
2. **Demand charge management** - The demand charge is a billing mechanism used to recover the cost of providing transmission and distribution service to commercial customers. The demand charge for a particular month is calculated based on the largest peak demand recorded over the month. ES systems are deployed to decrease the monthly peak load demand and decrease the total customer demand charge.
3. **Voltage Management** - The ES can be deployed at the customer site to provide voltage regulation applications for the end-user. This scenario could be particularly beneficial for the feeders with high percentages of distributed PV generation.

5.1.3 Energy Storage Deployment

Depending on the feeder and utility requirements, the energy storage system can be integrated into a distribution circuit in different deployment stages.

For instance, if a substation supplies a feeder with large percentages of PV integration, voltage violations and reverse power flow are primary concerns for the feeder. In this case, the utility may upgrade only the feeder instead of the entire distribution circuit supplied by the substation. This type of ES deployment is referred to as the feeder-level deployment. If, instead, the load demand is the major problem, the utility may plan ES integration at the substation-level to defer the transmission and distribution (T&D) upgrades. This deployment is referred to as the substation-level deployment. The type of storage deployment will depend upon the upgrade requirements and utility preferences. In this chapter, both substation-level and feeder-level ES deployment cases are discussed using different application scenarios.

Note that, the ES can be programmed to simultaneously provide multiple/stacked benefits at the substation-level, at the feeder-level, or at the customer-level. Deploying ES for stacked benefits makes the ES deployment cost-effective. In case of stacked benefits, first, based on a distribution circuit's characteristics, a primary application for ES deployment is identified. The primary application should also provide significant monetary benefits to the utility company justifying the cost of deploying ES. Based on the primary application scenario, the ES deployment type (substation or feeder-level deployment) is identified. Next, ES is programmed for the secondary application scenarios as identified in the stacked application scenario.

5.1.3.1 Substation-level Deployment

In this case, utilities plan to deploy ES for a given substation to meet substation-level requirements. This deployment strategy may be adopted by the utility if the potential substation-level benefits of the ES are higher than

the cost of installing ES. The substation-level benefits may include T&D deferral, providing ancillary services using frequency regulation, energy arbitrage, etc.

5.1.3.2 Feeder-level Deployment

ES may also be deployed at the feeder-level. In this case, utilities upgrade individual feeders supplied by the substation. Depending on the technological changes, instead of the entire substation, only a particular feeder may require upgrades. In this case, ES may be sized to address the primary concerns of only the affected feeder. Note that if the sum of ES systems deployed for the individual feeders equals the required ES capacity for the substation-level application case, feeder-level ES deployment will be able to meet the substation-level benefits as well.

5.2 Distributed Energy Storage Analysis - Proposed Framework

The objective of this chapter is to develop a methodology to evaluate the grid impacts and benefits of integrating distributed ES systems. To do so, this chapter presents a framework to integrate ES into the distribution system. The proposed approach includes the following stages: determining the requirement for ES, calculating ES size, identifying ES locations, and evaluating grid impacts of integrating ES. Several potential application scenarios for ES deployment are simulated, and the grid impacts and benefits of ES in meeting the simulated application scenarios are assessed. The method for the ES integration analysis is detailed as following.

5.2.1 Define Application Scenarios

The first step is to identify the ES application scenarios for the given feeder. The application of ES for both feeder and substation level deployments are investigated in this chapter using the following application scenarios. Note that the proposed approach can be easily applied to plan ES deployment for other application scenarios as well.

1. **N-1 Contingency (Substation-level deployment)** : For this application case, ES is primarily deployed to satisfy the N-1 contingency requirement for the substation transformer. The ES application period is assumed to be 3 to 5 years.
2. **Increase PV Hosting Capacity (Feeder-level deployment)** : The ES is deployed to increase the feeder's PV hosting capacity. For the selected case study, the feeder is required to accommodate a total PV generation equal to 75% of the feeder's peak load demand.
3. **Voltage management (Feeder-level deployment)** : In this application scenario the ES is deployed to provide voltage regulation services through reactive power (volt-var) control. This analysis assumes PV modules cause unacceptable voltage variations for the selected feeder and ES is required to mitigate the voltage concerns.

5.2.2 Identify Starting Point for ES Analysis

Once the application scenarios are defined, the next step is to identify the starting circuit conditions for the ES grid impact analysis. The starting conditions will depend on the selected application scenario. For example, if ES is deployed to defer the substation upgrade, the starting point for the analysis will be the year substation overloading is projected. On the other hand, if the

application scenario is PV integration, a circuit already experiencing adverse impacts due to PV integration will be selected as the starting condition.

Therefore, in this step, based on the ES application scenario, the initial circuit conditions are simulated. To simulate the initial circuit condition, several assumptions for ES deployment are specified. The assumptions may include:

1. Yearly load profile used for the analysis.
2. Load growth rate.
3. The number of years ES will be used to defer substation or feeder upgrade.
4. Initial percentage penetration of distributed energy resources (DERs), for example, PVs.
5. Feeder's PV hosting capacity.
6. Assumptions regarding the PV variability.

5.2.3 Determine ES Size

Energy storage needs to be sized for two systems, the power subsystem (MW) and the energy subsystem (MWh). The power subsystem (MW) rating defines the largest power demand the energy storage can supply. The energy subsystem rating (MWh) defines the total energy the energy storage can provide without recharging. The size of both subsystems are obtained based on the application scenario.

5.2.4 Identify ES Locations

The next task is to identify potential ES locations. The ES locations are more flexible for system-level benefits. Utilities can deploy storage units at any feasible location along the feeder including the substation, at feeder-ends,

or at mid-feeder. For customer level benefits, however, ES must be deployed at the individual customer locations. If multiple ES locations are possible, the best ES locations for providing stacked benefits are identified.

5.2.5 Conduct Grid Impact Analysis

The grid impacts of ES are quantified using a time-series load flow analysis simulated for each ES application scenario. The analysis demonstrates the usefulness of ES in meeting the desired grid objective. A three-phase load flow analysis is conducted for each energy storage deployment scenario, and the corresponding distribution system parameters are calculated. The grid impact analysis involves evaluating the utility of ES in improving the performance of the distribution system for a given grid objective or planning criteria.

5.3 Application 1 - Energy storage to meet N-1 Contingency

This case study demonstrates the application of ES systems in meeting the N-1 contingency requirement for the substation transformer. The case study simulates two identical substation transformers supplying for two distribution feeders with identical load demand characteristics and equal peak load demands. Under the N-1 contingency case, one of the transformers is out-of-service, and the other transformer is supplying both feeders. The ES is deployed to avoid the transformer overloading under the N-1 contingency case. The ES is planned to operate for 5 years. The steps for integrating and evaluating the effectiveness of ES are detailed as follows.

5.3.1 Selected Distribution Circuit

The one-line diagram for the distribution circuit under analysis is shown in Figure 5.2. Two identical 40 MVA transformers are connected to the substation. Each transformer serves a distribution feeder with a peak load demand of 20.6 MW measured in year 2013. It is assumed that under normal condition, both transformers are in service. Clearly, under normal operating condition, none of the transformers records an overloading.

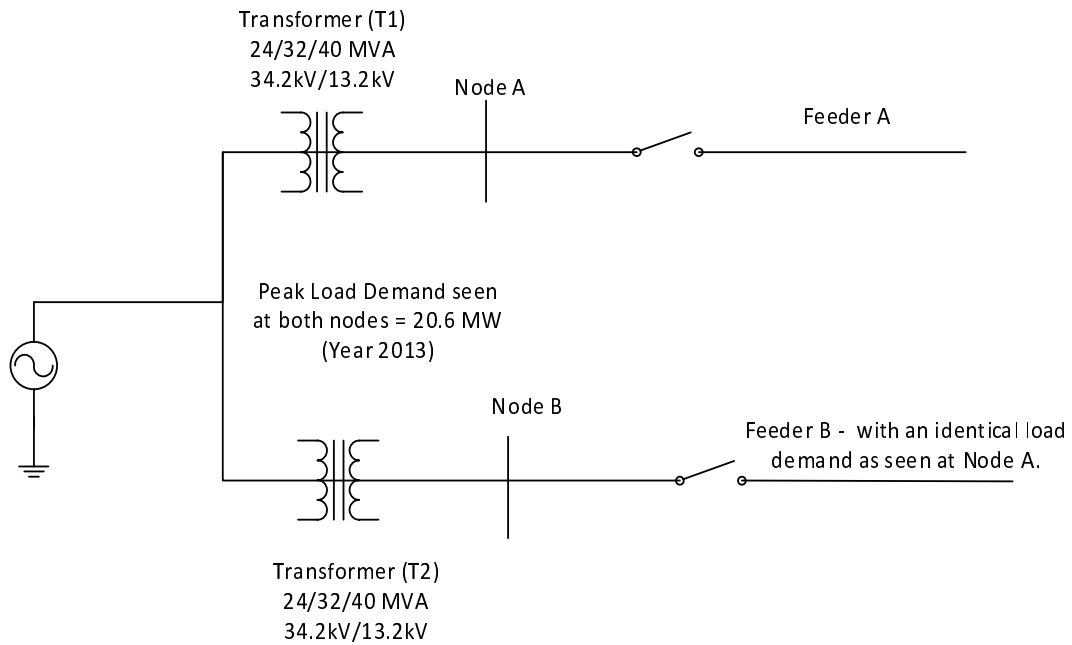


Figure 5.2: One-line Diagram of the Distribution Circuit Selected for Analysis (Courtesy of the electric utilities).

Next, the N-1 contingency condition is simulated by applying a fault at the secondary terminal of one of the transformers so that the transformer (T1) is out-of-service. In this case, the other 40 MVA transformer (T2) is required to serve both feeders (see Figure 5.3). Based on the peak load demands of

both feeders, the worst-case demand of transformer T2 in year 2013 is $20.6 + 20.6 = 41.2$ MW. Since the worst-case load demand exceeds the transformer rating, the N-1 contingency requirement is not satisfied for year 2013.

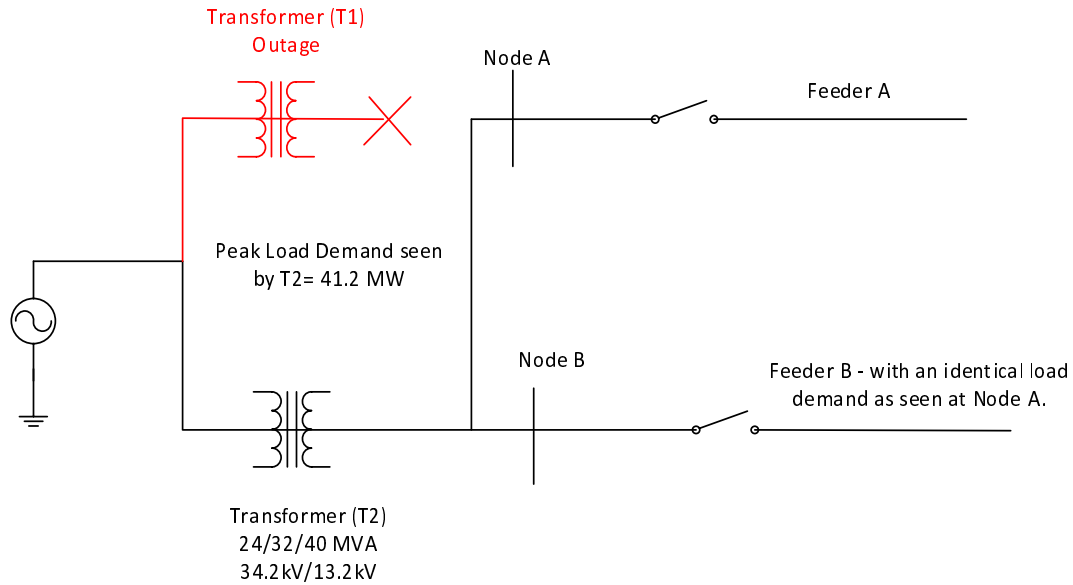


Figure 5.3: Simulated N-1 Contingency Case (Courtesy of the electric utilities).

The task of this case study is to demonstrate the application of ES in meeting the N-1 contingency requirement for the substation transformer. The ES is planned for 5 years after the year the N-1 contingency is not met. In the simulated case study, the N-1 contingency requirement is not met in year 2013. Therefore, ES will be planned for years 2013 to 2017.

The assumptions made for the ES integration study are as follows:

1. **Criteria for ES deployment:** ES will be required starting from the year when the N-1 contingency requirement is not met.
2. **The number of years ES is planned:** The ES is planned for 5 years since the N-1 contingency requirement is not met. In this case, the

contingency requirement for the substation transformer is not met in year 2013. Therefore, ES will be planned for years 2013 to 2017.

3. **Load assumptions:** For each feeder, the peak load demand recorded for year 2013 is assumed to be 20.6 MW. This results in a total peak load demand of 41.2 MW.
4. **Load shape profile:** The yearly load shape profile (for Year 2013) provided for the Feeder A is used for the analysis (Figure 5.4).
5. **Load growth rate:** A 3% load growth rate per year is assumed for the selected feeders. Using 3% load growth and the load demand profile measured for year 2013, the peak load demands and yearly load profiles for the future years are projected.

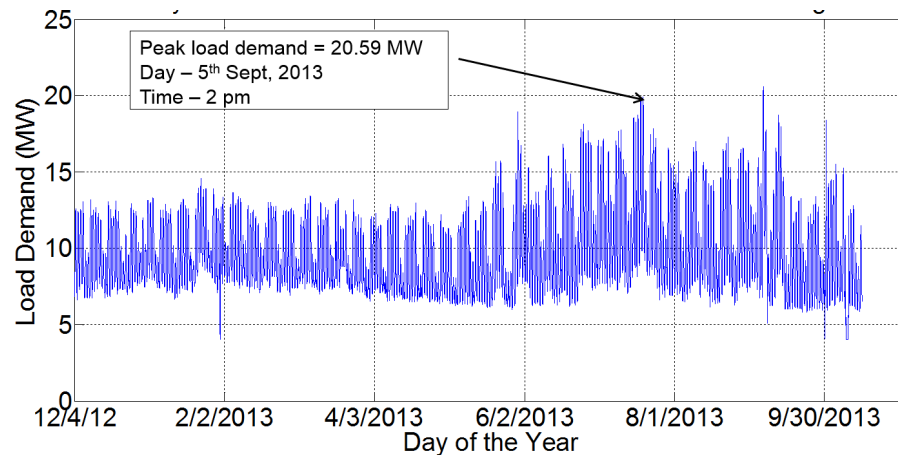


Figure 5.4: Yearly load shape profile measured at the Node A (Year 2013).

5.3.2 Identify Starting Point for ES Analysis

In this case, two identical 40-MVA transformers are connected at the substation and supply two identical feeders, each with a peak load demand of 20.6 MW measured in year 2013. During N-1 contingency case, one of the

transformers is out-of-service, and both feeders are served by one 40-MVA transformer. The objective is to determine if the transformer is adequate to meet the load demand for both feeders. The N-1 contingency requirement is satisfied if the transformer can supply both feeders without recording any overloading. As detailed in the previous section, for the simulated case study, the substation is not able to provide N-1 contingency requirement for Year 2013, necessitating ES deployment in year 2013.

5.3.3 Determine Energy Storage Size

The next objective is to identify a suitable ES size so that the N-1 contingency can be met for a duration of 5 years starting from year 2013. ES needs to be sized for the power subsystem (MW) and energy subsystem (MWh). The power subsystem rating defines the largest capacity that ES can supply. The energy subsystem rating defines the total energy an ES can provide without recharging. Since sizing the ES for the worst case peak load and duration could be expensive and wasteful, ES MW rating and duration are calculated using a typical peak load demand and overload duration. The ES size is determined according to the statistical analysis of the peak load demand and the energy supplied during the overload condition using the current and projected substation load demand for years 2013 to 2017.

Note that the load demand is available for a total of 315 days for year 2013 in hourly intervals. The available load demand data for Year 2013 results in 7560 (315×24) data points corresponding to each hour of the day. The yearly profile for year 2013 is projected to future years at a load growth rate of 3% per year. The measured and projected load demand are analyzed together to understand the loading condition for the ES plan duration (i.e., from 2013-

2017). The current and projected yearly load demands for Years 2013 to 2017 result in a total of 37800 data points (dataset), with 7560 data points for each year. A percentile analysis is done on the obtained data set to obtain ES size. The details of the analysis approach are as follows.

5.3.3.1 Percentile Analysis

The objective of the percentile analysis is to obtain a representative size for the ES based on the feeder's typical peak load and its duration. Given the uncertainty in the load demand, sizing ES based on the worst case peak load demand is not advisable. Instead, a statistically representative peak load should be selected. A percentile analysis assists in doing the same. Additionally, the percentile analysis helps in quantifying the risk as well. For example, if a median (50th-percentile) value is selected for the peak load, there is a 0.5 probability that if a transformer overloading occurs, the selected ES size will not be able to mitigate the overloading concern. Note that the probability of the peak load occurring should be included while calculating the net N-1 transformer contingency parameter. Assume that over the span of 5 years, a transformer overloading is expected to occur with a probability p . Let the ES be sized for 50 percentile peak load. In this case, the N-1 contingency for the transformer will not be met with a $p_{fail} = 0.5 \times p$ probability.

5.3.3.2 Energy Storage Power System Rating

The ES MW capacity required to mitigate transformer's overloading concern is determined using the current and projected load demand profiles. The required ES MW capacity for each overloading condition is determined by subtracting the recorded overload demand and the substation transformer rating

(40 MVA). A percentile analysis is done on the obtained ES MW capacities and a representative ES MW rating is identified. The percentile plot for the ES MW capacity is shown in Figure 5.5.

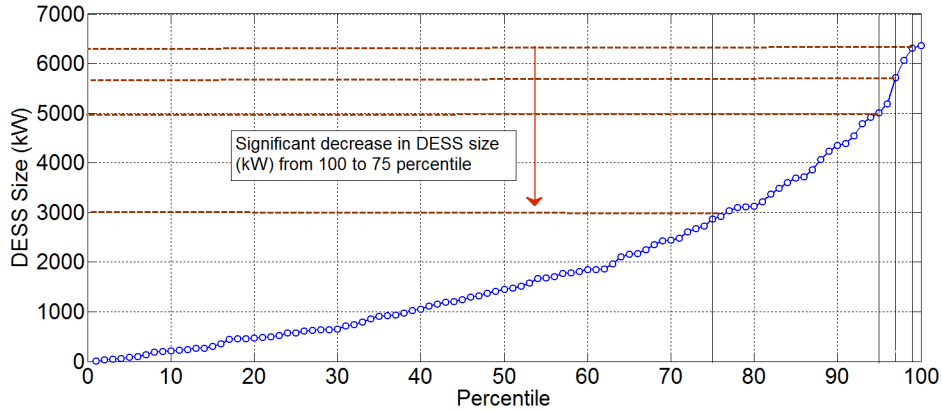


Figure 5.5: Percentile plot of ES size based on overload recorded for Years 2013-2017.

From the figure, the required ES capacity to meet N-1 contingency requirement decreases significantly from the 100th-percentile to the 75th-percentile value. Assuming 3% load growth, the required ES capacity decreases from 6.37 MW (100th-percentile) to 2.8 MW (75th-percentile). The 75th-percentile shows that, under the worst-case scenario, there is a 0.25 probability that the ES will be not be able to mitigate a transformer overload resulting from an N-1 contingency scenario. For the simulated case study, in a span of 5 years (2013-2017), a transformer overloading is recorded only for a total of 111 hours. This results in a 0.0029 probability of observing an overvoltage for the duration of 5 years. While calculating the absolute probability of ES being unable to meet N-1 contingency requirement, the probability of observing an overvoltage over the duration for which ES is deployed should be included. Essentially, if the ES capacity corresponding to a 75th-percentile value is deployed, the N-1 contingency may not be met with a probability of 7.34×10^{-4} (0.0029×0.25).

5.3.3.3 Energy Storage Energy System Rating

Next, the energy subsystem rating, or the energy storage MWh capacity, is determined. For the worst-case scenario, the ES MWh capacity should, at least, equal the largest energy (MWh) supplied above the substation transformer rating. For this analysis, the daily energy served above the substation transformer rating for the 5-year duration under consideration is calculated. To do so, the area between the load demand curve and substation transformer rating is calculated. Next the percentile analysis is done for the energy served above transformer rating (see Figure 5.6). Using Figure 5.6 the ES MWh capacity for a selected percentile value can be obtained. For a 3% load growth, the required ES MWh capacity is 9.95 MWh for the 75th-percentile value.

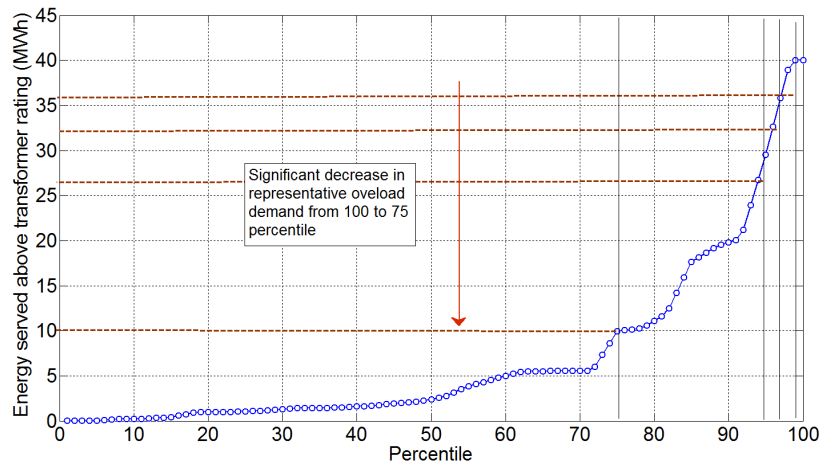


Figure 5.6: Percentile plot of the energy served above transformer rating for Year 2013-2017.

The detailed results for the percentile calculation are shown in Table 5.1. The table also shows the probability of not meeting N-1 contingency requirement corresponding to each percentile value. Note that the actual probability

of not meeting contingency will also depend upon the probability of observing a fault at either of the transformer terminals. For the results shown in Table 5.1, it is assumed that the fault occurs with a 100% certainty.

Table 5.1: Percentile values for the required ES capacity based on load demand for years 2013-2017 and using a 3% load growth

Percentile	ES power subsystem rating (MW)	ES energy subsystem rating (MWh)	Probability that N-1 contingency not met
100	6.37	40.01	0
99	6.31	40.01	0.29×10^{-4}
97	5.71	35.81	0.84×10^{-4}
95	5.01	29.52	1.45×10^{-4}
90	4.35	19.8	2.9×10^{-4}
75	2.8	9.95	7.34×10^{-4}
50	1.5	2.4	14.5×10^{-4}

5.3.4 Determine Energy Storage Location

To satisfy the N-1 contingency criteria, the ES can be located anywhere along the distribution feeder. Figure 5.7 portrays some potential locations of the ES with regard to this particular case study. For each ES location in the figure, when one of the transformers is out of service under the fault condition, the ES can be dispatched successfully to mitigate the potential overloading of the healthy transformer.

5.3.5 Conduct Grid Impact Analysis

The utility of deploying a 75th-percentile ES capacity, which corresponds to 2.8 MW/9.95MWh ES, on meeting N-1 contingency criteria for Years 2013-2017 is demonstrated in this section. Figure 5.8 shows the reduction in the overload demand recorded from Years 2013-2017. It can be seen that the

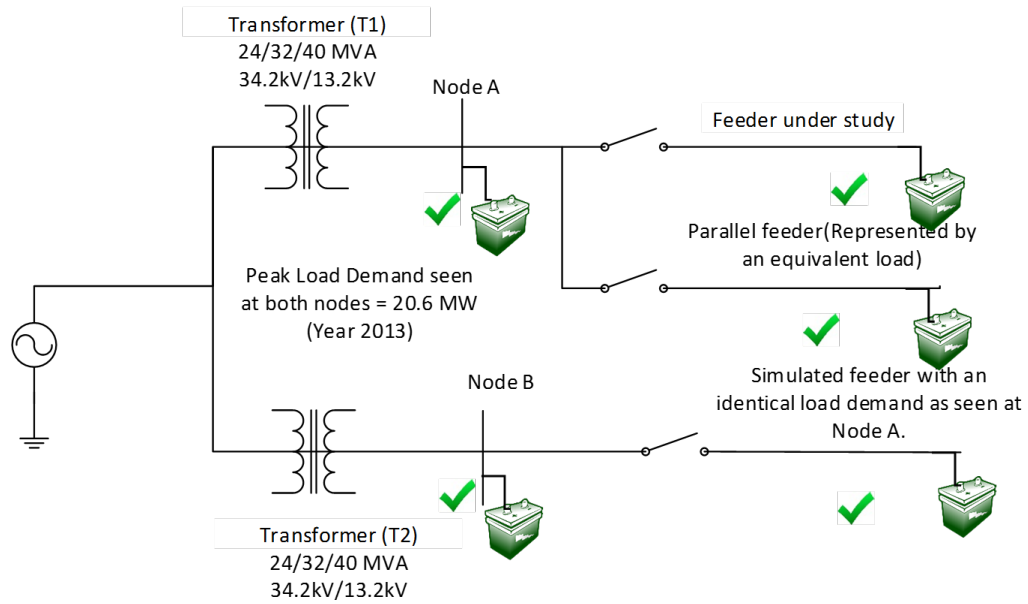


Figure 5.7: Potential Locations for Energy Storage Deployment to meet N-1 contingency requirement (Courtesy of the electric utilities).

deployed ES is able to provide for the contingency requirements for most of the time. At the 75th-percentile, the N-1 contingency requirement is not met for a few hours. Note that the ES is programmed to discharge to keep the substation load demand less than 40 MW and the ES is programmed to begin charging at 2 am.

The total energy served above the transformer rating and the total number of hours the transformer overloading is recorded for each year is shown in Table 5.2. For years 2013 and 2014, no event of transformer overloading is expected. However, when a 75th-percentile ES capacity is deployed, at the worst case, the transformer will be required to supply 12.64, 41.92 and 95.61 MWh above its rating for years 2015, 2016, and 2017, respectively.

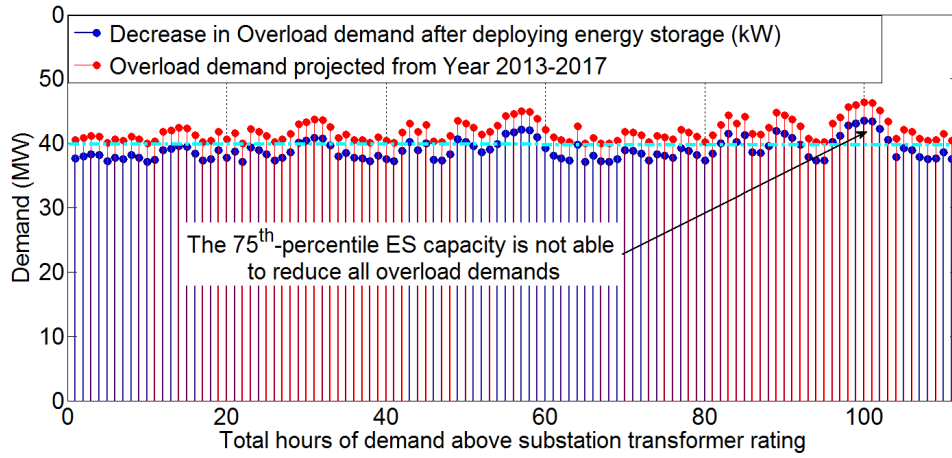


Figure 5.8: Application of energy storage is the substation mitigating transformer overloading during an N-1 contingency scenario.

Table 5.2: Energy served above transformer rating for Years 2013-2017

Year	Energy served above transformer rating (MWh)	Time above transformer rating (hr)
2013	0.00	0
2014	0.00	0
2015	12.64	10
2016	41.92	29
2017	95.61	55

5.4 Application 2 - Energy Storage to Increase PV Hosting Capacity

In this application scenario, ES is deployed to increase the PV hosting capacity of the distribution circuit. As discussed in Chapter 4, the PV hosting capacity of a distribution feeder is defined as the largest PV generation capacity that the feeder can accommodate without violating the feeder’s normal operating conditions. PV hosting capacity can be defined with respect to several impacts criteria including overvoltage concerns, voltage deviation, reverse

power flow, and protection related issues. This study however aims to mitigate overvoltage concerns of integrating PV and calculates hosting capacity using feeder overvoltages only.

The application scenario is detailed as following. The selected distribution feeder is required to accommodate a total PV generation equal to the 75% of the feeder's peak load demand. First, the PV hosting capacity of the selected distribution circuit without any energy storage unit is calculated. Next, the ES system is sized depending upon the feeder's PV hosting capacity and required PV accommodation limit. Finally, the PV hosting capacity for the feeder is calculated after deploying ES. The impact of ES locations on feeder's PV hosting limit is also investigated. In this study, the PV hosting capacity is calculated only for the overvoltage concerns. The PV hosting capacity for other impact criteria could be calculated and included in the analysis as well.

5.4.1 Selected Distribution Circuit

The selected 12.47-kV distribution circuit is supplied by a 24-MVA substation transformer and is connected to a total of 1.196 MW of PV system. The distribution circuit serves 1218 customer loads out of which 71% are residential customers. The feeder records a peak load demand of 12.5 MW for year 2013. The objective of this ES application scenario is to increase the PV hosting capacity of the feeder so that 75% of the feeder's peak load demand i.e. 9.375 MW is supplied by PV units.

5.4.1.1 Feeder's PV Hosting Capacity

Next, the PV hosting capacity of the selected feeder is calculated using the stochastic analysis framework proposed in Chapter 4. The method, anal-

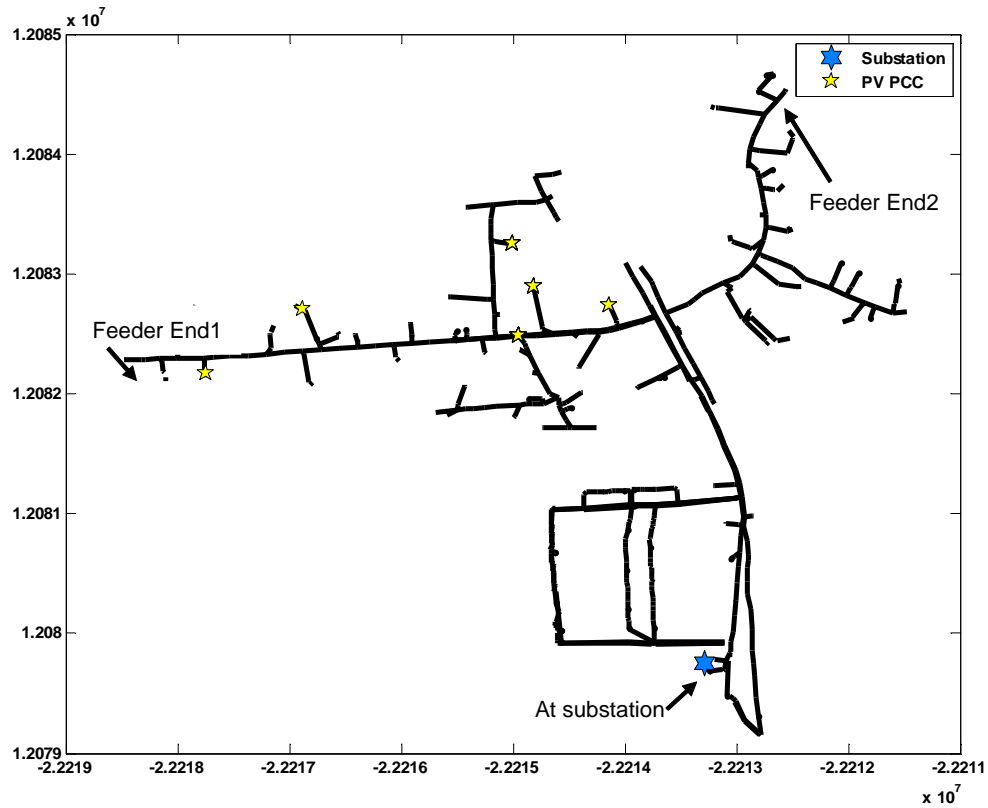


Figure 5.9: One-line diagram of the selected distribution feeder (Courtesy of the electric utilities).

ysis, and results are detailed in Chapter 4. Based on the analysis, the selected feeder can accommodate 6.084 MW of additional PV without resulting in any case of overvoltage violations. Beyond 6.084 MW and up to 6.374 MW, a few PV deployment cases may record an overvoltage while others may not. After including 6.374 MW of additional PV, the selected feeder is expected to record an overvoltage violation irrespective of the PV locations. Considering the most conservative case where the feeder records no case of voltage violation (irrespective of PV locations), the feeder can accommodate 6.084 MW additional PV and 1.196 kW of existing PV. The actual PV hosting capacity

of the feeder is $(6.084+1.196)$ MW = 7.28 MW.

5.4.1.2 Assumptions for ES Deployment

The objective is to increase feeder's PV hosting capacity so that it can accommodate a total PV generation equal to 75% of the feeder's peak load demand, i.e. 9.375 MW. Therefore, it is required to increase the feeder's PV hosting capacity by 2.095 MW. An overvoltage condition is observed due to the excess PV generation. To compensate for the excess PV generation, ES should operate as a sink for active power generated using PV panels. Therefore, ES is sized and programmed to charge (act as load) when the excess PV generation may result in a case of overvoltage violation.

The assumptions for ES deployment are as follows:

- **Circuit load condition** - PV hosting is calculated using the effective minimum load obtained for the feeder. The details regarding the effective load calculation is given in Chapter 4.
- **Energy storage control** - To mitigate overvoltage regulation concerns, ES is programmed to charge using the excess PV generation thus allowing the feeder to accommodate additional PV capacity.
- **Energy storage size** - Energy storage size is determined based on the required PV hosting capacity of the feeder. In this case, it is required to increase the PV hosting capacity of the feeder to 75% of the feeder's peak load demand, i.e. 9.375 MW. The ES should be sized so that it can absorb the excess PV generation beyond the feeder's PV hosting limit.
- **Energy storage location** - Three location scenarios are simulated: 1) at substation, 2) at FeederEnd1, and 3) at FeederEnd2 (see Figure 5.9).

5.4.2 Energy Storage Size

The PV hosting capacity calculated for the feeder is shown in Figure 5.10. The results shown in Figure 5.10 includes 1.196 MW of the existing PV. Based on the case study, the PV hosting capacity should be increased to 9.375 MW. The energy storage should absorb the excess PV generation above the feeder's PV hosting capacity limit.

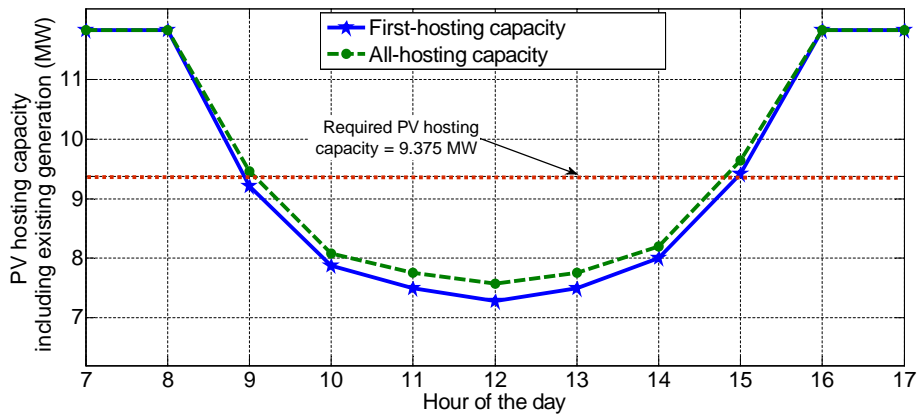


Figure 5.10: PV hosting capacity for overvoltage concern (Additional + Existing PV generation).

5.4.2.1 Energy Storage Power Subsystem Rating

The ES should provide for the peak power generation beyond the feeder's hosting capacity. The ES MW size is determined by subtracting the feeder's PV hosting capacity by the required PV hosting capacity. Therefore, to increase the PV hosting capacity to 9.375 MW, an ES with power subsystem rating equal to $9.375 - 7.28 = 2.095$ MW is required.

5.4.2.2 Energy Storage Energy Subsystem Rating

The ES should provide for the energy generated beyond the feeder's hosting capacity limit. The ES MWh size is determined by calculating the area between the required PV hosting capacity and the feeder's hourly first hosting capacity plots. The obtained MWh capacity for the ES is equal to 8.37 MWh.

5.4.3 Energy Storage Location

To understand the impact of ES location on feeder's PV hosting limit, three location scenarios are simulated. The ES is deployed at the substation, FeederEnd1, and FeederEnd2 (see Figure 5.9). An ES of size 2.095MW/8.37MWh is deployed at the three selected locations separately and is programmed to charge. The PV hosting capacity of the feeder is calculated using the proposed PV hosting analysis framework (see Chapter 4). The PV accommodation limit after deploying ES is compared against the feeder's actual PV hosting capacity.

5.4.4 Grid Impact Analysis

The PV hosting capacity calculated for each ES location scenario is shown in Table 5.3. On integrating ES, the PV hosting capacity for feeder overvoltage concern increases for each location scenario. The increase in the hosting capacity, however, depends upon the ES location. The feeder can accommodate a larger PV capacity on placing the ES at feeder ends compared to when placed at the substation. Therefore, based on the findings, for increasing the PV accommodation limit of the feeder, the ES should be placed towards feeder ends.

Table 5.3: PV Hosting Results

Cases		PV Hosting Capacity (Existing + Additional) (kW)
No Energy Storage	First-hosting Capacity ($H_{1,k}$)	6,084
	All-hosting Capacity ($H_{100,k}$)	6,374
At substation	First-hosting Capacity ($H_{1,k}$)	7,610
	All-hosting Capacity ($H_{100,k}$)	7,900
At Feeder End 1	First-hosting Capacity ($H_{1,k}$)	9,617
	All-hosting Capacity ($H_{100,k}$)	9,864
At Feeder End 2	First-hosting Capacity ($H_{1,k}$)	9,277
	All-hosting Capacity ($H_{100,k}$)	9,535

5.5 Application 3 - Energy Storage to Mitigate PV Variability

High penetrations of photovoltaic generation (PV) in the distribution circuit can cause voltage variability concerns. For example, a sudden drop in PV generation caused by rapid cloud movements can cause feeder voltages to suddenly ramp up or ramp down to unacceptable levels. This section demonstrates the application of energy storage units in regulating voltage variations caused by PV generation. The case study investigates the effectiveness of ES in providing voltage regulation services using reactive power control (Volt/Var) in the event when the existing PV generation suddenly ramps up or down. The location of ES units affect their ability to mitigate voltage regulation concerns. To understand ideal ES placement, ES is deployed at several locations along the feeder. Then, voltage variation levels for feeders with and without ES systems are recorded and compared. Finally, using actual PV generation data, the ability of ES to mitigate feeder voltage variation concerns is demonstrated.

5.5.1 PV Variability

An example PV generation profile recorded on a typical day at a PV plant is shown in Figure 5.11. The figure shows the 24-hour PV generation profile on a high variability day due to cloud transients. It can be seen from the figure that, depending on the weather conditions, the PV profile may be highly variable, with sudden generation drops from 1 pu to as low as 0.2 pu.

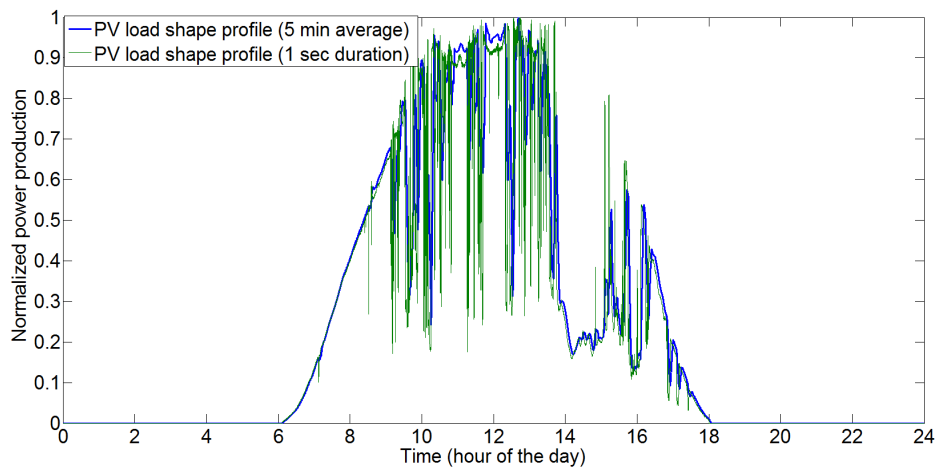


Figure 5.11: A typical PV generation profile with cloud transients.

Energy storage (ES) systems can be used to provide active and/or reactive power support to mitigate voltage regulation concerns caused by PV variability. When used for providing active power support, the energy storage units will be programmed to charge and discharge in accordance with the rate of change in PV generation. Therefore, in this case the ES compensates for the sudden change in PV generation thus effectively mitigating variability on the PV generation itself and in turn reducing the voltage variability. However, when ES is used to provide reactive power (VAR) support, the ES will not

affect active PV power generation. Instead, the ES will directly mitigate voltage variability concerns by generating or absorbing reactive power. Note that the reactive power based voltage regulation is preferred over the active power control because ES based active power support requires battery to charge and discharge thus deteriorating battery's life-cycle. This section demonstrates the effectiveness of using ES reactive power support to mitigate voltage variation concerns caused by PV variability.

5.5.1.1 Mathematical Analysis of Voltage regulation Concern

The analytical derivation of the voltage variation observed due to PV panels injecting active power into the grid is presented here. The change in feeder voltages on changing the active power generation of the PV panels is obtained using the Z_{bus} matrix of the distribution circuit. For a distribution circuit, assuming PV panels are the current injection sources, the voltage deviation depends upon the real part of the Z_{bus} matrix, termed as R_{bus} matrix. The detailed derivation is as follows.

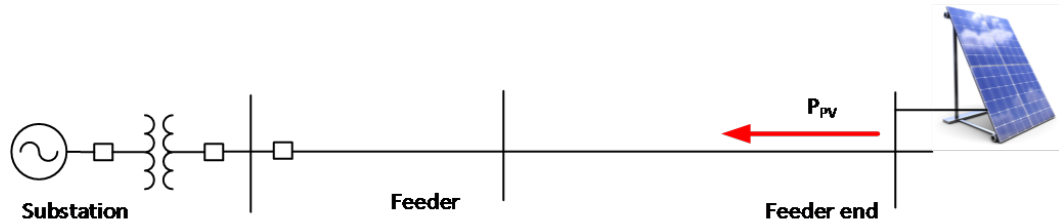


Figure 5.12: A simplified one-line diagram of the distribution feeder connected to PV.

The bus voltages recorded for the feeder is given by (5.1), where loads and distributed generation units are represented as the current injection sources.

$$V_{bus} = Z_{bus} \times I_{inj} \quad (5.1)$$

$$Z_{bus} = R_{bus} + jX_{bus} \quad (5.2)$$

$$I_{inj} = \frac{(P_{inj} + jQ_{inj})^*}{V_{norm}} \quad (5.3)$$

Substituting (5.2) and (5.3) in (5.1)

$$V_{bus} = (R_{bus} + jX_{bus}) \times \frac{(P_{inj} + jQ_{inj})^*}{V_{norm}} \quad (5.4)$$

Next, the change in bus voltage with respect to the change in injected active (dP_{inj}) and reactive power (dQ_{inj}) is given as following:

$$dV_{bus} = \frac{\partial V_{bus}}{\partial P_{inj}} dP_{inj} + \frac{\partial V_{bus}}{\partial Q_{inj}} dQ_{inj} \quad (5.5)$$

Since, PV is assumed to be generating at the unity power factor, $dQ_{inj}=0$.

The change in bus voltages with respect to active power injected at PV bus is obtained by differentiating (5.4) with respect to change in injected active (∂P_{inj}).

$$\frac{\partial V_{bus}}{\partial P_{inj}} = \frac{R_{bus}}{V_{norm}} - j \frac{X_{bus}}{V_{norm}} \quad (5.6)$$

Ignoring the imaginary component in (5.6) we obtain:

$$\frac{\partial V_{bus}}{\partial P_{inj}} = \frac{R_{bus}}{V_{norm}} \quad (5.7)$$

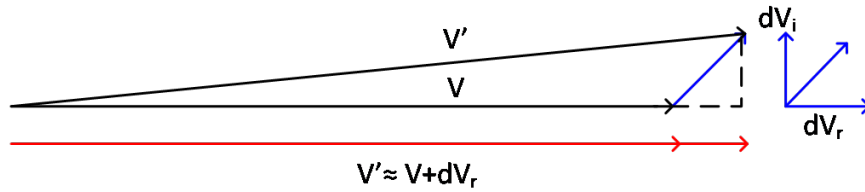


Figure 5.13: Change in voltage.

Therefore, the change in bus voltage with respect to the change in injected active (dP_{inj}) is equal to

$$dV_{bus} = \frac{R_{bus}}{V_{norm}} dP_{inj} \quad (5.8)$$

It can be observed from (5.8), that the voltage deviation observed due to PV generation depends upon the R_{bus} matrix of the distribution circuit and the rate of change of PV generation.

5.5.1.2 Energy Storage to mitigate Voltage Regulation Concern

The utility of energy storage (ES) in mitigating voltage variations resulting from the PV generation variability is analyzed. To do so, ES units are connected to a few selected feeder locations. The feeder voltages before and after implementing ES are derived. Finally, the reactive power required to mitigate voltage variability resulting from PV generation is calculated.

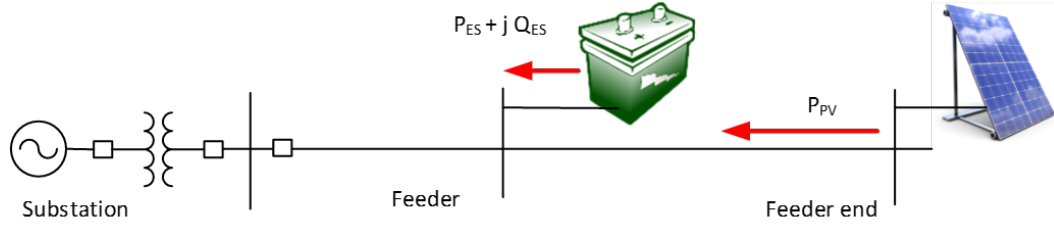


Figure 5.14: Mitigating PV voltage variation concern using ES.

Prior to implementing ES units, the change in bus voltages with respect to the change in injected active power due to PV units is given as:

$$dV_{bus} = \frac{R_{bus}}{V_{norm}} dP_{inj} \quad (5.9)$$

After implementing ES, the change in bus voltages is as follows:

$$dV'_{bus} = \frac{R_{bus}}{V_{norm}} (dP_{inj} + dP_{ES}) + \frac{X_{bus}}{V_{norm}} dQ_{ES} \quad (5.10)$$

The objective of installing ES is to result in a lesser or no voltage deviation due to PV generation, i.e. $dV'_{bus} \simeq 0$. From (5.10), it is clear that to mitigate voltage variations, the ES can be programmed for both active (Volt/Watt) and reactive power (Volt/Var) control. The Volt/Var control, however, unlike Volt/Watt control, does not involve the cycling of battery and hence does not affect ES life-cycle cost.

Assuming ES is only providing reactive power support, the reactive power required by ES to mitigate voltage variability is obtained as follows:

$$dQ_{ES} = -X_{bus}^{-1} \times R_{bus} \times dP_{inj} \quad (5.11)$$

Note that ES reactive power requirement depends upon the feeder's R/X ratio.

5.5.2 Selected Distribution Feeder and Assumptions

The objective of this scenario is to demonstrate the use of ES in providing voltage regulation services for the feeder for year 2013. Note that the selected feeders are connected to a total of 1.196 MW of existing PV generation. The locations and installed capacities of the existing PV panels for the selected feeder are shown in Figure 5.15.

In order to understand the impacts of PV variability on the feeder voltages and the utility of ES in mitigating the voltage concerns, two extreme PV variability cases are simulated. The simulated scenarios are described as follows:

1. **Case 1 - PV Ramping Up** : In this case, the existing PV generation ramps up from zero to the full rated power output of 1.196 MW in 1

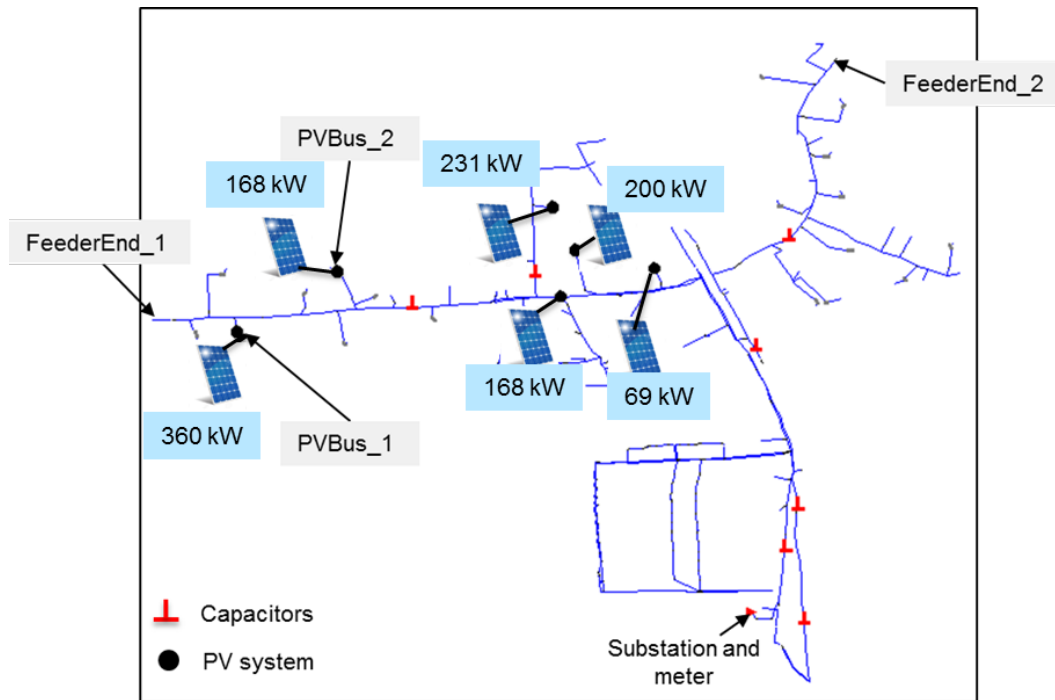


Figure 5.15: One-line diagram of the selected distribution feeder with existing PV locations and generation capacities (Courtesy of the electric utilities).

minute. As the PV generation ramps up, the feeder voltages are expected to ramp up as well. The energy storage is required to decrease the rate of voltage ramping by providing reactive power support.

2. **Case 2 - PV Ramping Down** : In this case, the existing PV generation ramps down from the full power output of 1.196 MW to zero in 1 min. In this case the feeder voltages will decrease as the PV generation ramps down and the ES is required to decrease the rate with which the feeder voltages ramp down by providing reactive power support.

The feeder loading conditions, criteria for voltage support using ES, ES size and locations, and PV variability assumptions are detailed as following.

- **Circuit Load Condition** - Circuit is operating at the minimum load

condition.

- **Energy Storage Control** - To mitigate voltage regulation concerns, ES is programmed to provide reactive power support (Volt/Var control).
- **PV Variability** - Time taken for PV generation to ramp up from 0 MW to full power (1.196 MW) or ramp down from full power (1.196 MW) to 0 MW = 1 min.
- **Simulation conditions** - The latency of the communication system is assumed to be 0.02 sec. This means that the information regarding the change in PV generation arrives at the energy storage location exactly 0.02 sec after the change in PV generation. The simulation for ES analysis is done for a total time duration of 300 sec at each 1 sec time step.

5.5.3 Energy Storage Size

In this application scenario the ES is deployed to provide reactive power support. Therefore, MW and MWh ES capacities do not directly depend upon this application scenario. For the simulation, it is assumed that ES was primarily deployed to increase feeder's PV hosting limit and providing voltage regulation service is a secondary application. Therefore, an ES of size 2.094 MW/8.37 MWh, as obtained from the PV hosting application scenario is selected for the study. Note that at any time the available reactive power at ES will depend upon its apparent power rating and current active power generation (5.12). For the study presented in this section it is assumed that 100% of reactive power is available for voltage regulation, i.e. $P_{ES} = 0$.

$$Q_{available} = \sqrt{(S_{ES})^2 - (P_{ES})^2} \quad (5.12)$$

where,

S_{ES} - is the apparent power rating of the smart inverter connected to ES.

P_{ES} - is the current active power generation of the ES unit.

5.5.4 Energy Storage Location

Several location scenarios are simulated to understand how the location of the energy storage system affects its ability to mitigate bus voltage variations caused by PV variability. The ES is placed on several buses along the feeder and programmed in Volt/Var control mode. The largest voltage variations with and without ES are recorded. The selected locations for ES deployment are shown in Figure 5.16. Starting with the substation, ES is deployed at thirteen different locations along the feeder. The distance of each ES deployment location with respect to the substation is shown in Figure 5.16 as well.

5.5.5 Energy Storage Control

For voltage regulation, the energy storage is used to absorb or generate reactive power. The relationship between the reactive power supplied/absorbed by ES and the change in PV generation is as follows:

$$Q_{storage} = P_{PV} \times \frac{R_{bus}}{X_{bus}} \quad (5.13)$$

where,

P_{PV} - is the change in PV generation power,

R_{bus} - is the real part of the short-circuit impedance (Z_{bus}) measured at the ES location.

X_{bus} - is the imaginary part of the short-circuit impedance (Z_{bus}) at the ES location.

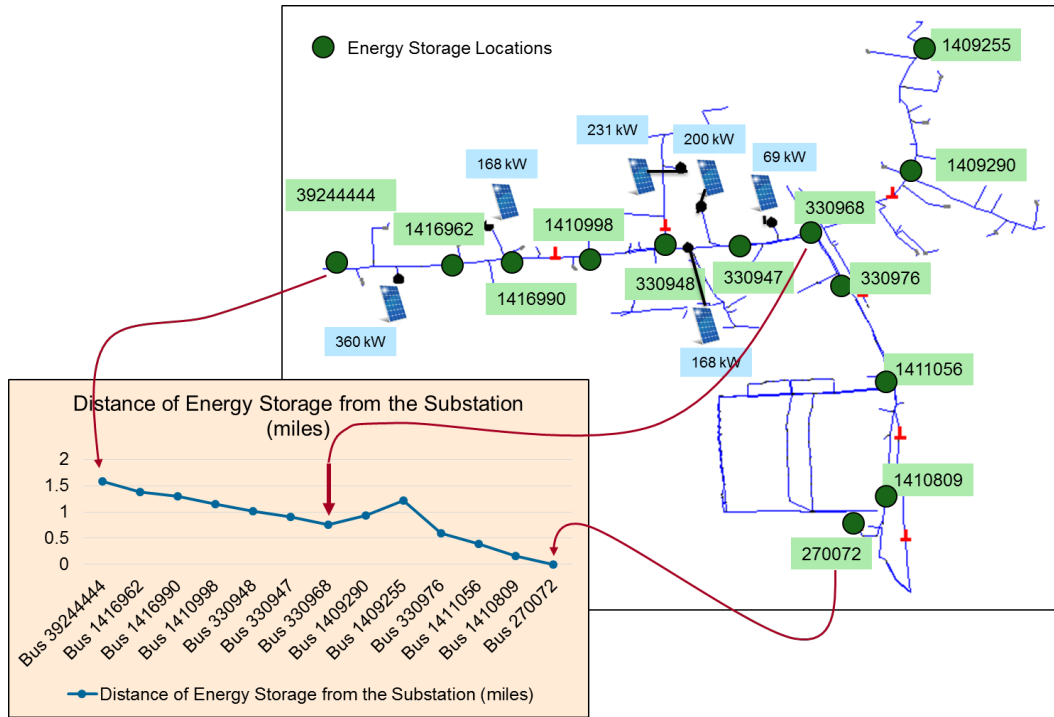


Figure 5.16: Energy Storage Locations (Courtesy of the electric utilities).

5.5.6 Grid Impact Analysis

The utility of ES as a reactive power support (Volt/Var control) to mitigate voltage variation caused by PV generation variability is illustrated in this section. Furthermore, the effect of different ES deployment locations on feeder voltage variations is also demonstrated. First, the ES is deployed at FeederEnd1 (see Figure 5.17) and programmed in the Volt/Var control mode. The largest voltage variations at four feeder buses are measured and shown in Figure 5.17 for both PV ramping up and down cases. From the figure, it can be seen that on deploying ES, the largest voltage variations decrease significantly for all buses. For example, the largest voltage variation at the FeederEnd1 decreases from 1.2% to 0.08%. Since, the ES is located closer to

the PV panels, it is more effective in mitigating voltage variability.

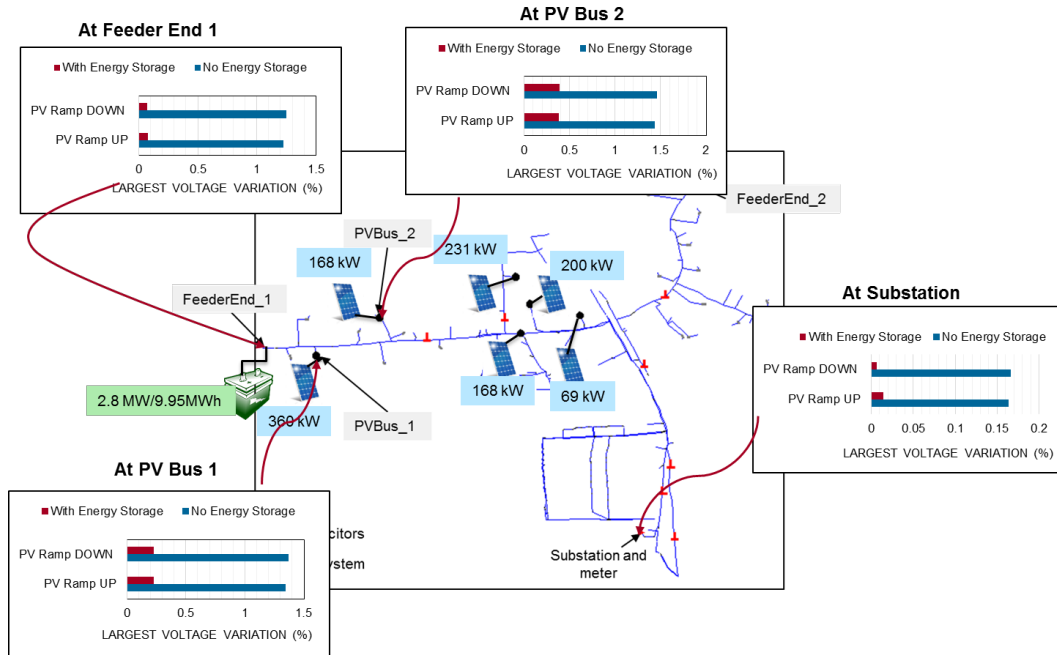


Figure 5.17: Voltage profiles (with and without energy storage), with energy storage located at FeederEnd1 (Courtesy of the electric utilities).

Next, the impact of ES locations on its ability to mitigate voltage variation concern is investigated. The ES is deployed at several feeder buses and programmed to absorb or supply reactive power for voltage regulation. At different ES locations, the largest voltages without energy storage and with energy storage are recorded. Figure 5.18 shows the largest voltage variations caused by both PV ramp up and PV ramp down cases, for different ES location scenarios. From Figure 5.18, the largest improvement in voltage profile at one of the PV buses (PVBus2) is observed when the ES is placed on Bus 3924444 (i.e. FeederEnd1) or at the buses closer to the PV buses, i.e. Bus 1416962, Bus 1416990, and Bus 1410998. On placing the ES farther away from

the PV locations, either at another feeder end or closer to the substation, a lesser improvement in the voltage profile is observed.

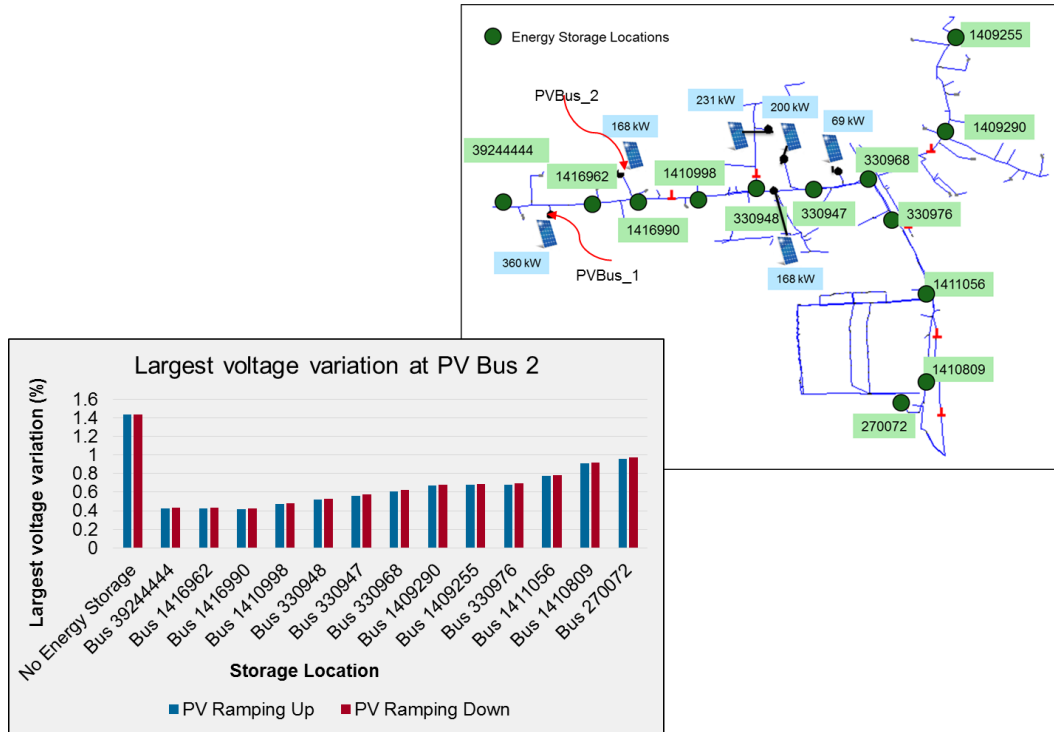


Figure 5.18: Largest voltage variation measured at PV bus 2 for different ES locations (Courtesy of the electric utilities).

Finally, the utility of deploying energy storage system for voltage management using volt-var control is demonstrated for actual PV generation data. The ES is programmed to supply reactive power when the PV generation is ramping down and vice versa. The PV irradiance profile for a high variability day, measured for an actual PV plant, is shown in Figure 5.19. The ES application scenario is simulated for 1 hour of the day, from 12 pm to 1 pm. The PV generation profile for the existing PV panels in the selected feeders is simulated using the high variability irradiance profile for 1 hour duration from

12:00 pm to 1:00 pm (see Figure 5.19). Note that the PV generation suddenly ramps up and down over the simulated time period, which could cause voltage variability.

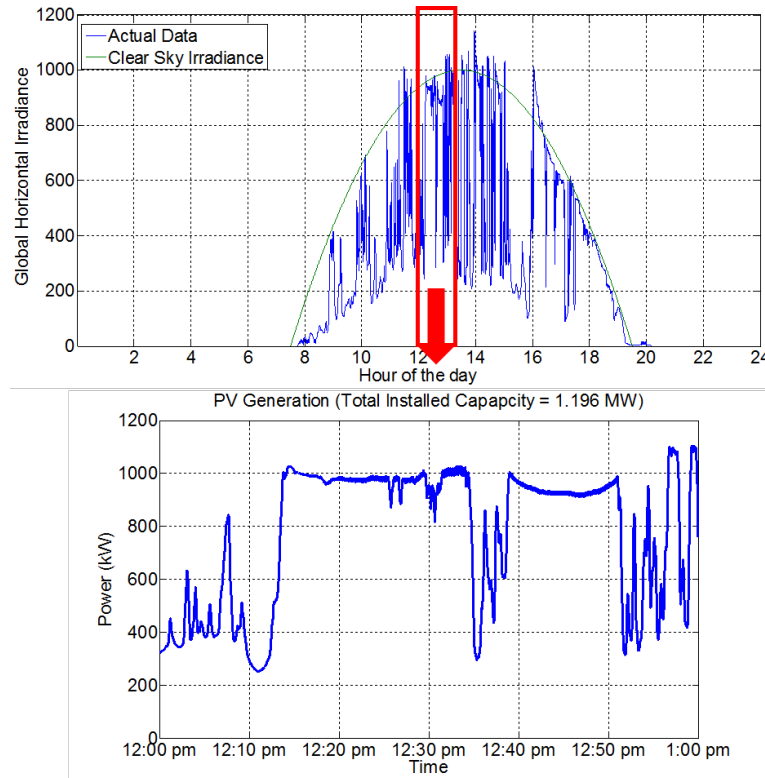


Figure 5.19: a) PV irradiance profile with high variability, b) Existing PV generation at the selected feeders from 12:00 pm to 1:00 pm using the high variability PV profile.

The voltage profiles with and without energy storage recorded at the substation, feeder end, and PV buses are shown in Figure 5.20. After deploying energy storage, the rate of change in feeder voltages due to PV variability decreases. Thus, the ES is successfully able to mitigate short-term voltage variations at each of the feeder buses. The voltage profile after ES deployment is smoother with a reduced rate of voltage ramping.

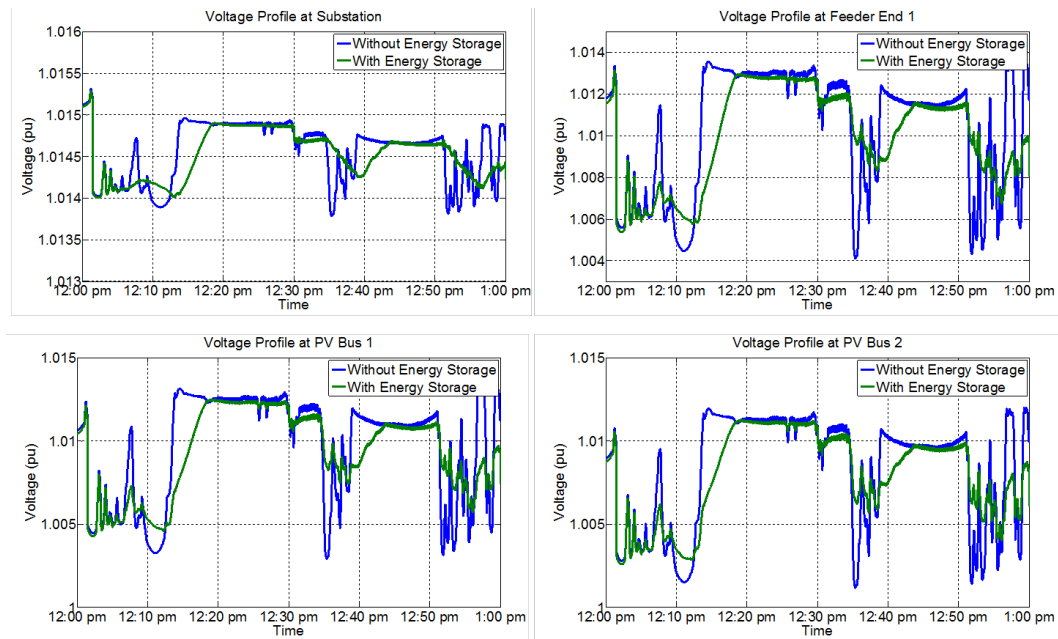


Figure 5.20: Voltage profiles (with and without energy storage) at; a) substation, b) FeederEnd1, c) PVBus1, d) PVBus2.

5.6 Conclusion

In recent years, the advancement of smart-grid technologies and the integration of distributed photovoltaic (PV) generation have led to an increase in distributed energy storage deployment. This calls for a standard methodology, analytics, and tools to quantitatively evaluate the effectiveness of energy storage solutions. In this chapter, a framework for evaluating the grid impacts and benefits of integrating ES systems into the distribution circuit is presented. The proposed framework begins with identifying application scenarios for ES deployment. Based on the selected application scenarios, the starting point for the analysis including ES deployment type, planning duration, feeder load conditions, and existing and future PV generation are identified. For each application scenario, the ES is sized for both power and energy system ratings

and potential ES locations are identified. Finally, the grid impact analysis is conducted to quantify the benefits of deploying ES and in meeting the desired grid service objective.

In this chapter, ES is deployed for the following application scenarios: 1) meeting substation N-1 contingency requirement, 2) increasing feeder's PV hosting capacity, and 3) mitigating voltage variability concerns due to PV generation variability. The finding of the study are as follows:

- ES systems can be deployed to provide multiple system-level benefits such as T&D upgrade deferral, DER integration, energy arbitrage, and frequency regulation, as well as customer-level benefits, for example, bus voltage management, and reliability benefits.
- The ES size will depend upon the application scenario. For example, for N-1 contingency requirement ES size is determined based on the feeder load demand recorded above the substation transformer rating. However, the ES size for increasing feeder's PV hosting limit will depend upon the required PV accommodation limit and current PV hosting capacity.
- Same as ES size, ES location will also depend upon the application scenario. When deployed for substation-level benefits, optimal locations would be close to the substation transformer thus avoiding power losses along the feeder. However, when deployed for feeder applications, such as voltage management or for increasing PV accommodation limit, optimal locations would be at the feeder ends or at the buses already observing voltage limit violations.

Chapter 6

Designing New Distribution Circuits

In the previous chapters, the effects of integrating smart grid technologies into the existing utility distribution circuits are discussed. To mitigate the impacts, various control schemes which can be incorporated into the existing distribution circuit are proposed. However, while installing a new utility distribution circuit or an islanded distribution circuit (such as, microgrids, distribution circuit for a multi-story building, and shipboard power systems), a complete circuit redesign could be more efficient and economical in meeting future service quality and reliability requirements. Therefore, as the challenges faced by the power distribution systems are expected to increase in the coming decades, we propose to design distribution circuit models more compatible for future service requirements.

At present, a majority of the distribution circuits are designed in radial topology; the design, operation, and analysis of which has been thoroughly analyzed and automated. However, with the integration of the distributed generation resources and the increased service reliability and power quality requirements, the distribution circuits supplying for urban and metropolitan area are increasingly adopting more complex topologies. Lately, in order to provide maximum reliability and operating flexibility, utilities are deploying spot and grid network systems in congested areas such as metropolitan and suburban business districts. Additionally, a high level of service reliability is of

primary concern for some microgrids for example, a shipboard power system in an all-electric ship. Given the trend towards more complex distribution architectures and the requirement for the improved service reliability, an analytical framework for designing new distribution circuits is required.

The work presented in this thesis aims to design a reliable circuit design for an all-electric shipboard power system. To achieve this objective, the design considerations of ship's primary distribution system and its secondary zonal distribution networks are considered separately. Note that ship's primary and zonal load centers interact in the same way as the primary and secondary circuits of the terrestrial power distribution system designed in a mesh topology. For ship's primary distribution system topology, we aim to investigate the reliability gains of designing three-dimensional power system topologies, spanning multiple levels of the ship, in contrast to the planar distribution systems that are currently used. As for ship's zonal distribution system, a new approach to design the distribution topology by prioritizing service reliability as the design objective is proposed. Although, the distribution circuit design framework is developed for a shipboard power system, the method is applicable to all kinds of new distribution circuit installations.

6.1 Shipboard Power Distribution System

A discussion on a typical shipboard power system deployed in an all-electric ship is presented in this section. As discussed before, same as terrestrial distribution systems, the shipboard power system is composed of a primary distribution and a secondary or zonal distribution system. The two systems are discussed separately in the following section.

6.1.1 Primary Distribution System

Figure 6.1 shows the primary distribution circuit of an all-electric ship designed in a breaker-and-a-half (BAAH) configuration. The shipboard power system shown in Figure 6.1 is supplying for nine equipment loads using four generators, two main and two auxiliary. The equipment loads supplied by the distribution circuit is as follows: radar, energy storage, pulsed load, port propulsion motor, starboard propulsion motor, and four zonal load centers.

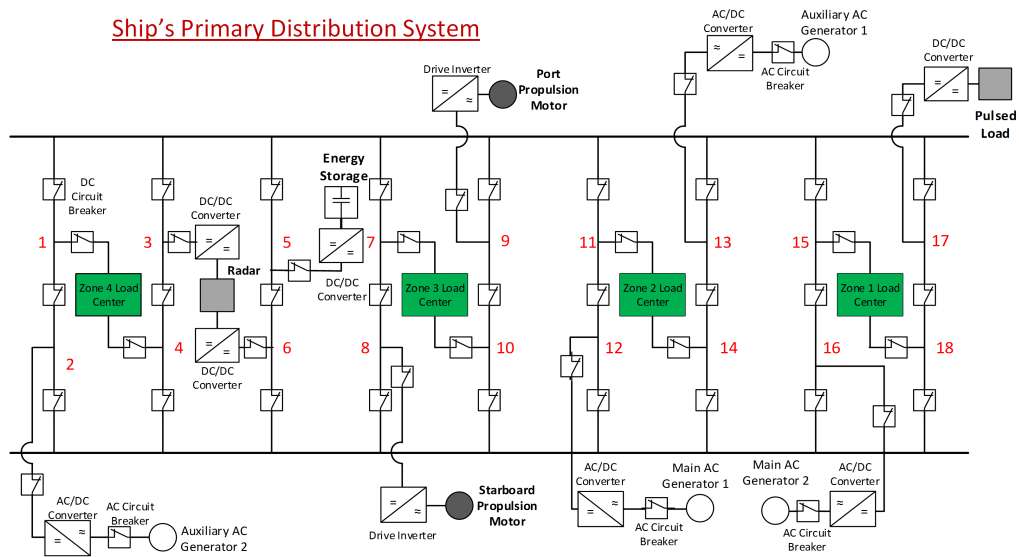


Figure 6.1: A shipboard distribution system in BAAH topology.

Several other configurations based on terrestrial distribution substation design can be adopted for the ship's primary distribution topology. Figure 6.2 shows simplified one-line diagrams of the additional topologies considered in this study, one is based in ring bus configuration and other is a double bus, double breaker arrangement (DBDB). In the ring bus topology, a ring of busbar runs around the ship's perimeter with circuit breakers sectionalizing the ring to connect several equipment loads and generators. In a BAAH topology, two

parallel bus bars run across the port and starboard side of the ship connected by several conducting wires called bays protected using three circuit breakers. Each incoming and outgoing wire is protected using 1.5 circuit breakers. In DBDB configuration, same as the BAAH topology, two parallel busbars are connected using cross-hull bays. Each bay is protected using two circuit breakers and contains only one line to equipment load or generator. Therefore, each incoming or outgoing line is protected using two circuit breakers.

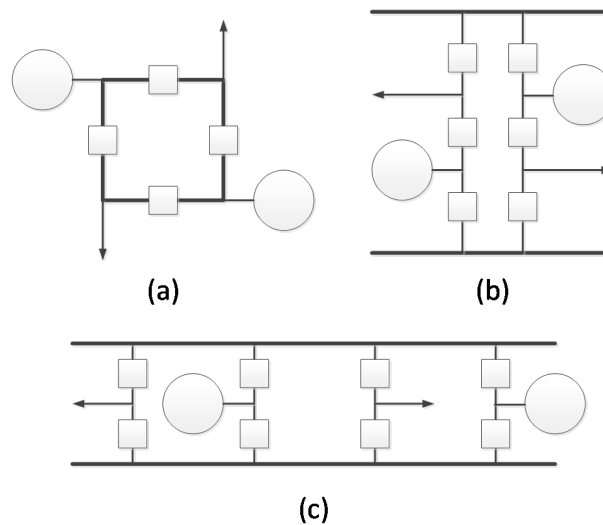


Figure 6.2: Comparison of (a) ring bus; (b) breaker-and-a-half; and (c) double breaker, double bus topologies.

6.1.2 Zonal/Secondary Distribution System

The ship's zonal load centers are similar to utility secondary distribution circuit supplying electric power to the end-users. To realize a high level of service reliability, ship's ZEDs are designed in a grid topology (see Figure 6.3). A ZED is usually doubly connected to the primary distribution system, thus allowing two levels of redundancy in the power supply. Note that several other

topologies based on terrestrial distribution circuits may be adopted for the ZED such as radial and loop topologies. The reliability of the other topologies will however be lower than the grid arrangement. Additionally, instead of selecting a given topology, a ZED distribution circuit could be designed for the required service availability measure.

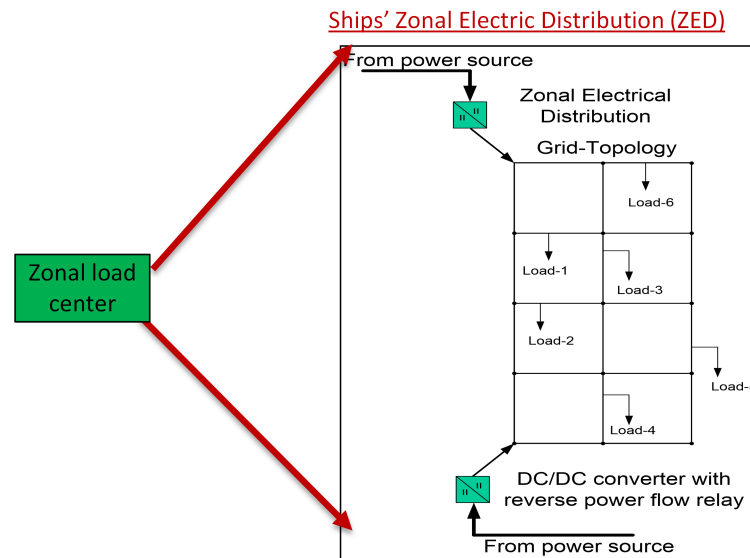


Figure 6.3: A zonal electric distribution (ZED) system in grid topology.

6.2 Shipboard Power System Reliability Analysis - A Literature Review

Ensuring the continuity of service of the shipboard power/electrical system (SPS) to the equipment loads in an all-electric ship is of paramount importance. A failure of the shipboard power system can result in critical loads and power equipment such as radar, weapons, and propulsion motors, to mention just a few, being left without service until repairs can be performed. Poor and irregular continuity of service may potentially pose serious threats to the crew

and the mission. Therefore, a SPS must be designed to achieve the desired reliability so as to minimize the frequency of unplanned service interruptions.

This section presents a short discussion on the state-of-the-art reliability analysis methods proposed for the shipboard power system. The probability that service to an equipment load might be interrupted depends on two factors: the overall topology of the distribution system and the relative placement of loads and generation units within the system [12]. In order to ensure the highest possible level of continuity of service in equipment loads, work to date has sought to improve the reliability of shipboard electrical distribution systems through the choice of distribution system topology [122–125]. Reliability of the shipboard’s power system, primarily the primary distribution circuit, is measured as the expected frequency and duration of service interruptions experienced by equipment loads resulting from failures of distribution system components. The reliability analysis undertaken has combined fault-tree analysis, used to identify the sets of component failures that lead to service interruptions, with Markov modeling, used to derive system reliability indices from component failure rates and mean times to repair [126]. Three notional topologies based on terrestrial distribution systems have been compared namely, ringbus, breaker-and-a-half (BAAH), and double-bus double-breaker (DBDB). An evolutionary algorithm to identify an optimal placement of equipment loads and generation units within an existing topology is also proposed [12].

6.2.1 Quantify Distribution System Reliability

During peacetime operations, service interruptions are most often caused by failures of individual components within the distribution system. In the

literature, methods have been proposed to evaluate the system reliability from the perspective of the overall distribution network topology, that is, the relationship between the reliability of a distribution circuit and the high-level topology of its connections. For example, [122] proposes a metric to calculate the peacetime quality of service (QOS) in shipboard power distribution systems. The QOS metric, defined as the mean time between service interruptions (MTBSI), has been applied to shipboard power system design, but these studies have primarily focused on design choices such as generator size and control interfaces, not on comparisons of overall system topologies [123, 124]. Several studies have proposed methods to quantify and compare the reliability metrics of terrestrial utility power system substation topologies [127, 128]. These studies propose a detailed computational technique for reliability calculation including Markov modeling approaches while incorporating complex failure scenarios.

A method to quantify the reliability of shipboard power system using Markov modeling and fault tree analysis is proposed in [125]. The method quantifies the reliability of a given SPS topology by calculating system interruption rate, mean time to repair, and total downtime for each equipment load connected to the SPS. The proposed approach results in a relationship between the reliability of a distribution circuit and the high-level topology of its connections. The method is specifically applied to the distribution system of an electric naval vessel, but the approaches described here can apply to most small-scale distribution systems, such as substations or microgrids.

6.2.2 Comparing Distribution System Topologies

Using the method proposed in [125], three notional shipboard distribution systems based on the ring bus, BAAH, and DBDB topologies found in terrestrial utility substations are compared for system reliability. The equipment reliability indices of three notional shipboard electrical distribution systems based on the three topologies are derived. The derived service interruption rates for each equipment system in each topology are compared in Figure 6.4. The details regarding the methodology and calculations can be found in [125].

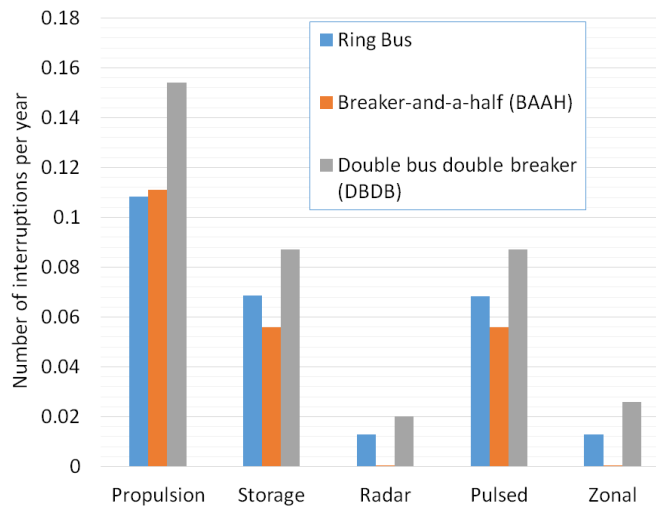


Figure 6.4: Equipment interruption rates for ring bus, BAAH, and DBDB topologies. For Radar and Zonal loads, the number of interruptions per year for BAAH topology are very small (not visible on the graph).

The BAAH topology, as shown in Figure 6.1, confers a greater level of reliability to the equipment loads than the other two topologies. The interruption rates shown for each equipment load signifies the expected number of service interruptions that equipment load will experience in a given year. With the exception of the propulsion system, in which the ring bus performs slightly

better than the BAAH, the BAAH topology has a lower rate of interruption than the other topologies. In the cases of the radar and zonal load centers, the BAAH interruption rate is so low as to not be visible on the chart. The DBDB topology, although contains more circuit breakers, results in a higher rate of service interruptions to every equipment system than the other two topologies.

6.2.3 Optimal Equipment Placement

Another way of improving SPS reliability is by optimally placing the equipment loads within a given shipboard distribution topology. In literature, the system reconfiguration problems, which aim to reconfigure the power path in a SPS to serve the critical loads in an event of fault or damage, have been extensively studied [129–133]. For example, [129] proposes a multi-agent system (MAS) to reconfigure the ship’s electric propulsion system in an event of fault. In [130], the SPS reconfiguration problem is formulated as a network flow problem in order to restore service to unfaulted sections of the system. An equipment placement problem is different from the system reconfiguration problem, as the latter is concerned with finding an optimal power path for a given SPS topology and equipment placement configuration.

An algorithm based on particle swarm optimization (PSO) is proposed in [12] to obtain an optimal equipment arrangement in a given SPS topology which will confer the highest level of system reliability, i.e., the smallest overall service interruption rate. The proposed algorithm simulates several candidate solutions, each candidate solution representing a particular equipment configuration. Next, the algorithm updates each candidate configuration, according to the candidate best and the global best solutions. The algorithm eventually

converges to the global optimized solution, representing the optimal equipment configuration.

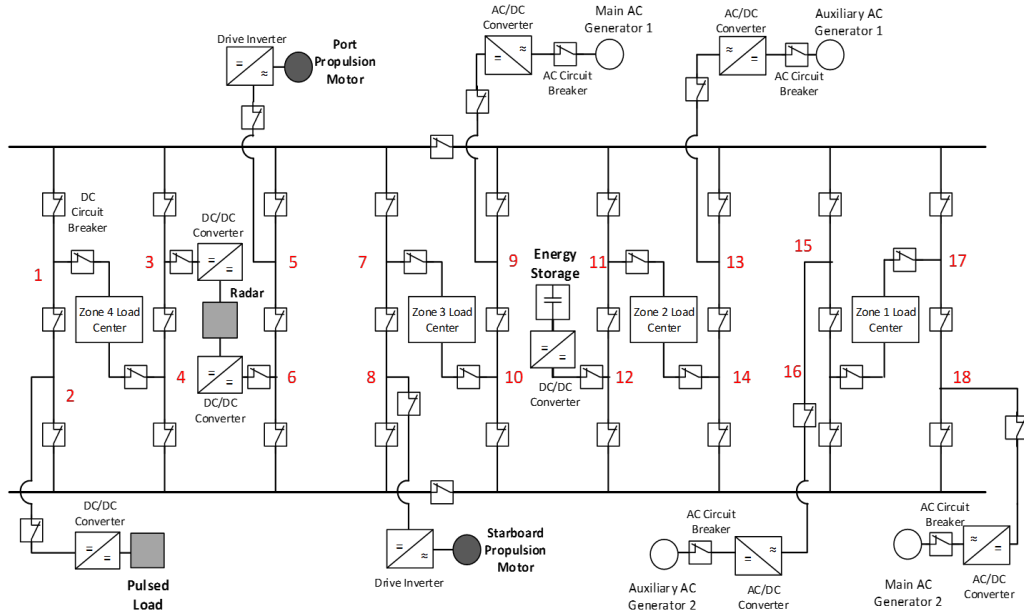


Figure 6.5: Optimal equipment placement within the breaker-and-a-half topology (BAAH).

The algorithm is implemented for BAAH topology and the results confirm that the proposed algorithm is able to improve the service reliability indices for the shipboard power system. On implementing the algorithm, the overall interruption rate for BAAH topology decreases to 0.221326453 as compared to 0.22253151 as recorded for the base case. Therefore, the overall system interruption rate decreases by 0.54%. Note that the improvement in the system reliability indices due to optimal equipment placement are not very significant, implying that the base case SPS in BAAH topology was close to optimal to begin with. Although the reliability gains are relatively small compared to those that are achieved through the choice of overall topology, but changes in equipment placement are easier and less costly design choices to implement

than changes in system topology. Placement choices also do not affect the number of required distribution system components, as can be the case with choices of system topology.

Table 6.1: Equipment Configuration Reliability Index Comparison

Topology	Equipment System	μ (interruptions per year)	MTTR (hours)	Total Downtime (hours per year)
Base Case	Propulsion	0.111011	3.162065	0.351022
	Energy Storage	0.055756	3.152356	0.175763
	Radar	0.000003	1.794887	0.000005
	Pulsed Loads	0.055756	3.152356	0.175763
	Zonal Load Centers	0.000009	2.030457	0.000018
Modified	Propulsion	0.110516	3.162060	0.349458
	Energy Storage	0.055756	3.171849	0.176850
	Radar	0.000016	1.980351	0.000032
	Pulsed Loads	0.055265	3.152356	0.174216
	Zonal Load Centers	0.000020	2.026110	0.000041

6.3 Proposed Approach to designing Distribution Systems for Improved Reliability

The objective of this work is to design distribution system topologies for improved service reliability and continuity. In this study, the reliability based designs for both ship's primary and zonal distribution systems are proposed. The previous work evaluated reliability gains obtained from the topological designs of the shipboard primary distribution systems. The topologies explored in the prior work, however, have been planar connecting equipment

loads and generation units at only one level of the ship. In this work, we propose to explore the reliability gains obtained from the three-dimensional shipboard designs. The service reliability of a ship's primary distribution system is quantified using expected frequency and duration of service interruptions to equipment loads caused by the component failure. Ship's planar topologies are extended into three-dimensional (3D) structures by distributing equipment loads to different planar SPS designs and connecting those using vertical tie-buses. Note that a 3D topology can be unfolded into multiple planar nets by simply disconnecting vertical tie-buses. The reliability analysis framework uses fault-tree approach and Markov modeling technique to compare the reliability of the SPS topologies.

As for the ship's zonal distribution system, a new approach to design distribution system topology aiming to achieve a desired network reliability/availability measure while using a minimum number of conductors is proposed. The service reliability for ZED systems is quantified in terms of network availability, which is defined as the steady-state probability of a network being in operational state. For a high level of service availability, the ship's ZED system is designed in a grid topology. A ZED topology using a lower number of conductors can be designed which can provide a desired level of network availability. The proposed approach is successful in designing reliable system topologies using a lesser number of conductors.

6.3.1 Three-dimensional Shipboard Power System Design

The objective of this work is to investigate the reliability gains obtained by designing a three-dimensional shipboard distribution system. In an electric ship, while the equipment loads served are distributed throughout all lev-

els of the ship, shipboard distribution system topologies investigated to date have themselves been planar. We propose looking into the gains in reliability that can be achieved through designing three-dimensional distribution systems, consisting of two or more planar topologies across different decks of the ship arranged in various configurations. The calculation of the system reliability indices for each equipment load is accomplished using a two-part process. First, the fault-tree analysis is used to identify a complete list of interruption scenarios for a given equipment load. Next, reliability indices are derived for the equipment load using Markov models.

6.3.1.1 Designing Three-dimensional Topologies

Several three-dimensional (3D) topologies based on notional ring bus and breaker-and-a-half topologies are designed and compared against the respective planar configurations. The 3D topologies are designed by connecting equipment loads across both upper and lower planes of the shipboard distribution system. The upper and lower planes are designed in several notional topologies and connected using four vertical tie-buses, two each on the port side and starboard side of the ship. A 3D topology adds structural robustness to the ship's primary distribution system. Since equipment loads are distributed in multiple decks of the ship, in an event of damage to one of the ship's decks, equipment loads in non-damaged decks may remain operational. 3D topologies also result in a slight improvement in the service reliability when compared with the respective planar configurations.

6.3.1.2 Reliability Concepts

Reliability analysis is, in general, the evaluation of how often systems or pieces of equipment are expected to fail, and how long such a failure is expected to persist before being repaired and returning to service. In the context of distribution systems, reliability is split into two related concepts: component reliability and system reliability.

Component reliability analysis assesses the expected frequency and duration of physical failures of distribution system components, such as circuit breakers, buses, and power converters. Component reliability is quantified through two indices: failure rate (λ) and mean time to repair (MTTR). In this study, component failures are grouped into three types: passive failures, active failures, and stuck breakers. Passive failures cause the failed component to act as an open circuit, preventing power from flowing through the component. Active failures disable the failed component and cause all adjacent circuit breakers to trip and isolate the fault. A stuck breaker fails to isolate a fault.

System reliability analysis assesses the expected frequency and duration of service interruptions, caused by component failures, to equipment loads served by the distribution system. Here, a service interruption to an equipment load is defined as the load being electrically isolated from all generation units. A shipboard distribution system serves five equipment systems: propulsion, energy storage, radar, pulsed loads (e.g., weapons systems), and zonal load centers (encompassing lighting, refrigeration, etc.). The reliability of each equipment system is evaluated separately.

6.3.1.3 Reliability Calculation Method

The analysis consists of two phases: the enumeration of failure scenarios through fault-tree analysis and the calculation of reliability indices through Markov modeling. Interruption scenarios are enumerated using an approach known as fault-tree analysis. In fault-tree analysis, a logical flowchart is constructed using system topology and causal relationships within the system. This flowchart ultimately connects a system interruption to the sets of component failures that constitute interruption scenarios. Fault trees are constructed from the top down, beginning with a system interruption block. The immediate cause or causes of the system interruption are identified and blocks representing these causes are connected to the system interruption block using logic gates. Each cause is then examined in the same manner, building further branches of proximate causes until each branch terminates with a component failure.

Once the interruption scenarios of a given system have been identified, reliability indices are calculated for each scenario. All component failures are assumed to be independent and uniformly distributed in time. Further, all second-order interruption scenarios considered are minimal sets of component failures. In other words, for a second-order interruption to be considered in this analysis, neither of the component failures in the interruption scenario can themselves be first-order interruption scenarios. The consequence of this restriction is that second-order interruption scenarios are considered repaired as soon as one component failure is repaired.

Scenario reliability indices are calculated through Markov modeling. In a Markov model, the system is assigned a set of states that it can potentially be found in, along with a set of rates of flow between states. A flowrate represents

the rate of change of the probability of the system being found in a given state. Flows out of a state lower the probability of being found in that state, while flows into the state raise this probability. Finally, in a Markov model, the probability of transitioning to a given state is solely dependent on the current state of the system. Thus, Markov models are said to be "memoryless".

6.3.2 Resilient Distribution Circuit Design

A distribution circuit design problem can be modeled to satisfy several different requirements such as ability to efficiently serve the load demand, minimize the circuit losses, adaptability to change in supply and demand, service continuity during outage etc. Clearly, the design problem satisfying all these constraints is complex. Therefore, the distribution circuit design problem is broken down into several smaller optimization problems by prioritizing the requirements. To date, the network design problem is approached from the perspective of minimizing the circuit losses and satisfying the load demand [15]. The reliability of the circuit operation and continuity of the service is ensured by installing the protection system on the top of the earlier designed distribution circuit.

The objective of this study is to design a distribution circuit with the continued ability of the circuit to perform its function in the face of damage and outages. As the service reliability is directly related to the distribution circuit topology, the reliable circuit design problem is approached from the aspect of topology computation. Mathematically, a distribution circuit can be represented by a network/graph. A network/graph is a collection of nodes and links (in electrical system loads and distribution lines) and a network topology is defined as the way in which a collection of nodes are connected

together using links [134]. For an electric distribution circuit, currently three kinds of network topologies are deployed by utilities: radial, loop and grid. The reliability of the network comes from the collective reliability of the network topology and thereby the manner in which nodes are connected. For example, in a radial topology there is only one path from the source to each load, thus failure of any one edge can lead to discontinuity of the service. However, in a grid topology there are multiple paths between the source node and the demand node, therefore grid topology offers increased reliability in terms of overall service continuity. Note that a path in a network/graph is a sequence of links/edges which connect a sequence of vertices. In the context of this study the path is defined as sequence of distribution lines connecting source to load.

In the context of network topology design, design economy is also a very important criterion. We can infinitely maximize the circuit reliability by increasing the number of conductors between nodes and thus by creating several alternate routes. However, after certain number of alternate paths, adding another path may only marginally increase the reliability while significantly increasing the cost. Furthermore, in the case of electric ship design, the space constraint calls for a reliable network topology design requiring a lesser number of conductors. Thus, a topology design problem need to address two conflicting criteria, maximize the reliability with minimum the design economy. In this work an algorithm is developed to find an optimal distribution topology which minimizes the number of conductors (or design economy) while satisfying a required reliability measure of the electric service. In the proposed algorithm, the service reliability is quantified using network availability. Network availability is defined as the steady-state probability of obtaining the system in its

operational state. Here, a network is said to be operational if the power supply is available to each load supplied by the network.

6.3.2.1 Network Availability

The network availability is defined for a probabilistic network/graph. A probabilistic graph $G = (V, E)$ is a set V of n nodes which represent the demand and supply nodes, together with a collection E of m links representing distribution lines, each associated with an index quantifying their probability of operation (a_i). The availability quantifies the ability of a network to carry out the desired network operation. The network availability is computed by enumerating the minpaths of the network. A minpath is a set of nodes and links that results in an operational network, but the removal of any one link will cause the network to fail.

6.3.2.2 Optimal Topology Design Problem

The algorithm aims to find an optimal network topology for a DC distribution circuit supplying for the zonal loads in an electric ship power system. The problem formulation begins with a typical grid topology for the distribution circuit, with a load connected at every node and each load is equally critical for a successful network operation. Clearly, the design economy is relatively higher for the complete grid network because of the multiple paths. The number of edges in the optimal circuit topology will be a subset of the edges in the original grid topology. The algorithm aims to find a minimal set of edges that ensures the desired network availability. The detailed problem formulation is presented in Chapter 8.

6.3.2.3 Proposed Algorithm - Successive Minpath Generation

For the context of the network design problem presented in this chapter, a network is said to be operational, if it contains at least one path from the source node to each node. The network availability is simply the probability of finding the network in its operational state, which means the probability of finding all nodes connected to the source node in a given network. Clearly, a minpath for a graph satisfying above reliability definition is a spanning tree.

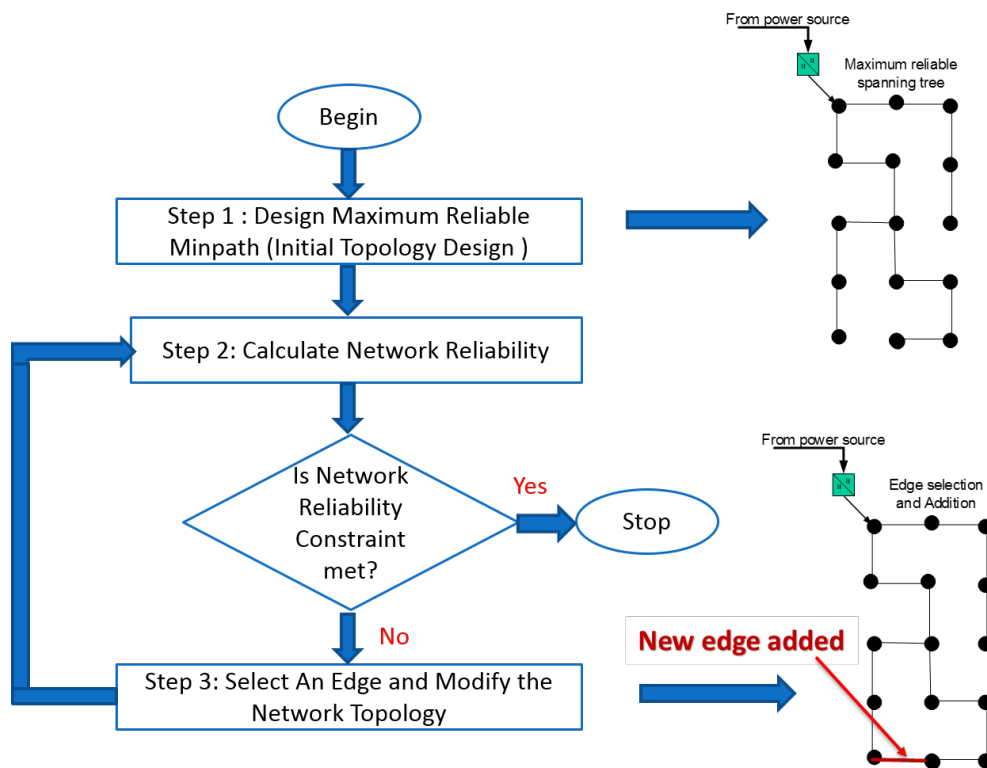


Figure 6.6: Flowchart for the proposed optimal topology design algorithm

The proposed algorithm begins with a minpath, thereby ensuring connectivity and successively adds minpaths to the network thus improving upon the availability while synthesizing an optimal network topology. The method is

primarily, divided into three stages; initial topology design, calculating and checking for the availability constraint, and successive edge selection and addition. The flowchart for the algorithm is shown in Fig. 6.6. The details regarding the problem formulation and methodology are discussed in Chapter 8. To test the algorithm the service availability resulting from different ZED topologies namely radial, loop, and grid are compared. Next, an optimal network topology that can ensure a desired probability of network operation while using a minimum number of conductors/links connecting load/nodes is designed.

Chapter 7

Three-dimensional Shipboard Power System Design

In an electric naval vessel, the mission success and personnel wellbeing depends heavily upon the proper functioning of the ship's power distribution system. A failure of the distribution system can disconnect important equipment loads such as radar or weapons from the power supply, potentially posing serious threats to the crew. Therefore, it is necessary to ensure that shipboard electrical distribution systems are designed to be as robust as possible with the highest level of service reliability [122].

In order to ensure the highest possible level of continuity of service in equipment loads, work to date has sought to improve the reliability of shipboard electrical distribution systems through the choice of distribution system topology. Reliability of a network is measured as the expected frequency and duration of service interruptions experienced by equipment loads resulting from failures of distribution system components. Previous work has been performed to establish metrics for calculating peacetime quality of service (QOS) in shipboard power distribution systems (SPS) [122–124]. Prior research has also investigated the reliability gains obtained through the choice of circuit topology [125, 127, 128]. The evaluation of system reliability from the perspective of the overall distribution network topology, that is, the relationship between the reliability of a distribution circuit and the high-level topology of

its connections has also been explored. It has been concluded that an SPS topology based on the breaker-and-a-half scheme results in greater reliability than equivalent distribution topologies based on the ring bus and double breaker, double bus designs [12, 125]. The topologies investigated in the prior work were, however, planar in design.

The objective of this work is to investigate the reliability gains obtained by designing a three-dimensional shipboard distribution system. In an electric ship, while the equipment loads served are distributed throughout all levels of the ship, shipboard distribution system topologies investigated to date have themselves been planar. We propose looking into the gains in reliability that can be achieved through designing three-dimensional distribution systems, consisting of two or more planar topologies across different decks of the ship arranged in various configurations. The calculation of the system reliability indices for each equipment load is accomplished using a two-part process. First, the fault-tree analysis is used to identify a complete list of interruption scenarios for a given equipment load. Next, reliability indices are derived for the equipment load using Markov models.

In this chapter, several three-dimensional (3D) topologies based on notional ring bus and breaker-and-a-half topologies are designed and compared against the respective planar configurations [13]. A primary distribution system topology for example BAAH topology can be extended into a 3D structure by distributing the ship's equipment loads to different planes of the ship where each plane is designed in the BAAH topology and connecting the different planes using vertical tie-buses. Several 3D topologies based on ship's planar topologies such as ring bus and BAAH, are simulated, and the reliability comparisons are made against the respective planar topologies. Compared

to planar topologies, 3D topologies slightly decrease the overall service interruption rates for each notional topology, thus improving the service reliability. Additionally, a 3D topology provides a more robust structure for the SPS. Since equipment loads are distributed in different decks of the ship, during an attack if one of the ship's decks are destroyed, loads located in another deck may remain functional.

7.1 Reliability Calculation

The reliability analysis is used to evaluate the expected frequency and duration of system or equipment failure. In the context of distribution systems, reliability analysis is split into two related concepts: component reliability and system reliability.

The expected frequency and duration of failures of individual distribution system components such as circuit breakers, buses, and power converters are characterized using component reliability analysis. In this study, three types of component failures are identified: passive failures, active failures, and stuck breakers. Passive failures cause the failed component to act as an open circuit, preventing power from flowing through the component. Passive failures only affect the failed component. An example of a passive failure is a circuit breaker false trip. Active failures, also referred to as short-circuit faults or overcurrents, not only disable the failed component, but also cause all adjacent overcurrent protective devices (i.e., circuit breakers) to trip and isolate the fault. Faults propagate through buses, stopping only at each successfully-opened circuit breaker. Examples of active failures include a bus short circuit or insulation breakdown in a circuit breaker or cables. A stuck breaker occurs when a circuit breaker is called upon to isolate a fault but fails to operate. When this

occurs, the fault propagates through the stuck breaker and must be contained by upstream breakers.

The system reliability analysis characterizes the expected frequency and duration of service interruptions to the equipment loads. Here, a service interruption to an equipment load is defined as the load being electrically isolated from all generation units. A shipboard distribution system serves five equipment loads: propulsion, energy storage, radar, pulsed loads, and zonal load centers. The system reliability indices are calculated individually for each equipment load.

7.1.1 Component Reliability Indices

Component reliability is quantified using two indices: failure rate (λ) and mean time to repair (MTTR). The failure rate is defined as the expected number of failures a given component will experience over the course of one year. The MTTR is defined as the expected length of time, in hours, that the component failure will persist before it is repaired. The inverse of MTTR is called the repair rate, denoted λ .

With the exception of stuck breakers, which by definition must occur simultaneously with an adjacent active failure, component failures are assumed independent of one another. Failure and repair rates are assumed to be constant, making component failures and repairs Poisson processes. In other words, the waiting times to a failure or a repair are given by exponential probability distributions. Each type of component has one set of reliability indices for each type of applicable component failure. The values for the component failure reliability indices used in this analysis are shown in Table 7.1. The values are either taken from manufacturer data or from independent testing

Table 7.1: Component Failure Reliability Indices

Component Failure	λ (failures per year)	MTTR (hours)
Circuit Breaker - Passive	0.01	4
Circuit Breaker - Active	0.01	4
Bus - Active	0.01	8
Converter - Passive	0.006	1
Converter - Active	0.006	1
Circuit Breaker - Stuck	5%	1

[135–137]. Note that, the stuck breaker failures are modeled differently than other failures.

7.1.2 System Reliability Indices

System reliability is quantified through three indices: the service interruption rate (μ), the system mean time to repair (MTTR), and total expected downtime. The service interruption rate is defined as the expected number of service interruptions that the equipment system may experience due to component failures over the course of a year. The system MTTR is defined as the expected number of hours that a service interruption will persist before service is restored through repairs to failed components. The total expected downtime is defined as the expected number of interruption in hours per year for a given equipment load.

The system reliability indices for each equipment load are calculated using a two-part process. First, fault-tree analysis is used to identify a complete list of interruption scenarios for a given equipment load [125]. An interruption scenario is a minimal set of one or more concurrent component failures that cause

the load in question to become disconnected from all generators. The number of individual component failures involved in an interruption scenario is called the scenario's order. Interruption scenarios up to second-order are considered, as third- and higher-order failures are exceptionally rare and therefore do not greatly affect reliability indices [127, 128]. Next, Markov models are used for deriving reliability indices for the equipment loads [126]. In a Markov model, the system is assigned a set of states that it can potentially be found in, along with a set of rates of flow between states. A flow rate represents the rate of change of the probability of the system being found in a given state. Flows out of a state lower the probability of being found in that state, while flows into the state raise this probability. The load's reliability indices are derived through such a model from the component reliability indices (failure rate λ and MTTR) shown in Table 7.1. Each interruption scenario is simulated in a Markov model, with each state of the model representing a combination of working and failed components. Flow rates between these states are defined by the applicable component failure rates and repair rates λ and π , as described in Table 7.1. There are three types of Markov models used to model an equipment system's various interruption scenarios: those representing first-order scenarios, second-order scenarios that do not involve a stuck breaker, and second-order scenarios that do involve a stuck breaker.

7.1.2.1 First-Order Interruption Scenarios

In the case of a first-order interruption scenario, there are only two states: component functioning (state 1) and component failed (state 2). The system will be interrupted in state 2. At time $t = 0$, we assume the component begins in a functioning state. In other words, $p_1(t = 0) = 1$ and $p_2(t = 0) = 0$,

where p_1 and p_2 are the probabilities of the system being in states 1 and 2, respectively, as functions of time. As time progresses, these probabilities will change, governed by the differential equation.

$$\dot{p}_i(t) = \sum_{j \neq i} \text{flowrate}(j \rightarrow i) \times p_j(t) - \sum_{i \neq j} \text{flowrate}(j \rightarrow i) \times p_i(t) \quad (7.1)$$

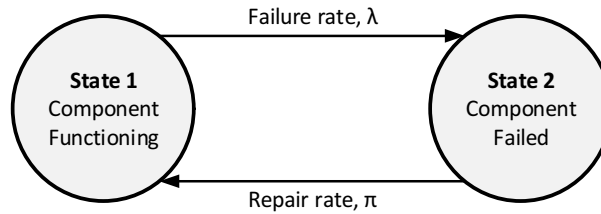


Figure 7.1: Markov model of a first-order interruption scenario.

In this two-state Markov model, the flowrate from state 1 to state 2 is the component failure rate λ , while the flowrate from state 2 to state 1 is the component repair rate π , as shown in Figure 7.1. Thus, the system of differential equations governing the behavior of this model can be expressed as:

$$\begin{bmatrix} \dot{p}_1(t) \\ \dot{p}_2(t) \end{bmatrix} = \begin{bmatrix} -\lambda & \pi \\ \lambda & -\pi \end{bmatrix} \begin{bmatrix} p_1(t) \\ p_2(t) \end{bmatrix} \quad (7.2)$$

As component failure rates tend to be very small, on the order of years between failures, the long-term behavior of the model must be considered. As t approaches infinity, the state probabilities will tend to steady-state values, P_1 and P_2 . These values can be obtained by setting the differential terms in (7.1) to 0. Additionally, states 1 and 2 are mutually exclusive, therefore $P_1 + P_2 = 1$.

Solving for P_1 and P_2 , we obtain.

$$\begin{bmatrix} P_1(t) \\ P_2(t) \end{bmatrix} = \begin{bmatrix} \frac{\pi}{\lambda + \pi} \\ \frac{\lambda}{\lambda + \pi} \end{bmatrix} \quad (7.3)$$

The total scenario interruption rate $\mu_{scenario}$ is given by the component failure rate (i.e., the flowrate from state 1 to state 2) times the probability of being in state 1, divided by the probability of not being in state 2 (in other words, the conditional rate of transition from a working state to a failed state, given that the system is not already in a failed state). Thus, the total scenario interruption rate is given by

$$\mu_{scenario} = \frac{\lambda \times P_1}{1 - P_2} = \lambda \quad (7.4)$$

The total scenario repair rate $\mu_{scenario}$ is similarly given by

$$\mu_{scenario} \frac{\pi \times P_2}{1 - P_1} = \pi \quad (7.5)$$

The total scenario $MTTR_{scenario}$ is thus given by $MTTR_{scenario} = \pi^{-1}$.

7.1.2.2 Second-Order Interruption Scenarios

In a second-order interruption scenario, there are four states: both components functioning (state 1), component 1 failed and component 2 functioning (state 2), component 1 functioning and component 2 failed (state 3), and both components failed (state 4). As interruption scenarios are assumed to be minimal sets of component failures, the system will be interrupted only in state 4. The Markov model for a second-order interruption scenario is visually represented in Figure 7.2.

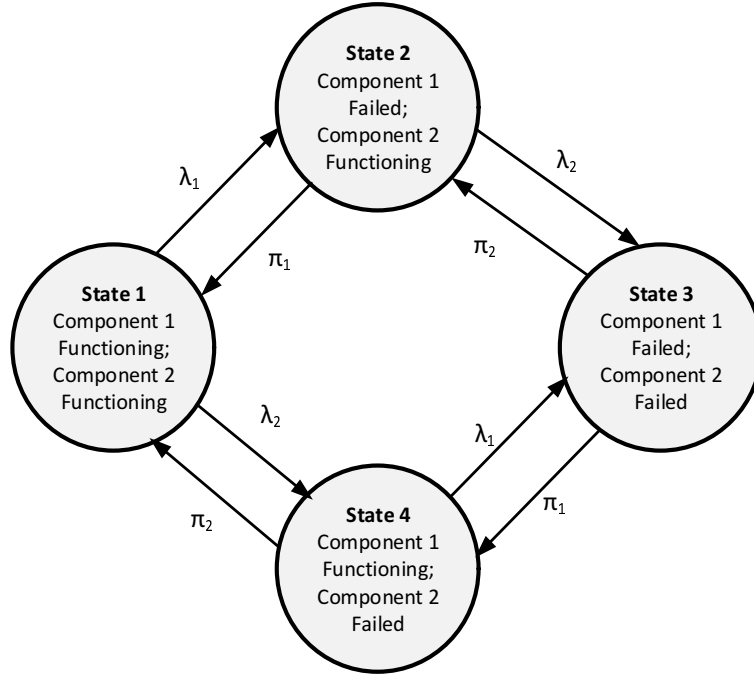


Figure 7.2: Markov model of a second-order interruption scenario.

From (7.1), the system of differential equations governing the behavior of this system is

$$\begin{bmatrix} \dot{p}_1(t) \\ \dot{p}_2(t) \\ \dot{p}_3(t) \\ \dot{p}_4(t) \end{bmatrix} = \begin{bmatrix} -(\lambda_1 + \lambda_2) & \pi_1 & \pi_2 & 0 \\ \lambda_1 & -(\lambda_2 + \pi_1) & 0 & \pi_2 \\ \lambda_2 & 0 & -(\lambda_1 + \pi_2) & \pi_1 \\ 0 & \lambda_2 & \lambda_1 & -(\pi_1 + \pi_2) \end{bmatrix} \begin{bmatrix} p_1(t) \\ p_2(t) \\ p_3(t) \\ p_4(t) \end{bmatrix} \quad (7.6)$$

Following the same procedure used above, steady-state probabilities P_1 , P_2 , P_3 , and P_4 are calculated. Therefore, for a second-order interruption scenario involving two component failures, neither of which is a stuck breaker failure, with failure rates λ_1 and λ_2 and repair rates π_1 and π_2 , the corresponding reliability indices $\mu_{scenario}$ and $MTTR_{scenario}$ are given as follows:

$$\mu_{scenario} \approx P_3 \times \lambda_1 + P_2 \times \lambda_2 \quad (7.7)$$

$$MTTR_{scenario} = (\pi_1 + \pi_2)^{-1}$$

where P_2 and P_3 are the steady-state probabilities of the system represented by the Markov model being in the states in which component 1 is functioning while component 2 is failed and vice versa, respectively.

7.1.2.3 Second-Order Interruption Scenarios Involving Stuck Break

Since stuck breaker failures occur simultaneously with an active failure on an adjacent component, they are modeled as a strict 5% probability of occurrence [9]. Thus, for a second-order interruption in which one component failure is a stuck breaker and the other component failure has failure rate λ , the corresponding reliability indices $\mu_{scenario}$ and $MTTR_{scenario}$ are calculated as follows:

$$\begin{aligned}\mu_{scenario} &\approx 0.05 \times \lambda \\ MTTR_{scenario} &= 1\end{aligned}\tag{7.8}$$

7.1.2.4 System Reliability Indices using Markov Model

Once the reliability indices for each interruption scenario of a given system interruption have been derived, the overall system reliability indices can be calculated. For a system with n associated interruption scenarios, the system can be represented by a Markov model with $n + 1$ states, as shown in Figure 7.3. State 1 represents the functioning system, while states 2 through $n + 1$ each represent one of the system's interruption scenarios. The flowrate from state 1 to state j is the scenario interruption rate of the interruption scenario associated with state j , while the reverse flowrate is that interruption scenario's repair rate.

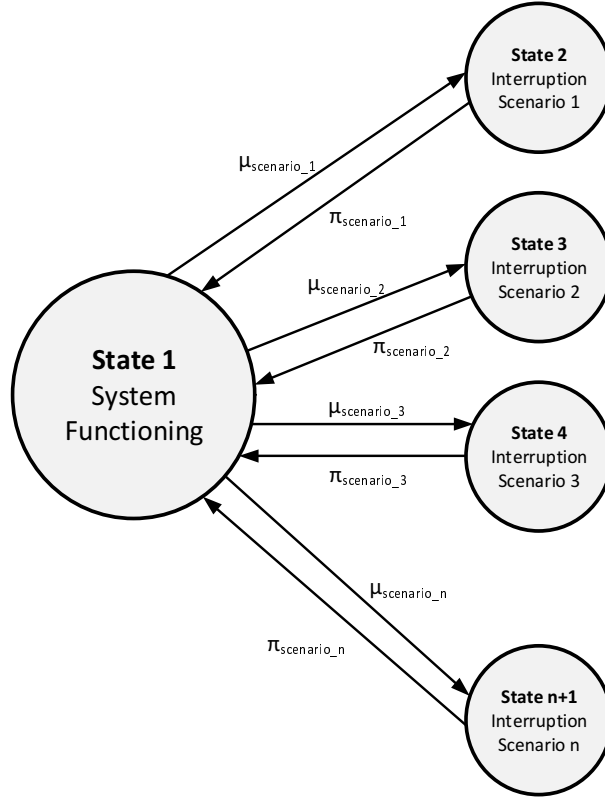


Figure 7.3: Markov model of a second-order interruption scenario.

Equipment reliability indices are derived from the collection of associated scenario indices calculated using (7.1)-(7.8). For an equipment system with n associated interruption scenarios, μ_{system} and $MTTR_{system}$ are calculated as follows:

$$\mu_{system} = \sum_{i=1}^n \mu_{scenario_i} \quad (7.9)$$

$$MTTR_{scenario} = \frac{\sum_{i=1}^n P_i}{\sum_{i=1}^n \pi_{scenario_i} \times P_i} \quad (7.10)$$

where, $\mu_{scenario_i}$ and $\pi_{scenario_i}$ are the interruption and repair rates of the system's i^{th} interruption scenario, respectively, and P_i is the steady-state proba-

bility of the system being in its i^{th} interruption scenario.

In order to facilitate simple comparisons between different topologies, a single overall interruption rate is calculated as a weighted sum of each load's interruption rate. The weights are used to reflect the relative severity of an interruption to each load [7]. The overall interruption rate is calculated as follows:

$$\mu_{overall} = 1.5 \times (\mu_{radar} + \mu_{pulsed}) + \mu_{propulsion} + 0.5 \times (\mu_{storage} + \mu_{zones}) \quad (7.11)$$

7.2 Planar Shipboard Power System Topologies

Three planar distribution system topologies for notional shipboard power system are studied in this work. The first topology is based on the ring bus arrangement, which is employed in most current electric naval vessels. Two different topologies are based on the breaker-and-a-half (BAAH) arrangement, BAAHv1, and BAAHv2. In BAAHv1, redundant connections for some equipment loads are sacrificed in order to reduce the number of circuit breakers used. Version two retains the same level of redundancy as in the ring bus topology [125].

In each topology, there are a total of thirteen generators and loads, collectively called objects. In all topologies except BAAHv1, eight objects have a single point of connection to the larger distribution system (the generators, energy storage unit, propulsion motors, and pulsed load), while five are connected at two points each (the radar and the zonal load centers). In BAAHv1, all objects are singly connected. Note that, the points on the distribution system to which objects are connected are referred to as slots.

7.2.1 Ring Bus

In a shipboard distribution system designed using the ring bus topology, the ring of busbar runs around the perimeter of the ship. The incoming and outgoing lines are connected to the buses running along the port and starboard sides of the ship, with two cross-hull buses connected at the bow and stern to complete the ring. The example of a ring bus-based SPS analyzed in this study is shown in Figure 7.4. In the ring bus topology (see Figure 7.4), the slots are split into two types. Singly connected objects can be connected to the eight slots located between each pair of bus circuit breakers along the port and starboard sides of the ship. The objects with two-point connections are connected across the port and starboard busbars

7.2.2 Breaker-and-a-Half

The BAAH topology consists of two parallel lengths of busbar connected by several conducting lines, called bays. Each bay is attached to two lines, either incoming or outgoing and is protected by three circuit breakers. One, called the common breaker, separates the two attached lines from each other. The other two, called the outside breakers, separate each line from its adjacent bus.

In a shipboard distribution system based on BAAH topology, loads and generators are connected to cross-hull lines, which are themselves connected to the buses running along the port and starboard sides of the ship. A BAAH topology requires 1.5 times as many circuit breakers as a ring bus topology with the same number of incoming and outgoing lines. As space and cost are often of great concern when designing a naval vessel, two versions of a BAAH-based DC distribution system are analyzed in this study. Note that, in

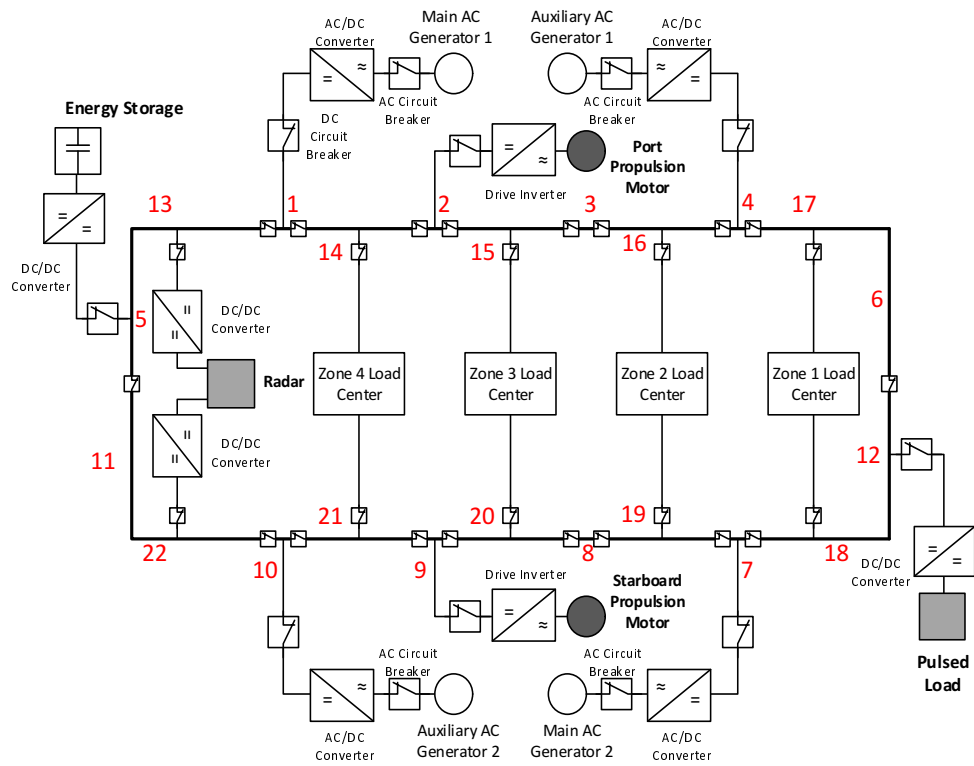


Figure 7.4: A shipboard distribution system with ring bus topology.

the simulated BAAH topology, both BAAHv1 and BAAHv2, a pair of circuit breakers are used to sectionalize the busses into two halves.

Version one, shown in Figure 7.5 contains roughly the same number of circuit breakers as the ring bus configuration in Figure 7.4. This is achieved by eliminating some of the redundant connections used in the distribution system shown in Figure 7.4 (specifically, those of the radar and zonal load centers). In version one, there are seven bays, each with two connection slots, for a total of fourteen slots. Version two, shown in Figure 7.6, is connected with the same amount of redundancy as the system in Figure 7.4, but uses a greater number of circuit breakers. Therefore, in Version two there are nine bays, for

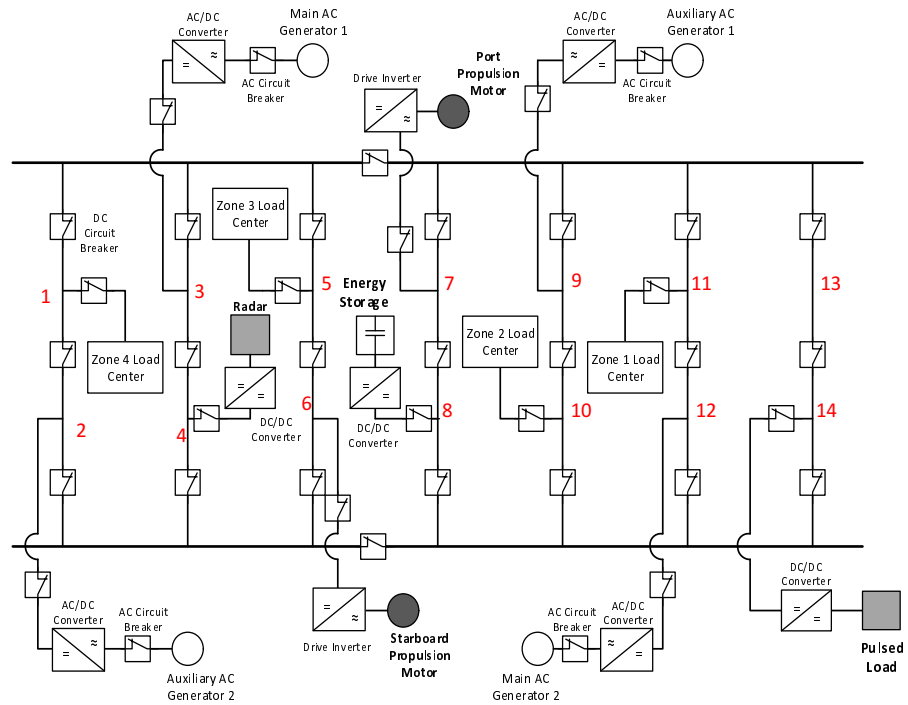


Figure 7.5: A shipboard distribution system with breaker-and-a-half topology (version one) - BAAHv1.

a total of eighteen slots and all slots are occupied in each configuration.

7.3 Three-Dimensional Shipboard Power System Topologies

The three-dimensional (3D) topologies are simulated based on the above three planar topologies. The objective is to distribute the equipment loads across the multiple decks of the ship by designing the shipboard power system topology in a three-dimensional architecture. The 3D distribution systems designed for the three planar topologies discussed in Section 7.2 are detailed in this section.

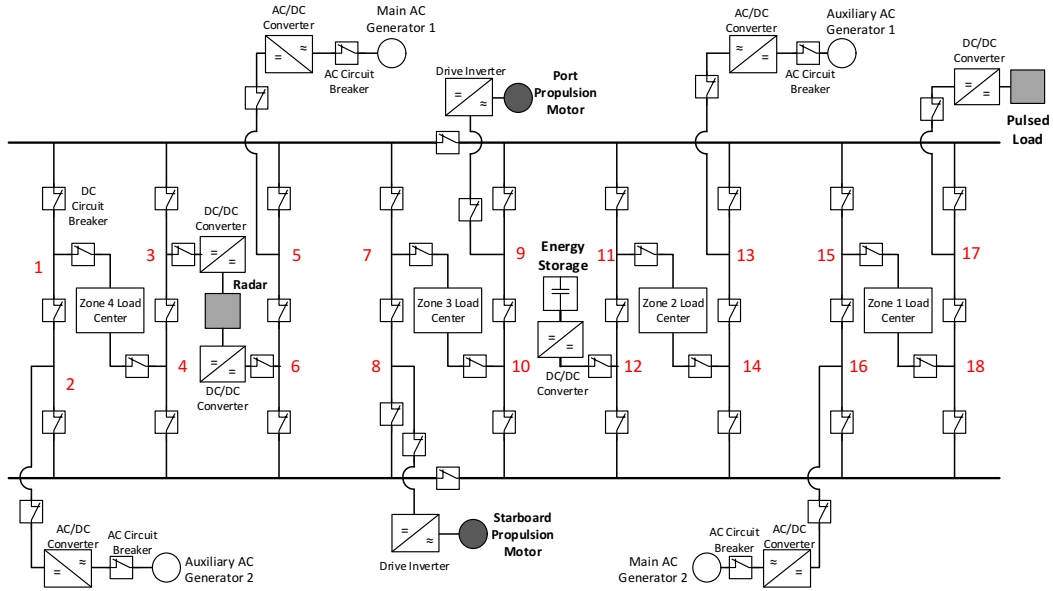


Figure 7.6: A shipboard distribution system with breaker-and-a-half topology (version two) - BAAHv2.

The 3D distribution systems are designed by arranging two or more planar topologies in parallel to one another. Two example three-dimensional topologies simulated by connecting the lower and the upper decks using four vertical buses, each protected by a bus-tie breaker, are shown in Figure 7.7 and Figure 7.8. Note that, in Figure 7.7, both planes are housed below decks while in Figure 7.8, the upper plane is housed within the ship's superstructure, and the lower plane is housed below the deck.

For each planar topology, two 3D arrangements for the shipboard distribution system are developed, 3D topology 1 and 3D topology 2. The 3D topology 1 is based on Figure 7.7 with both planes housed below the deck and both planes are of approximately same size. The 3D topology 2 is based on Figure 7.8 with the upper plane relatively smaller than the lower plane and housed within ship's superstructure. A few sample 3D topologies for ring bus

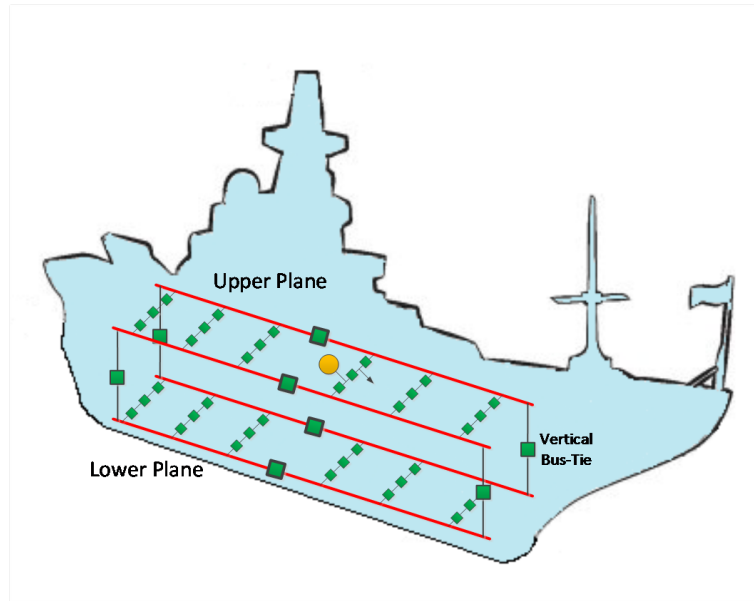


Figure 7.7: Designed three-dimensional SPS topology - 3D topology 1.

and BAAH distribution systems are presented in the following sections.

Note that in order to obtain practical 3D shipboard power system architectures, a few constraints regarding the location of the equipment loads within ship's structure are observed. While designing 3D topologies, it is assumed that ship's main generators can be housed only in the lower deck of the ship. Ship's main generators are typically of the capacity in hundreds of MW, therefore, housing them in the upper deck may result in stability issues. Similarly because of smaller capacity, auxiliary generators are placed in the upper deck. Additionally, to facilitate the navigation, the radar system is always placed in the upper deck of the ship.

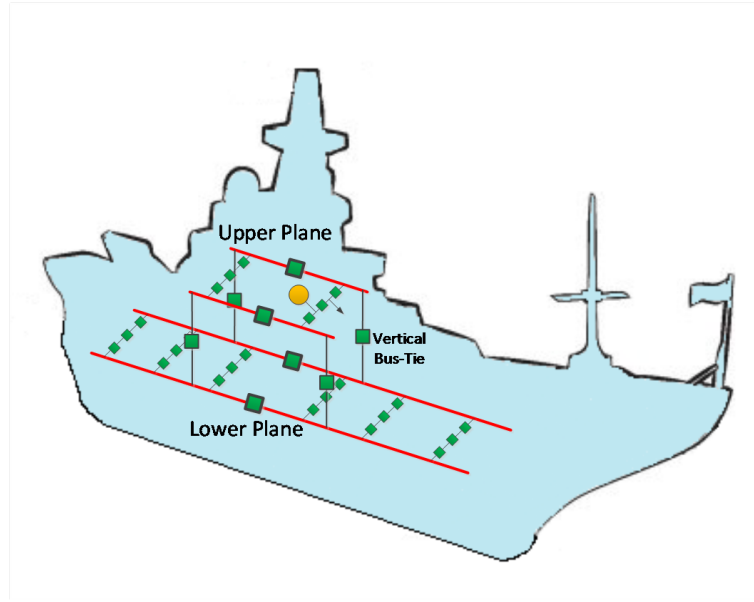


Figure 7.8: Designed three-dimensional SPS topology 2 - 3D topology 2.

7.3.1 Three-Dimensional Ring Bus Topologies

The 3D distribution systems designed for shipboard power system based on ring bus topology are shown in Figure 7.4. Note that both upper (dark gray) and lower decks (light gray) of the ship are designed in a ring bus arrangement, where the busbar runs around the ship structure in both upper and lower planes. In 3D topology 1 (see Figure 7.9), the upper plane is connected to radar, energy storage unit, and one of the zonal load centers. The rest of the loads are connected to the lower level. In 3D topology 2 (see Figure 7.10), the equipment loads are distributed across both planes of the ship with radar, pulsed load, and one of the zonal load centers supplied by the upper plane, while rest of the loads are powered by the lower plane. The two planes of both 3D topologies are connected using four DC circuit breakers, two connected on the port side while the other two on the starboard side. Note that compared

to the planar topology, a 3D ring bus topology requires four additional DC circuit breakers.

7.3.2 Three-Dimensional Breaker-and-a-Half Topologies

The 3D distribution systems designed in BAAHv2 topology for the shipboard power system are shown in Figure 7.6. Same as the 3D ring bus topology, here both upper and lower planes are designed in BAAHv2 arrangement. In 3D topology 1, both planes are of approximately same size. In 3D topology 2, the upper plane is housed in the ship's superstructure, and thus is smaller in size as compared to the lower plane. The upper plane is only supplying for radar while the rest of the equipment loads are powered by the lower plane. Both decks are connected using four DC circuit breakers, two connected on the port side and two on the starboard side. Both 3D BAAHv2 topologies also require four additional DC circuit breakers that are used to connect ship's upper and lower planes (see Figure 7.11 and Figure 7.12). Same as BAAHv2, two 3D topologies based on Figure 7.4 are simulated for BAAHv1 configuration.

7.4 Results and Discussions

This section compares the equipment reliability indices of the simulated three-dimensional topologies against respective planar shipboard power systems. The three-dimensional topologies are simulated by connecting the lower and the upper levels of SPS using four vertical buses, each protected by a bus-tie breaker. Note that in 3D topology 1, both upper and lower levels are housed below ship's decks and, therefore, are of approximately same size. In 3D topology 2, the upper level is housed within ship's superstructure and, therefore, is smaller in size. The lower level is however below ship's deck and,

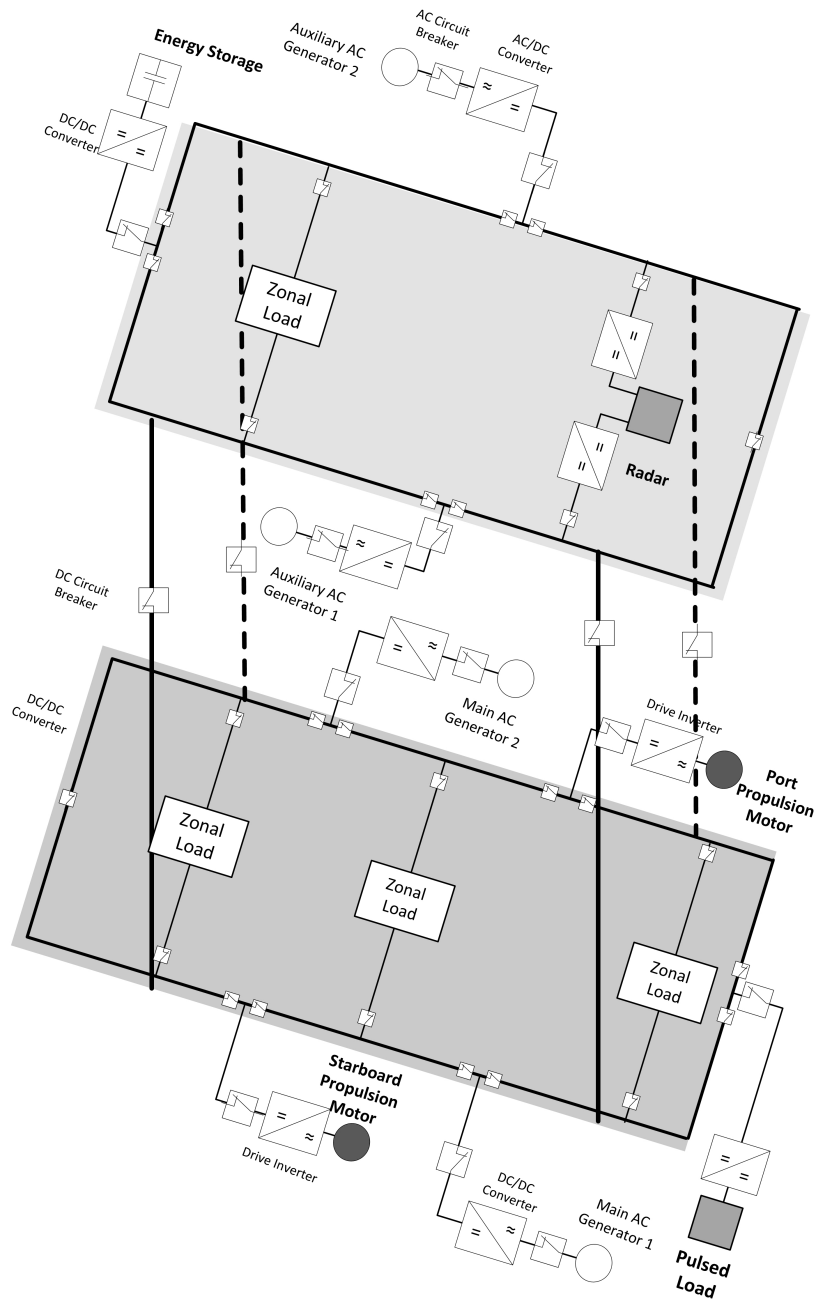


Figure 7.9: Three-dimensional ring bus topology by connecting upper and lower decks of the ship.

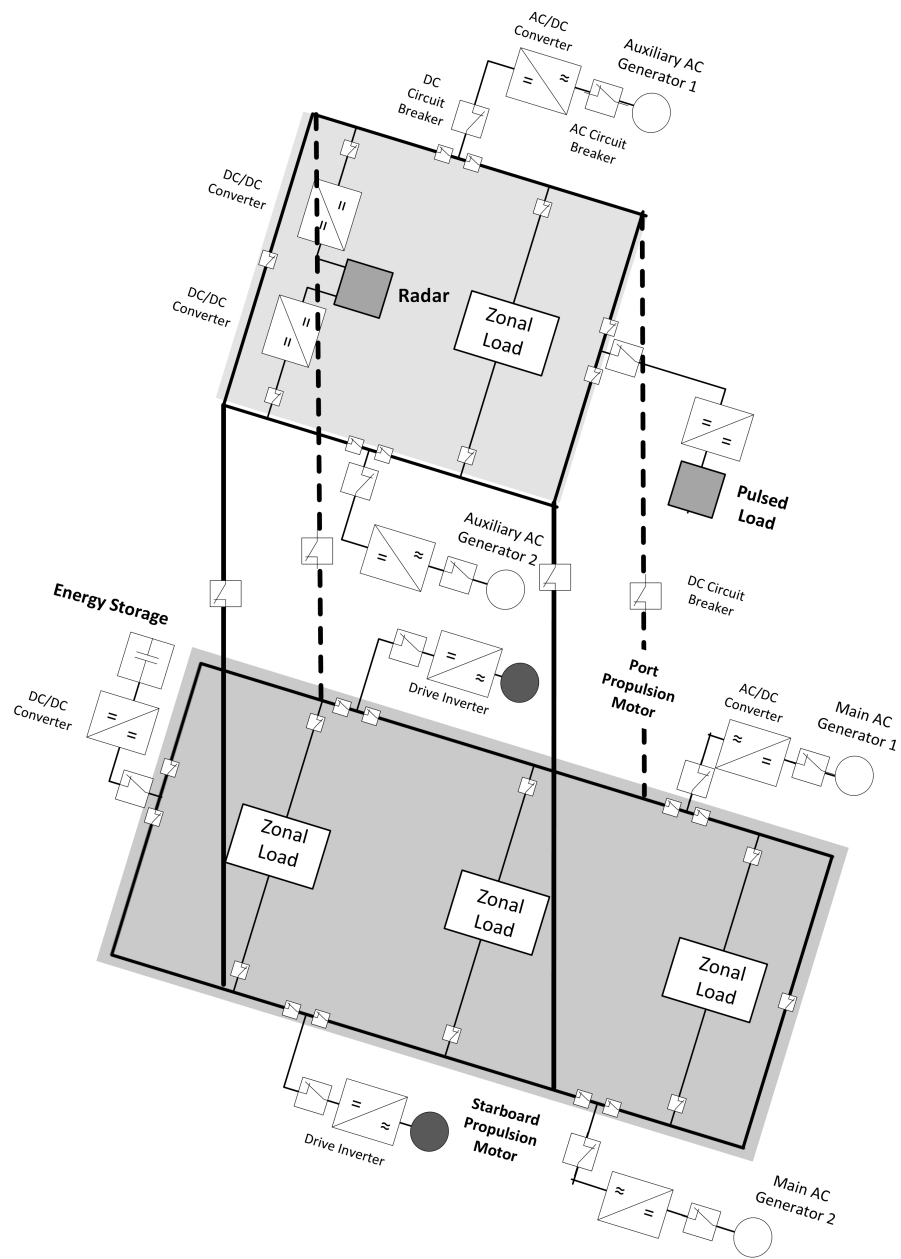


Figure 7.10: Three-dimensional ring bus topology by connecting upper and lower decks of the ship.

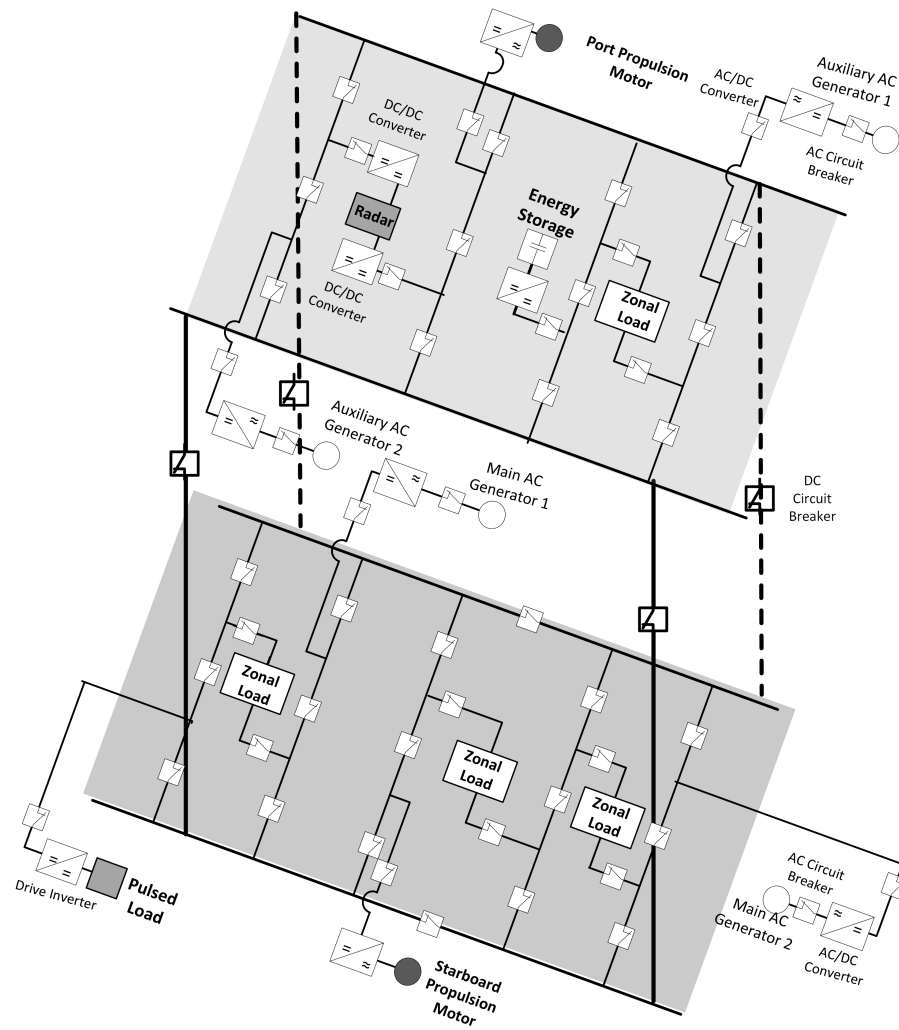


Figure 7.11: Three-dimensional BAAHv2 topology by connecting upper and lower decks of the ship.

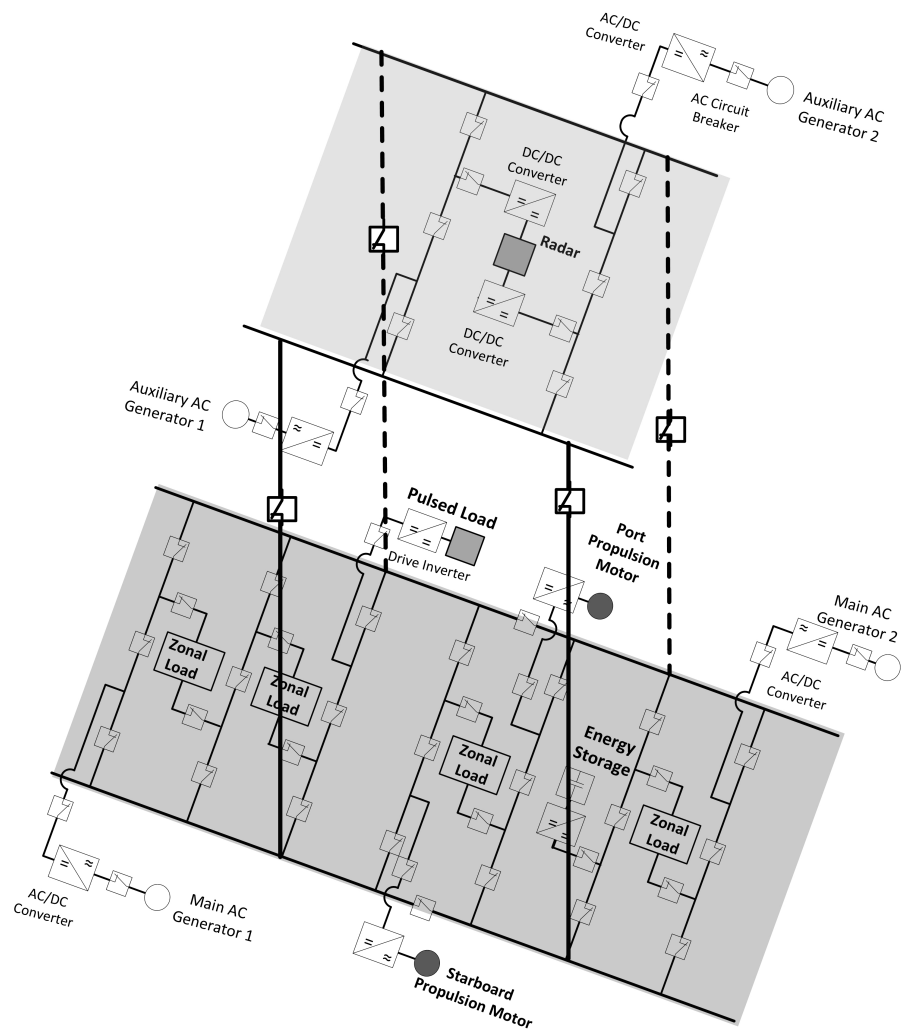


Figure 7.12: Three-dimensional BAAHv2 topology by connecting upper and lower decks of the ship.

therefore, is supplying for most of the equipment loads.

7.4.1 Reliability Indices

The results of the reliability analysis for each simulated 3D distribution systems corresponding to each planar topology is presented in this section. The detailed results comparing reliability indices for each equipment load for the planar and 3D topologies designed for ring bus SPS are shown in Table 7.2. The reliability indices compared are interruptions per year (μ), mean-time-to-repair in hours (MTTR), and total downtime in hours per years. Here, system total downtime is the total expected time the system will spend in an interrupted state per year, the product of the service interruption rate and MTTR.

For ring bus topology, as compared to planar topology, for both 3D topologies, the MTTR improves for each equipment load. The number of interruptions per year, however, slightly increases for zonal loads and radar. The total downtime also slightly increases for radar and zonal loads. The rest of the equipment loads, i.e. propulsion, energy storage, and pulsed load, however, record a decrease in number of interruptions per year and total downtime. The overall interruption rate also decreases from 0.270778421 for a planar topology to 0.248217682 for both 3D topologies.

The overall interruption rates are compared for planar and 3D topologies deployed in ring bus, BAAHv1, and BAAHv2 in Table 7.3 and Figure 7.13. Compared to respective planar topologies, the overall interruption rate decreases for each 3D topology. For BAAHv1, the overall interruption rate decreases from 0.387396438 for a planar topology to 0.387145662 for 3D topology 1 and 0.248217682 for 3D topology 2. A similar reliability improvement is

Table 7.2: System Reliability Indices - Ring Bus Topology

Equipment	Topological Arrangement	μ (interruptions per year)	MTTR (hours)	Total Downtime (hours per year)
Propulsion	Planar	0.108413	3.21388	0.348428
	3D Topology 1	0.109605	3.18973	0.349611
	3D Topology 2	0.109605	3.18973	0.349611
Energy Storage	Planar	0.068502	3.59850	0.246504
	3D Topology 1	0.055402	3.16603	0.175404
	3D Topology 2	0.055402	3.16603	0.175404
Radar	Planar	0.012905	3.32509	0.042909
	3D Topology 1	0.013403	3.23853	0.043405
	3D Topology 2	0.013403	3.23853	0.043405
Pulsed Load	Planar	0.068202	3.60993	0.246204
	3D Topology 1	0.055402	3.16603	0.175404
	3D Topology 2	0.055402	3.16603	0.175404
Zonal Load Centers	Planar	0.012909	3.32474	0.042919
	3D Topology 1	0.015409	2.94757	0.045420
	3D Topology 2	0.015409	2.94757	0.045420

Table 7.3: Overall Interruption Rates

System Topology	Topological Arrangement		
	Planar	3D Topology 1	3D Topology 2
Ring Bus	0.270778421	0.248217682	0.248217682
BAAHv1	0.387396438	0.387145662	0.387146803
BAAHv2	0.22253151	0.221779707	0.222280985

recorded for BAAHv2. The overall interruption rate for the BAAHv2 planar topology is 0.22253151 while the interruption rate comes out to be 0.221779707 and 0.222280985 for 3D topology 1 and 3D topology 2, respectively.

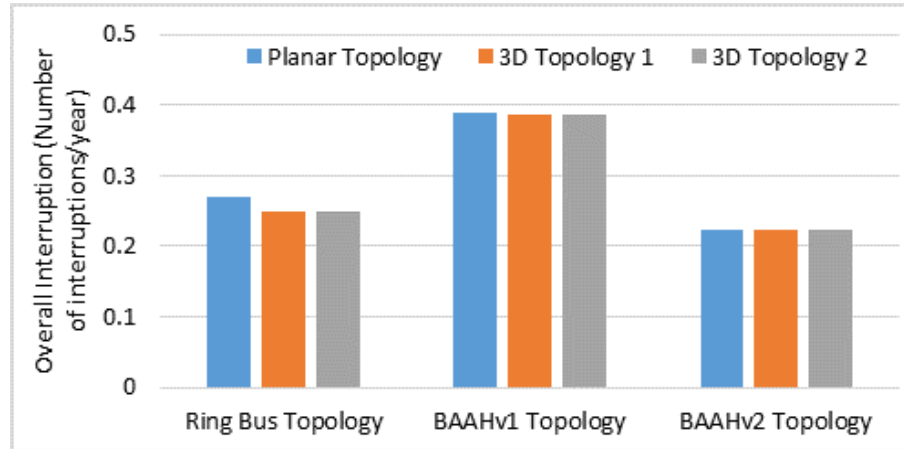


Figure 7.13: Comparing overall interruption rates.

7.4.2 Component Count Comparison

For the consideration of space and cost concerns, the numbers of circuit breakers and power electronic converters required for each topology are compared in Table 7.4. Note that each 3D topology requires four additional DC circuit breakers compared to the corresponding planar topologies. The additional breakers are used to connect the upper and lower planes of the shipboard power system.

7.5 Conclusion

This chapter evaluates the reliability gains obtained by designing shipboard distribution system in a three-dimensional arrangement. The three-dimensional structures are designed based on three notional distribution topologies ring bus, BAAHv1, and BAAHv2. The system reliability indices of planar SPS are compared to those designed in 3D architectures. Compared to planar topologies, 3D topologies decrease the overall service interruption rates for each

Table 7.4: System Topology Component Count Comparison

System Topology	Equipment Arrangement	Number of Components Required				
		AC Breaker	DC Breaker	AC/DC Conv.	DC/DC Conv.	Drive Inverter
Ring Bus	Planar	4	36	4	4	2
	3D topologies	4	40	4	4	2
BAAH v1	Planar	4	34	4	3	2
	3D topologies	4	38	4	3	2
BAAH v2	Planar	4	45	4	4	2
	3D topologies	4	49	4	4	2

notional topology. Depending upon the topology and equipment placement, for 3D topologies the equipment reliability indices, however, improves for a few equipment loads while remains unchanged or becomes worse for others.

The absolute gain or loss in equipment reliability, however, is not significant when compared to the planar topology. This is because the alternate paths obtained using the 3D architecture while decreases the second- and higher-order interruption scenarios, the first-order interruption scenarios remain unchanged. Since, first-order interruption scenarios will have a higher contribution towards the system interruption rate, the reliability gains obtained using 3D architectures are small. A 3D topology, however, may be preferred given that it results in a structurally robust architecture where the most critical loads may potentially function even when one of the decks are destroyed during the attack.

Chapter 8

Resilient Distribution Circuit Topology Design

In recent years, with the increased dependence on electric power systems, the requirement for a resilient and fault-tolerant distribution circuit is increasing. For example, ensuring a higher level of service continuity is important for shipboard distribution circuits in all-electric ships, microgrids with variable energy sources, and secondary distribution networks in metropolitan cities. Additionally, in an all-electric ship, the limited space, weight, and number of onboard spare parts necessitates the use of a minimal amount of equipment while ensuring the highest level of network availability. This work is motivated by the service availability requirements and design constraints for an all-electric ship zonal distribution circuit (ZED). The availability is the steady-state probability that a component or a system is operational. Mathematically, network availability is defined as the probability of finding the circuit operational at time t , given that it was operational and good as new at time zero.

Generally, the distribution circuit design problem is approached from the perspective of minimizing circuit losses and satisfying load demand [15, 138–144]. However, in recent years, in order to provide improved service continuity [145], several work have sought to develop circuit architectures with improved service reliability. For example, [146–151] aim to achieve a higher service reli-

ability in a microgrid while optimizing a defined economic criteria. A method to calculate and improve the availability of microgrids during natural disaster is presented in [152]. The paper targets to improve network availability by the use of distributed generation and energy storage systems. The effects of renewable energy resources on the availability of microgrids are evaluated in [153]. The paper [153] also presents a method of improving network availability by deploying energy storage units. A qualitative method to evaluate the availability of microgrids for different microgrid architectures is proposed in [154]. The paper calculates the occupancy probability of the minimum cut set and compares the effect of topological structure on network availability. Furthermore, the analysis also models the impact of local generation and energy storage units on availability. Additionally, [155] develops a method to include energy storage unit for increasing the availability of PV generation. The paper develops a Markov-chain-based energy storage model for evaluating PV generation availability. Authors conclude that the developed energy storage model may assist in planning grid integrated PV generation, both large and small-scale. Furthermore, several research articles have also focused on designing communication infrastructure in the smart grids, including communication protocols, routing algorithm, and security. [156–160].

For a given distribution circuit, a higher level of network availability can be ensured either by deploying components with low failure rates or by providing redundancies for the power supply by modifying the circuit topology. A circuit topology is characterized by the node interconnections within a circuit. In literature, several works have characterized the vulnerability of the electric transmission system due to circuit's structural topology [161–165]. A close correlation between the topological structure of the network and its resilience

to survive a failure has been reported. Although the relation between the circuit topology and its resiliency or service availability has been investigated, none have explored the problem of designing a circuit topology while aiming to improve its availability. Thus, the availability-based methods for designing distribution circuits have not been investigated.

In this chapter, we aim to design a resilient circuit topology ensuring the highest level of network availability while using a minimum number of conductors. The objective is to ensure the availability of electrical service to each load in a given all-electric ship ZED system. Additional service requirements such as system losses, equipment reliability, and other operational requirements can be satisfied on the designed circuit topology. First, a mathematical framework for the design of a resilient circuit topology, subject to network availability constraint, is developed. Next, to efficiently solve the topology design problem, a novel graph-theory based algorithm, termed successive minpath generation, is proposed. The proposed algorithm reduces the search space for the resilient circuit topology to polynomial time, thus providing a significant computational advantage. Additionally, by prioritizing network availability as the objective, this work presents a new approach to designing distribution circuits.

The algorithm is successfully applied to design distribution circuit topologies for ZEDs supplied by both single as well as multiple power sources. For the single-power source case, the circuit topology with network availability more than 0.99 is obtained by using 3 fewer and 12 fewer conductors for a 15-node and a 30-node ZED, respectively, as compared to the corresponding grid topologies. As for the ZED supplied by two power sources, network availability more than 0.99 is obtained by using 6 fewer conductors than the corresponding grid topology. By designing the circuit topology, this work prioritizes network

availability as the design objective and thus presents a new approach to the distribution circuit design problem. The results confirm the success of the proposed algorithm in designing distribution circuit topologies.

8.1 Scope of the Work

This work presents a method for designing resilient distribution circuit topologies. System resiliency is defined as the ability to maintain an acceptable level of service during faults. System resiliency can be quantified using several parameters such as system reliability, recoverability, stability, etc. The objective of this work is to design circuit topologies that can continue to supply power even in the case of multiple faults. Therefore, for the context of this paper, network resiliency is quantified in terms of service availability. The method is specifically applied to design circuit topologies for ship's zonal distribution systems. The proposed approach can be successfully extended to design utility distribution circuits as well.

The proposed method aims to design a distribution circuit topology with improved service availability using a minimum number of feeders/conductors. Here, service availability is defined as the steady state probability that a given network is operational. In the context of the distribution circuit design problem, the selected distribution circuit is assumed to be operational if there is a path from the source to each load node. The availability as defined in this work is not contingent upon the reliability of the protection equipment. Instead the availability solely depends upon the circuit topology and the availability of the feeders. Additionally, it is assumed that as soon as the fault occurs in the feeder, the faulty feeder is isolated and the rest of the circuit is operating normally.

The proposed algorithm is based on the availability index measuring the steady-state probability of observing the system in an operational state. Generally, the reliability of the power distribution system is quantified by measuring the frequency and duration of service interruptions. For example, ASUI (average service unavailability index) defined as the average annual outage time, is commonly used by distribution providers to measure service reliability. The proposed approach, however, can be extended to design distribution circuits for other reliability parameters as well. In fact, the algorithm is applied to design distribution circuits while aiming to decrease service interruption rates and mean time to repair.

It should be note that, while designing distribution systems, several other requirements including feeder voltage class, cable type, capacity, impedance, etc. need to be satisfied. The circuit design problem satisfying all these objectives is complex. Therefore, by prioritizing the requirements, the design problem is broken down into several smaller optimization problems. Generally, the design begins with the selection of a distribution circuit topology (radial, loop or grid). Next, an optimal distribution circuit is designed, to satisfy different service requirements such as ability to efficiently serve the load demand, minimize the circuit losses, maximize operational economy, etc. At the end, to ensure circuit reliability and service continuity, a protection system is designed for the distribution circuit. Note that in the traditional distribution circuit design approach, a reliable service operation is achieved using the protection system. This work, however, aims to prioritize improved service availability as the distribution circuit design objective. Once a resilient topology is designed, the additional service requirements such as system losses, equipment reliability, and other operational requirements can be satisfied on

the designed circuit topology.

8.2 Network Availability - Definitions

A network availability problem is modeled on a probabilistic graph where each edge has an associated probability of failure/operation. Basic graph theory definitions and relevant network availability parameters are defined in this section.

8.2.1 Probabilistic Graph and Network Topology

A graph or a network is a collection of nodes and edges. A distribution circuit is mathematically represented using a probabilistic graph. A probabilistic graph $G = (V, E)$ is a set V of n nodes representing load and source nodes together with a set E of m edges representing distribution lines, where each edge is associated with an availability index (a_e). The index (a_e) quantifies the availability of edge e , which is equal to the probability that edge e is operational at time t , given that it was operational at time zero.

Using reliability theory, the availability of edge e depends upon its failure rate, λ_e , and repair rate, μ_e , and is given by (8.1).

$$a_e = 1 - \left(\frac{\lambda_e}{\lambda_e + \mu_e} \left(1 - \exp^{-(\lambda_e + \mu_e)t} \right) \right) \quad (8.1)$$

Assuming t to be large, the steady-state availability of edge e simplifies to (8.2).

$$a_e = \frac{\mu_e}{\lambda_e + \mu_e} \quad (8.2)$$

A network topology is defined as the way in which the nodes are connected using edges. For an electrical distribution system, nodes and edges correspond

to loads and distribution lines, respectively. Currently, three types of network topologies are deployed for distribution circuits: radial, loop, and grid.

8.2.2 Network Availability

As mentioned before, the availability is the steady-state probability that a component or a system is operational. Here, network availability ($A(G)$) is defined as the probability that the network is in operating state at time t , given that the network was operating and good as new to begin with. The network operating state is characterized based on the desired network operation. For an electric distribution circuit, the desired network operation is defined as the case when electric service is available to each load served by the circuit. Therefore, in the context of this work, a network is said to be operational if there is a path from the source node to each load node. A network fails if any one of the load nodes are disconnected from the source node and thus has no electric service. An example of the operational and failed networks for a distribution circuit designed in a grid topology is shown in Figure 8.1. Note that while an operational network connects each load to the source, in failed networks, one or more loads are disconnected.

Here, network availability ($A(G)$) is computed using minpaths [166]. The implemented availability calculation algorithm does not use any approximation and calculates the actual network availability for a given graph. A minpath is a set of nodes and edges that characterize an operational network, but the removal of any one edge results in a loss of service; such a case is defined as network failure. A minpath would be defined differently depending upon the definition of the operational network. For example, the minpath for the grid topology (G) shown in Figure 8.1 is characterized by a minimal subgraph of

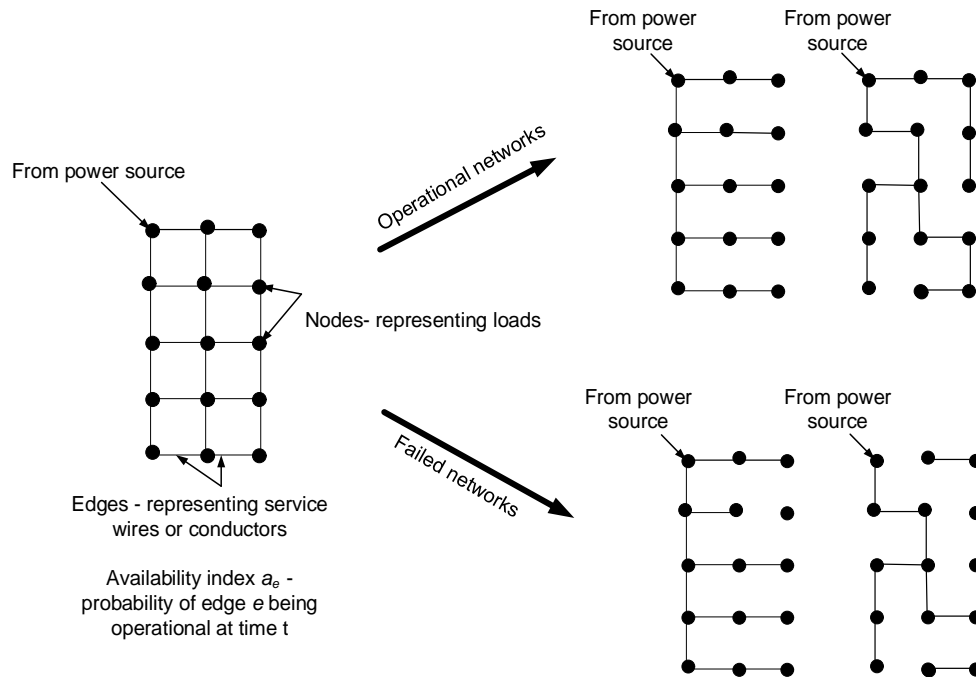


Figure 8.1: Defining operational and failed networks for a distribution circuit. A network is identified as operational if and only if there is a path from the supply node to each load node. The network fails if any one of the load nodes are disconnected from the supply node.

G connecting all nodes of G .

8.3 Resilient Network Topology Design

The problem formulation begins with a typical grid topology ($G = (V, E)$) for the distribution circuit where a load is connected at every node and each load is equally critical for a successful network operation (Figure 8.1). Because of the multiple paths, the design economy is relatively higher for the grid topology. Therefore, the aim is to find a minimal subset of edges in $G = (V, E)$ such that the resulting network topology meets the network availability target.

8.3.1 Problem Formulation

We begin with a probabilistic graph $G = (V, E)$ with a set V of n nodes and a set E of m edges designed in a grid topology. Every edge $e \in E$ has an associated availability index, a_e , which gives the probability of that edge being operational at time t , given that the edge was operational at time zero. An example graph for the distribution circuit laid out in the grid topology is given in Figure 8.1.

First, for every subset $F \subseteq E$, an incidence vector $\chi^F = (\chi_e^F)_{(e \in E)}$ is induced by setting:

$$\chi_e^F = \begin{cases} 1, & \text{if } e \in F \\ 0, & \text{otherwise} \end{cases} \quad (8.3)$$

Likewise, a subgraph $G^F = (V, F)$ of the graph $G = (V, E)$ is induced by the corresponding incidence vector χ^F . In this way any subgraph for the graph G can be characterized.

Now, for each edge $e \in E$ in the graph $G = (V, E)$, we associate a variable $x_e \in \mathbb{R}$. For any subset of edges $F \subseteq E$, we define:

$$x(F) = \sum_{e \in E} x_e$$

Based on the above definitions, the problem of finding a resilient circuit topology with network availability greater than or equal to p is formulated as follows:

$$\min_{\forall F \in \mathcal{P}(E)} x(F) \quad (8.4)$$

subject to

1. $A(G^F) \geq p$ for a given p where $0 < p < 1$
2. $0 \leq x_e \leq 1 \forall e \in E$

3. x_e is integral $\forall e \in E$

The optimization problem defined in (8.4) is a non-linear integer program. Note that $\mathcal{P}(E)$ is the powerset of E . Also, based on above formulation, $x(F)$ is equal to the total number of edges in the subgraph G^F .

8.3.2 Complexity of the Topology Design Problem

To date, the algorithms developed to calculate network availability are exponential in the number of edges [166], requiring computation time that grows exponentially with the number of edges. Thus, using a closed form expression for $A(G)$ and solving the optimization problem given in (8.4) is impractical.

A practical approach to calculating the network availability is using minpaths P_1, P_2, \dots, P_h of the graph $G = (V, E)$. The required network topology can be designed by selecting a subset of minpaths satisfying the availability constraint in (8.4). Although seemingly simple, the method of enumerating all minpaths and selecting a subset of minpaths is exponential in the number of nodes. The number of minpaths in a network can be exponential in the number of nodes. Furthermore, enumerating all subsets of minpaths will introduce another exponential term, thereby making the algorithm computationally intractable. Hence, an efficient algorithm is required for the circuit topology design problem.

8.3.3 Theoretical Discussion

Prior to discussing the proposed algorithm, a few additional observations and results related to the network design problem defined in (8.4) are discussed.

Definition 1: Connected Graph - A graph $G = (V, E)$ is connected when there is a path between every pair of nodes. Thus, in a connected graph each node is reachable from every other node.

Definition 2: Spanning Tree - A spanning tree $T = (V, E_{sub})$ of a graph $G = (V, E)$ is a selection of edges of G forming a tree, T , that spans every vertex.

Definition 3: Edge Contraction - In a graph $G = (V, E)$ with n vertices and m edges, the contraction of an edge $e \in E$ with endpoints (u, v) , where $u \in V$ and $v \in V$ is defined as the operation of deleting the edge e and merging vertices u and v . The resulting graph $G.e = (V^c, E^c)$ has $n - 1$ vertices and $m - 1$ edges.

Definition 4: Edge Deletion - In a graph $G = (V, E)$ with n vertices and m edges, the deletion of an edge $e \in E$ with endpoints (u, v) , where $u \in V$ and $v \in V$, is defined as the operation of deleting the edge e while vertices u and v are retained. The resulting graph $G - e = (V, E^d)$ has n vertices and $m - 1$ edges.

Observation 1: A graph $G = (V, E)$ with $A(G) \geq p$, where $0 < p < 1$, is a connected graph.

The availability of a graph is defined as the probability of finding a path from the source to each load node. In a disconnected graph there is no path between one or more nodes, implying that one or more nodes are not reachable from the source. Thus the availability of a disconnected graph is zero. Therefore, by contradiction, a graph G with availability greater than zero will be a connected graph.

Observation 2: Corresponding to the availability problem defined in

(8.4), the minpath for a graph $G = (V, E)$ with n vertices, is a spanning tree with $(n - 1)$ edges.

By the definition of network availability, the minpath for G is a subgraph connecting all vertices using the minimum number of edges. Also, the minimal connected graph for a set of n vertices is a spanning tree with $(n - 1)$ edges. Thus, by definition, the minpath is a spanning tree.

Proposition 1: Let $G^S = (V, S)$ be a subgraph of $G = (V, E)$, such that $S \subset E$. Define $G^{S^e} = (V, S \cup e)$ where $e \in (E \cap S)$. Then, $A(G^{S^e}) > A(G^S)$. Note that the above proposition implies that on adding an edge, the network availability of any graph $G = (V, E)$ will increase.

Proof: In a graph $G = (V, E)$, for an edge $e \in E$ with availability equal to a_e , (8.5) holds for $0 < a_e < 1$ [166].

$$A(G.e) > A(G - e) \quad (8.5)$$

Next, the availability of the graph $G^{S^e} = (V, S \cup e)$ can be expressed as a function of two graphs obtained by contracting and deleting an edge $e \in E$ (see (8.6)). Then the above proposition can be proved using (8.5) as follows:

$$\begin{aligned} A(G^{S^e}) &= a_e A(G^{S^e}.e) + (1 - a_e) A(G^{S^e} - e) & (8.6) \\ &> a_e A(G^{S^e} - e) + (1 - a_e) A(G^{S^e} - e) \\ &> a_e A(G^S) + (1 - a_e) A(G^S) \\ &> A(G^S) \end{aligned}$$

Based on the above observations, we propose an efficient graph theory based algorithm for the circuit topology design problem. The algorithm begins by generating a minpath (in this case a spanning tree) for the network,

thus ensuring that the network is connected so that network availability is greater than zero. Note that the minpath achieves non zero network availability using a minimum number of edges. Next, the edges are selected and successively added to the network, thereby increasing the number of minpaths and improving network availability. The process terminates when the availability constraint is satisfied. The proposed algorithm successfully reduces the search space of the topology design problem defined in (8.4) from double exponential to polynomial time, thereby making the design problem tractable. The proposed algorithm and its complexity are discussed in detail in the following section.

8.4 Proposed Algorithm : Successive Minpath Generation

In the context of the network design problem presented in this chapter, a network is said to be operational if it contains at least one path from the source node to each load node. Network availability is simply the probability of finding the network in its operational state at time t , given that it was operational at time zero. The proposed algorithm begins with a minpath, thereby ensuring connectivity, and successively adds minpaths to the network, thus improving upon the network availability. The method consists of three stages: designing initial topology, evaluating network availability constraint, and selecting and adding an edge. The proposed topology design algorithm is given by Algorithm 1. The three steps of the proposed algorithm are discussed in detail in the following section.

8.4.1 Initial Topology Design

The algorithm begins by identifying a maximum available spanning tree $T = (V, E_{sub})$ of the graph $G = (V, E)$, as shown in Figure 8.2. The problem of finding a maximum available tree is similar to that of finding a maximum cost spanning tree [134]. A standard min-cost spanning tree algorithm is adapted to generate a maximum available spanning tree $T = (V, E_{sub})$ for graph $G = (V, E)$, and the steps are presented in Algorithm 2.

Note that the network represented by the spanning tree contains only one minpath for the successful operation. Therefore, the network availability for the tree $T = (V, E_{sub})$ spanning the graph $G = (V, E)$ is given as:

$$A(T) = \prod_{\forall e \in E_{sub}} a_e \quad (8.7)$$

Prim's algorithm [134] is originally applied to find either a minimum cost tree or a maximum capacity spanning tree; both quantities are represented by additive functions. The same algorithm can be applied to the availability

Algorithm 1 Obtain the required circuit topology satisfying a given network availability constraint, $A(G^F) \geq p$

Require: A non-empty connected weighted graph $G = (V, E)$ with vertices V and edges E . The weights are component availability indices for edges (a_e).

Obtain maximum available spanning tree ($T = (V, E_{sub})$) using Algorithm 2.

Define $G^F = (V, F)$ where, $F = E_{sub}$.

Calculate $A(G^F)$.

while $A(G^F) < p$. **do**

 Define {rem-edge} = $\{e | e \in E \setminus F\}$.

 Select an edge and obtain the updated network topology, $G^{F'} = (V, F')$ (Use Algorithm 3).

 Redefine $G^F = G^{F'}$ and Calculate $A(G^F)$.

end while

return The graph $G^F = (V, F)$. The graph G^F represents the required circuit topology.

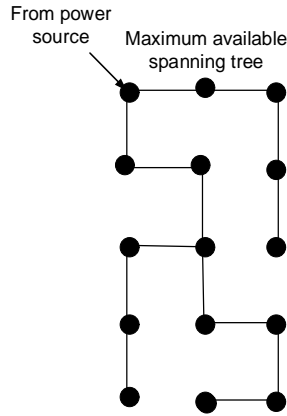


Figure 8.2: Initial topology design- spanning tree.

function shown in (8.7) by simply taking the logarithm of the function and converting it to an additive function. The algorithm starts with a vertex and, among all possible connected vertices, selects an edge with maximum availability index (a_e). It then moves forward from the other end of the selected edge and repeats until a tree connecting all vertices of the graph is found. The complexity of Prim's algorithm is $\mathcal{O}(|V|^2)$; therefore a maximum available spanning tree is found in polynomial time.

8.4.2 Availability Calculation

The principle of a minpath-based availability calculation algorithm is discussed here. Let P_1, P_2, \dots, P_h be minpaths of $G = (V, E)$. Let E_i be the event that all edges in minpath P_i are operational and $Pr[E_i]$ denotes the probability of such an event. The network availability is then simply the probability that one or more events E_i occur. Note that E_i are not disjoint events. Thus, the

availability of graph G is given by:

$$A(G) = \sum_{j=1}^h (-1)^{(j+1)} \sum_{I \subseteq \{1,2,\dots,h\}, |I|=j} Pr[E_I] \quad (8.8)$$

where, E_I is the event that all paths P_i with $i \in I$ are operational. This is referred to as standard inclusion-exclusion expansion [166].

To make the availability computation further tractable, the standard inclusion-exclusion approach to the availability calculation discussed in (8.8) is modified. The method of disjoint products [166] is used, which makes event E_i (the event that all edges in minpath P_i are operational) disjoint. This modification makes the network availability calculation recursive and thus computationally efficient.

Algorithm 2 Obtain maximum available spanning tree

Require: A non-empty connected weighted graph $G = (V, E)$ with vertices V and edges E. The weights are availability indices for edges (a_e).

{conn-node} = { x }, where x is an arbitrary selected node (starting point) from the set of node V.

{rem-node} = $\{V \setminus x\}$.

{conn-edge} = {}.

while {conn-node} \neq V. **do**

 Choose the edge $\{u, v\}$ with the maximum weight

 s.t. $u \in$ {conn-node} and $v \in$ {rem-node}.

 Add v to {conn-node}.

 Delete v from {rem-node}.

 Add $\{u, v\}$ to {conn-edge}.

end while

Define $E_{sub} =$ {conn-edge}.

return The tree $T = (V, E_{sub})$. Note that, T is the maximum available spanning tree that can be extracted from the given circuit topology.

8.4.3 Edge Selection and Addition

Once the network is connected, the next step is to meet the availability constraint. The edge selection algorithm selects the edge amongst the remaining edges which maximizes network availability. For this purpose, all remaining edges are added separately to the current network topology and the availability of the modified topology is computed. The additional edge resulting in maximum network availability for the modified network topology is selected and added. The edge selection algorithm is shown in Algorithm 3. Since the edge resulting in the maximum network availability is selected, at each iteration the algorithm results in the maximum improvement in the network availability.

To understand the complexity of edge selection and addition algorithm, let us consider a $(n \times n)$ grid graph $G = (V, E)$, where $(n \times n = |V|)$. The total number of edges in the given grid graph will be: $|E| = n \times (n - 1) + (n - 1) \times n = 2n^2 - 2n$. Also, the spanning tree $T = (V, E_{sub})$ for the graph $G = (V, E)$ contains $|E_{sub}| = n^2 - 1$ edges.

Algorithm 3 Edge selection and addition algorithm

Require: A weighted graph $G = (V, E)$ with vertices V and edges E . The weights are availability indices for edges (a_e) .

Require: A subgraph $G^F = (V, F)$ of $G = (V, E)$ s.t. $F \subseteq E$.

$\{\text{opt-edge}\} = \{e | e \in F\}$.

$\{\text{rem-edge}\} = \{e | e \in E \setminus F\}$.

for all $s(i) \in \{\text{rem-edge}\}$. **do**

Define $F^i = F \cup \{s(i)\}$ and obtain $G^{F^i} = (V, F^i)$.

Calculate $A(G^{F^i})$.

end for

Select s_{opt} with maximum value of $A(G^{F^i}) \forall s(i) \in \{\text{rem-edge}\}$.

Define $F' = F \cup \{s_{opt}\}$ to obtain new topology $G^{F'} = (V, F')$.

return Updated network topology $G^{F'} = (V, F')$ after edge addition.

Note that in the worst case, the edge selection and addition step has to look for $|E| - |E_{sub}| = n^2 - 2n + 1$ edges. Therefore, in big-O notation the complexity of searching the possible edge space is $\mathcal{O}(n^2)$ or $\mathcal{O}(|V|)$. The proposed algorithm reduces the double exponential search space for the resilient topology to a polynomial search space in the number of nodes.

8.5 Results and Discussion

This section demonstrates the proposed algorithm for its application in designing the circuit topology with improved network availability. The analysis begins with the simulation of a sample network, representing a zonal electric distribution (ZED) circuit for an electric ship supplied by a single power source. The network contains 15 nodes with a load connected at each node. For the system under evaluation, the network availability ($A(G)$) resulting from different circuit topologies, i.e. radial, loop, and grid, are first compared. Next, using the proposed algorithm, resilient circuit topologies are designed while satisfying a given network availability ($A(G)$) constraint. This case study confirms that the proposed algorithm is efficient in designing optimal circuit topologies with the required network availability.

Furthermore, for a detailed evaluation of the stage-by-stage development of the proposed algorithm, a 30-node distribution circuit supplied by a single power source is simulated. The analysis demonstrates that the proposed algorithm improves the network availability by increasing the number of alternate paths in the topology. Also, as the value of $A(G)$ parameter is increased, the proposed algorithm increases the number of loops in the optimal topology, which increases the number of alternate paths.

Because a secondary distribution circuit is generally connected at multiple

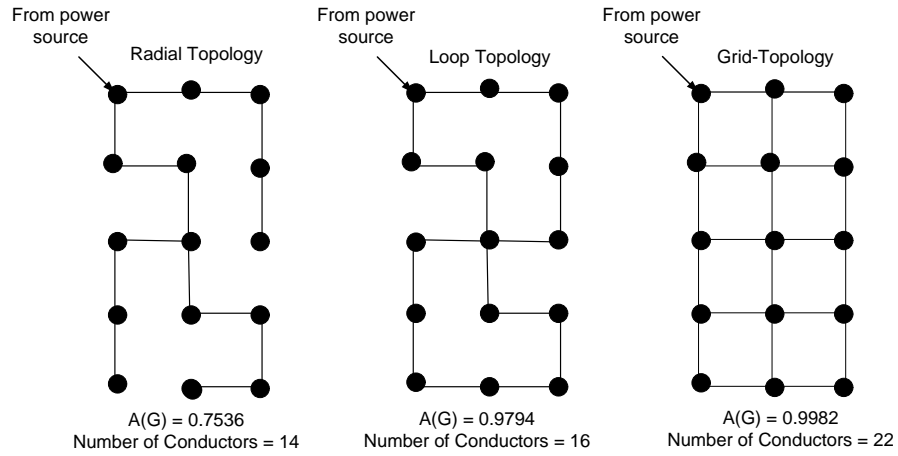


Figure 8.3: Distribution circuit topologies, a) Radial b) Loop and c) Grid.

points to the primary circuit, the proposed algorithm is extended to the distribution circuit supplied by multiple power sources. First, the modifications made in the proposed algorithm to include multiple power sources are discussed. Then the algorithm is applied to design the resilient circuit topology for a 15-node ZED supplied by two power sources. The results show that the proposed algorithm is efficient in designing resilient topologies for the distribution circuits supplied by both single and multiple power sources.

8.5.1 Comparison of Existing Circuit Topologies

For the selected 15-node distribution circuit, the loads are connected in a radial, a loop, and a grid topology as shown in Figure 8.3. Let, the probability of finding an edge operational is 0.98. The network availability of the three topologies are calculated and compared in Table 8.1.

As shown in Table 8.1, the network availability of the radial topology is the lowest among the three selected topologies. The radial topology is calculated

Table 8.1: Comparison of different distribution circuit topologies

Circuit Topology	Network Availability ($A(G)$)	Number of conductors
Radial	0.7536	14
Loop	0.9794	16
Grid	0.9982	22

to be available with a probability of 0.75 using 14 conductors. By adding only two conductors, however a loop topology is obtained with network availability of about 0.98. Note that a significant improvement in network availability is obtained using only two additional conductors. In contrast to a radial topology with only a single operational path, the loop topology results in multiple operational paths and therefore significantly improves network availability. Due to several alternate paths, the grid topology results in the maximum number of operational networks and, therefore, maximum network availability (more than 0.99). However, the grid topology is obtained by adding 6 additional conductors in the loop topology, thus significantly increasing the design cost. It is possible that a few of the additional conductors in the grid topology contribute significantly less towards the improved network availability. Therefore, using the proposed algorithm, we aim to find a circuit topology that uses fewer conductors than in a grid topology, while satisfying the required network availability constraint.

8.5.2 Designed Resilient Circuit Topology

In this section, the resilient circuit topologies are designed to meet a given network availability measure ($A(G)$). The objective is to satisfy a network availability measure using a minimum number of conductors. We consider three cases for resilient circuit topology design with a required network avail-

ability greater than 0.98, 0.99 and 0.995. Note that each service wire (conductor) has $a_e = 0.98$.

Figure 8.4(a) shows the circuit topology designed to satisfy network availability $A(G) > 0.98$. Note that the circuit topology for a service availability greater than 0.98 is obtained using only 16 conductors, which is the same as the number of conductors used in the loop topology (Figure 8.3). Since the service availability offered by the loop topology is lower than the designed topology (see Table 8.2), the proposed algorithm is efficient in designing a low cost topology with maximum availability.

Next, Figure 8.4(b) and Figure 8.4(c) show the designed resilient network topologies with network availability greater than 0.99 and 0.995. Note that network availability greater than 0.99 and 0.995 is obtained using only 17 and 19 conductors, respectively. Clearly by intelligently selecting the conductors, the proposed algorithm is able to design a low cost circuit topology with network availability comparable to the grid topology. Also, based on the designed circuit topologies, the additional conductors in the grid topology (with 22 conductors) shown in Figure 8.3 contribute significantly less towards improving network availability.

Using the proposed algorithm, a detailed case study is conducted to understand a stage-by-stage development of the circuit topology. A 30-node distribution circuit is simulated and the required network availability index ($A(G)$) is increased from 0.6 to 0.99. The resilient circuit topologies generated for several network availability indices are shown in Figure 8.5. The designed circuit topologies are compared for the availability and number of conductors in Table 8.2. Note that the complete grid topology for the 30-node system requires 49 conductors and results in a service availability of 0.9982. However,

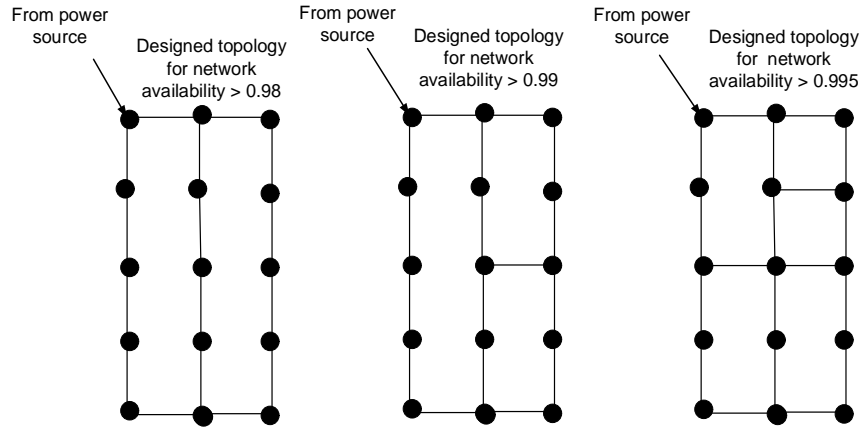


Figure 8.4: Resilient distribution circuit topology with, a) $A(G) > 0.98$ b) $A(G) > 0.99$ c) $A(G) > 0.995$.

Table 8.2: Comparison of different distribution circuit topologies

Circuit Topology	Network Availability ($A(G)$)	Number of conductors	Number of loops
A	0.5566	29	0
B	0.8285	31	2
C	0.9374	32	4
D	0.9712	33	10
E	0.9843	35	30
F	0.9902	37	116

using the proposed algorithm, a circuit topology with a network availability greater than 0.99 is obtained using only 37 conductors, which implies a significant saving in design cost. By comparing the topologies designed for a 15-node system to a 30-node system, it is evident that the saving in design cost increases significantly with the increase in the size of the distribution circuit.

From Table 8.2, it can be observed that the number of loops in the de-

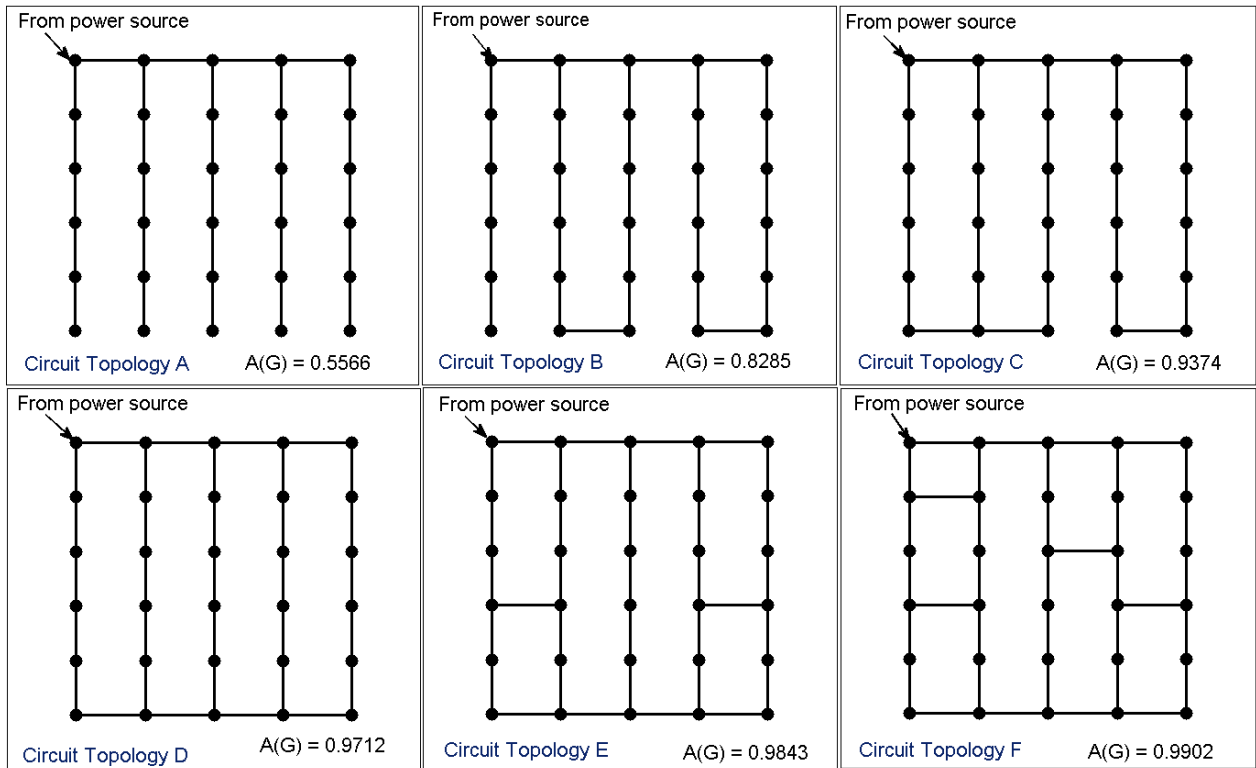


Figure 8.5: Resilient distribution circuit topologies designed for the 30-node system.

signed circuit topology increases significantly with the increase in the network availability index. This observation illustrates the working principle of the proposed algorithm. In order to maximize the number of alternate paths, the algorithm aims to maximize the number of loops in the designed circuit topologies. At every iteration, the algorithm intelligently selects the edge that results in the number of alternate paths or maximum number of loops. By maximizing the number of operation paths, the proposed algorithm leads to a maximum improvement in network availability while using a minimum number of conductors.

8.5.3 Designed Resilient Circuit Topology with Multiple Sources

Generally, secondary distribution circuits in metropolitan cities or in all-electric ships are connected at multiple points to the primary distribution circuit; thus, they are effectively supplied by multiple power sources. This section presents an extension of the proposed topology design algorithm for distribution circuits supplied by multiple power sources. The objective is to design a resilient circuit topology for a distribution circuit simultaneously supplied by more than one power source using the minimum number of conductors.

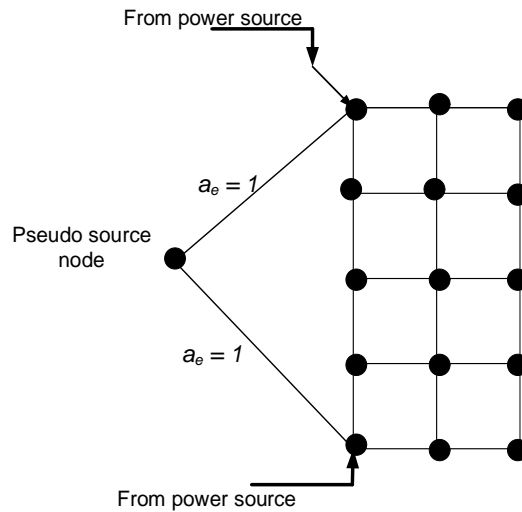


Figure 8.6: A distribution circuit supplied by multiple power sources and the pseudo source node added to solve the resilient circuit design problem.

The proposed modification is illustrated using a 15-node circuit laid out in a grid topology and connected at two different points to the primary distribution circuit, as shown in Figure 8.6. To include multiple sources into the topology design problem, a pseudo source node is added and connected to each source node supplying for the distribution circuit, as shown in Figure 8.6. Since power sources are assumed 100% available, the edges connecting

the pseudo source node and the source nodes in G have availability equal to $a_e = 1$. Next, the proposed topology design algorithm (Algorithm 1) is implemented on the modified distribution circuit with the pseudo source node. The important point to note is that the proposed modification enables us to apply the same algorithm proposed for circuits supplied by a single power source (Algorithm 1) to the one supplied by multiple power sources.

The proposed modification is implemented and tested to design resilient circuit topologies with network availability greater than 0.99 for the 15-node system shown in Figure 8.6, supplied by two power sources. As expected, as the number of power sources supplying for the circuit is increased, the number of conductors in the designed topology decreased. Network availability was observed to also depend upon the location of power sources. The circuit topologies designed for the distribution circuits supplied by two power sources are shown in Figure 8.7. Both designed circuits are using 16 conductors and provide a network availability greater than 0.99. The network availability of the circuit show in Figure 8.7(b) is greater than that of Figure 8.7(a) only because of the difference in the location of the power sources. Also, for the same distribution circuit supplied by only one power source, the designed topology resulted in a network availability of about 0.97. As expected, a significant improvement in network availability is observed by adding an additional power source.

8.6 Conclusion

This chapter develops a novel mathematical formulation and an efficient graph-theory based algorithm for the design of a resilient distribution circuit topology while satisfying a given network availability requirement. The pro-

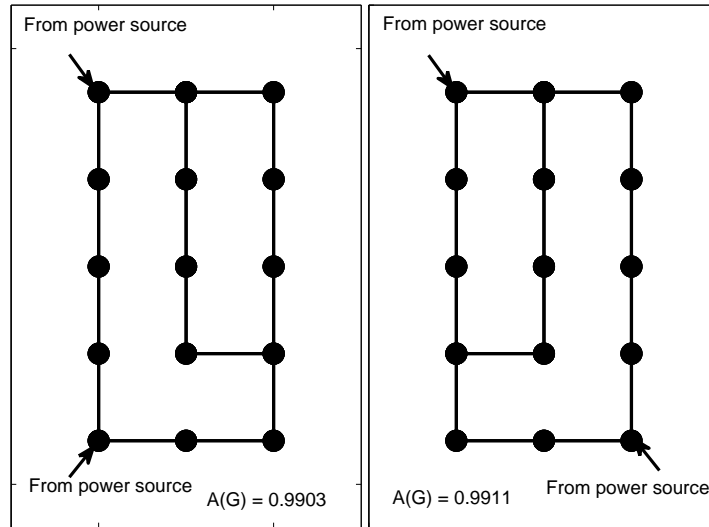


Figure 8.7: Resilient distribution circuit topologies for the distribution circuits supplied by two power sources.

posed algorithm, termed successive minpath generation, is tested and validated using distribution circuits supplied by single as well as multiple power sources. The results confirm that the proposed algorithm is significantly efficient in designing resilient circuit topologies. Furthermore, it is also demonstrated that the algorithm maximizes the number of operational paths at each iteration, therefore resulting in the maximum possible improvement in network availability at a particular iteration. By optimizing the distribution circuit topology, the proposed approach presents a new perspective on the general distribution circuit design problem. The designed circuit topology can be further optimized for additional service requirements (capacity, voltage regulation, etc.), thus prioritizing service continuity as the distribution circuit design objective.

Chapter 9

Conclusion

The modern power distribution grid is gradually evolving from a centralized, unidirectional, and deterministic system to a distributed, bidirectional, stochastic, and dynamic system. The objective of this dissertation is to facilitate this shift in the power distribution system architecture. Notably, to mitigate the undesirable impacts of new technologies and to realize the improved power quality and reliability standards, the study presents methods to control and design power distribution systems. The dissertation is divided into two parts: first concerning the evaluation and mitigation of the impacts of integrating new technologies, and second regarding reliability based approaches for distribution circuit design. The first goal is realized using existing utility distribution systems and the second objective is achieved using a shipboard power system.

For the existing distribution circuits, the impacts and solutions of integrating distributed technologies including electric vehicles (EVs) and photovoltaic systems (PVs) into the distribution circuit are evaluated. The task includes designing circuit and equipment models, identifying simulation criteria, evaluating grid impacts of the new technologies, and developing control strategies to mitigate the impacts and facilitate the integration. Furthermore, the utility of distributed energy storage (ES) systems in providing distribution circuit applications is also investigated. For new distribution circuits, methods for

designing distribution circuits with improved service reliability are proposed. The objectives are explored using a shipboard power distribution system (SPS) for an all-electric ship. Note that in an electric naval vessel, the proper functioning of equipment loads, such as radar, weapons, and propulsion motors is of paramount importance and therefore, it is necessary to ensure that the SPS is designed to be as resilient as possible. The reliability of the distribution circuit are evaluated from the topological perspective.

First, EV integration analysis is conducted for an actual 13.8-kV distribution feeder primarily supplying for residential loads. To evaluate EV charging impacts, three different models for EV loads are developed namely: a time-domain model, an average-value model (AVM) model, and a constant-power model; each model suitable for a different integration study. Notably, the EV charger AVM representing the average dynamics corresponding to the time-domain model, is proposed to obtain a relatively faster model for the voltage quality study. The proposed AVM is successfully able to approximate the EV charger's switching dynamics while significantly decreasing the simulation time. Next, EV impact analysis framework is proposed to evaluate the grid impacts of EV integration both at local and at global circuit level. The analysis identifies several factors concerning EV integration such as the effects of location, size, clustering, and percentage penetration on the distribution circuit. Various methods to mitigate EV load impacts including infrastructural change, indirectly controlled charging using TOU pricing, and direct EV charging control using smart charging algorithms are evaluated next. It is concluded that the additional voltage drops due to EV load charging are efficiently mitigated by upgrading the distribution circuit using an additional transformer; however, the method requires infrastructural changes and hence

is expensive. Implementing a TOU pricing schedule efficiently shifts the EV load charging to off-peak load hours. Furthermore, to optimally mitigate EV charging concerns while avoiding inconveniencing customers, the off-peak rates should begin between 11 pm and 12 am. The controlled charging algorithm designed to mitigate voltage quality issues due to EV charging significantly decreases the substation load demand as well. The proposed method optimally shifts the EV load demand to off-peak load hours thus simultaneously benefiting utility companies as well.

Next, the impacts and solutions of integrating large percentages of distributed PV systems into the distribution circuit are evaluated. First, a mathematical formulation for the hosting capacity problem is developed. To solve the formulated problem, an hourly stochastic analysis approach is proposed. The method is illustrated by calculating the hosting capacity of an actual 12.47-kV feeder for overvoltage concerns. The results obtained using the proposed method are compared against those obtained using a fixed minimum load condition. The method to quantify the percentage accuracy of the hosting capacity results is also presented. It is observed that the voltage quality impact of PV system varies with the loading condition. Additionally, for the same customer penetration level, the PV system impact varies with the PV deployment scenario, depending on the relative PV locations and sizes. PV deployment scenarios with larger PVs at farthest load nodes result in higher impacts on the voltage quality. Also, primary buses farther away from the substation are most likely to observe overvoltages. Methods to mitigate feeder overvoltage concerns due to PV generation using smart inverters are investigated as well. It is observed that smart inverter based active and reactive power control is efficient in mitigating PV related voltage regulation concerns.

Although, the results are demonstrated using overvoltage condition, the proposed framework can be applied to determine the hosting capacity for other impact criteria such as voltage deviation, voltage imbalance, etc. In sum, by developing a mathematical formulation, an hourly stochastic analysis framework, and an approach to quantify the percentage accuracy of the results, a comprehensive understanding of the PV hosting capacity problem is presented in this work.

Many of the challenges for utility distribution system due to the integration of new technologies can be solved using energy storage systems. A framework to evaluate the benefits of integrating the distributed energy storage systems is presented. The applications of ES deployment are investigated for the following three cases, 1) to meet substation N-1 contingency requirement, 2) to increase feeder's PV hosting capacity, and 3) to mitigate voltage variability concerns due to PV generation variability. It is concluded that ES can successfully provide multiple grid and customer benefits. The ES size and optimal deployment locations, however, depends upon the application scenario.

The objectives for new distribution circuits are explored using the primary and zonal distribution circuits of an all-electric shipboard power system. The study demonstrates that the reliability of a distribution system is fundamentally linked to the high-level topology of its connections. For primary distribution circuit, reliability gains obtained using 3D power system topologies are evaluated. The reliability of 3D topologies are compared against respective planar structures. A 3D topology is observed to add structural robustness to the ship's primary distribution system. Since equipment loads are distributed in multiple decks of the ship, in an event of damage to one of the ship's decks, equipment loads in non-damaged decks may remain operational. 3D topologies

also result in a slight improvement in the service reliability when compared with the respective planar configurations.

Another contribution of this work is a proposed framework for designing a reliable distribution circuit topology for the ship's zonal electric distribution (ZED) system. The service reliability for ZED systems is quantified in terms of network availability, which is defined as the steady-state probability of a network being in operational state. The objective is to design a resilient circuit topology ensuring the highest level of network availability while using a minimum number of conductors. We propose a mathematical formulation and an efficient graph theory based algorithm to solve the topology design problem for the ship's ZED system. The reliability constraint topology design is a combinatorial optimization problem with a double exponential search space in the number of edges/conductors. The proposed algorithm reduces the search space to linear in the number of edges and thus provides a significant computational advantage. The proposed algorithm, termed as successive minpath generation, is evaluated using 15 and 30 node ZED systems. The findings confirm that the algorithm is significantly efficient in designing optimal circuit topologies while minimizing the number of conductors (or design economy). Compared to grid topology, the proposed approach results in ZED systems with network availability more than 0.99 by using 3 fewer and 12 fewer conductors for a 15-node and a 30-node ZED, respectively. Additionally, the proposed algorithm maximizes the number of operational paths at each iteration, therefore resulting in a maximum possible improvement in service reliability at a particular iteration.

Bibliography

- [1] OpenDSS. [Online]. Available: <http://sourceforge.net/projects/electricdss/>
- [2] A. Dubey, S. Santoso, and M. Cloud, “Average-value model of electric vehicle chargers,” *Smart Grid, IEEE Transactions on*, vol. 4, no. 3, pp. 1549–1557, Sept 2013.
- [3] —, “Average-value model for plug-in hybrid electric vehicle battery chargers,” in *Power and Energy Society General Meeting, 2012 IEEE*, July 2012, pp. 1–8.
- [4] —, “Understanding the effects of electric vehicle charging on the distribution voltages,” in *Power and Energy Society General Meeting (PES), 2013 IEEE*, July 2013, pp. 1–5.
- [5] A. Dubey, “Impact of electric vehicle loads on utility distribution network voltages,” Master’s thesis, Dept. of Electrical and Computer Eng., University of Texas at Austin, Austin, TX, 2012.
- [6] A. Dubey, S. Santoso, and M. Cloud, “A practical approach to evaluate voltage quality effects of electric vehicle charging,” in *Connected Vehicles and Expo (ICCVE), 2013 International Conference on*, Dec 2013, pp. 188–194.
- [7] —, “Comparative analysis of effects of electric vehicle loads on distribution system voltages,” in *T D Conference and Exposition, 2014 IEEE*

PES, April 2014, pp. 1–5.

- [8] A. Dubey, S. Santoso, M. Cloud, and M. Waclawiak, “Determining time-of-use schedules for electric vehicle loads: A practical perspective,” *Power and Energy Technology Systems Journal, IEEE*, pp. 1–8, 2015.
- [9] A. Dubey and S. Santoso, “Electric vehicle charging on utility distribution systems: Impacts and mitigations,” *selected for publication in IEEE Access*, July 2015.
- [10] —, “A stochastic analysis framework to determine pv hosting capacity of distribution circuits,” *submitted to IEEE Transactions on Power Delivery*, July 2015.
- [11] A. Dubey, S. Santoso, and A. Maitra, “Understanding photovoltaic hosting capacity of distribution circuits,” in *Power and Energy Society General Meeting, 2015 IEEE*, July 2015, pp. 1–8.
- [12] B. Stevens, A. Dubey, and S. Santoso, “On improving reliability of shipboard power system,” *Power Systems, IEEE Transactions on*, vol. 30, no. 4, pp. 1905–1912, July 2015.
- [13] A. Dubey, S. Santoso, and A. Arapostathis, “Reliability analysis of three-dimensional shipboard electrical power distribution systems,” in *Electric Ship Technologies Symposium (ESTS), 2015 IEEE*, June 2015.
- [14] A. Dubey and S. Santoso, “Availability-based distribution circuit design for shipboard power system,” *selected for publication in IEEE Transactions on Smart Grid*, April 2015.

- [15] H. L. Willis, *Power Distribution Planning Reference Book*. CRC Press, 1997.
- [16] Us department of energy multi-year program plan 2011-2015: Vehicle technologies program (2010). [Online]. Available: https://www1.eere.energy.gov/vehiclesandfuels/pdfs/program/vt_mypp_2011-2015.pdf
- [17] Cymdist. [Online]. Available: <http://www.cyme.com/software/cymdist/>
- [18] Matlab and simulink, the mathworks, inc. as of september 2006. [Online]. Available: <http://www.mathworks.com>
- [19] Metropolitan washington council of governments: Electric vehicles in metropolitan washington, oct. 2012. [Online]. Available: http://www.mwcog.org/store/item.asp?PUBLICATION_ID=449
- [20] C. Farmer, P. Hines, J. Dowds, and S. Blumsack, "Modeling the impact of increasing phev loads on the distribution infrastructure," in *System Sciences (HICSS), 2010 43rd Hawaii International Conference on*, Jan 2010, pp. 1–10.
- [21] C. Roe, E. Farantatos, J. Meisel, A. Meliopoulos, and T. Overbye, "Power system level impacts of phev," in *System Sciences, 2009. HICSS '09. 42nd Hawaii International Conference on*, Jan 2009, pp. 1–10.
- [22] J. Taylor, A. Maitra, M. Alexander, D. Brooks, and M. Duvall, "Evaluation of the impact of plug-in electric vehicle loading on distribution system operations," in *Power Energy Society General Meeting, 2009. PES '09. IEEE*, July 2009, pp. 1–6.

- [23] —, “Evaluations of plug-in electric vehicle distribution system impacts,” in *Power and Energy Society General Meeting, 2010 IEEE*, July 2010, pp. 1–6.
- [24] S. Rahman and G. Shrestha, “An investigation into the impact of electric vehicle load on the electric utility distribution system,” *Power Delivery, IEEE Transactions on*, vol. 8, no. 2, pp. 591–597, Apr 1993.
- [25] J. Taylor, J. Smith, and R. Dugan, “Distribution modeling requirements for integration of pv, pev, and storage in a smart grid environment,” in *Power and Energy Society General Meeting, 2011 IEEE*, July 2011, pp. 1–6.
- [26] A. Hajimiragha, C. Canizares, M. Fowler, and A. Elkamel, “Optimal transition to plug-in hybrid electric vehicles in ontario, canada, considering the electricity-grid limitations,” *Industrial Electronics, IEEE Transactions on*, vol. 57, no. 2, pp. 690–701, Feb 2010.
- [27] Y. Chen, A. Oudalov, and J. Wang, “Integration of electric vehicle charging system into distribution network,” in *Power Electronics and ECCE Asia (ICPE ECCE), 2011 IEEE 8th International Conference on*, May 2011, pp. 593–598.
- [28] S. Hadley, “Evaluating the impact of plug-in hybrid electric vehicles on regional electricity supplies,” in *Bulk Power System Dynamics and Control - VII. Revitalizing Operational Reliability, 2007 iREP Symposium*, Aug 2007, pp. 1–12.
- [29] J. Gomez and M. Morcos, “Impact of ev battery chargers on the power quality of distribution systems,” *Power Delivery, IEEE Transactions on*,

vol. 18, no. 3, pp. 975–981, July 2003.

- [30] S. Shao, M. Pipattanasomporn, and S. Rahman, “Challenges of phev penetration to the residential distribution network,” in *Power Energy Society General Meeting, 2009. PES '09. IEEE*, July 2009, pp. 1–8.
- [31] O. Warweg, F. Schaller, S. Ritter, and P. Bretschneider, “Technical and regulatory challenges for the integration of electric vehicles into the energy system,” in *Innovative Smart Grid Technologies (ISGT Europe), 2011 2nd IEEE PES International Conference and Exhibition on*, Dec 2011, pp. 1–8.
- [32] K. Clement-Nyns, E. Haesen, and J. Driesen, “The impact of charging plug-in hybrid electric vehicles on a residential distribution grid,” *Power Systems, IEEE Transactions on*, vol. 25, no. 1, pp. 371–380, Feb 2010.
- [33] F. Koyanagi, T. Inuzuka, Y. Uriu, and R. Yokoyama, “Monte carlo simulation on the demand impact by quick chargers for electric vehicles,” in *Power Engineering Society Summer Meeting, 1999. IEEE*, vol. 2, 1999, pp. 1031–1036 vol.2.
- [34] A. Boulanger, A. Chu, S. Maxx, and D. Waltz, “Vehicle electrification: Status and issues,” *Proceedings of the IEEE*, vol. 99, no. 6, pp. 1116–1138, June 2011.
- [35] Q. Wu, A. Nielsen, J. Ostergaard, S. T. Cha, and Y. Ding, “Impact study of electric vehicle (ev) integration on medium voltage (mv) grids,” in *Innovative Smart Grid Technologies (ISGT Europe), 2011 2nd IEEE PES International Conference and Exhibition on*, Dec 2011, pp. 1–7.

- [36] J. Pillai and B. Bak-Jensen, "Impacts of electric vehicle loads on power distribution systems," in *Vehicle Power and Propulsion Conference (VPPC), 2010 IEEE*, Sept 2010, pp. 1–6.
- [37] G. Putrus, P. Suwanapingkarl, D. Johnston, E. Bentley, and M. Narayana, "Impact of electric vehicles on power distribution networks," in *Vehicle Power and Propulsion Conference, 2009. VPPC '09. IEEE*, Sept 2009, pp. 827–831.
- [38] Electric power research institute, "transportation electrification: a technology overview," 2011. [Online]. Available: <http://www.epri.com/abstracts/Pages/ProductAbstract.aspx?ProductId=000000000001021334/>
- [39] R. C. Leou, C. L. Su, and C. N. Lu, "Stochastic analyses of electric vehicle charging impacts on distribution network," *Power Systems, IEEE Transactions on*, vol. 29, no. 3, pp. 1055–1063, May 2014.
- [40] M. Gray and W. Morsi, "Power quality assessment in distribution systems embedded with plug-in hybrid and battery electric vehicles," *Power Systems, IEEE Transactions on*, vol. 30, no. 2, pp. 663–671, March 2015.
- [41] S. Bohn, M. Agsten, A. Dubey, and S. Santoso, "A comparative analysis of pev charging impacts -an international perspective," in *SAE Technical Paper*, Jan 2015.
- [42] C. Weiller, "Plug-in hybrid electric vehicle impacts on hourly electricity demand in the united states," *Energy Policy*, vol. 39, no. 6, pp. 3766 – 3778, 2011. [Online]. Available: <http://www.sciencedirect.com/science/article/pii/S0301421511002886>

- [43] J. Axsen and K. Kurani, “The early US market for PHEVs: Anticipating consumer awareness, recharge potential, design priorities and energy impacts,” Univ. California at Davis, UCD-ITS-RR-08-22, Tech. Rep., 2008.
- [44] K. Parks, P. Denholm, and T. Markel, “Costs and emissions associated with plug-in hybrid electric vehicle charging in the Xcel Energy Colorado service territory,” National Renewable Energy Laboratory, NREL/TP-640-41410, Tech. Rep., 2007.
- [45] J. Cook, C. Churchwell, and S. George, “Final evaluation of San Diego Gas & Electric plug-in electrical vehicle TOU,” San Diego Gas & Electric, Tech. Rep., 2014. [Online]. Available: <https://www.sdge.com/sites/default/files/documents/1681437983/SDGE%20EV%20%20Pricing%20%26%20Tech%20Study.pdf>.
- [46] S. Schey, D. Scoffield, and J. Smart, “A first look at the impact of electric vehicle charging on the electric grid in the ev project,” in *EVS26 International Battery, Hybrid and Fuel Cell Electric Vehicle Symposium*, May 2012.
- [47] S. Shao, T. Zhang, M. Pipattanasomporn, and S. Rahman, “Impact of tou rates on distribution load shapes in a smart grid with phev penetration,” in *Transmission and Distribution Conference and Exposition, 2010 IEEE PES*, April 2010, pp. 1–6.
- [48] Y. Gao, C. Wang, Z. Wang, and H. Liang, “Research on time-of-use price applying to electric vehicles charging,” in *Innovative Smart Grid Technologies - Asia (ISGT Asia), 2012 IEEE*, May 2012, pp. 1–6.

- [49] S. W. Hadley, "Impact of plug-in hybrid vehicles on the electric grid," Oak Ridge Nat. Lab., Oak Ridge, TN, USA, Tech. Rep., 2007. [Online]. Available: http://www.ornl.info/info/ornlreview/v40_2_07/2007_plug-in_paper.pdf
- [50] P. Denholm and W. Short, "An evaluation of utility system impacts and benefits of optimally dispatched plug-in hybrid electric vehicles," Nat. Renew. Energy Lab., Golden, CO, USA, Tech. Rep., 2006.
- [51] K. Clement-Nyns, E. Haesen, and J. Driesen, "The impact of charging plug-in hybrid electric vehicles on a residential distribution grid," *Power Systems, IEEE Transactions on*, vol. 25, no. 1, pp. 371–380, Feb 2010.
- [52] K. Mets, T. Verschueren, W. Haerick, C. Develder, and F. De Turck, "Optimizing smart energy control strategies for plug-in hybrid electric vehicle charging," in *Network Operations and Management Symposium Workshops (NOMS Wksp)*, 2010 IEEE/IFIP, April 2010, pp. 293–299.
- [53] E. Sortomme, M. Hindi, S. MacPherson, and S. Venkata, "Coordinated charging of plug-in hybrid electric vehicles to minimize distribution system losses," *Smart Grid, IEEE Transactions on*, vol. 2, no. 1, pp. 198–205, March 2011.
- [54] S. Deilami, A. Masoum, P. Moses, and M. Masoum, "Real-time coordination of plug-in electric vehicle charging in smart grids to minimize power losses and improve voltage profile," *Smart Grid, IEEE Transactions on*, vol. 2, no. 3, pp. 456–467, Sept 2011.
- [55] S. Shao, M. Pipattanasomporn, and S. Rahman, "Demand response as a load shaping tool in an intelligent grid with electric vehicles," *Smart*

- Grid, IEEE Transactions on*, vol. 2, no. 4, pp. 624–631, Dec 2011.
- [56] ———, “Grid integration of electric vehicles and demand response with customer choice,” *Smart Grid, IEEE Transactions on*, vol. 3, no. 1, pp. 543–550, March 2012.
- [57] L. Gan, U. Topcu, and S. Low, “Stochastic distributed protocol for electric vehicle charging with discrete charging rate,” in *Power and Energy Society General Meeting, 2012 IEEE*, July 2012, pp. 1–8.
- [58] S. Han, S. Han, and K. Sezaki, “Development of an optimal vehicle-to-grid aggregator for frequency regulation,” *Smart Grid, IEEE Transactions on*, vol. 1, no. 1, pp. 65–72, June 2010.
- [59] E. Sortomme and M. El-Sharkawi, “Optimal scheduling of vehicle-to-grid energy and ancillary services,” *Smart Grid, IEEE Transactions on*, vol. 3, no. 1, pp. 351–359, March 2012.
- [60] J. de Hoog, T. Alpcan, M. Brazil, D. Thomas, and I. Mareels, “Optimal charging of electric vehicles taking distribution network constraints into account,” *Power Systems, IEEE Transactions on*, vol. 30, no. 1, pp. 365–375, Jan 2015.
- [61] Z. Li, Q. Guo, H. Sun, S. Xin, and J. Wang, “A new real-time smart-charging method considering expected electric vehicle fleet connections,” *Power Systems, IEEE Transactions on*, vol. 29, no. 6, pp. 3114–3115, Nov 2014.
- [62] T. Markel, M. Kuss, and P. Denholm, “Communication and control of electric drive vehicles supporting renewables,” in *Vehicle Power and Propulsion Conference, 2009. VPPC '09. IEEE*, Sept 2009, pp. 27–34.

- [63] G. Shrestha and B. Chew, “Study on the optimization of charge-discharge cycle of electric vehicle batteries in the context of singapore,” in *Power Engineering Conference, 2007. AUPEC 2007. Australasian Universities*, Dec 2007, pp. 1–7.
- [64] Y. Cao, S. Tang, C. Li, P. Zhang, Y. Tan, Z. Zhang, and J. Li, “An optimized ev charging model considering tou price and soc curve,” *Smart Grid, IEEE Transactions on*, vol. 3, no. 1, pp. 388–393, March 2012.
- [65] W. Shi and V. Wong, “Real-time vehicle-to-grid control algorithm under price uncertainty,” in *Smart Grid Communications (SmartGridComm), 2011 IEEE International Conference on*, Oct 2011, pp. 261–266.
- [66] Y. He, B. Venkatesh, and L. Guan, “Optimal scheduling for charging and discharging of electric vehicles,” *Smart Grid, IEEE Transactions on*, vol. 3, no. 3, pp. 1095–1105, Sept 2012.
- [67] C. Jin, J. Tang, and P. Ghosh, “Optimizing electric vehicle charging: A customer’s perspective,” *Vehicular Technology, IEEE Transactions on*, vol. 62, no. 7, pp. 2919–2927, Sept 2013.
- [68] P. Richardson, D. Flynn, and A. Keane, “Local versus centralized charging strategies for electric vehicles in low voltage distribution systems,” *Smart Grid, IEEE Transactions on*, vol. 3, no. 2, pp. 1020–1028, June 2012.
- [69] M. M. A. M. Chris and G. David, *Power Electronics in HEVs: Plugin Hybrid Electric Vehicles*, in *Hybrid Electric Vehicles: Principles and Applications with Practical Perspectives*,. UK: John Wiley & Sons Ltd, 2011.

- [70] A. Collin, S. Djokic, H. Thomas, and J. Meyer, “Modelling of electric vehicle chargers for power system analysis,” in *Electrical Power Quality and Utilisation (EPQU), 2011 11th International Conference on*, Oct 2011, pp. 1–6.
- [71] M. Chan, K. Chau, and C. Chan, “Modeling of electric vehicle chargers,” in *Industrial Electronics Society, 1998. IECON '98. Proceedings of the 24th Annual Conference of the IEEE*, vol. 1, Aug 1998, pp. 433–438.
- [72] R. Horton, J. Taylor, A. Maitra, and J. Halliwell, “A time-domain model of a plug-in electric vehicle battery charger,” in *Transmission and Distribution Conference and Exposition (T D), 2012 IEEE PES*, May 2012, pp. 1–5.
- [73] P. Murali and S. Santoso, “Dynamic modeling of short-circuit behavior of a six-pulse rectifier,” in *Electric Ship Technologies Symposium (ESTS), 2011 IEEE*, April 2011, pp. 486–491.
- [74] H. Zhu, R. Burgos, F. Lacaux, A. Uan-Zo-li, D. Lindner, F. Wang, and D. Boroyevich, “Average modeling of three-phase and nine-phase diode rectifiers with improved ac current and dc voltage dynamics,” in *Industrial Electronics Society, 2005. IECON 2005. 31st Annual Conference of IEEE*, Nov 2005, pp. 1–6.
- [75] S. Chiniforoosh, J. Jatskevich, V. Dinavahi, R. Iravani, J. Martinez, and A. Ramirez, “Dynamic average modeling of line-commutated converters for power systems applications,” in *Power Energy Society General Meeting, 2009. PES '09. IEEE*, July 2009, pp. 1–8.

- [76] I. Jadric, D. Borojevic, and M. Jadric, "Modeling and control of a synchronous generator with an active dc load," *Power Electronics, IEEE Transactions on*, vol. 15, no. 2, pp. 303–311, Mar 2000.
- [77] J. Jatskevich, S. Pekarek, and A. Davoudi, "Parametric average-value model of synchronous machine-rectifier systems," *Energy Conversion, IEEE Transactions on*, vol. 21, no. 1, pp. 9–18, March 2006.
- [78] B. Zhang and S. Pekarek, "Analysis and average value model of a source-commutated 5-phase rectifier," in *Power Electronics Specialists Conference, 2004. PESC 04. 2004 IEEE 35th Annual*, vol. 1, June 2004, pp. 362–368 Vol.1.
- [79] J. Taylor, J. Smith, and R. Dugan, "Distribution modeling requirements for integration of pv, pev, and storage in a smart grid environment," in *Power and Energy Society General Meeting, 2011 IEEE*, July 2011, pp. 1–6.
- [80] I. Khan, "Battery chargers for electric and hybrid vehicles," in *Power Electronics in Transportation, 1994. [Proceedings]*, Oct 1994, pp. 103–112.
- [81] S. Bae and A. Kwasinski, "Spatial and temporal model of electric vehicle charging demand," *Smart Grid, IEEE Transactions on*, vol. 3, no. 1, pp. 394–403, March 2012.
- [82] W. Schalkwijk and B. Scrosat, *Charging, Monitoring, and Control: Advances in Lithium-Ion Batteries*. Springer, 2002.
- [83] O. W. P. Krause and S. Sudhoff, *Analysis of electric machinery and drive systems*. Wiley-IEEE press, 2002.

- [84] [pscad/emtdc] power system simulation software manual. monitoba hvdc research center. [Online]. Available: <https://hvdc.ca/pscad/>
- [85] R. Vicini, O. Micheloud, H. Kumar, and A. Kwasinski, "Transformer and home energy management systems to lessen electrical vehicle impact on the grid," *Generation, Transmission Distribution, IET*, vol. 6, no. 12, pp. 1202–1208, December 2012.
- [86] F. Uriarte, A. Toliyat, A. Kwasinski, and R. Hebner, "Consumer-data approach to assess the effect of residential grid-tied photovoltaic systems and electric vehicles on distribution transformers," in *Power Electronics for Distributed Generation Systems (PEDG), 2014 IEEE 5th International Symposium on*, June 2014, pp. 1–8.
- [87] Nissan leaf. [Online]. Available: <http://www.nissanusa.com/leaf-electric-car/index#/leaf-electric-car/index>
- [88] Chevrolet volt. [Online]. Available: <http://www.chevrolet.com/volt-electric-car/>
- [89] P. Joskow and C. Wolfram, "Dynamic pricing of electricity," *American Economic Review*, pp. 381–385, 2012.
- [90] "Solar Market Insight Report 2014," GTM Research/SEIA:U.S. Solar Market Insight, Tech. Rep., 2014.
- [91] F. Katiraei and J. Aguero, "Solar pv integration challenges," *Power and Energy Magazine, IEEE*, vol. 9, no. 3, pp. 62–71, May 2011.

- [92] C. Masters, "Voltage rise: the big issue when connecting embedded generation to long 11 kv overhead lines," *Power Engineering Journal*, vol. 16, no. 1, pp. 5–12, Feb 2002.
- [93] Y. Liu, J. Bebic, B. Kroposki, J. de Bedout, and W. Ren, "Distribution system voltage performance analysis for high-penetration pv," in *Energy 2030 Conference, 2008. ENERGY 2008. IEEE*, Nov 2008, pp. 1–8.
- [94] E. Liu and J. Bebic, "Distribution system voltage performance analysis for high-penetration photovoltaics," GE Global Research, Niskayuna, NY, Rep. NREL/SR-581-42298, 2008, Tech. Rep., 2008.
- [95] M. Thomson and D. Infield, "Impact of widespread photovoltaics generation on distribution systems," *Renewable Power Generation, IET*, vol. 1, no. 1, pp. 33–40, March 2007.
- [96] P. Barker and R. de Mello, "Determining the impact of distributed generation on power systems. i. radial distribution systems," in *Power Engineering Society Summer Meeting, 2000. IEEE*, vol. 3, 2000, pp. 1645–1656 vol. 3.
- [97] A. Woyte, V. Van Thong, R. Belmans, and J. Nijs, "Voltage fluctuations on distribution level introduced by photovoltaic systems," *Energy Conversion, IEEE Transactions on*, vol. 21, no. 1, pp. 202–209, March 2006.
- [98] Y. T. Tan and D. Kirschen, "Impact on the power system of a large penetration of photovoltaic generation," in *Power Engineering Society General Meeting, 2007. IEEE*, June 2007, pp. 1–8.

- [99] R. Tonkoski, D. Turcotte, and T. El-Fouly, “Impact of high pv penetration on voltage profiles in residential neighborhoods,” *Sustainable Energy, IEEE Transactions on*, vol. 3, no. 3, pp. 518–527, July 2012.
- [100] M. Alam, K. Muttaqi, and D. Sutanto, “An approach for online assessment of rooftop solar pv impacts on low-voltage distribution networks,” *Sustainable Energy, IEEE Transactions on*, vol. 5, no. 2, pp. 663–672, April 2014.
- [101] H. Pezeshki, P. Wolfs, and G. Ledwich, “Impact of high pv penetration on distribution transformer insulation life,” *Power Delivery, IEEE Transactions on*, vol. 29, no. 3, pp. 1212–1220, June 2014.
- [102] Y. Agalgaonkar, B. Pal, and R. Jabr, “Distribution voltage control considering the impact of pv generation on tap changers and autonomous regulators,” *Power Systems, IEEE Transactions on*, vol. 29, no. 1, pp. 182–192, Jan 2014.
- [103] E. Demirok, D. Sera, R. Teodorescu, P. Rodriguez, and U. Borup, “Clustered pv inverters in lv networks: An overview of impacts and comparison of voltage control strategies,” in *Electrical Power Energy Conference (EPEC), 2009 IEEE*, Oct 2009, pp. 1–6.
- [104] A. Toliyat, A. Kwasinski, and F. Uriarte, “Effects of high penetration levels of residential photovoltaic generation: Observations from field data,” in *Renewable Energy Research and Applications (ICRERA), 2012 International Conference on*, Nov 2012, pp. 1–6.
- [105] “For Electric Power Systems and Equipment-Voltage Ratings (60 Hertz),” *American National Standard, ANSI C84.1-2011*, 2012.

- [106] A. Hoke, R. Butler, J. Hambrick, and B. Kroposki, “Steady-state analysis of maximum photovoltaic penetration levels on typical distribution feeders,” *Sustainable Energy, IEEE Transactions on*, vol. 4, no. 2, pp. 350–357, April 2013.
- [107] R. Shayani and M. de Oliveira, “Photovoltaic generation penetration limits in radial distribution systems,” *Power Systems, IEEE Transactions on*, vol. 26, no. 3, pp. 1625–1631, Aug 2011.
- [108] C. Debruyne, J. Desmet, J. Vanalme, B. Verhelst, G. Vanalme, and L. Vandeveldel, “Maximum power injection acceptance in a residential area,” in *Proceedings of the International Conference on Renewable Energies and Power Quality*. European Association for the Development of Renewable Energies, Environment and Power Quality, 2010, pp. 1–6.
- [109] L. Cipcigan and P. Taylor, “Investigation of the reverse power flow requirements of high penetrations of small-scale embedded generation,” *Renewable Power Generation, IET*, vol. 1, no. 3, pp. 160–166, September 2007.
- [110] A. Navarro, L. Ochoa, and D. Randles, “Monte carlo-based assessment of pv impacts on real uk low voltage networks,” in *Power and Energy Society General Meeting (PES), 2013 IEEE*, July 2013, pp. 1–5.
- [111] J. Smith, R. Dugan, M. Rylander, and T. Key, “Advanced distribution planning tools for high penetration pv deployment,” in *Power and Energy Society General Meeting, 2012 IEEE*, July 2012, pp. 1–7.
- [112] J. Smith, “Stochastic analysis to determine feeder hosting capacity for distributed solar pv,” EPRI, Technical Report 1026640, Tech. Rep.,

2012.

- [113] R. J. Broderick, J. E. Quiroz, M. J. Reno, A. Ellis, J. Smith, and R. Dugan, "Time series power flow analysis for distribution connected pv generation," Sandia National Laboratories SAND2013-0537, Tech. Rep., 2013.
- [114] W. Erdman, "Secondary network distribution systems background and issues related to the interconnection of distributed resources," National Renewable Energy Laboratory, Tech. Rep., 2005.
- [115] L. Victor, M. Kay, and I. Povey, "Reverse power flow capability of tap changers," *18th International Conference and Exhibition on Electricity Distribution, CIRED*, 2005.
- [116] J. Rittershausen and M. McDonagh, "Moving Energy Storage from Concept to Reality," Southern California Edison, Tech. Rep., 2011. [Online]. Available: <https://www.edison.com/content/dam/eix/documents/innovation/smart-grids/Energy-Storage-Concept-to-Reality-Edison.pdf>
- [117] A. A. Akhil, G. Huff, A. B. Currier, B. C. Kaun, D. M. Rastler, S. B. Chen, A. L. Cotter, D. T. Bradshaw, and W. D. Gauntlett, "DOE/EPRI 2013 Electricity Storage Handbook in Collaboration with NRECA," Sandia National Laboratories, Tech. Rep., July 2015. [Online]. Available: <http://www.sandia.gov/ess/publications/SAND2013-5131.pdf>
- [118] "Public Interest Energy Research (PIER) Program Interim/Final Project Report - Energy Storage Cost-Effectiveness Methodology and Prelim-

inary Results,” California Energy Commission (CEC)-DNV KEMA, Tech. Rep., June 2013. [Online]. Available: http://www.cpuc.ca.gov/NR/rdonlyres/A7FF0A4E-44FA-4281-8F8F-CFB773AC2181/0/DNVKEMA_EnergyStorageCostEffectiveness_Report.pdf

[119] “Energy Storage for the Electricity Grid: Benefits and Market Potential Assessment Guide,” Sandia Report, SAND2010-0815, Tech. Rep., Feb 2010. [Online]. Available: <http://www.sandia.gov/ess/publications/SAND2010-0815.pdf>

[120] “Cost-Effectiveness of Energy Storage in California: Application of the EPRI Energy Storage Valuation Tool to inform the California Public Utility Commission Proceeding R. 10-12-007,” EPRI report, TR3002001164, Tech. Rep., Dec 2013.

[121] P. C. Butler, “Battery Energy Storage for Utility Applications: Phase I Opportunities Analysis,” SAND94-2605, Tech. Rep., Oct 1994.

[122] N. Doerry and D. Clayton, “Shipboard electrical power quality of service,” in *Electric Ship Technologies Symposium, 2005 IEEE*, July 2005, pp. 274–279.

[123] N. Doerry, “Designing electrical power systems for survivability and quality of service,” *Naval Engineers Journal*, vol. 119, no. 6, pp. 25–34, 2007.

[124] N. Doerry and J. Amy, “Implementing quality of service in shipboard power system design,” in *Electric Ship Technologies Symposium (ESTS), 2011 IEEE*, April 2011, pp. 1–8.

- [125] B. Stevens and S. Santoso, "Reliability analysis of a shipboard electrical power distribution system based on breaker-and-a-half topology," in *Electric Ship Technologies Symposium (ESTS), 2013 IEEE*, April 2013, pp. 387–393.
- [126] P. M. Anderson, *Power System Protection*. IEEE Press, 1999.
- [127] M. Grover and R. Billinton, "A computerized approach to substation and switching station reliability evaluation," *Power Apparatus and Systems, IEEE Transactions on*, vol. PAS-93, no. 5, pp. 1488–1497, Sept 1974.
- [128] R. Allan and M. de Oliveira, "Reliability modeling and evaluation of transmission and distribution systems," in *Proceedings of the Institution of Electrical Engineers*, vol. 124, no. 6, June 1977, pp. 1–8.
- [129] Q. Yu and N. Schulz, "Multi-agent based reconfiguration of an electric propulsion system for all electric-ships," in *Power Symposium, 2007. NAPS '07. 39th North American*, Sept 2007, pp. 153–158.
- [130] K. Butler, N. Sarma, and V. Ragendra Prasad, "Network reconfiguration for service restoration in shipboard power distribution systems," *Power Systems, IEEE Transactions on*, vol. 16, no. 4, pp. 653–661, Nov 2001.
- [131] K. Butler and N. Sarma, "General reconfiguration methodology for ac radial shipboard power systems," in *Power Engineering Society Winter Meeting, 2000. IEEE*, vol. 2, 2000, pp. 1226–1230 vol.2.
- [132] M. Baran and N. Mahajan, "System reconfiguration on shipboard dc zonal electrical system," in *Electric Ship Technologies Symposium, 2005 IEEE*, July 2005, pp. 86–92.

- [133] P. Mitra and G. Venayagamoorthy, "Implementation of an intelligent reconfiguration algorithm for an electric ship power system," in *Industry Applications Society Annual Meeting, 2009. IAS 2009. IEEE*, Oct 2009, pp. 1–8.
- [134] T. L. M. Ravindra K. Ahuja and J. B. Orlin, *Network flows: theory, algorithms, and applications*. Prentice-Hall, 1993.
- [135] R. Brown, "Failure rate modeling using equipment inspection data," in *Power Engineering Society General Meeting, 2004. IEEE*, June 2004, pp. 693–700 Vol.1.
- [136] Y. C. Wu and W. F. Chang, "A study on optimal reliability indices in an electrical distribution system," in *Power System Technology, 2000. Proceedings. PowerCon 2000. International Conference on*, vol. 2, 2000, pp. 727–732.
- [137] R. Brown and J. Ochoa, "Distribution system reliability: default data and model validation," *Power Systems, IEEE Transactions on*, vol. 13, no. 2, pp. 704–709, May 1998.
- [138] T. Gonen and A. Mahmoud, "Bibliography of power distribution system planning," *Power Apparatus and Systems, IEEE Transactions on*, vol. PAS-102, no. 6, pp. 1778–1787, 1983.
- [139] T. Gonen and I. Ramirez-Rosado, "Review of distribution system planning models: a model for optimal multistage planning," *Generation, Transmission and Distribution, IEE Proceedings C*, vol. 133, no. 7, pp. 397–408, 1986.

- [140] S. Khator and L. Leung, "Power distribution planning: a review of models and issues," *Power Systems, IEEE Transactions on*, vol. 12, no. 3, pp. 1151–1159, 1997.
- [141] T. Gonen, *Electric Power Distribution system Engineering*. McGraw Hill, 1986.
- [142] T. Gonen and B. Foote, "Distribution-system planning using mixed-integer programming," *Generation, Transmission and Distribution, IEE Proceedings C*, vol. 128, no. 2, pp. 70–79, 1981.
- [143] G. L. Thompson and D. L. Wall, "A branch and bound model for choosing optimal substation locations," *Power Apparatus and Systems, IEEE Transactions on*, vol. PAS-100, no. 5, pp. 2683–2688, 1981.
- [144] Y.-Y. Hsu and J.-L. Chen, "Distribution planning using a knowledge-based expert system," *Power Delivery, IEEE Transactions on*, vol. 5, no. 3, pp. 1514–1519, 1990.
- [145] K. Moslehi and R. Kumar, "A reliability perspective of the smart grid," *Smart Grid, IEEE Transactions on*, vol. 1, no. 1, pp. 57–64, June 2010.
- [146] A. Basu, S. Chowdhury, and S. P. Chowdhury, "Impact of strategic deployment of chp-based ders on microgrid reliability," *Power Delivery, IEEE Transactions on*, vol. 25, no. 3, pp. 1697–1705, 2010.
- [147] J. Mitra, S. Patra, and S. Ranade, "Reliability stipulated microgrid architecture using particle swarm optimization," in *Probabilistic Methods Applied to Power Systems, 2006. PMAAPS 2006. International Conference on*, 2006, pp. 1–7.

- [148] M. Vallem and J. Mitra, "Siting and sizing of distributed generation for optimal microgrid architecture," in *Power Symposium, 2005. Proceedings of the 37th Annual North American*, 2005, pp. 611–616.
- [149] M. Erol-Kantarci, B. Kantarci, and H. Mouftah, "Reliable overlay topology design for the smart microgrid network," *Network, IEEE*, vol. 25, no. 5, pp. 38–43, 2011.
- [150] R. Yokoyama, T. Niimura, and N. Saito, "Modeling and evaluation of supply reliability of microgrids including pv and wind power," in *Power and Energy Society General Meeting - Conversion and Delivery of Electrical Energy in the 21st Century, 2008 IEEE*, 2008, pp. 1–5.
- [151] S. Patra, J. Mitra, and S. Ranade, "Microgrid architecture: a reliability constrained approach," in *Power Engineering Society General Meeting, 2005. IEEE*, 2005, pp. 2372–2377.
- [152] A. Kwasinski, V. Krishnamurthy, J. Song, and R. Sharma, "Availability evaluation of micro-grids for resistant power supply during natural disasters," *Smart Grid, IEEE Transactions on*, vol. 3, no. 4, pp. 2007–2018, Dec 2012.
- [153] J. Song, M. Bozchalui, A. Kwasinski, and R. Sharma, "Microgrids availability evaluation using a markov chain energy storage model: a comparison study in system architectures," in *Transmission and Distribution Conference and Exposition (T D), 2012 IEEE PES*, May 2012, pp. 1–6.
- [154] A. Kwasinski, "Quantitative evaluation of dc microgrids availability: Effects of system architecture and converter topology design choices,"

Power Electronics, IEEE Transactions on, vol. 26, no. 3, pp. 835–851, March 2011.

- [155] J. Song, V. Krishnamurthy, A. Kwasinski, and R. Sharma, “Development of a markov-chain-based energy storage model for power supply availability assessment of photovoltaic generation plants,” *Sustainable Energy, IEEE Transactions on*, vol. 4, no. 2, pp. 491–500, April 2013.
- [156] W. Meng, R. Ma, and H.-H. Chen, “Smart grid neighborhood area networks: a survey,” *Network, IEEE*, vol. 28, no. 1, pp. 24–32, January 2014.
- [157] C. Gentile, D. Griffith, and M. Souryal, “Wireless network deployment in the smart grid: Design and evaluation issues,” *Network, IEEE*, vol. 26, no. 6, pp. 48–53, November 2012.
- [158] Y. Zhang, R. Yu, M. Nekovee, Y. Liu, S. Xie, and S. Gjessing, “Cognitive machine-to-machine communications: visions and potentials for the smart grid,” *Network, IEEE*, vol. 26, no. 3, pp. 6–13, May 2012.
- [159] D. He, S. Chan, Y. Zhang, M. Guizani, C. Chen, and J. Bu, “An enhanced public key infrastructure to secure smart grid wireless communication networks,” *Network, IEEE*, vol. 28, no. 1, pp. 10–16, January 2014.
- [160] Z. Fadlullah, M. Fouda, N. Kato, X. Shen, and Y. Nozaki, “An early warning system against malicious activities for smart grid communications,” *Network, IEEE*, vol. 25, no. 5, pp. 50–55, September 2011.

- [161] P. Lagonotte, J. Sabonnadiere, , J. Leost, and J. Paul, “Structural analysis of the electrical system: application to secondary voltage control in france,” *Power Systems, IEEE Transactions on*, vol. 4, no. 2, May 1989.
- [162] Y. Koc, Warnier, M., R. Kooij, and F. Brazier, “Structural vulnerability assessment of electric power grids,” *American Institute of Physics, arXiv:1312.6606v1*, December 2013.
- [163] P. Holme, B. Kim, C. Yoon, and S. Han, “Attack vulnerability of complex networks,” *Phys. Rev. E*, vol. 65, no. 5, May 2002.
- [164] E. Cotilla-Sanchez, P. Hines, B. C., and S. Blumsack, “Comparing the topological and electrical structure of the north american electric power infrastructure,” *Systems Journal, IEEE*, vol. 6, no. 4, pp. 616–626, December 2012.
- [165] A. Holmgren, “Using graph models to analyze the vulnerability of electric power networks,” *Risk Analysis*, vol. 26, no. 4, pp. 955–969, December 2006.
- [166] C. J. Colbourn, *The Combinatorics of Network Reliability*. Oxford University Press, 1987.

Vita

Anamika Dubey was born in Rewa (M.P.), India on 3rd March 1988, the daughter of Late Mr. Rakesh Kumar Dubey and Dr. Usha Dubey. After completing high school from Kendriya Vidyalaya, Rewa, India in 2005, she attended Indian Institute of Technology (IIT) Roorkee, and received her Bachelor's in Technology (B.Tech) degree in Electrical Engineering in May, 2010.

She started her doctoral studies in the Department of Electrical and Computer Engineering under the supervision of Dr. Surya Santoso at The University of Texas at Austin in August 2010. During her doctoral studies, she worked on investigating and providing solutions to the problem of integrating intermittent/variable load and generation, such as electric vehicles, photovoltaic distributed generation, and energy storage into the existing utility distribution systems. She also worked on designing new distribution circuit topologies for improved service availability. During her studies, she held positions as a graduate research assistant and a teaching assistant, and authored or co-authored six journal articles, ten conference publications, and two book chapters. She also worked as an intern at Mitsubishi Electric Research Laboratories at Boston under the guidance of Dr. Hongbo Sun, and resulted in two patent applications. She received her Master of Science in Engineering (MSE) degree from The University of Texas at Austin in August 2012.

Email: ana.iitr@gmail.com

Permanent address:

H.No.-125/14, Arun Nagar, Rewa (M.P.), India, Pincode - 486001